OPTIMIZATION OF THE AIR HANDLING SYSTEM OF A MULTI-CYLINDER LIGHT-DUTY ENGINE RUNNING ON REACTIVITY CONTROLLED COMPRESSION IGNITION – A SIMULATION STUDY

By:

ANAND NAGESWARAN BHARATH

A Dissertation submitted in partial fulfillment of

the requirements for the degree of:

Doctor of Philosophy

(Mechanical Engineering)

at the:

UNIVERSITY OF WISCONSIN-MADISON COLLEGE OF ENGINEERING

2016

Date of Final Oral Examination: May 31st 2016

The dissertation is approved by the following members of the Final Oral Committee:

Rolf D. Reitz, Wisconsin Distinguished Professor, Mechanical Engineering (co-chair)
Christopher J. Rutland, Professor, Mechanical Engineering (co-chair)
David A. Rothamer, Associate Professor, Mechanical Engineering
Sage L. Kokjohn, Assistant Professor, Mechanical Engineering
Riccardo Bonazza, Professor, Engineering Physics

OPENING PRAYER

"Gurur Brahma, Gurur Vishnu, Gurur Devo, Maheshwara:
Guru Saakshaat, Param Brahma, Tasmai Shri Gurave Namah:
Guruve Sarva Lokanam, Bhishaje Bhava Roginam,
Nidhaye Sarva Vidhyanam, Sri Dakshinamurthaye Namo Namah:"

Translation

Guru is Brahma, the Creator; Guru is Vishnu, the Preserver;
Guru is Lord Maheshwara (Lord Shiva), the Destroyer;
The Guru alone is the Supreme Brahman, the Absolute.
I offer my Namaskarams (salutations) and utmost respect to such a Guru.
He who is the Guru for the whole world, He who removes the worldly diseases
and is the repository of all knowledge,
I Salute Him, the God Dakshinamurthy, who faces the South direction.

I dedicate this dissertation to my parents Chi. Bharath Dharmarajan Ganesan and Smt. Srividya Lokanayaki Bharath, as well as my family deity Lord Muruga, and the God of Knowledge, the Supreme Guru Sri Dakshinamurthy (an incarnation of Lord Shiva).

ABSTRACT

While Low Temperature Combustion (LTC) Strategies such as Reactivity Controlled Compression Ignition (RCCI) exhibit high thermal efficiency and low NOx and soot emissions, stable low load operation and a maximum limit in the high load range are some of the drawbacks faced that prevent such strategies from being implemented in production engines. LTC strategies such as RCCI are highly sensitive to intake conditions, which are in turn heavily influenced by the gas exchange process. Because the gas exchange process is dependent on the characteristics of the air handling system, which includes the exhaust gas recirculation system (EGR), turbocharger/supercharger performance and valve timing, a study on how to optimize the air handling system for the improved performance of RCCI combustion is necessary. Three major objectives were considered: 1. Improve combustion stability and efficiency while mitigating unburnt hydrocarbon (UHC) and carbon monoxide (CO) emissions at low load operation, 2. Determine system parameters and air handling configurations for high load operation and 3. Examine variable valve actuation (VVA) and manifold redesign strategies to maximize fuel efficiency by reducing pumping and friction work. The work involved the use of zero-dimensional and one-dimensional gas dynamics simulations using GT-Power for the gas exchange process, and a multi-dimensional combustion model in KIVA-3V for the in-cylinder combustion. Early Exhaust Valve Opening (EEVO) using fully flexible variable valvetrains and a cam-phased variable valve train, as well as cylinder deactivation, were studied for their potential to increase exhaust gas temperatures at low load, so that the Diesel Oxidation Catalyst can light off at low load points to improve the UHC and CO conversion efficiency. It was shown that for near-idle conditions of 1 Bar BMEP at 1,500 RPM, opening the exhaust valve at 80 degrees After Top Dead Center (ATDC) significantly improved UHC and CO conversion efficiency to > 90% for both valvetrains; however, fuel economy deteriorated by 9.6% for the fully flexible valvetrain. The fuel economy deterioration was even worse (at 90%) for the cam phaser due to increased pumping work that occurred as a result of residual exhaust gas recompression. The cylinder deactivation strategy in which only one cylinder was fired while the rest were motored gave the best fuel economy while still increasing exhaust gas temperatures. The DOC unburnt hydrocarbon and carbon monoxide conversion efficiency was the best for the cylinder deactivation

case as well due to the lower exhaust gas flow rates through the catalyst. For the second objective of performing high load system simulation, an 18 Bar IMEP at 2,000 rev/min load point was simulated. The stock multi-cylinder engine model was modified to include a low pressure (LP) EGR circuit and a throttle was added at the turbine outlet to increase backpressure for driving the LP EGR flow. At high load, medium speed operation, HP EGR could not be used as the pre-turbine pressure would not be sufficient to drive the EGR flow at that point. Moreover, if part of the flow were used for EGR, not all the exhaust energy is available to the turbine, resulting in a decrease in boost pressure.

For the 3rd and final part of this research, the exhaust manifold of the stock RCCI engine was redesigned using a concept known as the Divided Exhaust Period (DEP), in which the exhaust manifold was split into two separate manifolds, one connected to each exhaust valve. The blowdown manifold was directly connected to the turbine inlet, while the scavenging manifold bypassed the turbine and was connected to the turbine outlet. By using a variable valve actuation system to separately actuate the exhaust valves, different valve timings were implemented for each exhaust valve. Varying the blowdown valve-scavenging valve overlap allowed control over the exhaust distribution between the two manifolds, which in turn regulated the exhaust enthalpy available to the turbine. With the DEP concept, due to the lower overall backpressure that arose from the exhaust split, the pumping penalty was reduced. However, the pumping benefit was negated by the parasitic losses from the supercharger which had to make up for the boost deficit. When the fixed geometry turbocharger was replaced with a scaled variable geometry turbocharger (VGT), the supercharger could be disconnected and a 1% improvement in Brake Specific Fuel Consumption (BSFC) over the stock engine configuration was observed. The DEP concept offers a pumping benefit for RCCI engines as well as elevated exhaust gas temperatures for thermal management at low loads, but may require the use of two-stage boosting systems that could negate the pumping benefit through parasitic losses. Further investigation of the concept over a wide range of engine speeds and load points is therefore required to fully conclude whether the DEP concept could be beneficial for LTC engines.

ACKNOWLEDGEMENTS

They say it takes a village to educate a child. This proverb could not be truer in my case; in fact, my PhD was possible due to the support and guidance of people from four different cities (probably even more!): Ann Arbor, Michigan, Madison, Wisconsin, Westmont, Illinois, and Singapore. The PhD has been a challenging yet very fulfilling journey; every minute and second of this journey was worth it. At this juncture, I want to thank everyone who has helped me achieve my childhood dream of obtaining the PhD.

First and foremost, I would like to thank my advisors Professor Rolf Reitz and Professor Christopher Rutland for giving me the opportunity to work in the Engine Research Center at the University of Wisconsin Madison, the best engine research institution in the country. I am extremely grateful for their support and guidance, and for always being available to help me learn and improve my knowledge of RCCI engine simulation and engine gas dynamics whenever I was stuck. I will indeed be in a tremendous amount of debt to them for the rest of my professional career. I also would like to thank my committee members Professor Riccardo Bonazza, Professor David Rothamer and Professor Sage Kokjohn for their guidance and support, and for providing invaluable suggestions and ideas about my research topic whenever I needed help. I am also very grateful to our ERC research scientists Michael Andrie and Dr. Randy Hessel, for their mentorship as well as their guidance on the details of engine modeling and validating engine models with experimental data.

I am grateful for the monetary and technical support I have received from the Direct Injection Engine Research Consortium (DERC), a consortium of 27 different automotive companies and government agencies to study advanced engine combustion technologies. Without the support from DERC, this research would not have been possible. In particular, I would like to thank Philip Wetzel, Brian Smith, Brendan Biller and Benjamin Meikle from Eaton Corporation (one of the DERC member companies) for supplying the compressor map of the TVS-410 Roots Supercharger, and giving me sound technical advice on how to model the Roots Supercharger in GT-Power.

The numerous colleagues that I have worked with in the Engine Research Center here over the past 4 years have also left a deep impact in my personal and professional life. I am especially grateful to my

direct colleagues whom I had the honor of working with in DERC Project 3, namely Dr. Johannes Eichmeier, Dr. Yifeng Wu, Nitya Kalva, Yangdongfang Yang and Ritwik Athalye. Yifeng and I in particular have become very good friends outside of work, and he is someone whom I can always count on to discuss any questions I have about engine research, and about life in general! I also had lots of great memories with my office mates Bishwadipa (Dipa) Das Adhikary, Jae-Hyung Lim, Lu Qiu, Zongyu Yue, Chaitanya Kavuri, Tyler Strickland, Arun Ravindran, Jian Gong, Dr. Anand Krishnasamy, Dr. Federico Perini and Chandrasekhar Viswanadha. In particular, I want to thank Dipa, Jae, Chaitanya, Jian, Arun and Tyler for all the meaningful research discussions and engine modeling suggestions which have been very helpful for my work. The aforementioned six people have not only been reliable and helpful colleagues, but they have also become some of my best friends here and I'm sure I will be keeping in touch with them for the rest of my life. I also want to thank Federico for his assistance with developing MATLAB scripts to interpolate injection profiles and for general help with KIVA-3V.

In addition, I would also like to thank my colleagues performing experimental research for providing the data to validate my models, as well as giving me practical advice on what can be achieved in experiments so that my modeling work is more rooted in the real world. I would especially like to thank my colleagues from DERC Project 2: Reed Hanson, Christopher Gross, Shawn Spannbauer and Jacob Riederer for providing me the experimental data from the General Motors 1.9L Engine to validate my models and for the insightful discussions about multi-cylinder engine experiments. I would also like to thank other experimentalists: Cory Adams, John Roberts, Javier Vera and Ryan Walker for their suggestions and advice about matching simulation with engine testing data.

I am especially grateful to Professors Gregory Nellis and Sanford Klein from the Solar Energy Laboratory, who are both authors of the simulation software tool Engineering Equation Solver (EES). They have both been very helpful in providing programming advice in EES as well as helping me troubleshoot the zero-dimensional engine model code that I wrote. I also want to thank their students, particularly, Rodrigo Barraza, Wenjie Zhou, Luis Diego Fonseca Flores and Amy Van Asselt, who have also been very helpful in helping to test and troubleshoot my code. These four in particular have become very good friends

of mine, especially Rodrigo and Wenjie with whom I studied for my qualifying exams during my 1st year at Wisconsin.

Joshua Leach, our ERC Systems Administrator, deserves a very special note of thanks. He is an invaluable staff member of the ERC who works pretty much all around the clock to ensure that all the computer hardware and software, as well as the internet network, are properly working. He has been amazing in helping me and my colleagues resolve any computer or network related issues in a timely fashion. The ERC without him would be a very different place.

The Mechanical Engineering Department staff have also been very helpful in ensuring that I am aware of the degree policies as well as the continuous support that they have provided to me and other graduate students during our education in Wisconsin. In particular, I would like to thank Kathie Keyes and Theresa Pilar-Groesbeck for their guidance and advising pertaining to degree requirements and administrative matters. I also would like to thank Steven Noftle, who has been helpful in coordinating purchases and conference reimbursements for the ERC.

Jody Hoesly, the Assistant Director for Information Systems and the liaison librarian for Mechanical Engineering at the Wendt Commons Engineering Library, also deserves a special note of thanks. She has been very helpful and knowledgeable about library resources, references and journal articles whenever I needed help looking for the right print/online resources for my research work.

At this point, I must definitely give my sincere acknowledgements to the University of Wisconsin Madison Writing Center. The writing center is one invaluable resource on campus which made the challenging task of writing the dissertation much easier and more manageable. The various weekly graduate writers' group writing sessions that were organized by the Writing Center provided me a conducive and focused environment for writing my dissertation and publication manuscripts. I want to thank the facilitators of the writing groups, in particular: Sarah Groeneveld, Brad Hughes, Leigh Elion and David Callenberger. These four individuals have not only been amazing facilitators; they have also been a great lending ear willing to discuss about other issues that graduate students face as well as give advice about writing techniques.

The technical support staff at Gamma Technologies, the company which publishes the GT-Power engine modeling software, have been of tremendous help in troubleshooting any software related problems, or giving advice about engine system modeling in general. I would especially like to thank Paramjot Singh, Daniel Schimmel, Miles Melka and Thomas Wanat, whom I have spent many hours on the phone with to resolve any problems or issues related to model setup and simulation execution. I would also like to thank Michael Arnett, Kevin Roggendorf, Ryan Dudgeon and Matthew Massaro, and any other technical support staff from Gamma Technologies for their assistance and support in this project. In addition, I also want to thank Patrick Niven and Martin Horacek from Ricardo for their assistance and support with 1-D gas dynamics modeling of engine systems.

My former supervisors and colleagues at the University of Michigan Walter E. Lay Automotive Laboratory also deserve a special mention, for it was the research work that I performed and the education that I received at Michigan during my Masters that encouraged me to choose the field of internal combustion engines for my career. I want to thank my former advisors at Michigan, Prof. Dennis Assanis (who is now the President of the University of Delaware at the time of writing) and John Hoard, whom I had the opportunity to work with on EGR Cooler Fouling before moving to Wisconsin. Anyone who has had the opportunity to work with Dennis or take a class from him would know him not just as an accomplished research scholar, but also a convincing salesman. It was his Introduction to Internal Combustion Engines class that I took in the Winter 2011 semester at Michigan that piqued my interest in the subject and convinced me to pursue research in this area for my PhD. As for John, he's one of the most knowledgeable engine and aftertreatment experimentalists I have had the pleasure of working with; his many years of experience at Ford before he joined Michigan as a research scientist have made him a great mentor who has amazing perspectives on the future of the automotive engineering field.

Sotirios Mamalis is another one of my former University of Michigan colleagues that I'd like to thank. Currently a professor at State University of New York at Stony Brook, he has been a great friend whom I can always rely on for advice about boosting system modeling in GT-Power. His generosity in taking time off to provide me with advice on GT-Power modeling and even sending me model templates

and files has been extremely helpful, and I hope to collaborate with him on more projects in the future should opportunities arise. I also want to thank my other supervisors at the University of Michigan: Research Scientists Dr. Jason Martz and Dr. Stani Bohac, who have been very helpful in taking time off from their busy schedules to give me advice on Low Temperature Combustion engine modeling, and even helping me out with professional advice on my future career plans.

One important person I would especially like to thank is Professor Volker Sick, who is the current director of the Walter E. Lay Automotive Laboratory and also the associate vice president of research in engineering at the University of Michigan. Prof. Sick was my section instructor for Thermodynamics as well as the Mechanical Engineering Laboratory class during my sophomore year at Michigan. Besides being a very dedicated and helpful instructor for my classes, he has also been a wonderful mentor. Whenever I needed advice about pursuing graduate school or my future career plans, he was always available and eager to meet with me and give me suggestions for my future career. Even now, almost five years after I left Michigan, I am still in touch with him and am able to seek his advice whenever I need it. He is always ready to assist all of his students, current and former in whatever way he can, and for that I am very grateful.

The past 4½ years in Madison have been fantastic, and I would like to thank all of my graduate school colleagues from other departments that I have had the pleasure of hanging out with, as well as all of my wonderful friends from outside the University community who have made Madison, Wisconsin a welcoming home that I will miss dearly when I leave.

At this juncture, two of the most important people in the world that I want to profusely thank at this point are my wonderful parents: my father Bharath Dharmarajan Ganesan, and my mother Srividya Lokanayaki Bharath, for their love as well as their words of encouragement and support throughout my graduate school career. They have always been and will always be my biggest cheerleaders, and were it not for their moral support and encouragement, as well as their prayers, I would never have made it this far in life. I will always be very grateful and owe them a tremendous amount of debt for the rest of my life, and will always love them and express my deepest respect for them, for all that they have done for me.

And last but not least, I must thank God, especially my family deity, Lord Muruga of Palani. Lord Muruga has always given me the strength to carry on despite the challenges I have faced during my graduate school journey, and He has always answered my prayers in times of need. I will always be thankful to the Lord for giving me this opportunity to do the PhD, which has been my childhood dream, as well as giving me the physical and mental fortitude to accomplish something as challenging as writing this dissertation! Without His blessings, I would never have been able to complete the dissertation and defense.

LIST OF FIGURES

LIST OF TABLES

NOMENCLATURE

ABBREVIATIONS/ACRONYMS

ACT	Active Control Turbocharging
AMEP	Accessory Mean Effective Pressure
A/R	Aspect Ratio (or Area-to-Radius Ratio)
ATDC	After Top Dead Center
BDC	Bottom Dead Center
BDSC	Blowdown Supercharging
BDVC	Blowdown Valve Closing
BDVO	Blowdown Valve Opening
BDVOD	Blowdown Valve Open Duration
BMEP	Brake Mean Effective Pressure
BSFC	Brake Specific Fuel Consumption
CA50	Crank Angle at 50% Total Heat Release
CDC	Conventional Diesel Combustion
CFD	Computational Fluid Dynamics
CO	Carbon Monoxide
CPSI	Cells per Square Inch
DEP	Divided Exhaust Period
DI	Direct Injected
DOC	Diesel Oxidation Catalyst
DOI	Duration of Injection
DPF	Diesel Particulate Filter
EGR	Exhaust Gas Recirculation
EES	Engineering Equation Solver
EEVO	Early Exhaust Valve Opening
EVC	Exhaust Valve Closing
EVO	Exhaust Valve Opening
FGT	Fixed Geometry Turbocharger

FMEP	Friction Mean Effective Pressure
GRI	Gas Research Institute
HCCI	Homogeneous Charge Compression Ignition
HP	High Pressure
HRR	Heat Release Rate
IVC	Intake Valve Closing
IVO	Intake Valve Opening
$IMEP_g$	Gross Indicated Mean Effective Pressure
$IMEP_n$	Net Indicated Mean Effective Pressure
ISFC	Indicated Specific Fuel Consumption
JANAF	Joint Army-Navy-NASA-Air Force
KH	Kelvin-Helmholtz
LFE	Laminar Flow Element
LP	Low Pressure
LR	Long Route
LNT	Lean NOx Trap
LTC	Low Temperature Combustion
MK	Modulated Kinetics
NIST	National Institute of Standards and Technology
NOx	Oxides of Nitrogen
PCCI	Premixed Charge Compression Ignition
PFI	Port Fuel Injection
PPC	Partially Premixed Combustion
PPM	Parts Per Million
PRF	Primary Reference Fuel
RCCI	Reactivity Controlled Compression Ignition
RGF	Residual Gas Fraction
RMEP	Rubbing Mean Effective Pressure
RNG	Re-Normalization Group
RT	Rayleigh-Taylor

SACI	Spark Assisted Compression Ignition
SCR	Selective Catalytic Reduction
SCVC	Scavenging Valve Closing
SCVO	Scavenging Valve Opening
SI	Spark Ignition
SOC	Start of Combustion
SOI	Start of Injection
SR	Short Route
UHC	Unburnt Hydrocarbons
VEMB	Valve Event Modulated Boost
VGT	Variable Geometry Turbocharger
VNT	Variable Nozzle Turbocharger
VVA	Variable Valve Actuation
VVT	Variable Valve Train

VARIABLES

$\boldsymbol{\rho}$	Density
V	Volume
$\boldsymbol{V_d}$	Displacement Volume
u	Flow Velocity
e	Internal Energy
$\boldsymbol{\bar{u}_p}$	Mean Piston Speed
h	Enthalpy
m	Mass
$\boldsymbol{\dot{m}}$	Mass Flow Rate
q	Heat
$\boldsymbol{\dot{q}}$	Heat Transfer Rate
p	Pressure
A	Area
T	Temperature
R	Specific Gas Constant
$\boldsymbol{\gamma}$	Specific Heat Ratio
d	Diameter

C_D	Discharge Coefficient
θ	Crank Angle
a_w	Wiebe Efficiency Factor
m_w	Wiebe Shape Factor
$\bar{h}_w$	Average Convective Heat Transfer Coefficient
$\bar{w}$	Average In-cylinder Gas Velocity
K_1, K_2	Woschni Gas Velocity Correlation Coefficients
a	Crank Radius
b	Bore
s	Stroke
L	Length
$x(\theta)$	Piston Pin Position
A_c	Cross-sectional Area
C_f	Friction Coefficient
h_g	Gas Heat Transfer Coefficient (in GT-Power)
A_s	Surface Area
$\bar{T}$	Mean Temperature
Re_D	Reynolds Number for Internal Pipe Flow
C_k	Pressure Loss Coefficient
C_p	Specific Heat Capacity
Pr	Prandtl Number
$\dot{m}_r$	Mass Flow Parameter
N_r	Speed Parameter
N	Speed
I_{tc}	Turbocharger Moment of Inertia
ω_{TC}	Turbocharger Angular Velocity
τ_t	Turbine Torque
τ_c	Compressor Torque
τ_{fr}	Friction Torque
$\eta_{s,t}$	Turbine Isentropic Efficiency
$\eta_{s,c}$	Compressor Isentropic Efficiency
$\vec{U}$	Droplet Velocity Vector
$\vec{U}_{inj}$	Injection Velocity Vector
$\vec{V}_g$	Gas Velocity Vector
r	Radius (or radial position)
x	Position downstream of spray axis (GASJET Model)

τ_{KH}	Kelvin-Helmholtz Primary Spray Break-up Time
r_c	Child Parcel Spray Radius
L_b	Empirical Break-up Length
d_0	Parent Parcel Diameter
Ω_{KH}	Kelvin-Helmholtz Wave Frequency
Λ_{KH}	Kelvin-Helmholtz Wavelength
K_{RT}	Rayleigh-Taylor Wave Number
Y_i	Mass Fraction of Species i
q_j	Reaction Progress Variable
v', v''	Forward (‘) and Reverse (‘’) Stoichiometric Coefficient
$k_{f,j}, k_{r,j}$	Forward (f) and Reverse (r) Rate Coefficients for Reaction j
$E_{a,j}$	Activation Energy for Reaction j
A_j	Pre-exponential Factor for Reaction j
b_j	Temperature Exponent for Reaction j
M_r	Atomic/Molecular Mass
M	Mach Number
u^*	Friction Velocity
Ψ_{PRF}	Primary Reference Fuel Octane Number
ω_{EGR}	EGR Fraction
ϕ	Fuel-to-Air Equivalence Ratio
ϕ'	Fuel-to-Charge Equivalence Ratio

SUBSCRIPTS AND SUPERSCRIPTS

cv	Control Volume
in	Inlet
ex	Exit
int	Intake
exh	Exhaust
HR	Heat Release
L	Heat Loss Subscript
0	Stagnation Quantities (Pressure, Temperature, Enthalpy, etc.)
f	Fuel
LHV	Lower Heating Value
i	Component i of n components
ivc	Quantity at Intake Valve Closure (Pressure, Temperature, etc.)
crd	Connecting Rod
turb	Turbine
atm	Atmospheric Quantity
tc	Turbocharger
comp	Compressor
ref	Reference Quantity
corr	Corrected Quantity
cyc	Open Cycle
cc	Closed Cycle
max	Maximum
g	Gas
l	Liquid
noz	Nozzle
w	Value of Quantity/Parameter at Cylinder Wall (or any boundary wall)
soot	Soot Quantities (mass, diameter, etc.)

TABLE OF CONTENTS

CHAPTER 1: INTRODUCTION

With increased consumer demand for fuel economy and more stringent governmental regulations and standards for improved fuel efficiency, automotive manufacturers are turning towards compression ignition engines. Compression ignition engines, in which the fuel-air mixture is compressed to a high temperature and pressure in order to achieve auto-ignition, are an attractive solution due to their ability to achieve high thermal efficiencies without knock. The high efficiencies achieved can be attributed to the following factors: i) high in-cylinder pressures reached due to high compression ratios [1], enabling greater expansion work, ii) combustion of a lean fuel-charge mixture, which has higher specific heat ratios [2], iii) no pumping losses due to the lack of a throttle [2], and iv) the ability to use forced induction through turbocharging or supercharging to increase working fluid quantity for higher power output (without having to worry about knock) [3].

However, traditional compression ignition engines that use direct-injected high reactivity fuels produce high levels of NOx (Oxides of Nitrogen) and particulates (mainly soot) [4]. High NOx emissions occur due to high combustion temperatures [5] reached in the cylinder, while soot forms due to the combination of both the high combustion temperatures (~1,800 K) and the presence of locally rich regions in the fuel-charge mixture [6].

Although the mixture in a direct injected compression ignition engine is globally lean, the fuel is not premixed, as in a port-fuel injected spark-ignition engine. Rather, as the name implies, the fuel is directly injected into the cylinder, leaving insufficient time for the fuel spray to break up into droplets, evaporate and then mix completely with the intake charge. This results in locally fuel-rich regions where pyrolysis of hydrocarbons in the fuel takes place due to the high temperatures, forming precursors for soot formation [7].

Numerous technologies have been developed to reduce these harmful emissions from the engine exhaust. Exhaust Gas Recirculation (EGR) [8], in which a fraction of the exhaust gas is recycled back into the cylinder for charge dilution, has been shown to lower combustion temperatures, thereby reducing NOx

emissions. EGR systems also utilize heat exchangers called EGR Coolers [9] to further reduce the exhaust gas temperature before recirculation to further lower combustion temperatures. Advances have also been made in engine aftertreatment systems, such as the Lean NOx Trap (LNT) [10–12] and Selective Catalytic Reduction (SCR) [13] to mitigate NOx emissions, and Diesel Particulate Filters (DPFs) [14] to trap particulate matter in the exhaust.

While these aftertreatment technologies are sufficient to meet current emissions regulations, they are usually expensive and add to the cost of the vehicle. There are also other drawbacks involved with aftertreatment systems such as increased fuel consumption, making it more difficult to meet fuel economy standards. Use of a DPF increases exhaust backpressure on the engine, thereby reducing thermal efficiency [15,16]. The DPF also needs to be cleaned to remove accumulated soot after a certain period of time in a process known as regeneration [17], which involves oxidizing soot on the filter walls by increasing the temperature of the exhaust gas flowing through the DPF through the use of post-injections, increasing fuel consumption. Moreover, integration of the aftertreatment systems with the engine system is a challenging process, making the entire vehicle system more complex. Hence, in order to meet the emissions and fuel economy targets while keeping engine and aftertreatment system development costs low, it is necessary to optimize the in-cylinder combustion process through the utilization of advanced combustion strategies. An overview of these strategies is provided in Section 1.1.

1.1 Advanced Combustion Strategies – An Overview of Low Temperature Combustion

As shown in the $\emptyset - T$ map in Figure 1-1 from Dec et al. [18], soot formation commences at equivalence ratios > 2 and relatively high combustion temperatures around 1,800 – 1,900 K, and NOx emissions are formed primarily at lean equivalence ratios and very high combustion temperatures (> 2,400 K). To avoid the NOx and soot contour islands, the ideal combustion strategy should lie somewhere in the gray-shaded region (labeled LTC) and the blue region (labeled HCCI). As mentioned earlier in the chapter, to achieve high combustion efficiencies, the equivalence ratio should also be lean to stoichiometric, as the higher specific heat ratio of lean mixtures improves thermal efficiency. In summary, to attain low NOx and particulate matter emissions while maintaining high thermal efficiency, any proposed combustion strategy

should satisfy the lean equivalence ratio and relatively low combustion temperature (< 1,800 K) requirements. Combustion strategies that meet these requirements are collectively grouped under the umbrella of Low Temperature Combustion (LTC).

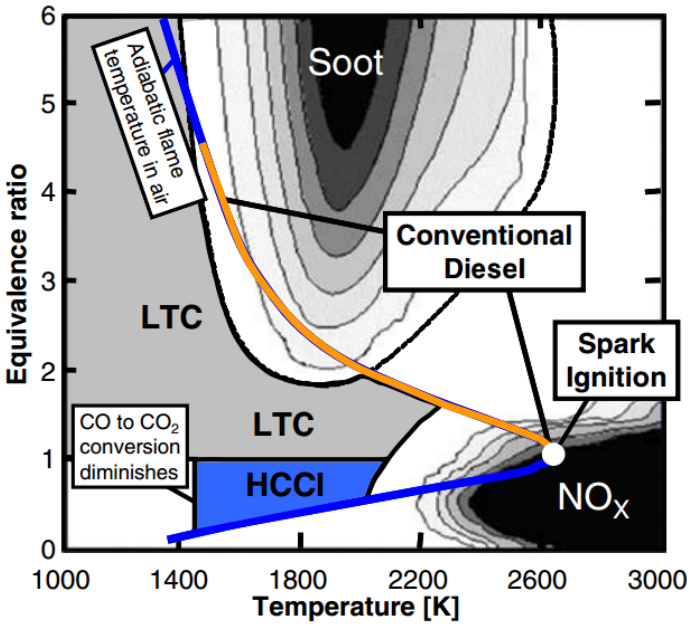

Figure 1-1: $\emptyset - T$ Map showing the regions for high soot and NOx formation, with different combustion strategies overlaid on map. Figure taken from [18].

Perhaps the most well-known LTC concept is Homogeneous Charge Compression Ignition (HCCI), in which a homogeneous mixture of fuel and air is inducted into the cylinder and compressed until auto-ignition occurs [19,20]. The heat release in HCCI combustion is controlled by chemical kinetics, and because the equivalence ratio and burned gas temperatures are low in relation to spark-ignited and conventional compression-ignition engines (< 2,000 K), NOx and soot production are significantly reduced. High thermal efficiency is achieved due to lower heat transfer losses and shorter combustion duration [21]. Despite these benefits, HCCI engines have not made their way into production because numerous operational challenges have to be addressed, the most important of which is the control of ignition timing/combustion phasing. The combustion phasing is heavily influenced by the chemical kinetics, which are in turn dependent on the in-cylinder charge temperature, pressure and degree of mixture homogeneity, which will be different from one engine cycle to the next, based on the engine speed and load, making

cycle-to-cycle HCCI control difficult in real world driving conditions. Moreover, there is also the possibility of rapid heat release rates in HCCI due to the near constant volume combustion, which can lead to high pressure rise rates and high peak pressures. This imposes a limit on the maximum load that can be achieved.

To address the controllability, high pressure rise rate and load limit issues with HCCI, several researchers have investigated the concept of Partially Premixed Combustion (PPC), which can be considered a strategy that lies somewhere between HCCI and Conventional Diesel Combustion (CDC), as well as Spark Assisted Compression Ignition (SACI) [22,23]. In SACI, a spark generates a propagating flame that burns part of the cylinder charge, raising the gas temperature and pressure and inducing compression ignition of the unburned gas. The spark timing acts as the control mechanism in this strategy, and by choosing an appropriate spark timing, combustion stability can be improved by preventing high peak pressure rise rates. As Persson et al. [24] noted, there is an orderly transition from SI to HCCI in the SACI regime that prevents the high pressure rise rates. The problem however, is that because the spark is initiated in a fuel-lean environment, the laminar flame speed of the propagating flame is very slow, and the onset of compression ignition is heavily influenced by the end-gas temperature at the flame front [25].

PPC has been referred to by a variety of different names: Premixed Charge Compression Ignition (PCCI) [26,27], Modulated Kinetics (MK) [28], and UNIBUS [29] to name a few, but the underlying concept in all these combustion strategies is the same. Basically, fuel is injected very early or late in the engine cycle to allow more time for mixing before combustion than in CDC, but because the fuel is still directly injected, the intake charge is not as homogeneous as the charge in HCCI. Injecting the fuel directly into the cylinder allows better control of combustion phasing through an appropriate selection of the Start of Injection (SOI) timing and Duration of Injection (DOI) such that auto-ignition occurs only after all the fuel has been injected. However, large EGR fractions of 70% or more are required to maintain the low NOx, as well as keep the peak pressure rise rate low if a highly reactive fuel such as diesel were used [30]. Large EGR rates increase the UHC and CO emissions, due to the lower combustion efficiencies as a result of the lower combustion temperatures.

To allow more mixing time, and potentially to reduce the EGR fractions, the use of low reactivity fuels such as gasoline for PPC has also been studied by researchers. Gasoline is attractive as a fuel due to its high volatility which allows early injection without having to worry about wall wetting. Kalghatgi et al. [31] showed that for the same combustion phasing and set of operating conditions, gasoline with its much longer ignition delay than diesel was more suitable for premixed combustion, producing low NOx and soot emissions. However, gasoline has poor ignitability at low load and idle operating conditions [32,33].

Bessonette et al. [34] and Inagaki et al. [35] discovered that the ideal fuel for HCCI combustion should have auto-ignition properties between those of gasoline and diesel, and that fuel reactivity stratification gives acceptable combustion noise. Based on their work, it was found that different blends of a high reactivity fuel with a low reactivity fuel would be required for different operating conditions. Fuel blending was further investigated by Kokjohn et al. [36] and Hanson et al. [37]; the authors incorporated in-cylinder fuel blending through port-fuel injection of gasoline and direct injection of diesel. It was discovered that decreasing fuel reactivity through the addition of gasoline significantly reduced the EGR fraction required to maintain optimal combustion phasing. The authors also found that to achieve higher load operation, a higher proportion of gasoline (or the less reactive fuel) was required for appropriate combustion phasing.

The work performed by Kokjohn and Hanson led to the development of a new LTC combustion strategy termed Reactivity Controlled Compression Ignition (RCCI). In RCCI, the low reactivity fuel (such as gasoline) is premixed through port-fuel injection, while the high reactivity fuel (such as diesel) is directly injected for in-cylinder fuel blending. This leads to stratification of fuel reactivity that in turn gives rise to lower pressure rise rates than those for other LTC strategies. By simply varying the ratio of the low reactivity fuel to the high reactivity fuel, the global octane number can be varied on a cycle-to-cycle basis, and a wide range of loads can be achieved, while achieving low soot and NOx emissions. In the following section (Section 1.2), the benefits of RCCI, as well as the current challenges, are further reviewed in detail.

1.2 Benefits and Challenges of Reactivity Controlled Compression Ignition (RCCI) Combustion

Further work by Kokjohn et al. [38] showed that compared with Conventional Diesel Combustion (CDC), the gas temperatures in the combustion chamber were significantly lower for RCCI, especially near the piston bowl, resulting in lower piston bowl heat transfer losses and improved thermal efficiency. Moreover, there is also improved control over the combustion event: CDC has an earlier start of combustion and a later end of combustion (i.e., longer combustion duration) than RCCI. Because of the earlier conclusion of combustion in RCCI, less expansion work is lost as compared to CDC which has late-cycle burning. Also, as mentioned in the previous section, the fuel blending leads to lower pressure rise rates and allows extension of the load limits. From the optical experiments executed by Splitter et al. [39], it was observed that the stratification of fuel reactivity achieved by in-cylinder fuel blending provides a reactivity gradient that provides a smooth transition from regions with more reactive fuel to less reactive fuel, which gives rise to the lower pressure rise rate and load limit extension benefits. Compared to diesel PPC, significantly lower EGR fractions are required by adding a less reactive fuel such as gasoline.

Despite the benefits of RCCI over CDC, and the better controllability over HCCI, there are still numerous operational challenges that need to be addressed. One of the main challenges is the low combustion efficiency at low load operating points. This is not a problem unique to RCCI; low load combustion efficiency is a problem with other LTC strategies as well. Due to the low combustion temperatures at low load, the oxidation rates of unburnt hydrocarbons (UHC) and carbon monoxide (CO) slow down [18,40] producing high UHC and CO emissions. The combustion stability also deteriorates during low load operation [41]. Moreover, the exhaust gas temperatures at low loads are insufficient to light off the diesel oxidation catalyst (DOC) for the oxidation of UHC and CO [42].

In addition to low combustion efficiencies at low load operating points, high load operation is another obstacle that must be addressed. Currently, due to maximum pressure rise rate constraints and high EGR fractions required for combustion stability at high load, the compression ratio must be lowered. Lowering the compression ratio will result in lower peak combustion temperatures, thereby resulting in an increase in the UHC and CO emissions [43], although the peak pressure will be reduced, resulting in

improved brake thermal efficiencies. Also, a lower compression ratio can reduce the volumetric efficiency, thereby reducing the amount of fresh air that can be trapped in the cylinder.

Implementing RCCI (or any LTC strategy) in a multi-cylinder engine system is another challenge. As Curran et al. [44] discovered, thermal efficiencies of a multi-cylinder RCCI engine were lower than those values for a single-cylinder version of the same engine, probably due to issues such as incomplete evaporation of port injected gasoline before the induction of intake air into the cylinder. The flow in the intake and exhaust manifolds is also not uniform for multi-cylinder engines due to unsteady gas dynamics, and this results in cylinder-to-cylinder variations in the mass of intake charge trapped at Intake Valve Closure (IVC), which in turn influences the discrepancies in the equivalence ratios between cylinders, and in essence the combustion variability among cylinders. Bittle et al. [45] found that the EGR distribution among cylinders was a major factor for the observed discrepancies. In addition, fuel economy can be adversely affected in multi-cylinder engines due to increased pumping work, a consequence of the high backpressure requirement for efficient turbocharger operation [46, 47] in LTC engine systems. The pumping penalty may be mitigated if a supercharger were used, but since the supercharger draws power directly from the cranktrain, there may be parasitic losses [48].

In addition, similar to other LTC strategies, RCCI is extremely sensitive to intake conditions such as intake temperature, intake pressure and equivalence ratio to name a few, as well as in-cylinder wall temperatures, making combustion control a difficult task [49]. The intake conditions are in turn determined by the gas exchange process, which is influenced by the characteristics/parameters of the air handling system, such as turbocharger/supercharger performance, valve timing, EGR fraction, etc. [50]. To understand and address the problems of combustion variation among cylinders, and to ensure proper mixture preparation, an in-depth study and optimization of the multi-cylinder engine air handling system is required.

The air handling system comprises the components that participate in the gas exchange process for inducting fresh air into the cylinders, and expelling exhaust gases out from the cylinders. These components include compressors such as turbochargers and superchargers, the intake and exhaust manifolds, the EGR

circuits, and the valvetrain. Due to the sensitivity of RCCI to intake conditions, it is vital to investigate the optimal valvetrain operation strategies and determine the necessary compressor specifications and manifold configurations for obtaining the ideal in-cylinder charge composition in preparation for RCCI combustion, so as to maximize thermal efficiency and fuel economy while minimizing harmful emissions throughout the load and speed range of a light-duty engine. In addition, the design and operating strategies of the air handling system will also impact the performance of the aftertreatment system in the further mitigation of emissions. It is therefore vital to investigate how the air handling system design and operation can be optimized to establish the appropriate in-cylinder conditions at IVC for a wide range of engine speeds and loads for LTC engine systems.

This study presents the development and analysis of operating strategies and air handling system configurations that optimize fuel economy and mitigate emissions for a light-duty engine running on Reactivity Controlled Compression Ignition (RCCI) through computer simulations. Although the study is focused on RCCI, the strategies presented in this dissertation may be applied to other LTC strategies such as HCCI, SACI and PPC, as the challenges present in these combustion strategies are the same as those faced in RCCI. The next section provides an overview of the approach used in this research and present a roadmap for the remainder of this dissertation.

1.3 Modeling Approach and Dissertation Roadmap

In this study, three different modeling and simulation techniques were used: a zero-dimensional filling-and-emptying model of the engine cylinder and the intake and exhaust manifolds, a one-dimensional gas dynamics model of the entire engine system including the compressors for forced induction and the EGR circuits, and a three-dimensional detailed computational fluid dynamics (CFD) model of the in-cylinder flow coupled with a chemical reaction mechanism comprising the individual chemical reactions of the combustion process.

Each technique has its advantages and shortcomings; therefore the techniques had to “work” in tandem with each other to obtain a complete picture of the system performance. The filling-and-emptying model developed using the Engineering Equation Solver (EES) for example does not accurately capture the

wave effects in the manifolds and cannot accurately evaluate boosting systems, but it has a very fast run time due to its low complexity and thus it was used for an initial evaluation of proposed design changes such as increased exhaust valve area and optimized valve timings to provide guidance for the air handling system design in the one-dimensional (1D) gas dynamics code GT-Power. GT-Power is able to evaluate the manifold flow characteristics, EGR flow characteristics, and the performance of the compressors and heat exchangers in the boosting systems accurately by capturing the wave-action effects and thus predict to a reasonable accuracy the in-cylinder initial conditions at Intake Valve Closure (IVC), but it does a poor job of simulating the combustion chemistry and the in-cylinder flows. GT-Power was therefore used to calculate the initial in-cylinder conditions for the multi-dimensional in-cylinder model in KIVA-3V as well as evaluate the impact of compressor configurations and EGR behavior on overall engine system performance. KIVA-3V predicts the heat release and emissions accurately by solving the coupled three-dimensional flow and chemistry differential equations, and was thus used to understand the impact of the system modifications made in GT-Power and EES on the emissions.

The rest of this dissertation is organized as follows: Chapter 2 reviews the literature on the current state-of-the-art in VVA and forced induction systems and their application to LTC strategies, and formulates the research objectives as well as presents the major contributions of this research work. Chapter 3 covers in detail the engine system specifications and the characteristics of each simulation technique used for the research, while Chapter 4 covers the validation of each of the modeling techniques described in Chapter 3 with experimental data. Chapter 5 presents the results of the low load optimization simulations of Early Exhaust Valve Opening (EEVO) and cylinder deactivation, followed by Chapter 6 which describes the modifications made to the stock engine configuration to attain high load operation. Chapter 7 then presents the results of the Divided Exhaust Period (DEP) simulation study to optimize the medium and high load operation. Finally, Chapter 8 summarizes the major conclusions of this research, and presents some proposed ideas for future work to improve upon the results of the current study.

CHAPTER 2: LITERATURE REVIEW

This chapter provides an overview of the current state-of-the-art on air handling systems, and evaluates the use of such systems in LTC strategies to improve thermal efficiency. The literature review itself is divided into the following sections. Section 2.1 describes in detail the theory and concepts behind Variable Valve Actuation (VVA), while Section 2.2 covers the topic of forced induction through the use of turbochargers and superchargers, and the application of such technologies to LTC concepts. Section 2.3 identifies the gaps in research from the current literature and formulates the research objectives, followed by Section 2.4 which reviews the literature on the proposed solutions to meet the research objectives. Section 2.5 concludes the chapter, detailing the contributions of this dissertation to the field of air handling system optimization for LTC engines.

2.1: Variable Valve Actuation (VVA)

Variable Valve Actuation (VVA) involves changing the times at which the intake and exhaust valves open and close during an engine cycle, and may involve control of the valve lifts as well. The objective of VVA is to optimize the gas exchange process to obtain improved combustion efficiency and reduced emissions over a wider range of operating points, which would not be possible with a fixed valvetrain system that is optimized for a specific point in the engine's operating range [51]. VVA systems are classified according to their actuation mechanisms, which may involve the use of traditional cam actuation, or non-conventional camless systems utilizing electromagnetic or hydraulic actuators. The mechanism used will affect the flexibility offered in the degree of valvetrain control. Figure 2-1 depicts the different variable valvetrain mechanisms available today.

The research performed for this dissertation (pertaining to VVA) was primarily an exploratory study on the effects of valve lift profiles generated by VVA mechanisms on RCCI combustion and engine performance through system simulations. Thus, a detailed study of the specific VVA mechanisms and their features was not performed. Therefore, this section only briefly reviews some of the VVA mechanisms listed in Figure 2-1 and provides some examples of such mechanisms used in production engines.

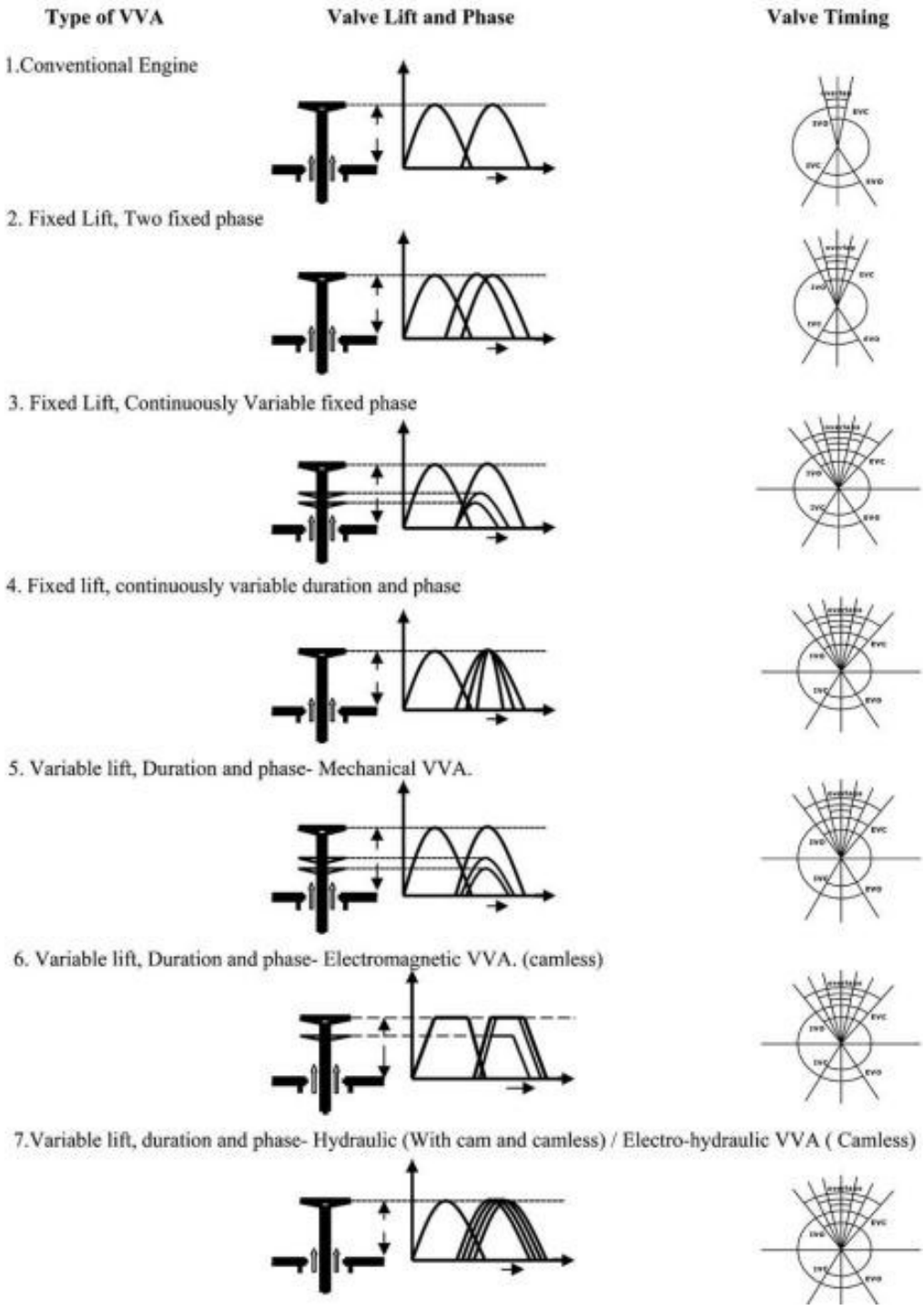

Figure 2-1: Different Variable Valve Actuation (VVA) Mechanisms. Figure taken from [52].

The most commonly used VVA mechanism in production engines today is the cam phaser. A cam phaser shifts the camshaft relative to the crankshaft, essentially translating the entire valve event by a certain angle value, thereby simultaneously changing both the closing and opening crank angles for the cycle [53].

The cam phaser can be used to simultaneously open and close the valves early or late, but usually there are physical limitations in achieving early valve events due to the risk of the valves hitting the piston during travel. Compared with a more flexible variable valvetrain system however, the controls for a cam phaser are much less complex, and installing a cam phaser on the camshaft is also a much simpler procedure due to the fewer components required.

VVA systems that offer a greater degree of freedom than the cam phaser can allow one to change the magnitude of the valve lift and/or the valve open duration. These systems may still utilize a cam, as in the case of Porsche's VarioCam Plus [54] and BMW's VANOS technologies [55], or could be camless, in which case, the camshaft is no longer used to open and close the valves. Instead, electromagnetic, hydraulic or pneumatic actuators are used to open and close the valves [56]. The drawback to more flexible systems is that they are more complex, and hence more expensive than cam phasers. Also, because of the more complicated control strategies involved in adjusting the valve lift and valve duration magnitudes, these systems are more prone to failure than the much less complex cam phasers. However, by controlling the duration and the lift magnitude, these systems allow a greater control over the gas exchange process, since the lift magnitude and duration can influence the intake and exhaust flow characteristics and hence the trapped mass.

2.1.1 Use of Variable Valve Actuation for Low Temperature Combustion Control

As mentioned earlier, low load operation of RCCI is challenging because of combustion instability and the high UHC and CO emissions due to poor combustion efficiencies. One way to achieve stable low load operation is by recycling hot exhaust gas through the use of EGR. While EGR has traditionally been used to dilute the intake charge and to lower combustion temperatures for NOx reduction for mid-load and high load operation, it can also be used to heat the intake charge and even recycle unburnt fuel from earlier combustion cycles for low load operation. EGR can be implemented through the use of an external EGR loop as demonstrated by Martinez-Frias et al. [57], or the use of internal EGR through VVA.

A widely used VVA technique to implement internal EGR for HCCI combustion is the Negative Valve Overlap (NVO) method to trap the burned gas in the cylinder before intake valve opening, developed

by Willand et al. [58], and shown in Figure 2-2. The NVO method involves early exhaust valve closing and late intake valve opening so that exhaust gas is retained in the combustion chamber during the compression stroke. By compressing and re-expanding the exhaust gas, the in-cylinder charge temperature can be maintained at a high enough value until it is mixed with the fresh intake air entering the cylinder. The higher intake charge temperatures in turn ensure improved combustion stability and higher combustion efficiency.

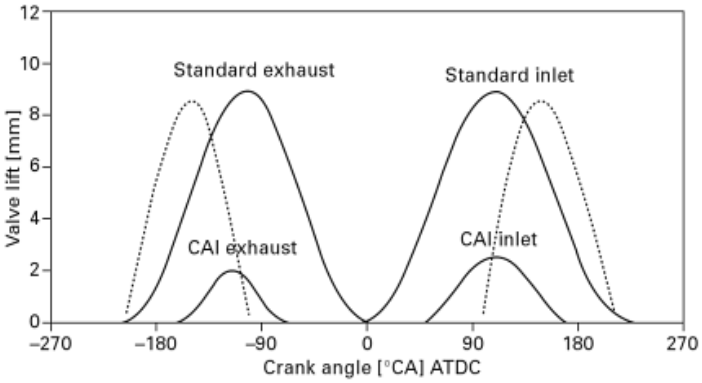

Figure 2-2: Negative Valve Overlap (NVO) Valve Timing Strategy. The exhaust valves are closed early and the intake valves open late to trap the residual gas in the cylinder for internal Exhaust Gas Recirculation (EGR). Figure obtained from [59].

However, as Borgqvist et al. [33] discovered in their research on gasoline PPC, NVO may result in lower net indicated efficiencies due to heat loss during the recompression of the exhaust gases. They proposed using the exhaust re-breathing technique, devised by Fuerhapter et al. [60] to reduce the heat losses while maintaining combustion stability. This technique, shown in Figure 2-3, involves the opening of the exhaust valves during the intake stroke to allow exhaust gases in the exhaust manifold back into the cylinder. While heat loss is minimized using this technique, rebreathing gives rise to lower residual gas temperatures and combustion efficiencies at low load than NVO does [61].

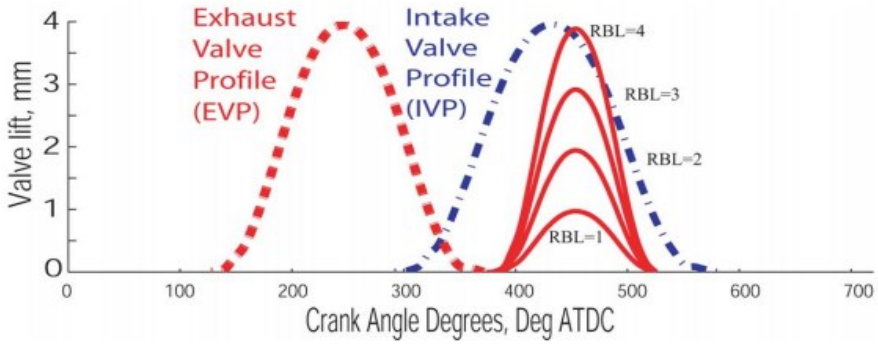

Figure 2-3: Exhaust Rebreathing. The exhaust valves are opened again during the intake stroke to allow exhaust gases back into the cylinder from the exhaust manifold. By adjusting the lift magnitude, the fraction of exhaust gas trapped can be varied. Figure obtained from [62].

A variation of the rebreathing technique, called Blowdown Supercharging (BDSC) was proposed by Hatamura et al. [63] and Kuboyama et al. [41, 64], in which the exhaust system is split among groups of cylinders, to allow the exhaust blowdown pressure wave from one cylinder to direct exhaust gas into the cylinder it is linked to through the shared exhaust system.

2.1.2 Variable Valve Actuation for LTC Aftertreatment System Optimization

The aforementioned studies in the previous sub-section have focused on optimizing the combustion process through VVA to reduce UHC and CO emissions, but limited information is available on further removal of said emissions in the aftertreatment systems. Designing an aftertreatment system for LTC strategies is a major challenge in itself; Three-way Catalysts (TWCs), which are used to reduce the NOx, UHC and CO emissions in spark-ignited engines, cannot be used as they require a stoichiometric fuel-charge equivalence ratio, while the charge for LTC strategies is highly lean [65]. Thus, a Diesel Oxidation Catalyst (DOC) used for lean-burn CDC is the feasible catalyst of choice, but activating it is an obstacle owing to the low exhaust gas temperatures from LTC concepts [66].

Numerous approaches have been investigated by researchers to improve DOC performance. Laing [67] and Socha et al. [68] proposed using an electrical heater to heat the catalyst, but this requires large electrical currents (150 – 250 A) for rapid catalyst warm-up [69], in turn placing a high power demand on the vehicle electrical power supply components (i.e., the alternator and the batteries) and leading to

deterioration in fuel economy [70]. Prikhodko et al. [71] experimented with the Pt/Pd ratio in the DOC to investigate the effect of precious metal loading, but found that due to the low exhaust gas temperatures of RCCI combustion, the metal loading did not improve DOC performance. Katare et al. [72] found that varying the exhaust gas composition to include hydrogen can lower the light-off temperature by up to 20℃, but at least one cylinder needs to run rich to generate hydrogen, and since H_2 concentration in the exhaust of lean combustion is very low; this increases particulate matter (PM) emissions in the exhaust.

It can therefore be seen that an ideal strategy for improving DOC efficiency is to increase the exhaust gas temperature. In addition to improved DOC performance, a higher exhaust gas temperature also means that high EGR fractions greater than 50% (which are the norm for low load operation) can be avoided, since lower EGR fractions can be used to provide the same heating effect for elevated combustion temperatures, thereby improving volumetric efficiency. Proposed strategies to increase the exhaust gas temperatures will be covered in Section 2.4.1.

2.2 Forced Induction

Forced induction involves the use of a compressor to increase the quantity of the working gas trapped in the cylinder and this in turn leads to higher power output. The compressor could be a supercharger driven by the engine's crankshaft, or a turbocharger driven by a turbine powered by the exhaust gas.

2.2.1 Turbocharging

Turbochargers for automotive applications comprise an axial or radial turbine mechanically linked by a shaft to a centrifugal compressor. Hot exhaust gas flowing through the turbine is accelerated to a high velocity as it expands through the turbine nozzle and is directed towards the turbine wheel, which in turn drives the centrifugal compressor. The velocity of the intake air is first increased by the compressor wheel before it passes through a diffuser, where a portion of its kinetic energy is converted to pressure energy. Since a turbocharger recycles waste heat from the exhaust that would otherwise be lost, the thermal efficiency is increased. Moreover, since the turbocharger increases power output, the engine can be

downsized by reducing the number of cylinders [73]. This improves fuel economy due to lower friction and heat losses from a smaller engine geometry, while maintaining the power output of the larger engine [74]. Figure 2-4 shows a typical automotive turbocharger comprising a radial turbine and a centrifugal compressor connected by a common shaft.

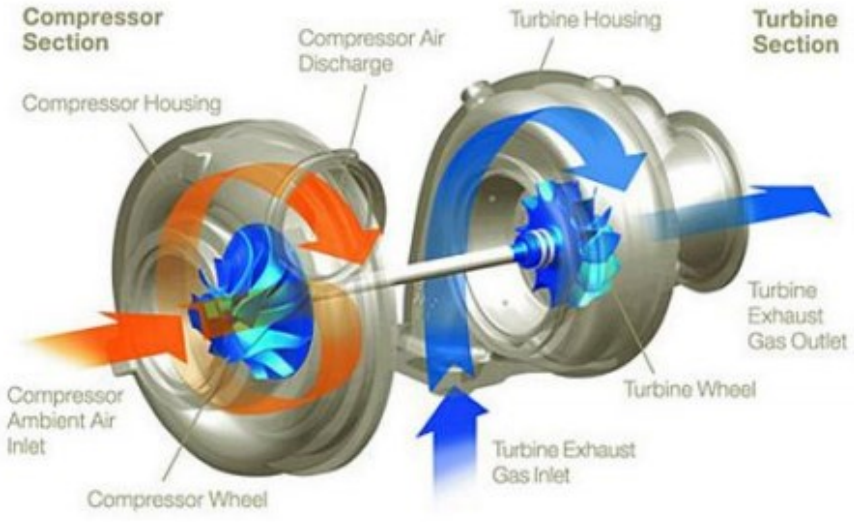

Figure 2-4: Diagram showing the components of a typical automotive turbocharger, which comprises a radial turbine lined by a shaft to a centrifugal compressor. (Source: [75])

A major challenge with traditional turbochargers (also known as fixed geometry turbochargers or FGTs) is that they are designed for optimal performance at a specific engine speed and load rather than over a wide range of speeds and load points [76]. This happens due to the differences in the flow characteristics between the two different machines: the piston engine is a positive displacement device, meaning the flow rate through the engine is directly proportional to its operating speed, while the turbocharger is a rotordynamic machine whose expansion ratio is approximately proportional to the square of the flow rate [77]. Moreover, since there is no mechanism or strategy to control the boost pressure in an FGT, the FGT may over-speed at other operating conditions, giving rise to exceedingly high boost pressures and in turn, high in-cylinder combustion pressures that may cause mechanical damage to the turbocharger and the engine [78]. To avoid this problem, a wastegate is incorporated into the turbine to regulate the turbine inlet pressure and hence the boost pressure.

A wastegate is essentially a pressure relief valve that diverts/bypasses a portion of the exhaust gas away from the turbine inlet. When the engine speed increases and the maximum allowable boost pressure is reached, the wastegate opens to allow a portion of the exhaust gas to bypass the turbine, thereby limiting the amount of exhaust energy that can be extracted and hence preventing overboosting. Wastegates can be internal (integrated into the turbine housing), such as the flap valve, or external (integrated into the exhaust manifold outside the turbine volute), like the poppet valve. Figure 2-5 shows the aforementioned valve types used as wastegates.

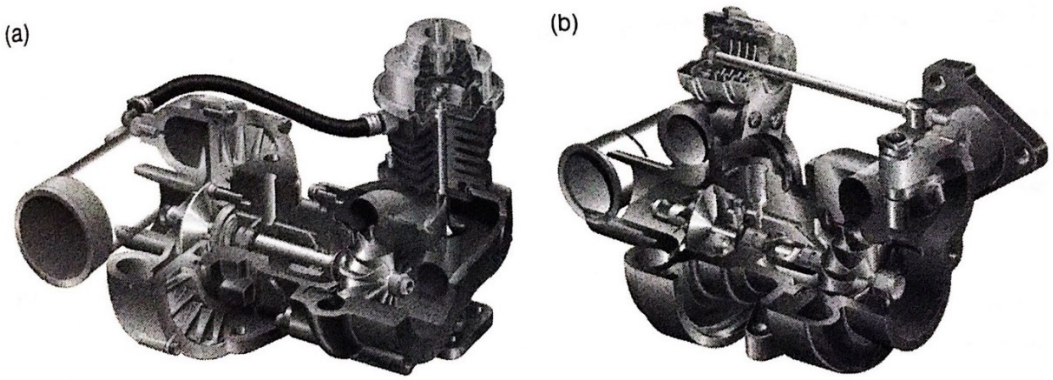

Figure 2-5: Two different types of wastegates: (2-5a, Left): A poppet valve wastegate. (2-5b, Right): A flap valve wastegate. (Source: [77])

The wastegate is opened and closed through the use of an actuation system that is pneumatic or electronic; of these two types, the pneumatic system is more widely used. Pneumatic actuators comprise a canister with a preloaded spring connected to the valve by an actuator rod [79, 80]. The compressor outlet pressure is monitored by a sensor, and when this pressure exceeds a threshold value, it exerts a force on the spring which causes the actuator rod to open the valve at the turbine inlet, directing the exhaust gas through a bypass to the turbine outlet. For a finer control of the valve opening to allow a wider range of operation, a pulse-width modulated signal may be sent from the ECU to the pneumatic line between the canister and the compressor outlet [81].

Although the wastegate allows some control over the exhaust flow through the turbine and thus the boost pressure, the fixed geometry turbine is not always able to extract sufficient work from the exhaust

gas to power the compressor, especially at low engine speeds and during transients [74]. Moreover, there may be throttling losses in the wastegate that will lower the turbine inlet pressure, which in turn will affect the turbine isentropic efficiency and hence the work supplied by the turbine to the compressor. To overcome the aforementioned problems of control and reduced pressure ratios across the turbine, a variable geometry turbocharger may be used.

A Variable Geometry Turbocharger (VGT) (also sometimes referred to as a Variable Nozzle Turbocharger (VNT)) incorporates a moving vane mechanism in the radial flow passage between the turbine wheel and the turbine housing. By changing the position of the vanes (referred to as vane position or rack position), the effective turbine nozzle area and thus the aspect ratio (A/R ratio) of the turbine housing can be altered, thereby adjusting the flow capacity of the turbine to match the engine requirements at a particular operating condition [82]. Changing the flow capacity in turn allows the backpressure to be adjusted so that a positive pressure difference can be generated between the exhaust manifold and the intake manifold to help drive EGR, especially high pressure EGR. The rack position may also be adjusted to raise exhaust temperatures for aftertreatment thermal management [83]. Figure 2-6 shows a schematic of a VGT from Mitsubishi Heavy Industries, with a cut-away showing the vanes in the turbine housing.

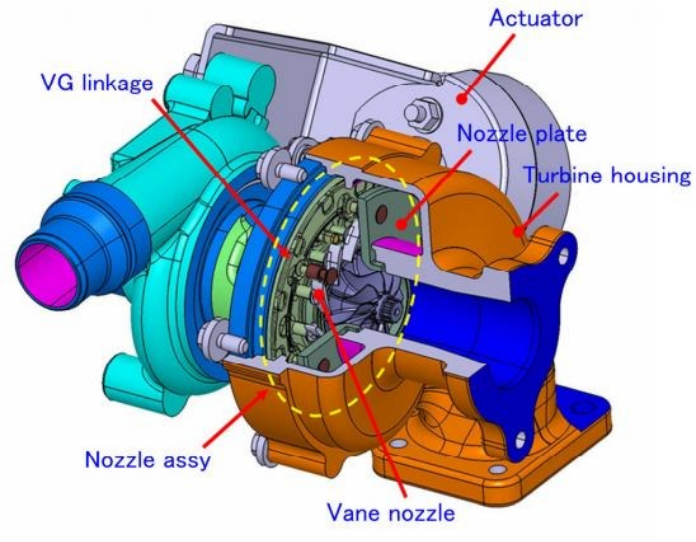

Figure 2-6: Schematic of a VGT from Mitsubishi Heavy Industries, with a cut-away view showing the vanes for adjusting the nozzle area and aspect ratio. (Source: [84])

2.2.2 Supercharging

Compressors used for superchargers are generally of the positive displacement type, meaning they force air into a given space and decrease the volume of this given space to raise the pressure [85]. Roots blowers and Lysholm compressors are two of the most commonly used positive displacement compressors for automotive superchargers today. These compressors are mechanically linked to the crankshaft through a system of gears and pulleys. Because they directly draw power from the engine through the crankshaft connection, and their rotational speed is directly proportional to the engine speed, superchargers do not experience the turbo lag phenomenon [86]. But compared with turbocharged engines, supercharged engines will experience a poorer fuel economy as the supercharger is a parasitic load that directly draws power from the engine, especially at higher engine speeds where a significant amount of friction will be generated, deteriorating the efficiency. Figure 2-7 shows two different types of positive displacement compressors: the Roots Blower and the twin-screw Lysholm compressor.

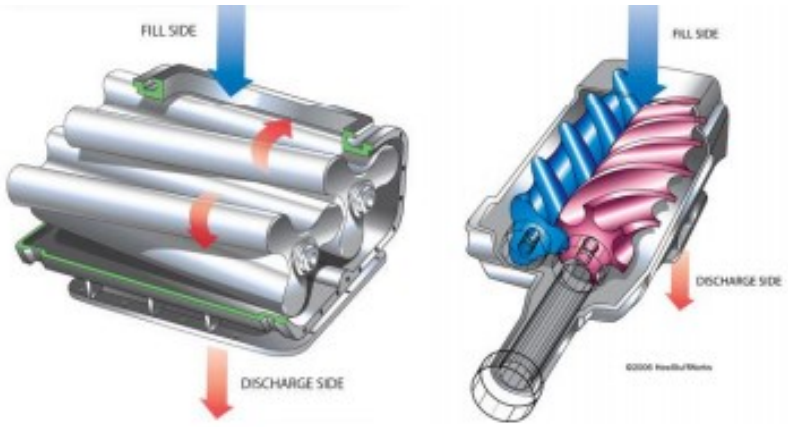

Figure 2-7: Two different types of positive displacement compressors used as superchargers for automotive applications. (2-7a, Left): The Roots Blower. (2-7b, Right): The Twin-screw Lysholm Compressor (Source: [75])

2.2.2.1 Pressure Wave Supercharging

A different type of compressor used as a supercharger is the pressure-wave compressor (also referred to as a wave rotor). As its name suggests, it uses the pressure waves from the high energy exhaust pulses to compress the intake air. Figure 2-8 shows a schematic of a pressure-wave supercharger. The

compressor consists of a cylindrical rotor flanked by two stationary end plates and linked to the cranktrain by means of a pulley belt drive. Within the rotor is an array of channels, while the end plates have ports through which the working fluid can enter or exit the channels.

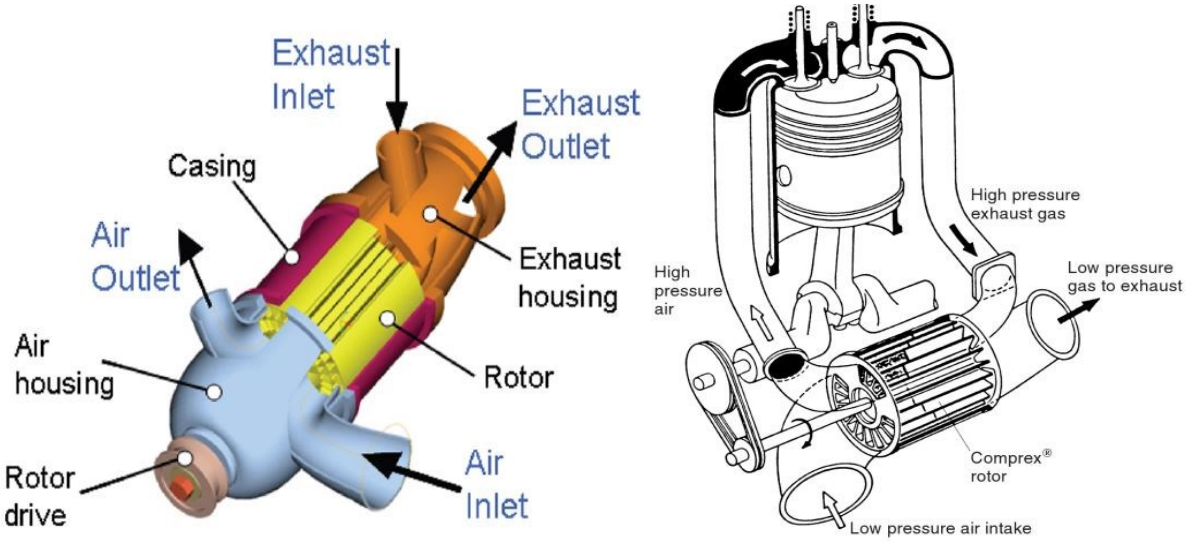

Figure 2-8: Schematic diagrams of a pressure wave supercharger. (2-8a, Left): CAD model showing the components of the pressure wave supercharger. Obtained from [87]. (2-8b, Right): Schematic showing how the pressure wave supercharger is connected to the engine; the wave rotor is linked to the cranktrain by means of a pulley belt drive. Obtained from [88].

As the rotor rotates at a speed of 4 to 5 times the engine speed [3], the channel ends are periodically exposed to different port pressures at the end plates. When the exhaust ports line up with the rotor channels during rotation, the high energy exhaust gas enters the channels, generating a compression wave that propagates at sonic velocity to the intake ports which are closed. As the compression wave gets reflected at the closed intake ports, it compresses the fresh air in the channel to a higher pressure. The pressurized intake air then leaves the channels and enters the intake ports when they open due to the rotation of the rotor.

Because the compression efficiency across a pressure wave is higher than that of a centrifugal compressor blade or the rotors of the Roots and Lysholm compressors, the pressure wave supercharger has the potential to be more efficient than a conventional turbocharger or supercharger [89]. Transient response of a pressure wave supercharger is also superior to that of a turbocharger because the flow through the wave rotor channels responds on the time scale of the pressure waves with no rotational intake inertial lag [90].

However, there are a number of disadvantages to using a pressure wave supercharger: pressure wave compressors are expensive to manufacture because they have to be tailor-made to a specific engine instead of being mass produced. The dimensions of the rotor and the channels for the optimal generation of pressure waves are highly dependent on the engine the compressor is fitted to. Moreover, because of heat transfer and mixing between the exhaust gas and the intake air in the channels, the intake air exiting the channels will be at a high temperature and intercooling is necessary [91].

2.2.3 Advanced Forced Induction Concepts – Multi-stage Charging

To further increase power output, more than one compressor may be used in a multi-stage charging setup (usually two-stage, but three-stage [92] is becoming more common to meet today's more stringent power and emissions regulations) to increase the overall pressure ratio. Besides increasing boost, appropriate selection of compressor size, type and/or configuration for each stage in a two-stage charging system can improve transient response by minimizing compressor inertia [93]. The most common multi-stage charging concept utilized today is that of two-stage turbocharging, which may further be divided into series sequential turbocharging and parallel sequential turbocharging. Another less common multi-stage concept is the twincharger, in which a supercharger is connected in series with a turbocharger.

In series sequential turbocharging, two turbochargers of different sizes are connected in series: a small high-pressure (HP) stage upstream and a larger low-pressure (LP) stage downstream [94, 95]. At low engine speeds and high loads, the system operates as a two stage system. At higher speeds, a bypass valve directs flow to only the LP stage, and the system essentially operates as a single stage system. Due to lower inertia of the smaller HP turbine and compressor, transient response is improved and turbo lag can be minimized. The smaller HP stage is also more efficient than the LP stage in converting the limited exhaust enthalpy available at low speeds to boost. However, because the two stages are in series, the flow range available is narrowed at the expense of higher boost, restricting the operating range [96].

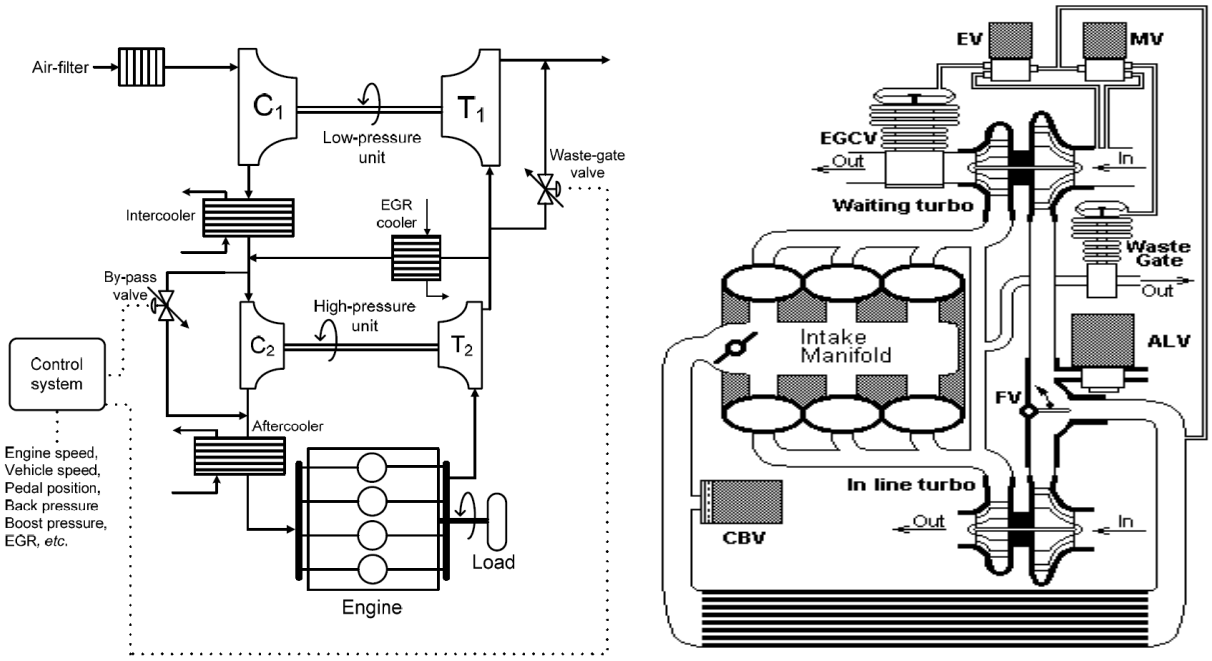

Figure 2-9. (Left, 2-9a): Series-Sequential Turbocharging Configuration. Taken from [93]. (Right, 2-9b): Parallel-Sequential Turbocharging Configuration. Taken from [97].

Parallel sequential turbocharging employs two turbochargers (of the same or different sizes) connected in parallel: intake air can enter the engine through two different compressor inlets simultaneously when both turbochargers are operating. At lower engine speeds, usually only one of the turbochargers is active, and the second turbocharger is activated as engine speed is increased to provide sufficient boost over the entire engine operating range. Compared with the series sequential configuration, the parallel sequential configuration allows a much wider flow range [93], although the pressure ratios reached will not be as high due to the lack of successive compression by two turbochargers connected in series.

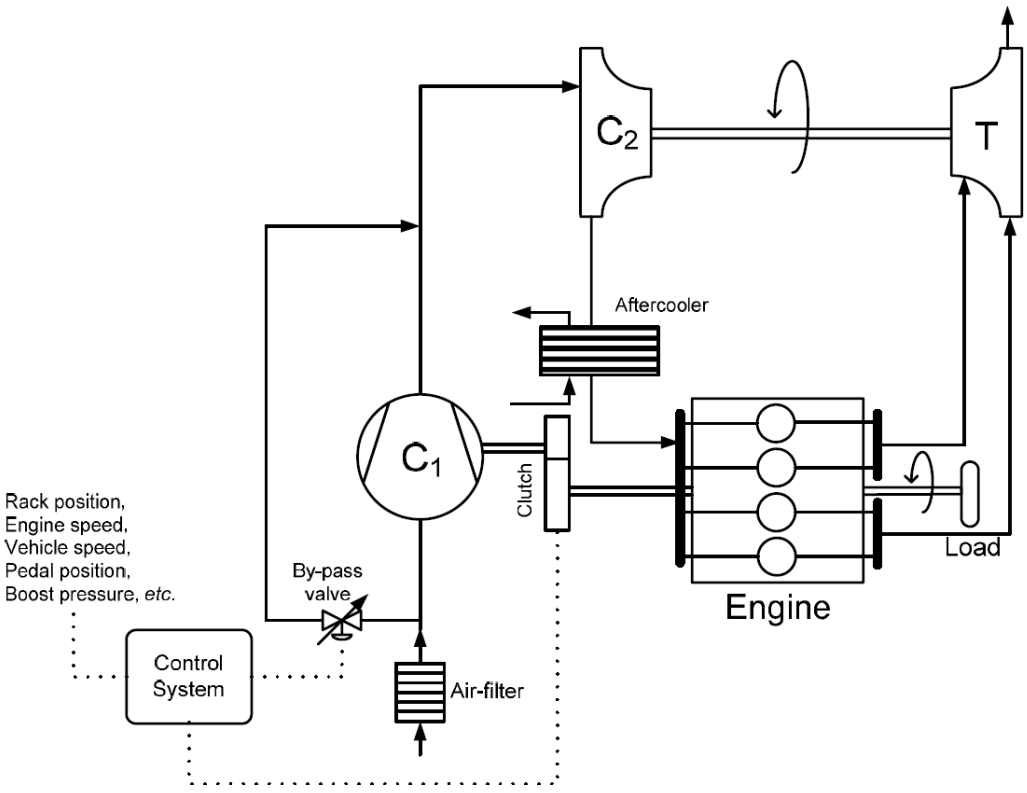

Figure 2-10. Twincharging (Turbocharger and Supercharger in series) Configuration. Taken from [93]

As an alternative to two stage turbocharging, a twincharging setup may be used, in which a supercharger is connected in series with a turbocharger [98]. Since a supercharger provides near-instant boost due to its direct dependence on engine speed, transient response is vastly improved. High pressure ratios are possible due to pressure ratios of both compressors in series being multiplied. Drawbacks of this configuration are the low efficiency of the positive displacement supercharger at high engine speeds, the increased fuel consumption due to the supercharger directly drawing power from the crankshaft, and the need for complex control systems to ensure smooth operation of two different compressor types [93].

2.2.4 Forced Induction for LTC Strategies

Forced induction technologies may be used to extend the upper load limit of LTC strategies, while still maintaining dilute conditions for low NOx formation [99]. As Christensen et al. showed, boosting allowed natural gas HCCI operation up to 14 Bar net IMEP [100]. A challenge in implementing boosting is that a higher trapped mass leads to advancement in combustion phasing, increasing pressure rise rates

and hence combustion noise, limiting the maximum load that can be achieved. To achieve even higher loads, pressure rise rates can be kept low by retarding combustion phasing, which is done by adding cooled EGR. Indeed, with cooled EGR, Christensen et al. [101] achieved 16 Bar net IMEP for natural gas HCCI, while Dec et al. [99] obtained a maximum load limit of 16 Bar IMEP for gasoline HCCI with an intake pressure of 3.25 Bar. Boosting also improves combustion efficiency, combustion stability, and reduces UHC emissions. The effect of elevated intake pressure on autoignition also reduces the need to preheat the intake air.

With regards to the boosting system used for LTC strategies, a number of studies have been conducted on compressor type and configuration to achieve the desired engine system performance. It was discovered by Olsson et al. [46] that while using a fixed geometry turbocharger for a dual fuel HCCI engine gave a BMEP of 16 Bar, the low exhaust gas enthalpy resulted in the need to use high exhaust backpressures for efficient exhaust energy conversion by the turbine, leading to high pumping losses. From the same research group, Wilhelmsson et al. [102] showed that pumping losses may be mitigated using a VGT through a well-defined operating strategy to apply just the right amount of boost, rather than "over-boosting". In addition, both Wilhelmsson [102] and Martins et al. [103] recommended that proper turbocharger matching to an engine is very crucial to achieve the desired high load with minimal pumping work throughout the operating range.

Shingne et al. [47] used GT-Power simulations to perform initial turbocharger matching for a 2-liter, 4-cylinder HCCI engine. The authors compared single VGT and two-stage series turbocharging configurations with naturally aspirated operation using currently available "off-the-shelf" turbocharger systems developed for conventional SI and CI engines. It was discovered that using either turbocharger configuration was able to significantly increase the load limit up to 8.53 Bar and 10.86 Bar BMEP for the single VGT and two-stage series turbocharger configurations respectively at an engine speed of $2{,}500\ \mathrm{rev} \cdot \mathrm{min}^{-1}$. However, as Figure 2-11 shows, the exhaust pressures for both turbocharging strategies were higher than the intake pressure for all engine speeds, with a significant jump in exhaust pressure observed from $2{,}000\ \mathrm{rev} \cdot \mathrm{min}^{-1}$ to $2{,}500\ \mathrm{rev} \cdot \mathrm{min}^{-1}$ and higher speeds. With the considerably higher exhaust pressures

at higher engine speeds, the pumping penalty showed a drastic increase (shown in Figure 11-b) as the engine speed increased due to the higher backpressures necessary to improve turbine work extraction efficiency.

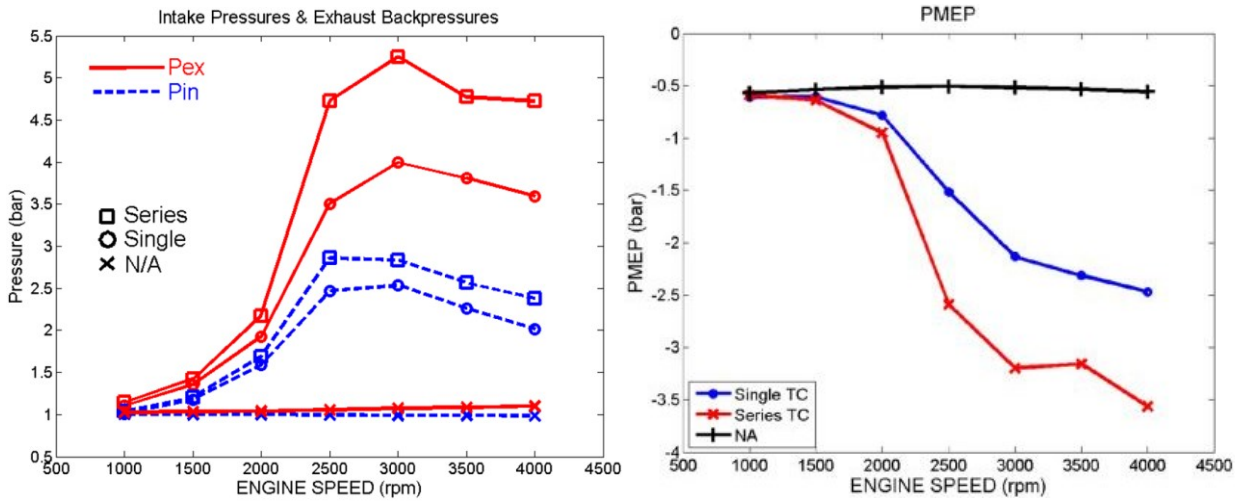

Figure 2-11. (Left, 2-11a): Intake and Exhaust Pressures as a function of engine speed for a naturally aspirated, single stage turbocharged and two-stage series turbocharged HCCI engine. (Right, 2-11b): PMEP as a function of engine speed for the aforementioned configurations. (Source: [47])

Mamalis et al. [48] compared different compressor configurations for a multi-cylinder HCCI engine through the use of GT-Power simulations to select the ideal boosting setup for HCCI operation. They found that a two-stage turbocharger configuration provided the greatest boost quantity, but resulted in the highest pumping work, while the supercharger gave the best indicated efficiency due to low pumping work but the worst brake efficiency due to parasitic losses. Further work by Mamalis [104] in a subsequent paper showed that using a VGT in conjunction with a Positive Valve Overlap (PVO) valve strategy instead of an NVO strategy significantly reduced pumping work, and that multi-stage compression was beneficial for high intake pressures required for medium and high loads.

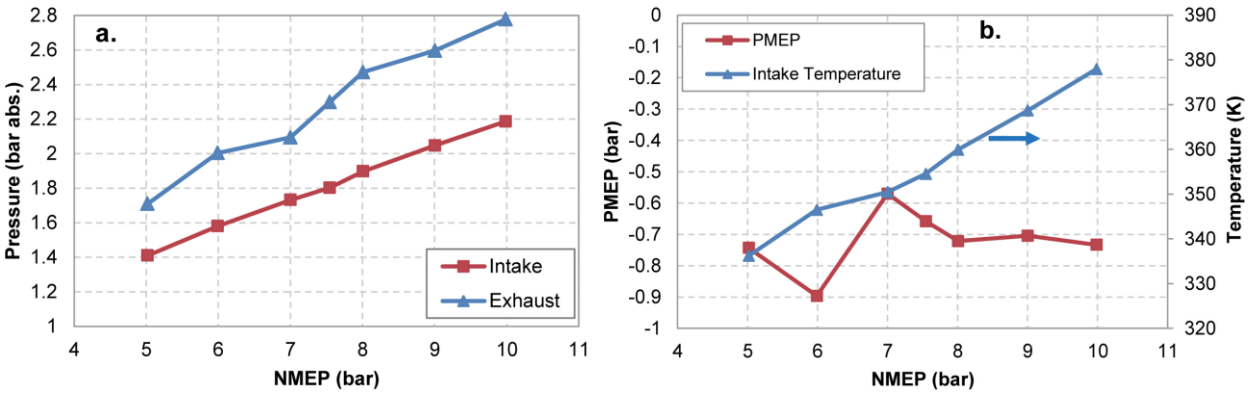

Figure 2-12. (Left, 2-12a): Intake and Exhaust Pressures as a function of the net IMEP for a VGT equipped HCCI engine. (Right, 2-12b): Intake Temperature and PMEP as a function of the net IMEP. (Source: [104])

Despite the improvement in pumping work observed from 6 Bar IMEP to 7 Bar IMEP as shown from Mamalis' follow-up paper (in Figure 2-12b), the PMEP still remained negative because of the exhaust manifold pressure being higher than the intake manifold pressure for all the operating points studied, giving an unfavorable pressure difference that deteriorates the gas exchange process.

Extending the work done by Mamalis, Shingne et al. [105] investigated two different operating strategies of the twincharger configuration and compared these operating strategies to the two-stage series turbocharging configuration for a multi-cylinder HCCI engine. They found that operating the twincharger configuration such that the same quantity of fresh charge is inducted as that of the two-stage turbocharging configuration gave better fuel economy than attaining the same intake manifold pressure as that of the two-stage turbocharging configuration. They also discovered that a twincharger configuration could provide boost at low engine speeds unlike the two-stage turbocharger configuration due to the low exhaust enthalpies and mass flow rates. Figure 2-13 shows the BSFC as a function of engine speed for the two different operating strategies.

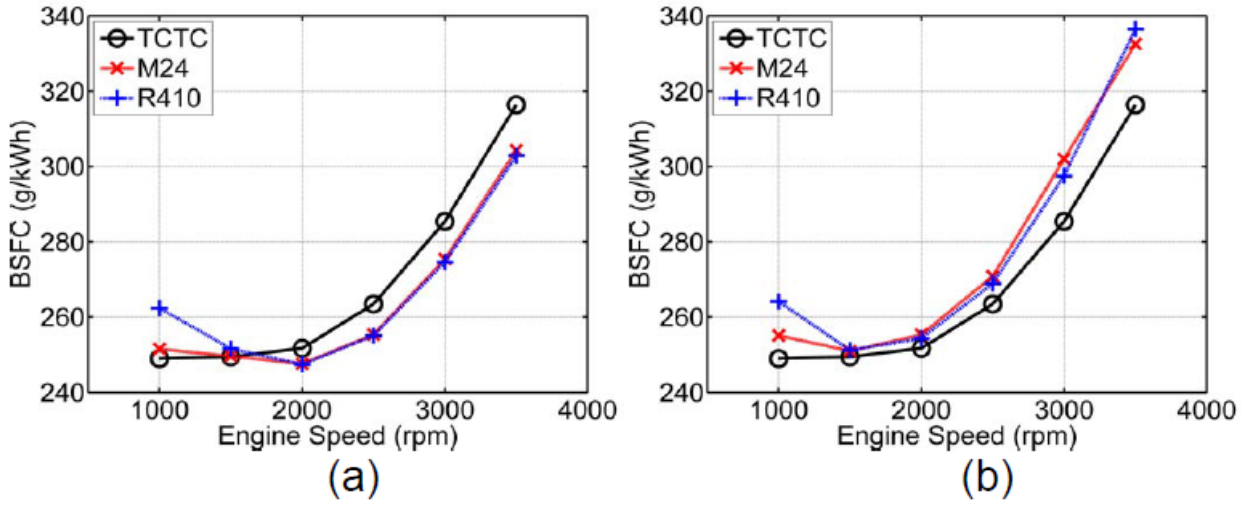

Figure 2-13: BSFC as a function of engine speed for two different twincharger operating strategies. (Left, 2-13a): Intake pressure match with two-stage turbocharger. (Right, 2-13b): Intake mass flow rate match with two-stage turbocharger. (Source: [105])

Building on the earlier papers of Mamalis' [48] and Wilhelmsson's [102], Taritas et al. [106] compared a series VGT and supercharger system with a single VGT for high load HCCI operation over a wide range of engine speeds from $1{,}000\ \text{rev} \cdot \text{min}^{-1}$ to $4{,}000\ \text{rev} \cdot \text{min}^{-1}$. They found that the combined VGT and supercharger system allowed high intake pressures, giving rise to higher loads than just the VGT alone, but at higher engine speeds, the frictional losses in the supercharger outweighed the pumping benefits and the VGT was more suited for boosting. The authors also found that the VGT vane position could function as a control knob to obtain sufficient boost while regulating the backpressure.

2.3 Gaps in Research and Formulation of Research Objectives

As discussed earlier in Section 2.1.2, major obstacles in low-load LTC operation are the high CO and UHC emissions due to the low combustion efficiencies and the poor catalyst efficiencies in oxidizing the aforementioned emissions at these operating points. The combustion efficiency may be improved through variable valve actuation strategies, such as negative valve overlap, but that does not solve the problem of low DOC efficiency as the exhaust gas temperatures are still too low to activate the catalyst. Conventional strategies to improve catalyst performance, such as heating the catalyst using an electrical heater cause fuel economy to deteriorate as they would draw a large amount of electrical power from the

automotive electrical systems. Thus, alternative strategies that increase exhaust gas temperatures for DOC light-off at low load need to be investigated.

Regarding high load LTC operation, while two-stage series turbocharging and twincharging can extend the load limit, the high pumping penalty due to high exhaust backpressures in two-stage turbocharged systems and the parasitic losses from the supercharger in twincharged systems negatively impact fuel economy. Moreover, the highest load point that was achieved for multi-cylinder engines in the studies presented in this literature review chapter was only 10.86 Bar BMEP [47], which is in the medium load range; although Olsson et al. managed to achieve 16 Bar BMEP [46], there was no discussion in that study about the combustion stability, i.e., whether the peak pressure rise rate could be maintained below the 10 bar/degree limit. Modeling and experimental studies on high load LTC up to 18 and 23 Bar IMEP [107–110] have only investigated what the in-cylinder initial conditions (pressure, temperature, charge composition, etc.) at Intake Valve Closure (IVC) and the injection strategies should be, but have not approached the issue from a system level perspective on how those IVC conditions can be achieved via calibration of the air handling system. Therefore, it is necessary to study the requirements and settings of the air handling system to identify how the load limit can be extended up to the 18 to 23 Bar IMEP range, while finding solutions to improve fuel economy by maximizing work extraction from the turbocharger turbine and minimizing the pumping penalty.

Based on the gaps in research identified in the preceding two paragraphs the following research objectives were established:

1. Investigate operating strategies that can raise the exhaust gas temperature at low load for enhanced DOC efficiency.
2. Determine the operating parameters and configuration of the air handling system to achieve high load operation of 18 Bar IMEP.
3. Examine VVA and manifold redesign strategies that can potentially mitigate the pumping penalty at medium and high load operation.

2.4 Proposed Solutions

2.4.1 Early Exhaust Valve Opening (EEVO) and Cylinder Deactivation

One VVA technique that shows great potential for increasing the exhaust gas temperature is Early Exhaust Valve Opening (EEVO). Bohac et al. [111] demonstrated that EEVO reduced catalyst light-off time in a spark-ignition engine by increasing the exhaust gas temperature. However, they also found that opening the exhaust valve early results in an increase in the UHC and CO emissions, and an increase in fuel consumption due to reduced duration of the expansion stroke. Parvate-Patil et al. [112] explained that the increased UHC and CO emissions were due to the quenching of the hydrocarbon and CO oxidation reactions when the exhaust valves are opened earlier in the cycle.

Roberts et al. [113] developed an experimentally validated model based on the first law of thermodynamics to predict the exhaust gas temperatures downstream of the turbine in a turbocharged 6-cylinder diesel engine that incorporated an EEVO strategy using a fully flexible variable valvetrain. The model showed that advancing the exhaust valve opening (EVO) timing results in a 30 to 100 K increase in the exhaust gas temperatures downstream of the turbine, but gives a deterioration between 2 and 5 % in the brake thermal efficiency.

The aforementioned EEVO studies, as well as other EEVO studies in literature, have so far, been performed only on gasoline spark ignition engines and conventional diesel engines, but not on LTC engines. In spite of the disadvantages of EEVO as listed in the preceding paragraphs, the potential of obtaining higher exhaust gas temperatures for a more rapid catalyst light-off is promising from a systems-level perspective and were explored further, especially for LTC engines where high UHC and CO emissions at low load operation are a major challenge.

EEVO can be implemented using either a fully flexible variable valvetrain or a cam phaser. As discussed in Section 2.1, both mechanisms have their advantages and disadvantages: a fully flexible variable valvetrain allows a great degree of autonomy and freedom in determining the shape, duration and magnitude of the valve lift profile, but it is complex, expensive and prone to failure due to the complicated control strategies involved in its operation. The cam phaser on the other hand is much easier to manufacture

and install on an engine and its controls are much less complex than a fully flexible variable valvetrain system, but the cam phaser only allows a translation of the valve lift profile and cannot modify the lift magnitude and duration. Thus, it is of interest to compare the engine performance between the two different VVA systems for the EEVO strategy.

To address the fuel economy penalty posed by EEVO, cylinder deactivation may be implemented [114]. By running a fewer number of cylinders at a higher load point while motoring the other cylinders with their intake and exhaust valves closed, the required fueling can be reduced, significantly improving fuel economy. Since the firing cylinders are running at a higher load point, the exhaust gas temperatures during deactivation will be higher, leading to an improved aftertreatment system performance. In fact, Lu et al. [115] demonstrated through experiments that cylinder deactivation generated exhaust gas temperatures of 793 – 843 K at highway cruising conditions for a heavy-duty truck engine, which are 170 to 220 K higher than when all cylinders are firing. In addition to the higher exhaust gas temperatures, the lower exhaust gas flow rates from the smaller number of fired cylinders may further improve the DOC efficiency.

As each of the aforementioned strategies to raise the exhaust gas temperatures has benefits and drawbacks, it is of interest to compare the impact of each strategy on engine performance, emissions and catalyst efficiency, so as to determine the best strategy for low load RCCI (and LTC) operation. Chapter 5 presents the methodology and results of the EEVO and cylinder deactivation strategies and determine the best strategy for low load operation by considering the impact of each strategy on engine fuel economy and DOC efficiency.

2.4.2 Divided Exhaust Period

One strategy that can mitigate pumping losses at medium and high load operation is the Divided Exhaust Period (DEP). The Divided Exhaust Period (DEP) is a gas-exchange system that divides the exhaust flow into two different exhaust manifolds by using separate valve timings for each of the exhaust valves. One exhaust valve is linked to the turbocharger (called the blowdown valve), and the other exhaust valve (called the scavenging valve) is connected to the manifold that bypasses the turbine and is directed to

the aftertreatment system. Using a variable valvetrain to individually control the timing, the blowdown valve is opened first, allowing the high energy blowdown pulse to be evacuated from the cylinder into the turbocharger turbine through the blowdown manifold. Once this high energy pulse has been evacuated, the blowdown valve is closed and the scavenging valve is opened, exposing the remaining exhaust gas in the cylinder to the scavenging manifold.

Since the scavenging manifold is at atmospheric pressure and the remaining exhaust gas bypasses the turbine, a positive pressure difference between the cylinder and the exhaust system can be maintained over a longer duration than in a conventional engine, thereby reducing the pumping penalty. In situations where boosting is not required (e.g., low load, cold-start), the blowdown valve can remain closed and all the exhaust gas can be emptied into the scavenging manifold, which can be used to warm up the catalyst. Figure 2-14 shows a schematic of the Divided Exhaust Period concept.

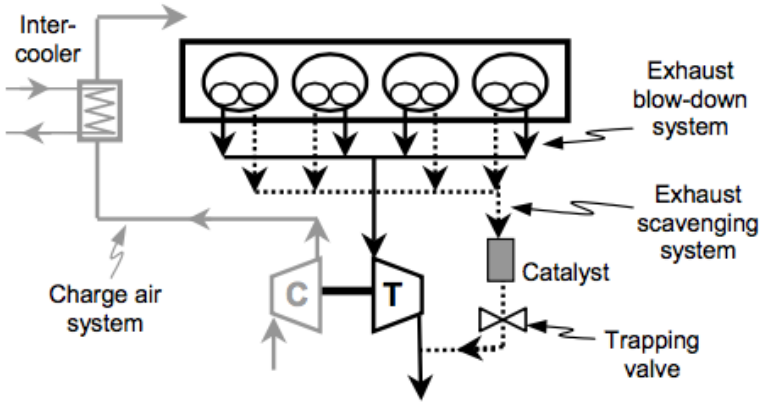

Figure 2-14: Divided Exhaust Period Concept (Source: [116])

The concept of DEP is not new; it was first introduced in a British patent from 1924 [117], and Moller et. al [116] implemented the concept in a gasoline spark-ignited engine in their 2005 paper. Moller's simulations and experiments showed that with DEP, the pumping penalty could be reduced by 1 Bar as compared to a standard turbocharged engine. The research also showed that by keeping the blowdown valve timings slightly longer than 180 degrees, pulse interactions between cylinders can be avoided, allowing a

more efficient pulse turbocharging process. Knocking resistance also improved as the residual gas content was lower compared to a standard engine due to a more efficient cylinder evacuation process.

One challenge that was encountered in Moller's study was the extended choking duration in the exhaust valves at high engine speeds that caused a deterioration in pumping work. The choking problem could be mitigated by using a larger exhaust valve area, but the geometric dimensions of the cylinder head limit the extent to which the exhaust valve area may be increased.

Extending the work done by Moller, Roth et al. [118] developed the Valve Event Modulated Boost (VEMB) system for spark-ignited engines. Unlike Moller's work which used a fully flexible VVA system, they used a concentric camshaft system to allow independent cam phasing of the blowdown and scavenging valves. Their work highlighted the following important points:

1. For a constant blowdown valve timing, a significant boost modulation can be achieved by retarding the scavenging valve timing, i.e., the overlap between the blowdown and scavenging valves. This happens due to the change in exhaust flow distribution between the blowdown and scavenging manifolds when the scavenging valve timing is changed.
2. The fuel economy of the engine could be improved over the entire speed and load range because of reduced pumping losses and reduced residual gas fraction (RGF) that allowed optimal combustion phasing at medium and high load.

In their follow-up study on the Valve Event Modulated Boost (VEMB) system [119], Roth et al. looked at the effects of adding EGR, and found that EGR helped lower the pumping penalty even further and therefore improved the Brake Specific Fuel Consumption (BSFC). They also introduced the concept of scavenge-sourced EGR (shown in Figure 2-15), where the exhaust gas in the scavenging manifold was exclusively used for supplying EGR flow. Scavenge-sourced EGR was also able to recycle a greater quantity of unburned hydrocarbons than conventional EGR, because a larger quantity of unburned hydrocarbons from the cylinder wall was expelled during the scavenging valve open period.

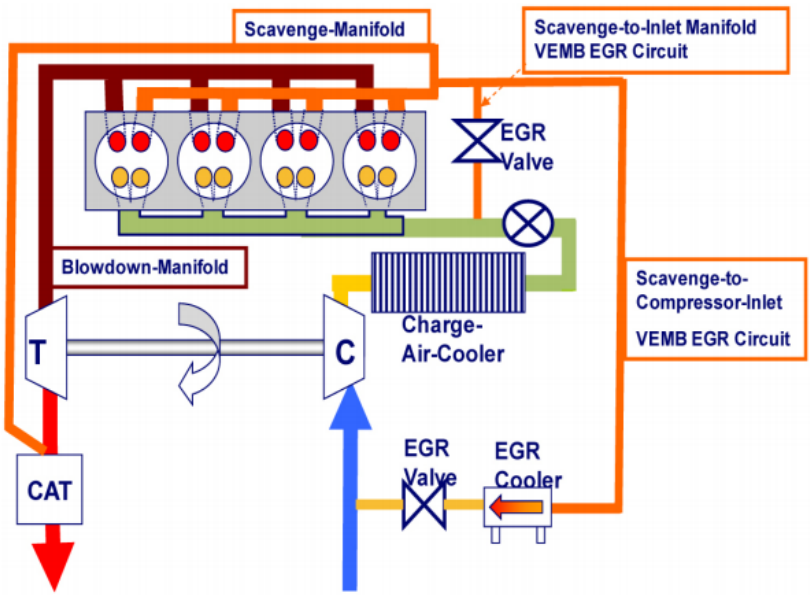

Figure 2-15: Scavenge-sourced EGR in the Valve Event Modulated Boost System. (Source: [119])

Hu et al. [120] conducted an optimization study of the scavenging valve duration and maximum lift on the Brake Specific Fuel Consumption (BSFC) at high load operation for a downsized turbocharged SI engine. They found that by increasing the scavenging valve lift at high speed, the blow-through effect increased, thereby reducing the Residual Gas Fraction (RGF), which in turn improves combustion stability by reducing the probability of knocking. They also found that the high load limit at low speed could be extended with the DEP concept by about 10% as a smaller turbine can be used as compared with the original engine.

Gundmalm et al. [121–123] investigated the DEP concept for a heavy-duty diesel engine and also studied the influence of blowdown valve-to-scavenging valve area ratio as well as external EGR on the performance of an engine equipped with DEP. They found that the ideal ratio of blowdown valve area to scavenging valve area is largely influenced by the exhaust valve timings. If the scavenging valve is opened late, a larger blowdown valve (than scavenging valve) is required to handle the larger flow rate through the blowdown valve to prevent choking at the blowdown port; if the scavenging valve is opened early, then the blowdown-to-scavenging valve area ratio should be smaller to prevent choking at the scavenging valve. The EGR circuit used also had an effect on the improvement observed; for cases with high pressure (HP)

(or Short Route (SR)), EGR there was a greater benefit to using DEP over the low pressure (LP) (or Long Route (LR)) EGR. This was due to high boost levels at medium engine speeds that caused choking at the blowdown valves, as with LP EGR, all the exhaust flows through the turbine before entering the EGR circuit.

To further improve work extraction by the turbocharger in the DEP concept, Williams et al. [124 – 126] pioneered a new two-stage turbocharger configuration called turbo-discharging. In this configuration, the scavenging valve is connected to the turbine of another turbo-compressor called the turbo-discharger. The outlet of the turbocharger turbine is connected to the compressor of the turbo-discharger, which is driven by the scavenging pulse. The compressor de-pressurizes the turbocharger turbine outlet, thereby leading to a higher turbine expansion ratio and hence greater work extraction from the turbocharger turbine. Turbo-discharging could especially be useful for increases in low-speed torque, and can also improve transient response due to the increased expansion ratio across the turbine during the initial transients.

In summary, the primary benefit of the Divided Exhaust Period (DEP) concept is the reduced pumping penalty as the exhaust gas is evacuated into two separate exhaust manifolds that are ideally at a lower pressure than the pressure in the cylinder such that a positive pressure gradient always exists between the cylinder and the exhaust manifolds for a more efficient evacuation process. This is done by separately actuating each exhaust valve at different times using a VVA system so that the high enthalpy blowdown pulse is routed to the turbine first, while the lower enthalpy remaining exhaust pulse is routed to the scavenging manifold that is at near atmospheric pressure. The DEP concept can also be used at low load operation by only opening the scavenging valve to bypass the turbocharger turbine so that the exhaust gas temperature is kept high enough for activation of the aftertreatment system. Furthermore, with a smaller exhaust flow rate through the turbocharger turbine, a smaller turbocharger can be used, which can also improve the transient response of the engine.

Thus far, the DEP concept has only been implemented on conventional SI and CI engines, but has not been explored for LTC engine concepts such as HCCI and RCCI. Given the ability of this concept to reduce the pumping penalty for turbocharged engines, this concept would potentially be able to reduce the

overall engine backpressure for LTC concepts, where the high backpressure due to the low exhaust enthalpy is a major challenge for turbochargers attached to LTC engines. Also, the overboosting problem that Wilhelmsson [102] and Martins [103] identified may be avoided by a proper selection of the blowdown and scavenging valve timings so that just the right quantity of boost is provided by regulating the exhaust flow through the turbine. Chapter 7 will present the methodology and results of the Divided Exhaust Period (DEP) concept applied to a light-duty engine running on RCCI.

2.5 List of Contributions

This section summarizes the list of contributions that were accomplished in the present research in order to meet the objectives listed in Section 2.3. The contributions are grouped pertaining to the objective that they meet.

Objective 1: Improve LTC combustion efficiency and stability at low load, and mitigate UHC and CO emissions

This objective was accomplished through the use of Early Exhaust Valve Opening (EEVO) and cylinder deactivation to obtain higher exhaust gas temperatures to improve DOC conversion efficiency of UHC and CO emissions. EEVO was accomplished through the use of a fully flexible VVA system and a cam phaser, and the impact of these two types of VVA systems on engine fuel economy was compared with the impact of cylinder deactivation on fuel economy. EEVO and cylinder deactivation are examined in detail in Chapter 5.

Objective 2: Determine the operating parameters and configuration of the air handling system to achieve high load operation of 18 Bar IMEP.

To achieve this objective, the 1-D simulation model of the stock multi-cylinder engine system was modified to include a Low Pressure (LP) EGR circuit, and any other modifications such as using a throttle at the turbine outlet for raising backpressure to run LP EGR were determined. The turbocharger performance was examined and reasons for the phenomena observed were identified. The system level performance was also compared to the stock diesel engine performance. The high load system setup is given in Chapter 6.

Objective 3: Examine VVA and manifold redesign strategies that can potentially mitigate the pumping penalty at medium and high load operation.

The Divided Exhaust Period (DEP) concept was implemented on the RCCI engine to meet this objective. The stock exhaust manifold was removed from the 1-D engine model and replaced with two separate exhaust manifolds: the blowdown manifold connected to the turbocharger and the scavenging manifold bypassing the turbocharger. The design and operating parameters of the newly designed divided exhaust system, in particular the exhaust valve area and the valve lift profiles were investigated through the guidance of a zero-dimensional filling-and-emptying model. The filling-and-emptying model was also used to determine the geometrical requirements of a new smaller turbocharger for the DEP engine, and a scaling procedure using dimensional analysis was used to perform the turbocharger selection. The DEP engine performance was compared with that of the stock engine at two different load points: 8 Bar BMEP at 3,000 rev/min and 18 Bar IMEP at 2,000 rev/min. Details of the DEP study are given in Chapter 7.

CHAPTER 3: RESEARCH METHODOLOGY

For this research project a zero-dimensional filling-and-emptying model and a one-dimensional gas dynamics model were used to investigate the gas exchange processes of the engine system as a whole, while a multi-dimensional combustion model was used to simulate the in-cylinder combustion process. In addition, turbocharger scaling was performed using dimensional analysis techniques to obtain a more compatible turbocharger geometry for the Divided Exhaust Period (DEP) concept. This chapter provides details of the engine specifications and the modeling techniques used as well as the turbocharger scaling procedure. Section 3.1 describes the engine system specifications, followed by Section 3.2 which presents an overview of the various engine simulation techniques. Sections 3.3 and 3.4 give detailed mathematical and scientific descriptions of the zero-dimensional and one-dimensional engine system models, while Section 3.5 introduces the equations used for the calculation of engine system performance parameters. Section 3.6 covers the features of the KIVA-3V multi-dimensional model used to simulate the combustion process. Finally, Section 3.7 concludes this chapter with a description of the generalized modeling procedure using the various modeling techniques covered in the preceding sections.

3.1 Engine System Specifications

The engine system simulations performed for this research were based on the General Motors Z19 DTH 1.9L light-duty diesel engine modified to run on RCCI. The specifications of the stock engine configuration are given in Table 3-1, and those of the turbocharger and the DOC are given in Tables 3-2 and 3-3, respectively. The turbine and compressor wheel dimensions given in Table 3-2 were obtained by calculating the average of the inducer and exducer diameters for each wheel. The reader is requested to consult Appendix A for more information about the wheel measurements and calculations.

Table 3-1. Engine specifications (Stock Configuration)

Bore	82 mm
Stroke	90.4 mm
Connecting Rod Length	145.54 mm
No. of Cylinders	4
Displacement	1.9 liters
Compression Ratio	*16.7 (Stock Piston)*
	15.1 (RCCI Piston)
Turbocharger	Honeywell Garrett M53 Variable Geometry Turbocharger
EGR	High Pressure EGR Loop
Intake Valve Closure (Degrees ATDC)	-132
Exhaust Valve Opening (Degrees ATDC)	112

Table 3-2 Turbocharger Specifications

Turbine Wheel Diameter (mm)	39.87
Compressor Wheel Diameter (mm)	41.92
Turbine A/R (Aspect Ratio)	0.56
Compressor A/R (Aspect Ratio)	0.42

Table 3-3. Catalyst specifications

Volume	0.6 L
Substrate	90 mm
Substrate length	90 mm
Substrate material	Metallic
Cpsi/wall	200/50 micron
Loading/washcoat	90 g/ft^3 Pt
Heat shield	Yes

3.2 Overview of Engine Modeling Techniques

Modeling and simulation techniques using high performance computers provide a cost-effective solution to investigate and optimize the various aspects of the combustion process, such as the spray modeling, in-cylinder mixing, combustion chemistry and the intake and exhaust gas dynamics, allowing automotive companies and researchers to develop control strategies with the objective of improving engine

efficiency and reducing pollutant emissions. Modeling techniques may be classified under two major categories depending on the process that they simulate in the engine cycle: (i) the gas exchange process, and (ii) the in-cylinder combustion. These two categories may be further divided into sub-categories based on the fidelity captured and the model complexity. Figure 3-1 shows the various types of modeling techniques in use today, and groups them according to whether they model the gas exchange process or the in-cylinder combustion.

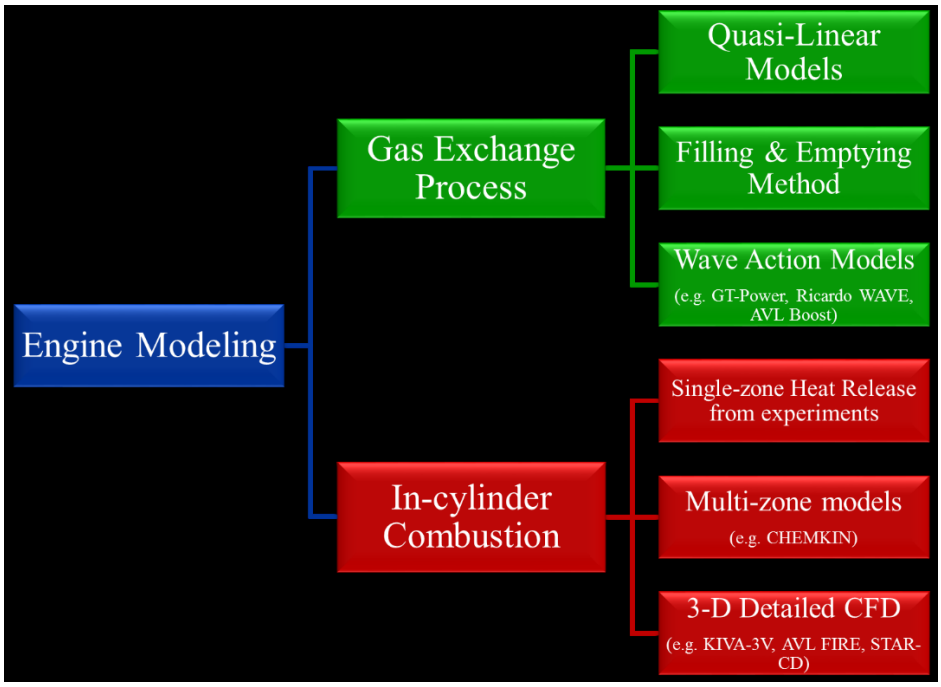

Figure 3-1: Various categories of engine modeling techniques, classified according to the process they simulate.

As the figure shows, the gas exchange process can be represented by quasi-linear models, the filling and emptying method, and wave action models, while the in-cylinder combustion process can be represented by single-zone heat release data from experiments, multi-zone models and three-dimensional detailed computational fluid dynamics. The following two sub-sections 3.2.1 and 3.2.2 offer an overview of the aforementioned techniques.

3.2.1 Gas Exchange Process Modeling

The gas exchange process refers to the movement of the working gas into and out of the cylinders during the valve open period, specifically the flow of intake air into the cylinders between intake valve

opening (IVO) and intake valve closing (IVC), and the flow of exhaust gas comprising the products of combustion out of the cylinder into the exhaust manifold between exhaust valve opening (EVO) and exhaust valve closing (EVC). As shown in Figure 3-1, the gas exchange process can be represented by quasi-linear models, the filling-and-emptying method, and wave action models. This sub-section presents an overview of the models used to simulate the gas exchange process.

3.2.1.1 Quasi-linear Methods

The simplest of the three aforementioned approaches is the quasi-linear (or quasi-steady) method, in which the engine and its components (such as the turbocharger and supercharger) are represented by empirically derived steady-state algebraic correlations or tabulated experimental data. Essentially, the engine system is represented as an analogue of an electrical circuit with the turbocharger/supercharger characteristics being considered as non-linear resistances. Due to their low complexity, quasi-linear methods offer the obvious advantage of minimal computational times, but since they are empirically derived, they are only valid for operating points where experimental data are available [127, 128]. Moreover, the empirical coefficients used to calibrate such models are highly specific to a particular engine and cannot be universally applied to any general engine system.

3.2.1.2 Filling-and-emptying Methods

"Filling-and-emptying" methods are more complex than quasi-linear models, and they involve the use of finite volumes to represent the manifolds. The mass flow of gas into and out of each finite volume, and the gas pressure and gas temperature are calculated at each crank angle degree by solving a set of first-order non-linear ordinary differential equations that represent the conditions in the manifolds. This solution method is more accurate than the quasi-linear method, as the variation of the gas properties with respect to time over an entire engine cycle is captured [129].

A drawback of the filling-and-emptying methods is that the manifold conditions are represented by one average temperature and pressure, which makes it difficult to study manifold tuning and mixture maldistribution in cylinders [127, 128]. In reality, the gas dynamics in the intake and exhaust manifolds are unsteady and this results in the propagation of pressure waves which can have an effect on the engine

performance, especially in engines that have long manifold pipe lengths and employ the use of pulse turbocharging. Hence, a detailed manifold analysis using wave action techniques is necessary for manifold design. Nevertheless, the zero-dimensional filling-and-emptying model offers invaluable insights into the thermodynamics of the entire system and generates results within a very short period of time. Therefore filling-and-emptying models can be used to quickly investigate the effectiveness of different operating strategies or technologies from a thermodynamic perspective before performing a more detailed analysis using higher dimensional modeling techniques. For this reason, a zero-dimensional filling-and-emptying model was developed using the software package Engineering Equation Solver (EES) to perform initial thermodynamic analyses. Details of this model are given in Section 3.3.

3.2.1.3 One-dimensional Wave Action Models

Wave action techniques [130 – 132] are used to solve the compressible flow equations of mass, momentum and energy in one dimension. Since the equations are hyperbolic, non-linear partial differential equations, the method of characteristics devised by Riemann or finite difference methods [133] are used to solve them. Because wave action techniques consider the propagation of pressure waves in the manifolds, they are able to accurately capture the physical resonances of the manifolds, which in turn gives a more realistic and accurate distribution of the gas flow through the manifolds and charge maldistribution effects in the cylinders. With the added complexity of pressure wave modeling, the computational time is increased, compared to quasi-steady and filling and emptying models. GT-Power by Gamma Technologies, Ricardo's WAVE and AVL Boost are the most commonly used wave action modeling software used by automotive manufacturers today. Details of the solution procedure used by the one-dimensional gas dynamics models are covered in Section 3.4.

3.2.2 In-cylinder Combustion Process Modeling

In-cylinder combustion models are used to analyze and evaluate the chemical reactions between the fuel species and air that occur during the combustion process and calculate the energy released by these reactions. The models can be classified into two major groups: thermodynamic (or zero-dimensional)

models, and multi-dimensional models. This sub-section provides an overview of the models, as well as their advantages and shortcomings.

In zero-dimensional models, the combustion chamber is divided into individual thermodynamic control volumes called zones, and the properties of the gas mixture, such as temperature and pressure are homogeneous within each zone, i.e., no spatial variation in properties is accounted for within a zone. The 1st Law of Thermodynamics and the conservation of mass are applied in the solution procedure to each zone, and a final equation of state for the gas in each zone is required to obtain closure for the system [134, 135]. The greater the number of zones the combustion chamber is divided into, the higher is the accuracy of the solution obtained since a larger number of zones can more realistically capture the charge and temperature distribution in the cylinder, which is stratified rather than homogeneous [136]. The drawback of using more zones is increased computational time since the continuity and energy equations have to be solved for more than one zone; nevertheless, the solution time is far shorter than that of a multi-dimensional model.

However, zero-dimensional models do not consider the fluid dynamics effects such as in-cylinder turbulence and the effect of EGR mixing on the combustion characteristics, resulting in inaccuracies in ignition delay prediction. Moreover, in combustion strategies where fuel is directly injected into the cylinder, zero-dimensional models may not be able to accurately represent the fuel spray break-up and the fuel-air mixing processes [137, 138]. Although empirical correlations for the injection process have been used in zero-dimensional models with limited success, these empirical correlations will only work for a narrow range of data points. Hence, to accurately predict the onset of combustion as well as the emissions, and to capture the experimental trends accurately, a multi-dimensional model that captures the details of the gas flow and spray behavior within the cylinder, and the role of turbulence in the fuel mixing process is needed.

Despite being computationally intensive compared with zero-dimensional models, multi-dimensional models are able to capture the detailed three-dimensional flow field [139] in the combustion chamber as well as the crevice regions. Capturing the detailed flow field enables one to model the mixing

between the fuel and the intake charge with a significantly higher fidelity than a multi-zone model, thereby achieving a more realistic representation of the charge preparation process, which has been shown to be an important factor in the successful operation of LTC strategies such as HCCI and RCCI [107, 140–143]. As a result, multi-dimensional models can better simulate the effects of inhomogeneity on the combustion process, in turn predicting the emissions trends more accurately. For this research, KIVA-3V was used for the multi-dimensional modeling of the in-cylinder combustion process. Details of the solution procedure used by KIVA-3V are covered in Section 3.6.

3.3 Zero-dimensional Filling-and-emptying Model

The system under consideration for the filling-and-emptying model is given in Figure 3-2. The cylinder and the exhaust manifold were modeled as separate control volumes in this model (as indicated by the dotted lines representing the control volume boundaries). For the turbocharger, the turbine was modeled as a nozzle with work output required to drive the compressor. The crank angle resolved intake manifold pressure is heavily dependent on the compressor operation, which is in turn influenced by the compressor geometry, requiring a tedious analysis of velocity triangles at the impellers, volutes and diffusers to calculate the flow losses. For simplicity the intake manifold was modeled as a constant pressure vessel with the desired cycle-averaged boost pressure value. Since the objective of using the filling-and-emptying model was to perform an initial thermodynamic analysis of the engine system to select operating points for a full coupled system analysis, only one of the cylinders was modeled, with a major assumption that the charge is distributed evenly among all cylinders and that the combustion process is similar across the cylinders.

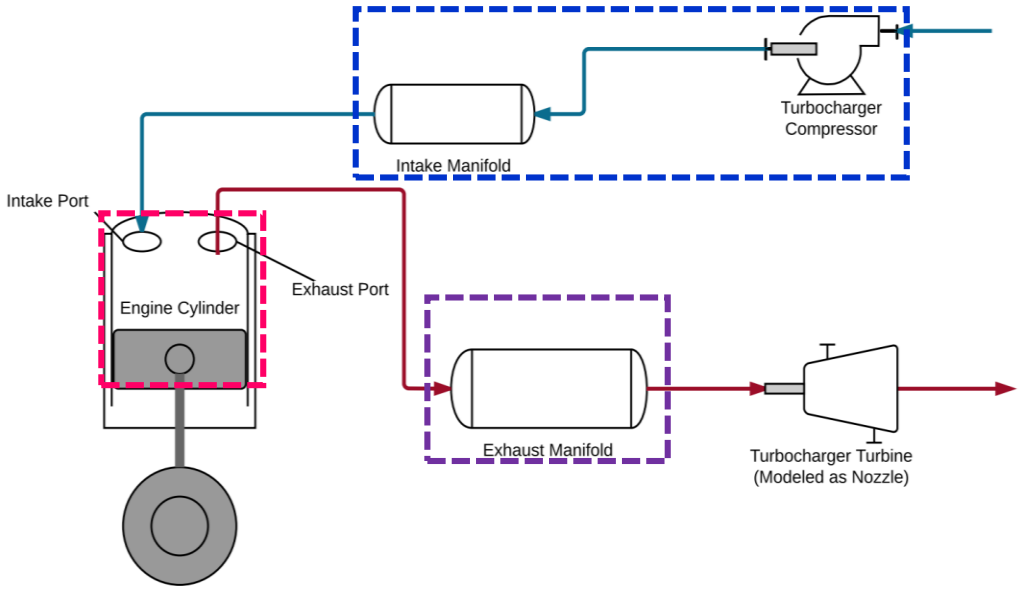

Figure 3-2: System Schematic used for the Zero-dimensional Filling-and-emptying Model. The dotted lines show the boundaries for the different control volumes considered in the model.

Equations for the conservation of mass and the conservation of energy were solved for the cylinder and the exhaust manifold as:

Conservation of Mass:

$$\frac{d}{dt}(\rho V) = \dot{m}_{cv,in} - \dot{m}_{cv,ex} \tag{3.1}$$

Conservation of Energy (1st Law of Thermodynamics):

$$\frac{\partial}{\partial t}(\rho e) = \sum_{in/out} \dot{q} - p \cdot \frac{dV}{dt} + \sum_{in,ex}^{n} h \cdot \frac{dm}{dt} \tag{3.2}$$

The terms $\dot{m}_{cv,in}$ and $\dot{m}_{cv,ex}$ represent the mass flow rate of the gas into and out of the control volume respectively, while $\sum_{in/out} \dot{q}$ represents the net heat transfer rate into/out of the control volume, $p \cdot \frac{dV}{dt}$ denotes the rate of internal energy change due to boundary work and $\sum_{in,ex}^{n} h \cdot \frac{dm}{dt}$ represents the rate of internal energy change due to the net enthalpy flow into/out of the control volume. Subsection 3.3.1

provides detailed descriptions of the modeling technique for the cylinder while subsection 3.3.2 describes the modeling technique for the exhaust manifold and the turbocharger turbine.

3.3.1 In-cylinder Combustion and Gas Exchange Modeling

The equations for the conservation of mass and energy for the cylinder are given by:

Conservation of Mass for Cylinder:

$$\frac{d}{dt}(\rho V) = \dot{m}_{int} - \dot{m}_{exh} \tag{3.3}$$

Conservation of Energy for cylinder (1st Law of Thermodynamics):

$$\frac{\partial}{\partial t}(\rho e) = \dot{q}_{HR} - \dot{q}_L - p_0 \cdot \frac{dV}{dt} + \sum_{int,exh}^{n} h \cdot \frac{dm}{dt} \tag{3.4}$$

3.3.1.1 Gas Flows through Intake and Exhaust Ports

The terms $\dot{m}_{int}$ and $\dot{m}_{exh}$ in Equation 3.3 refer to the gas flows through the intake and exhaust ports, respectively. Because flow through the ports is assumed to be adiabatic and isentropic, the equations for $\dot{m}_{int}$ and $\dot{m}_{exh}$ depend on whether the flow is subsonic or sonic (Sonic condition: $\frac{p_T}{p_0} < 0.528$) [3, 133]:

$$\dot{m}_{int} = \begin{cases} \dfrac{p_{int}A_{int}}{\sqrt{T_{int}}} \cdot \sqrt{\dfrac{\gamma}{R}\left(\dfrac{2}{\gamma+1}\right)^{\frac{\gamma+1}{(\gamma-1)}}} & \dfrac{p_0}{p_{int}} < 0.528 \quad (3.5a) \\ \dfrac{p_{int}A_{int}}{\sqrt{RT_{int}}} \cdot \left(\dfrac{p_0}{p_{int}}\right)^{\frac{1}{\gamma}} \cdot \sqrt{\dfrac{2\gamma}{\gamma-1}\left(1-\left(\dfrac{p_0}{p_{int}}\right)^{\frac{\gamma-1}{\gamma}}\right)} & \dfrac{p_0}{p_{int}} > 0.528 \quad (3.5b) \end{cases}$$

$$\dot{m}_{exh} = \begin{cases} -\frac{p_0 A_{exh}}{\sqrt{T_0}} \cdot \sqrt{\frac{\gamma}{R}\left(\frac{2}{\gamma+1}\right)^{\frac{\gamma+1}{(\gamma-1)}}} & \frac{p_{0,exh}}{p_0} < 0.528 \quad (3.6a) \\ -\frac{p_0 A_{exh}}{\sqrt{RT_0}} \cdot \left(\frac{p_{0,exh}}{p_0}\right)^{\frac{1}{\gamma}} \cdot \sqrt{\frac{2\gamma}{\gamma-1}\left(1-\left(\frac{p_{0,exh}}{p_0}\right)^{\frac{\gamma-1}{\gamma}}\right)} & \frac{p_{0,exh}}{p_0} > 0.528 \quad (3.6b) \end{cases}$$

In these equations, p_{int} refers to the intake pressure/compressor outlet pressure (which is the cycle-averaged boost pressure value), p_0 refers to the in-cylinder pressure, $p_{0,exh}$ refers to the exhaust turbine inlet pressure (which is the crank angle resolved stagnation pressure in the exhaust manifold), T_0 refers to the in-cylinder temperature, T_{int} refers to the cycle-averaged intake manifold temperature, R is the specific gas constant for air at $287\ \mathrm{J \cdot kg^{-1}K^{-1}}$, and γ refers to the temperature dependent specific heat ratio of air.

The effective intake flow area A_{int} and the effective exhaust flow area A_{exh} are given by:

$$A_{int} = C_{D,int} \cdot \frac{\pi d_{int}^2}{4} \quad (3.7a)$$

$$A_{exh} = C_{D,exh} \cdot \frac{\pi d_{exh}^2}{4} \quad (3.7b)$$

where C_D is the valve discharge coefficient. The subscripts *int* and *exh* correspond to the intake and exhaust valves respectively. The discharge coefficient is in turn a function of the valve lift-to-diameter ratio, as shown by Figure 3.3 [144].

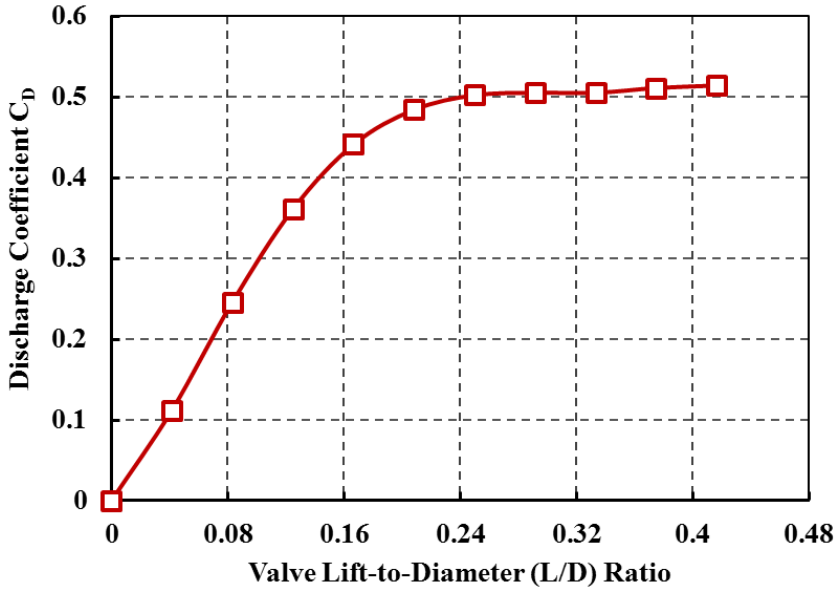

Figure 3-3: Valve discharge coefficient as a function of the lift-to-diameter ratio [144]

From Figure 3-3, it can be seen that the discharge coefficient varies with valve lift, L, which in turn is a function of crank angle. As a result, the intake and exhaust flow will not be constant and will also vary with the crank angle. (For more details on the discharge coefficient and effective valve area representation in the zero-dimensional code, the reader is requested to consult Appendix B.)

3.3.1.2 Energy Equation for In-cylinder Processes

The energy equation for the cylinder is given by:

$$\frac{\partial}{\partial t}(\rho e) = \dot{q}_{HR} - \dot{q}_L - p_0 \cdot \frac{dV}{dt} + \sum_{in,ex}^{n} h_0 \cdot \frac{dm}{dt} \qquad (3.8)$$

The terms $\dot{q}_{HR}$ and $\dot{q}_L$ represent the rate of heat released from combustion and the rate of heat loss to the cylinder walls by convection respectively.

3.3.1.2.1 Combustion Model: The Vibe (or Wiebe) Function

Assuming a single-zone combustion model, the total heat release from the fuel q_{HR} is represented by a Vibe (more commonly referred to as Wiebe) Function, developed by Ivan Vibe [145] to characterize the chain reaction events that happen during the combustion process. The function is given by:

$$q_{HR} = q_f \cdot \left[1 - e^{-a_w \cdot \left(\frac{\theta - \theta_{SOC}}{\Delta\theta}\right)^{m_w}}\right] = \left(\sum_{i=1}^{n} m_{f,i} \cdot q_{LHV,i}\right) \cdot \left[1 - e^{-a_w \cdot \left(\frac{\theta - \theta_{SOC}}{\Delta\theta}\right)^{m_w}}\right] \quad (3.9)$$

where q_f is the total fuel energy, given as the product of the ith fuel mass $m_{f,i,}$ and the lower heating value of the ith fuel $q_{LHV,i}$. θ_{SOC} is the crank angle at the start of combustion, while $\Delta\theta$ is the duration of combustion. The exponent, a_w, known as the Wiebe efficiency factor (denoted by [146]), is dependent on the efficiency of the combustion process, while the shape parameter, m_w, determines the shape of the heat release curve. Differentiating the Wiebe function, the heat release rate term $\dot{q}_{HR}$ in the energy equation is obtained:

$$\dot{q}_{HR} = \frac{dq_{HR}}{d\theta} \cdot \frac{d\theta}{dt} = \left(a_w \cdot m_w \cdot q_f \cdot \left(\frac{\theta - \theta_{SOC}}{\Delta\theta}\right)^{m_w - 1} \cdot e^{-a_w \cdot \left(\frac{\theta - \theta_{SOC}}{\Delta\theta}\right)^{m_w}}\right) \cdot \frac{d\theta}{dt} \quad (3.10)$$

3.3.1.2.2 In-cylinder Convective Heat Loss: Woschni Correlation for Heat Transfer Coefficient

The heat loss to the cylinder walls by convection is given by the well-known Newton's Law of Cooling equation:

$$\dot{q_L} = \bar{h}_w \cdot A_w \cdot (T_0 - T_w) \quad (3.11)$$

where $\bar{h}_w$ is the average convective heat transfer coefficient, A_w is the surface area of the cylinder wall, and T_w is the cylinder wall temperature. The convective heat transfer coefficient is in turn given by the widely used Woschni correlation [147]:

$$\bar{h}_w = 3.26 \cdot b^{-0.2} \cdot p_0^{0.8} \cdot T_0^{-0.55} \cdot \bar{w}^{0.8} \quad (3.12)$$

where $\bar{w}$ is the average in-cylinder gas velocity, given by:

$$\bar{w} = K_1 \bar{u}_p + K_2 \cdot \frac{V_d T_{ivc}}{p_{ivc} V_{ivc}} \cdot (p_0 - p_m) \quad (3.13)$$

In developing the above correlation for $\bar{w}$, Woschni assumed that the average gas velocity is proportional to the mean piston speed $\bar{u}_p$ during the intake, compression and exhaust strokes. During the

combustion process, he attempted to account for the increase in the gas velocity caused by the density change that occurs as a result of combustion by introducing a term proportional to the pressure rise during combustion: $(p_0 - p_m)$, where p_m is the crank angle resolved motoring pressure. In this pressure rise term, V_d refers to the cylinder displacement volume, while T_{ivc}, p_{ivc}, and V_{ivc} refer to the in-cylinder temperature, in-cylinder pressure and cylinder volume, respectively, at Intake Valve Closure (IVC) timing.

Based on the aforementioned assumptions about the in-cylinder gas velocity, Woschni calculated the constants K_1 and K_2 $for\ use$ in Equation 3.13, as shown in Table 3-4.

Table 3-4. Woschni Gas Velocity Correlation Constants K_1 and K_2

	K_1	K_2
Gas Exchange Period ($\theta_{EVO} < \theta < \theta_{IVC}$)	6.18	0
Compression Period (θ_{IVC} to TDC)	2.28	0
Combustion and Expansion Period (TDC to θ_{EVO})	2.28	$3.24 \cdot 10^{-3}$

3.3.1.2.3 Cylinder Boundary Work and Enthalpy Flow Terms

The cylinder volume at a given crank angle is given by the slider-crank equation:

$$V(\theta) = V_c + \frac{\pi b^2}{4}\Big(L_{crd} + a\ - x(\theta)\Big) \tag{3.14}$$

where V_c is the cylinder clearance volume, b is the cylinder bore, L_{crd} is the connecting rod length, a is the crank radius and $x(\theta)$ is the piston pin position. The piston pin position is a function of crank angle θ and is given by Equation 3.15:

$$x(\theta) = a_c \cdot \cos\theta + \sqrt{L_{crd}^2 - a^2 \cdot \sin^2\theta} \tag{3.15}$$

The rate of change of volume with respect to crank angle is found by differentiating Equation 3.14 with respect to θ:

$$\frac{dV}{d\theta} = \frac{\pi b^2}{4} \cdot \frac{dx}{d\theta} = -\frac{\pi b^2}{4} \cdot \frac{a^2 \cdot \sin(2\theta)}{2\sqrt{L_{crd}^2 - a^2 \cdot \sin^2\theta}} \tag{3.16}$$

Using the chain rule, the rate of volume change $\frac{dV}{d\theta}$ for the cylinder can then be re-expressed (with respect to time) as:

$$\frac{dV}{dt} = \frac{dV}{d\theta} \cdot \frac{d\theta}{dt} \tag{3.17}$$

The final set of terms in the energy equation for the cylinder is the set of terms for the enthalpy flows into and out of the cylinder through the intake and exhaust ports, given as:

$$\sum_{in,ex}^{n} h \cdot \frac{dm}{dt} = \begin{cases} \dot{m}_{exh} \cdot h_0(T_0), & t_{evo} < t \leq t_{ivo} \\ \dot{m}_{exh} \cdot h_0(T_0) + \dot{m}_{int} \cdot h_{int}(T_{int}), & t_{ivo} < t \leq t_{evc} \\ \dot{m}_{int} \cdot h_{int}(T_{int}), & t_{evc} < t \leq t_{ivc} \\ 0 & OTHERWISE \end{cases} \tag{3.18}$$

where h_0 is the stagnation enthalpy of the gas in the cylinder and h_{int} is the stagnation enthalpy of the gas in the intake manifold. The stagnation enthalpies are in turn functions of the respective gas temperatures.

3.3.2 Exhaust Manifold Modeling

The continuity equation for the exhaust manifold is given by:

$$\frac{d}{dt}(\rho V) = -\dot{m}_{exh} - \dot{m}_{in,turb} \tag{3.19}$$

where $\dot{m}_{exh}$ is the exhaust gas mass flow rate from the cylinder into the exhaust manifold, given by Equations 3.6, and $\dot{m}_{in,turb}$ is the exhaust mass flow rate out of the exhaust manifold into the turbine. (Equations for the mass flow rate into the turbine are developed in subsection 3.3.3.)

Since the exhaust manifold is modeled as an adiabatic constant volume reservoir, the volume change and heat transfer terms in the energy equation are zero for the manifold. As a result, the energy equation for the exhaust manifold can be simplified as:

$$\frac{\partial}{\partial t}(\rho e) = \sum_{in,exh}^{n} h \cdot \frac{dm}{dt} = -\dot{m}_{exh} \cdot h_0(T_0) - \dot{m}_{in,turb} \cdot h_0\left(T_{0,exh}\right) \tag{3.20}$$

Here $h_0(T_{0,exh})$ represents the stagnation enthalpy of the exhaust gas in the exhaust manifold at the stagnation exhaust temperature of $T_{0,exh}$.

3.3.3 Turbocharger Turbine Modeling

Because the zero-dimensional filling-and-emptying model will be used to establish the design parameters of the ideal turbocharger for an RCCI engine and the characteristics of said turbocharger are not known, a simplified turbocharger model that does not consider the device geometry was used to simulate the boosting process initially. This simplified model, implemented by Watson and Janota [78], and Payri et al. [148], involves representing the turbocharger turbine as an adiabatic nozzle (of equal effective area to the turbine in question) placed immediately downstream of the exhaust manifold. The mass flow rate through the turbine is given by a variant of the mass flow rate equations for the intake and exhaust ports:

$$\dot{m}_{in,turb} = \dot{m}_{out,turb} = \begin{cases} \dfrac{p_{0,exh}A_T}{\sqrt{T_{0,exh}}} \cdot \sqrt{\dfrac{\gamma}{R}\left(\dfrac{2}{\gamma+1}\right)^{\frac{\gamma+1}{(\gamma-1)}}} & \dfrac{p_{atm}}{p_{0,exh}} < 0.528 \quad (3.21a) \\ \dfrac{p_{0,exh}A_T}{\sqrt{RT_{0,exh}}} \cdot \left(\dfrac{p_{atm}}{p_{0,exh}}\right)^{\frac{1}{\gamma}} \cdot \sqrt{\dfrac{2\gamma}{\gamma-1}\left(1-\left(\dfrac{p_{atm}}{p_{0,exh}}\right)^{\frac{\gamma-1}{\gamma}}\right)} & \dfrac{p_{atm}}{p_{0,exh}} > 0.528 \quad (3.21b) \end{cases}$$

In Equations 3.21, $p_{0,exh}$ refers to the stagnation pressure in the exhaust manifold, A_T refers to the effective nozzle area equivalent to the turbine, $T_{0,exh}$ refers to the stagnation temperature of the exhaust gas in the exhaust manifold, and p_{atm} is the atmospheric pressure. As Equations 3.21 show, by modeling the turbine as a nozzle, it is assumed that the turbine does not store/accumulate mass over time.

The aforementioned equations and relations were incorporated in a computer program written using the Engineering Equation Solver (EES). EES was chosen as the programming platform due to its comprehensive library of thermodynamic properties, its interpolation capabilities and the convenience it

offers in performing numerical integration. EES uses a semi-implicit adaptive step-size integration technique to solve the coupled system of differential equations [149]. The full EES code for the stock engine configuration can be found in Appendix B.

3.4 One-Dimensional Gas Dynamics Modeling

A model of the multi-cylinder engine with pipes, flow-splits and orifices was created in GT-Power, and the entire system was discretized into many volumes, with each flow-split being represented by a single volume and each pipe being divided into one or more volumes. (The stock engine system model was already created in GT-Power by researchers at the General Motors Collaborative Research Laboratory [144] and was modified and adjusted by the author for RCCI studies.) Figure 3-4 shows the GT-Power model of the stock engine configuration.

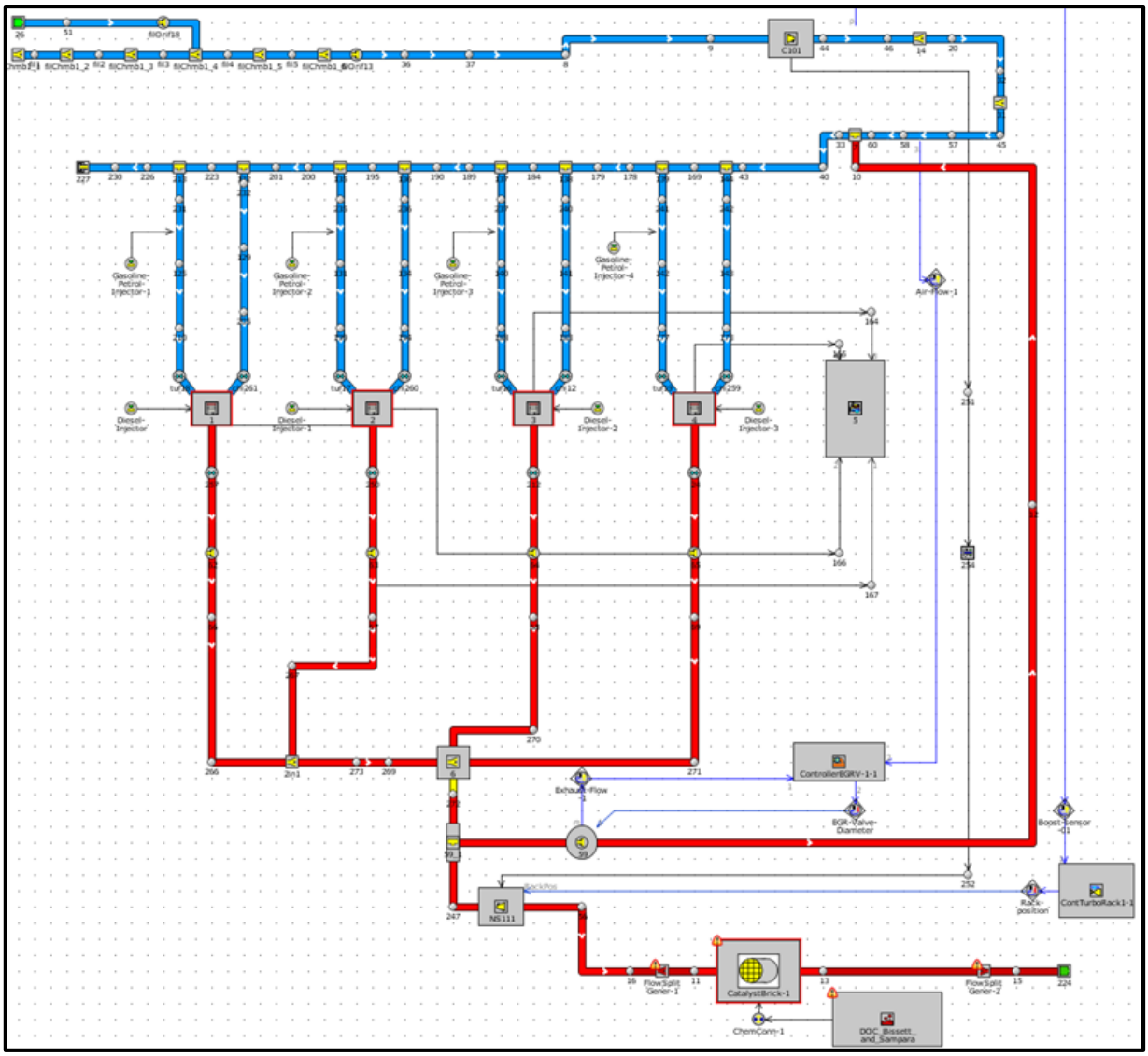

Figure 3-4: GT-Power Model of the General Motors Z19 DTH 1.9L Multi-cylinder Engine [144]. 4 PFI Injectors have been added to the intake manifold for RCCI.

A "staggered-grid" approach [150] was used for discretization (shown in Figure 3-5): scalar variables such as pressure, temperature, density and enthalpy are uniform throughout the volume and are calculated at the volume centroid, while vector quantities such as velocity and mass fraction fluxes are calculated at the boundaries.

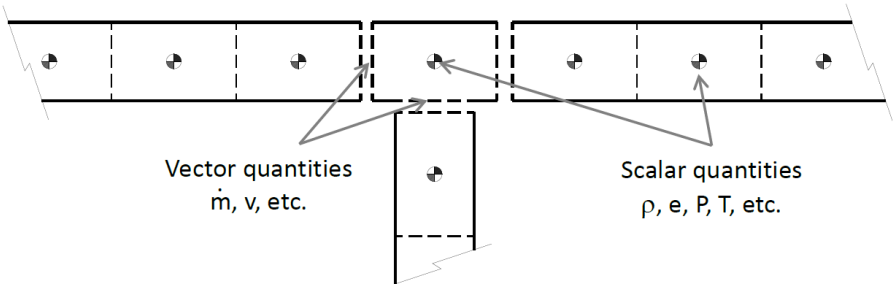

Figure 3-5: Schematic representation of the staggered-grid approach used in GT-Power. (Source: [151])

The continuity, momentum and energy equations for compressible flow through the flow components are solved in one dimension [151]:

Continuity:

$$\frac{dm}{dt} = \sum_{boundaries} \rho A_c u \tag{3.23}$$

Momentum (One-Dimensional):

$$\frac{d(\rho A_c u)}{dt} = A_c \cdot \frac{dp}{dx} + \frac{d}{dx}\left[\sum_{boundaries} (\rho A_c u \times u)\right] - \frac{4C_f \rho u^2 A_c}{2D} - \frac{d}{dx}\left(\frac{C_k}{2} \cdot \rho u^2 A_c\right) \tag{3.24}$$

Energy:

$$\frac{d(me)}{dt} = -p \cdot \frac{dV}{dt} + \sum_{boundaries} (\dot{m}h) - h_g A_s(\bar{T} - T_w) \tag{3.25}$$

The Fanning friction factor C_f, which is used to model the frictional flow losses in pipes, is calculated as a function of the Reynolds number and wall surface roughness [152]. The equation used to calculate the friction factor depends on whether the flow regime in the pipes was laminar or turbulent (determined by the Reynolds Number Re_D):

$$C_f = \begin{cases} \dfrac{16}{Re_D} & Laminar\ Regime\ (Re_D < 2{,}000) \quad (3.26a) \\ \dfrac{0.08}{Re_D^{0.25}} & Turbulent\ Regime\ (Re_D > 4{,}000) \quad (3.26b) \end{cases}$$

The pressure loss coefficient, which is used to account for flow losses in pipe bends, is defined by:

$$C_k = \frac{p_{in} - p_{ex}}{\frac{1}{2\rho} u_{in}^2} \tag{3.27}$$

where $p_1 and\ p_2$ are the inlet and outlet pressures respectively, ρ is the inlet density and u_{in} is the inlet flow velocity.

The gas flowing through the intake and exhaust manifolds is assumed to be ideal, so the ideal gas equation of state is used to describe the gas behavior:

$$p_{int,exh} V_{int,exh} = m_{int,exh} R T_{int,exh} \tag{3.28}$$

In the energy equation, the heat transfer from the gases flowing inside the manifolds to the walls is calculated using a heat transfer coefficient, computed according to the Colburn Analogy [153]:

$$h_g = \frac{1}{2} C_f \rho u_{eff} C_p \cdot Pr^{-\frac{3}{2}} \tag{3.29}$$

Where C_f is the friction factor of the pipe, ρ is the gas density, u_{eff} is the effective velocity outside the boundary layer, C_p is the specific heat and *Pr* is the Prandtl Number.

The aforementioned equations of continuity, momentum and energy are integrated over time using an explicit method. In this method, the right hand side of the conservation equations is evaluated using values from the previous time step, giving the derivatives of the variables of mass flow rate, density and internal energy. The derivatives are then integrated over the time step to obtain the values at the new time. The solver then iterates on the pressure and temperature at that particular time step until they satisfy the calculated density and energy, which are defined as functions of pressure and temperature.

3.4.1 Modeling of Turbocharger Performance

The turbocharger was modeled in GT-Power using manufacturer-generated performance maps of the turbine and compressor provided by the user. Turbine data from the manufacturer typically consists of isentropic efficiency and mass flow parameter (sometimes also called reduced mass flow rate) expressed

as functions of speed parameter and pressure ratio (or expansion ratio), and are given in the form of lookup tables. The mass flow parameter and speed parameter are given by:

Mass Flow Parameter $\dot{m}_r$:

$$\dot{m}_r = \frac{\dot{m}_{exh}\sqrt{T_{0,exh}}}{p_{0,exh}} \tag{3.30}$$

Speed Parameter:

$$N_r = \frac{N_{tc}}{\sqrt{T_{0,exh}}} \tag{3.31}$$

In a typical turbine map, the mass flow parameter and efficiency values from the lookup tables are plotted against pressure ratio to obtain the turbine characteristic curves for each speed parameter. Figure 3-6 shows the turbine performance map for the stock Honeywell Garrett M53 Variable Geometry Turbocharger. Note the different groups of curves labeled T10-T100 which represent the different vane openings (or rack position) of the variable vanes that control the aspect ratio of the turbine volute.

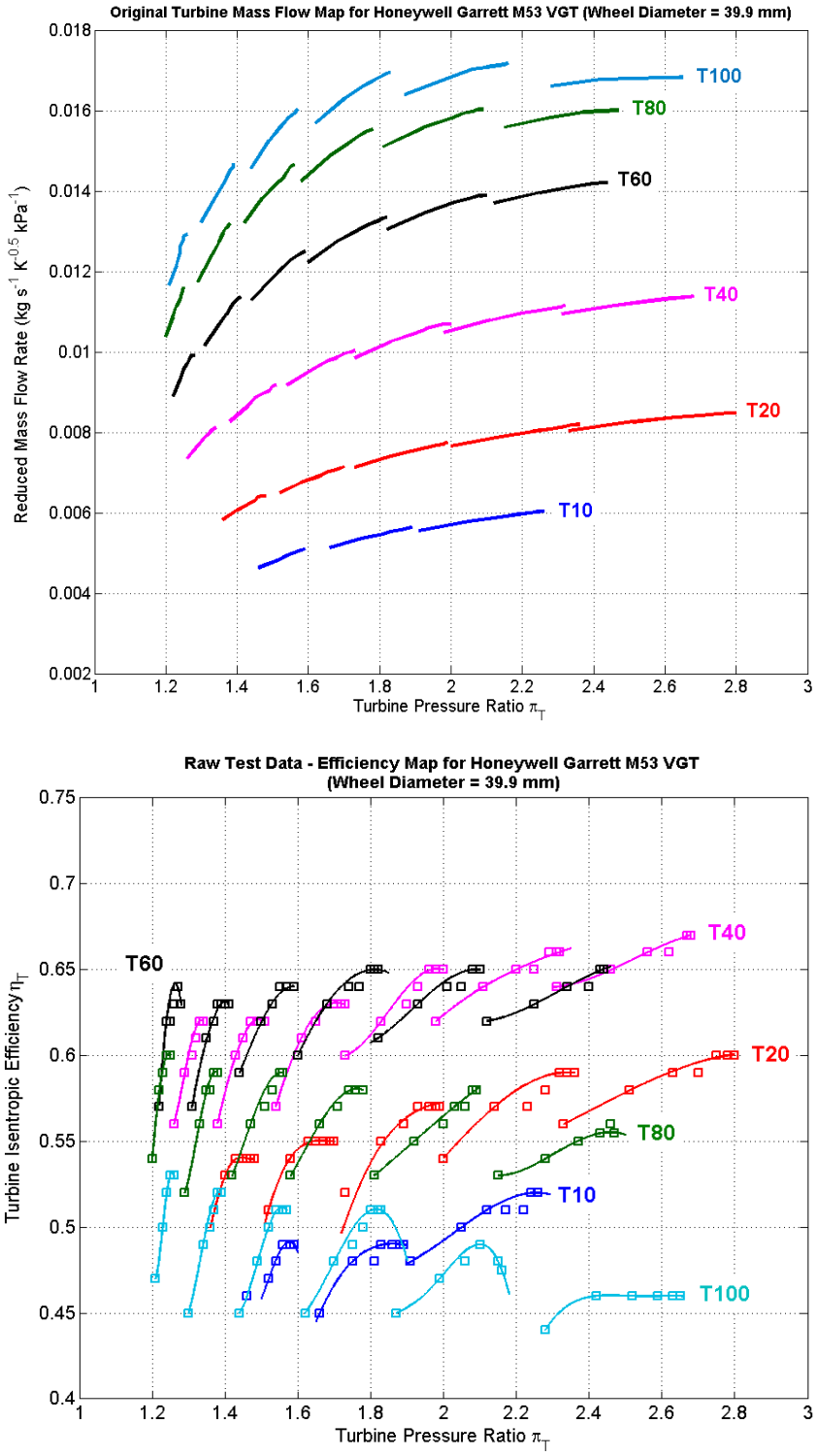

Figure 3-6: Raw Turbine Map for the Honeywell Garrett M53 VGT [144]

As Figure 3-6 shows, the test data from Honeywell only covers a very limited range at all rack positions. Interpolation within this data range may give unacceptable results due to the non-linear behavior

of the turbine flow characteristics. To overcome this problem, the raw test data must first undergo a curve fitting procedure to improve the data resolution in preparation for simulation studies. The raw data is fed into the "TurbineMapVGT" template in GT-Power which performs a polynomial curve fit on the dataset to smooth the mass flow parameter vs. pressure ratio and the efficiency vs. pressure ratio plots. The data at each rack position is fed into the template as a separate turbine map, and each map undergoes a curve fitting procedure to improve its data resolution. Figure 3-7 shows the fitted turbine map obtained from GT-Power for a rack position of 0.6 (T60 family of curves). The reader is requested to consult Appendix C for the curve fits at other rack positions.

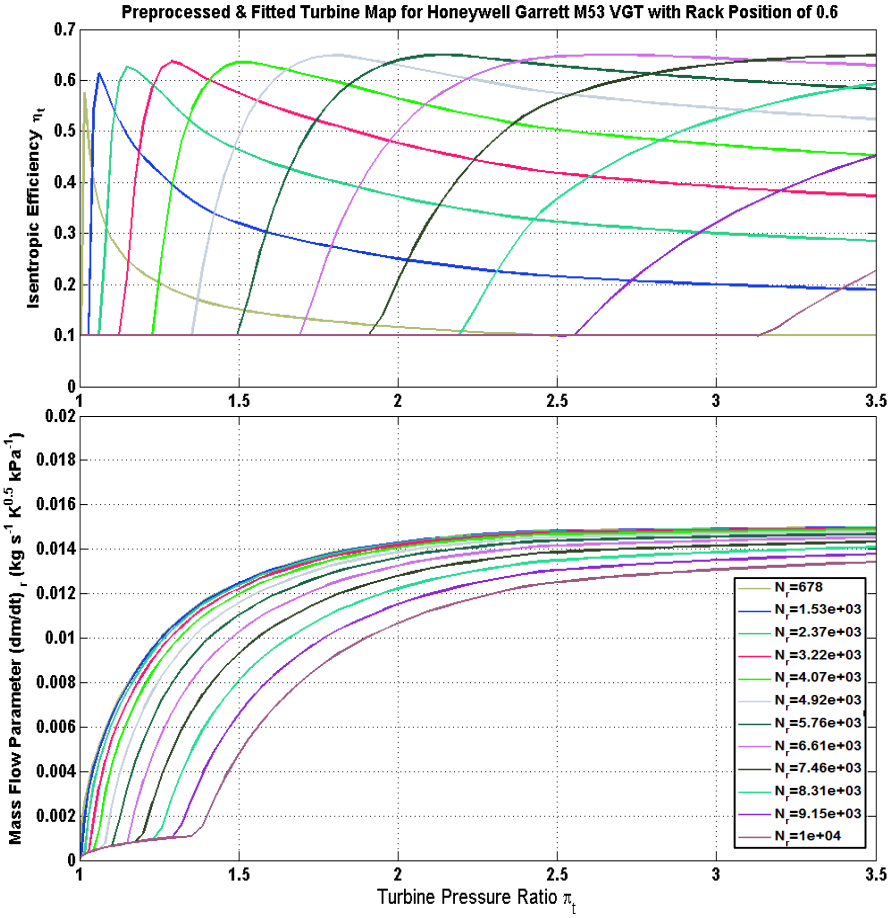

Figure 3-7: Preprocessed and Fitted Turbine Map from GT-Power for the Honeywell Garrett M53 Stock VGT at a Rack Position of 0.6 (T60 Family of Speed Lines).

The compressor data from the manufacturer consists of the compressor isentropic efficiency expressed as a function of pressure ratio, corrected mass flow rate and corrected speed. The corrected mass

flow rate and corrected speed are the compressor mass flow rate and rotational speed that would be observed if the inlet conditions were at a particular reference temperature and pressure and are given as:

Corrected Mass Flow Rate:

$$\dot{m}_{comp,corr} = \frac{\dot{m}_{comp}\sqrt{\frac{T_{int}}{T_{ref}}}}{\frac{p_{int}}{p_{ref}}} \tag{3.32}$$

Corrected Speed:

$$N_{comp,corr} = \frac{N_{comp}}{\sqrt{\frac{T_{int}}{T_{ref}}}} \tag{3.33}$$

where $\dot{m}_c$ and N_c are the actual mass flow rate and actual speed, T_{in} and p_{in} are the actual temperature and pressure at the compressor inlet, and T_{ref} and p_{ref} are the reference temperature and pressure. Usually the reference temperature and pressure would be ambient conditions at sea level (i.e. 298.15 K and 1 atm.), but for the M53 VGT, the reference temperature and pressure were 302.78 K and 0.962 bar, respectively. The raw compressor map from Honeywell is shown in Figure 3-8.

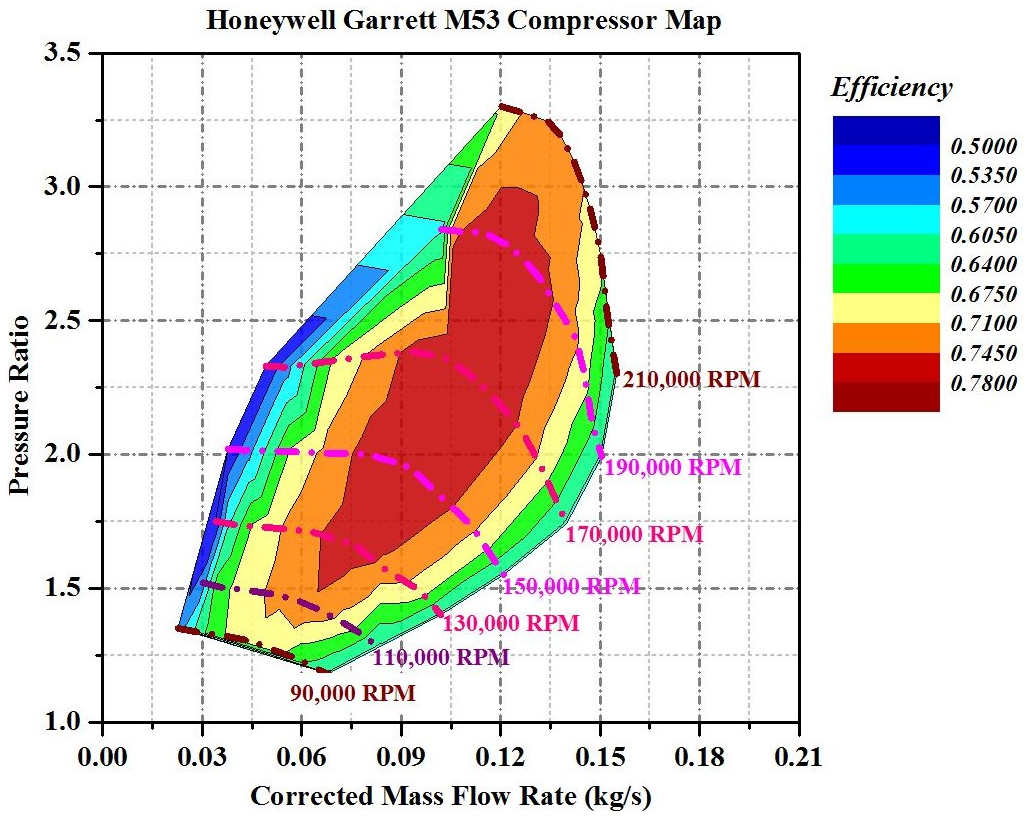

Figure 3-8: Honeywell Garrett M53 Stock Compressor Map showing Corrected Mass Flow Rate and Corrected Speed Values [144]

GT-Power predicts the turbocharger speed and the pressure ratio across each turbine and compressor at every time step, and determines the corresponding mass flow rates through the turbines and compressors, as well as the device efficiencies from the performance maps. The turbocharger speed is calculated using the turbocharger torque equation as:

Turbocharger Torque Equation (Newton's 2nd Law for Angular Momentum Conservation):

$$I_{tc} \cdot \frac{d\omega_{tc}}{dt} = \tau_t - \tau_c - \tau_{fr} \tag{3.34}$$

The iteration method used by GT-Power to simulate the turbocharger is described as follows [154]:

1. GT-Power starts the calculation of the turbocharger speed using an initial guess value (the calculation is not very sensitive to the guess value), and attempts to find a convergence of the solution to the torque equation through iteration.

2. The pressure ratios across the turbine(s) and compressor(s) are obtained from the pressures in the adjacent flow components immediately upstream and downstream of the turbine(s) and compressor(s), which in turn are dependent upon the behavior of the entire engine system.
3. The device efficiencies corresponding to the pressure ratios and mass flow rates (on the performance maps) are then used to calculate the enthalpy changes across the turbine and the compressor, which in turn are used to evaluate the turbine and compressor outlet temperatures. The equations for the enthalpy change across the turbine and compressor are given as:

Enthalpy change across turbine:

$$\Delta h_t = \eta_{s,t}(h_{t,in} - h_{t,ex}) = c_p T_{0,exh} \eta_{s,t} \left[1 - \left(\frac{p_{0,exh}}{p_{ex,turb}} \right)^{\frac{\gamma-1}{\gamma}} \right] \tag{3.35}$$

Enthalpy change across compressor:

$$\Delta h_c = \frac{h_{comp,in} - h_{comp,ex}}{\eta_{s,c}} = \frac{c_p T_{0,int}}{\eta_{s,c}} \left[1 - \left(\frac{p_{in,comp}}{p_{int}} \right)^{\frac{\gamma-1}{\gamma}} \right] \tag{3.36}$$

4. Steps 2 and 3 are repeated until the solution to the torque equation has converged and the torque balance is satisfied. (For the relationship between the turbocharger torque and the thermodynamic variables, please refer to Equations 3.63 and 3.64.)

3.4.2 Flow across Intake and Exhaust Valves

The equations for the flow through the exhaust and intake valves are given by Equations 3.7 and 3.8, respectively. The effective valve area term for both these equations is given by Equation 3.9, and the valve discharge coefficient follows the trend given by the plot in Figure 3-3.

3.4.3 Aftertreatment System Modeling

GT-Power was also used to model the aftertreatment processes using the built-in DOC model developed by Bissett and Sampara [155] as a base-line. Exhaust gas properties such as gas composition,

exhaust flow rate and exhaust temperature from the engine system model and the manufacturer catalyst specifications are used as inputs to the DOC model.

3.5 Calculation of Engine Performance Parameters

The engine performance was evaluated by analyzing the in-cylinder pressure trace, the gas exchange process during a single engine cycle, and the impact of the engine system components on the system behavior. System performance analysis was done for both the EES and GT-Power models. This section defines the system performance parameters and describes their calculation procedures.

By analyzing the in-cylinder pressure trace and the Pressure-Volume (p-V) diagram of an engine cycle, the work output from the cylinder may be evaluated for each cycle. The work output during an engine cycle is given by:

$$W_{cyc} = \oint p_0 \cdot dV \tag{3.37}$$

The **Net Indicated Mean Effective Pressure** $\boldsymbol{IMEP_n}$ is the work per cycle divided by the cylinder displacement:

$$IMEP_n = \frac{W_{cyc}}{V_d} \tag{3.38}$$

The net indicated mean effective pressure is a representation of the work output over the entire engine cycle, during both the gas exchange period when the valves are open and during the combustion, compression and expansion stages when the valves are closed. As such, it is also considered to represent the open cycle work output. The **Gross Indicated Mean Effective Pressure** $\boldsymbol{IMEP_g}$ is the work output during the closed portion of the cycle, defined mathematically as the integral from the volume at -180 degrees crank angle to the volume at 180 degrees crank angle. This value is essentially the work output from the compression and expansion strokes of the cycle:

$$IMEP_g = \frac{W_{cc}}{V_d} = \int_{V_{-180}}^{V_{180}} p_0 \cdot dV \tag{3.39}$$

The Pumping Mean Effective Pressure PMEP is obtained by subtracting the gross indicated mean effective pressure from the net indicated mean effective pressure as follows:

$$PMEP = IMEP_n - IMEP_g \tag{3.40}$$

The PMEP gives an indication of the efficiency of the gas exchange process. Pumping work is either added to or subtracted from the closed cycle work because of the flow of the intake air and exhaust gases into and out of the cylinder, respectively, through the intake and exhaust ports. PMEP is usually negative due to the work done by the piston displacement in expelling gases out of the cylinder during the exhaust stroke and inducting fresh intake air into the cylinder during the intake stroke. If a compressor such as a supercharger or turbocharger is used to assist in the induction of fresh air, PMEP may be positive.

The **Friction Mean Effective Pressure FMEP** is an indication of the work losses due to mechanical friction in the bearings and the cranktrain as well as any parasitic losses due to the components and accessories connected to the cranktrain, such as superchargers, alternators, etc. FMEP is defined by:

$$FMEP = RMEP + AMEP \tag{3.41}$$

where RMEP is the Rubbing Mean Effective Pressure and AMEP is the Accessory Mean Effective Pressure. RMEP gives an idea of the friction in the piston bearings, friction in the cranktrain, and friction due to the rubbing motion of the piston against the cylinder wall. It can be calculated using the Chen-Flynn Correlation [156]:

$$RMEP = A \cdot p_{0,max} + B \cdot \overline{u_p} + C \cdot \overline{u}_p^2 \tag{3.42}$$

where $p_{0,max}$ is the maximum cylinder pressure, $\overline{u}_p$ is the mean piston speed, and A, B and C are constants obtained using a curve fit for a particular engine. The mean piston speed is calculated from the engine speed N using the following equation:

$$\overline{u_p} = 2 \cdot s \cdot \frac{N}{60} \tag{3.43}$$

where s is the stroke, which for the 1.9L engine is 0.0904 m. For the General Motors 1.9L engine, the constants A, B and C are given in Table 3.5 [144]:

Table 3-5: Chen-Flynn Friction Correlation Equation Coefficients

Peak Cylinder Pressure Factor, A	0.001
Mean Piston Speed Factor ($\mathrm{Bar \cdot s \cdot m^{-1}}$), B	0.07
Mean Piston Speed Squared Factor ($\mathrm{Bar \cdot s^2 \cdot m^{-2}}$),C	0.0053

The AMEP indicates the friction work needed to operate the engine components connected to the cranktrain, such as mechanical superchargers and alternators.

By subtracting the FMEP from the $IMEP_n$, the **Brake Mean Effective Pressure BMEP** may be obtained. BMEP gives an indication of the actual useful work output that is transmitted to a generator for electric power generation in a genset or railroad locomotive, or to the automotive transmission for a road vehicle. The BMEP is the value that is measured by a dynamometer in a test cell.

Knowledge of fuel consumption is crucial to understand the efficiency of the fuel conversion process by an engine. The fuel consumption is expressed in terms of specific fuel consumption, which is the fuel consumed to produce a unit of power per unit time. Two specific fuel consumption quantities can be defined: the **Indicated Specific Fuel Consumption ISFC** and the **Brake Specific Fuel Consumption BSFC** defined by:

$$ISFC = \frac{m_f}{W_{cyc}} \cdot 3.6X10^6 = \frac{m_f}{IMEP_n \cdot V_d} \cdot 3.6X10^6 \tag{3.44}$$

$$BSFC = \frac{m_f}{BMEP \cdot V_d} \cdot 3.6X10^6 \tag{3.45}$$

where m_f is the mass of fuel consumed per engine cycle. ISFC and BSFC are typically expressed using the units of $\mathrm{g \cdot kWh^{-1}}$, so the conversion factor of $3.6X10^6$ is used to convert the energy per cycle which is expressed in Joules to units of kWh.

3.6 In-cylinder Closed Cycle Simulations using KIVA-3V

GT-Power only computes the solution pertaining to the gas flow through the intake and exhaust manifold components. The in-cylinder fuel injection and combustion processes were simulated using the multi-dimensional engine combustion code KIVA-3V. Figure 3-9 provides a brief overview of the various physics and chemistry models used in KIVA-3V, which are covered in this section.

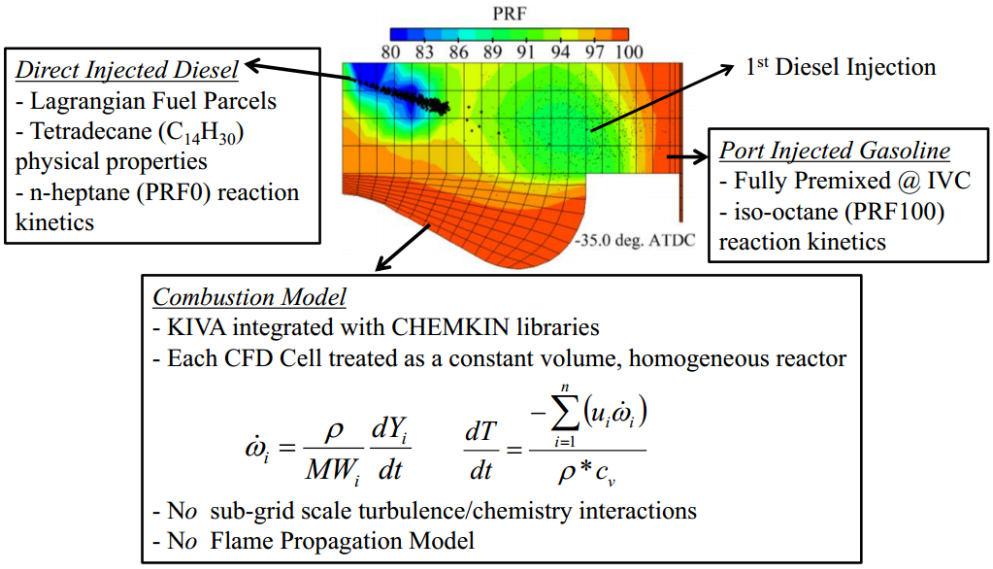

Figure 3-9: Illustration of the major features of the KIVA-3V model. Taken from [157].

3.6.1 Multi-dimensional CFD Grid/Mesh Geometry

Two different piston geometries were used for the KIVA-3V simulations: the stock piston with a re-entrant bowl for low-load operation, and a newly designed flat-bottomed RCCI piston for medium and high-load operation. The decision to swap the stock re-entrant bowl piston with the flat-bottomed piston was based on recommendations made in previous piston bowl optimization studies [158–161], where the flat-bottomed piston geometry was shown to be optimal for RCCI mixture preparation and combustion.

A 1/7-sector mesh of each geometry with periodic boundary conditions was used to simulate the combustion process, since the DI fuel injector has 7 injector holes in a symmetrical configuration. Details of the sector mesh are given in Table 3-6, and the sector mesh geometries are shown in Figure 3-10.

Table 3-6. Computational grid specifications

Computational grid	Stock	RCCI
Cells at IVC	9,738	6,213
Cells at TDC	3,528	2,034
Radial resolution (mm)	2.1	2.6
Azimuthal resolution (deg.)	2.9	

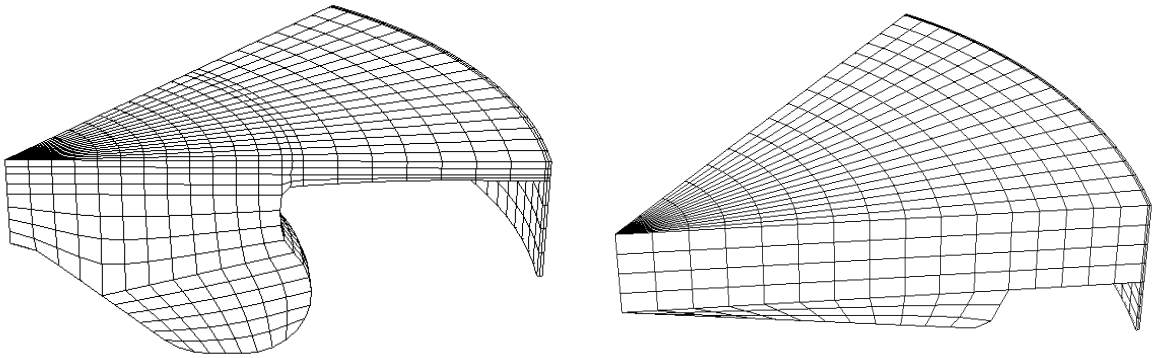

Figure 3-10. Stock Piston Mesh (Left, 3,528 Cells at TDC) and RCCI Piston Mesh (Right, 2,034 Cells at TDC)

3.6.2 Spray Model

The Lagrangian-Drop Eulerian-Fluid technique is used to model spray behavior in KIVA-3V. This technique uses the GASJET model of Abani et al. [162, 163], which assumes that the relative velocity between a droplet and the fuel vapor (gas phase) is equal to the relative velocity between a droplet and a turbulent gas jet with the same mass and momentum of the injected fuel. In this model, an axial component of the gas phase velocity is imposed as a function of the distance from the nozzle, which is used in the droplet acceleration equation given by:

$$\frac{d\vec{U}}{dt} = \frac{3}{8} C_D \cdot \frac{\rho_g}{\rho_l r_d} \left|\vec{U} - \vec{V}_g\right| \cdot (\vec{U} - \vec{V}_g) \tag{3.46}$$

where $\vec{U}$ is the droplet velocity vector, C_D is the Reynolds number dependent droplet drag coefficient, ρ_g and ρ_l are the gas and liquid phase densities respectively, r_d is the droplet radius, and $\vec{V}_g$ is the velocity vector of the gaseous phase, given as: $\vec{V}_g = \langle \tilde{V}_{g,x}, \tilde{V}_{g,y}, \tilde{V}_{g,z} \rangle$. The gas velocity components perpendicular to the spray axis $\vec{V}_{g,y}$ and $\vec{V}_{g,z}$ are obtained from the Eulerian gas phase solution while the axial component $\vec{V}_{g,x}$ is found from gas-jet theory:

$$\vec{V}_{g,x} = \min\left[\vec{U}_{inj}, \frac{3\vec{U}_{inj} d_{noz}}{K_{entr} x}\sqrt{\frac{\rho_l}{\rho_g}}\left(1 + \frac{12r^2}{K_{entr}^2 x^2}\right)^{-2}\right] \tag{3.47}$$

where $\vec{U}_{inj}$ is the injection velocity, d_{noz} is the injector nozzle diameter, K_{entr} is a model constant taken to be 0.7, x is the position downstream of the nozzle on the spray axis, and r is the radial position. An advantage of using the GASJET model is that the grid size dependency of the spray is reduced, allowing a more accurate spray simulation on a relatively coarse grid.

In KIVA-3V the liquid fuel is broken up into parcels that are injected as spheres with the same diameter as that of the effective injector nozzle hole. These fuel parcels then undergo break-up as modeled by the Kelvin-Helmholtz/Rayleigh-Taylor (KH-RT) hybrid spray break-up model, developed by Beale and Reitz [164]. This model comprises two sub-models; the Kelvin-Helmholtz (KH) instability model used to simulate the primary break-up of the fuel parcels, and the Rayleigh-Taylor (RT) used to model the secondary (aerodynamic) break-up, as illustrated in Figure 3-11.

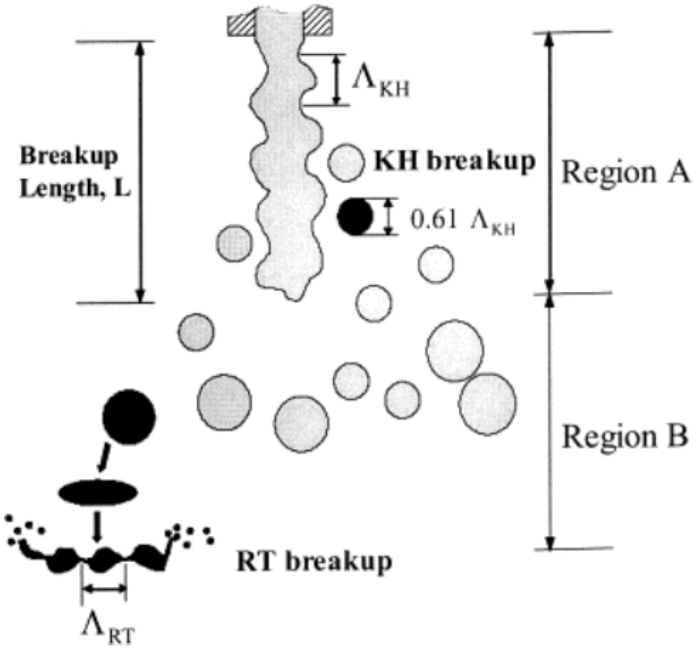

Figure 3-11: Kelvin-Helmholtz Rayleigh-Taylor Spray Breakup Model (Source: [157])

The KH model predicts the primary break-up process by calculating the break-up time τ_{KH} given by:

$$\tau_{KH} = 3.726 \cdot \frac{B_1 r}{\Omega_{KH} \Lambda_{KH}} \tag{3.48}$$

where B_1 is a parameter that adjusts the fuel vapor distribution in the combustion chamber, and Ω_{KH} and Λ_{KH} are the calculated frequency and wavelength respectively of the fastest growing wave. The radii r_c of the derivative child parcels from the primary KH break-up are given by:

$$r_c = B_0 \Lambda_{KH} \tag{3.49}$$

where B_0 is a constant with a value of 0.6.

An empirical break-up length, L_b, is calculated to determine the transition from primary to secondary break-up:

$$L_b = C_b d_0 \sqrt{\frac{\rho_l}{\rho_{air}}} \tag{3.50}$$

where d_0 is the diameter of the parent parcel and C_b is an adjustable parameter given a value of 1.9. At distances from the injector tip greater than this break-up length, the RT model is used to predict the secondary break-up.

In the RT model, Rayleigh-Taylor waves grow on the surface of a given droplet if the wavelength of the fastest growing wave on that droplet is smaller than the droplet diameter. The droplet breaks up once the wave growth time is equal to the break-up time. The radius of the resulting child droplet is given by:

$$r_c = \frac{\pi C_{RT}}{K_{RT}} \tag{3.51}$$

where K_{RT} is the calculated wave number and C_{RT} is a constant used to adjust the in-cylinder fuel vapor distribution. The value of C_{RT} is typically set to 0.10.

3.6.3 In-cylinder Flow and Combustion Modeling

The CHEMKIN II chemistry solver [165] integrated into KIVA-3V is used to couple the chemical reactions with the in-cylinder flow solutions. The KIVA CFD model transmits to the CHEMKIN solver the mixture composition and thermodynamic conditions in each computational cell at every flow field solver time step. CHEMKIN then computes the mixture composition as well as the energy released or absorbed due to chemical reactions, and returns this updated information to the CFD model.

The Re-Normalization Group (RNG) $k-\in$ model was used for turbulent flow calculations [166], but sub-grid turbulence-chemistry interactions were not considered. Instead, the chemistry solver treats each computational cell as a well-stirred homogeneous reactor, with the rate of change of any species Y_i in the cell given by:

$$\frac{dY_i}{dt} = \frac{M_{r,i}}{\rho} \sum_{j=1}^{n_r} (v''_{j,i} - v'_{j,i}) \cdot q_j \tag{3.52}$$

where ρ is the average mixture density, $M_{r,i}$ is the molecular mass of Y_i, $v''_{j,i}$ and $v'_{j,i}$ are the forward and reverse stoichiometric coefficients, respectively, corresponding to Y_i of the jth chemical reaction (in a chemical reaction mechanism comprising n_r chemical reactions), and q_j is the reaction progress variable. The reaction progress variable q_j is in turn given by:

$$q_j = k_{f,j} \prod_{j=1}^{n_s} \left(\frac{\rho Y_i}{M_{r,i}} \right)^{v'_{k,j}} - k_{r,j} \prod_{j=1}^{n_s} \left(\frac{\rho Y_i}{M_{r,i}} \right)^{v''_{k,j}} \quad (3.53)$$

where $k_{f,j}$ is the forward reaction rate coefficient, $k_{r,j}$ is the reverse reaction rate coefficient and n_s is the number of species. The forward reaction rate coefficient is given by the Arrhenius Equation:

$$k_{f,j}(T) = A_j T^{b_j} e^{-\frac{E_{a,j}}{RT}} \quad (3.54)$$

where A_j is the pre-exponential factor, b_j is the temperature exponent and $E_{a,j}$ is the activation energy for the forward reaction. The reverse reaction rate coefficient can be obtained using the same equation, but is usually calculated from the equilibrium constant for each reaction.

For the combustion chemistry, a reduced Primary Reference Fuel (PRF) mechanism with 48 species and 142 reactions [167] was used. Iso-octane was used as the surrogate fuel to model the chemical and physical properties of gasoline, while n-heptane was used as the surrogate for diesel chemistry and tetradecane for the diesel spray break up, collision and evaporation. The reader is requested to consult Appendix D for the reactions considered in the PRF mechanism.

Since each of the reactions in the mechanism involves only a small number of species, the stoichiometric coefficient matrix for the differential equation is sparse. Hence, an analytical Jacobian algorithm called SpeedCHEM developed by Perini et. al. [168] was used to reduce the Chemistry computation time. Simulation time was further reduced through the use of cell clustering [169].

3.6.4 Wall Heat Transfer Model

Since the boundary layer of the in-cylinder flow is very thin relative to the computational grid resolution, a wall heat transfer model based on turbulent flow theory is needed to compute the convection heat transfer between the gas and solid boundaries. In KIVA-3V, the wall heat transfer model of Han and Reitz [170] is used. In this model, the wall heat flux is proportional to the logarithm of the ratio of the gas temperature to the solid wall temperature due to the variation in gas density within the cylinder. The wall heat flux q_w is given by:

$$q_w = \frac{\rho c_p u^* \bar{T} \cdot \ln\left(\frac{T}{T_w}\right)}{2.1 \ln(y^+) + 2.5} \tag{3.55}$$

where u^* is the friction velocity, $\bar{T}$ is the average temperature between the gas and the wall (i.e. $\bar{T} = \frac{T+T_w}{2}$), T_w is the wall temperature, and y^+ is the dimensionless distance from the wall.

3.6.5 Emission Formation Models

Pollutant species modeled using the reduced PRF mechanism include NOx and soot. NOx emissions are predicted using the Gas Research Institute (GRI) NO formation mechanism, which comprises 4 species and 12 reactions [171]. The GRI mechanism is itself part of the PRF mechanism, and is given by Equations 100 to 112 in Appendix D.

Soot emissions are evaluated using a phenomenological two-step soot model based on the work by Hiroyasu et al. [172] and are implemented in the code by Kong et al. [173]. This model uses acetylene (C_2H_2) as the soot inception species and determines the rate of change of soot mass within each computational cell using:

$$\frac{dm_{soot}}{dt} = \frac{dm_{soot,f}}{dt} - \frac{dm_{soot,o}}{dt} \tag{3.56}$$

where $\frac{dm_{soot,f}}{dt}$ is the rate of soot formation and $\frac{dm_{soot,o}}{dt}$ is the rate of soot oxidation. The soot formation rate is in turn proportional to the mass of acetylene $m_{C_2H_2}$, and is given by:

$$\frac{dm_{soot,f}}{dt} = A_f m_{C_2H_2} P^n e^{-\frac{E_{a,f}}{RT}} \tag{3.57}$$

The rate of soot oxidation is based on the Nagle and Strickland model of carbon oxidation [174, 175]:

$$\frac{dm_{soot,o}}{dt} = \frac{6M_{r,C}}{\rho_{soot} D_{soot}} \cdot m_{soot} R_{ox} \tag{3.58}$$

where $M_{r,C}$ is the atomic mass of carbon, ρ_{soot} is the soot density with a value of 2 g cm^{-3} and D_{soot} is the soot particle diameter with a value of 0.025 μm.

3.7 Turbocharger Map Scaling Procedure using Dimensional Analysis

To accommodate the lower exhaust gas flow rates through the turbocharger turbine in the Divided Exhaust Period (DEP) concept, a smaller turbocharger would have to be used. In addition, the new turbocharger should be able to efficiently utilize the low exhaust gas enthalpy from Low Temperature Combustion to generate the required boost over a wide range of operating points so that the pumping penalty can be mitigated. In order to accomplish the aforementioned criteria, the new turbocharger must be properly matched to the engine such that its geometry and flow characteristics are compatible with the flow characteristics of the engine over the engine's operating range.

Turbocharger matching has traditionally been done through trial-and-error, which is time consuming and laborious. Moreover, turbine and compressor test data from turbocharger manufacturers is often proprietary and hence difficult to obtain. Therefore, a more systematic method that allows one to generate new turbocharger maps from existing maps is required. One such method involves the use of dimensional analysis. This section presents the dimensional analysis techniques described by [176] and [177] used to express turbine and compressor maps in terms of non-dimensional parameters and select the required turbine and compressor wheel diameters.

The turbine mass flow parameter and speed parameter are first converted to the non-dimensional quantities of mass flow coefficient $\emptyset_{turb}$ and the rotor/blade tip Mach Number M_{turb} given by:

Turbine Mass Flow Coefficient:

$$\emptyset_{turb} = \frac{\dot{m}_r\sqrt{R_{exh}}}{d_{turb}^2} = \frac{\dot{m}_{exh}\sqrt{R_{exh}T_{0,exh}}}{p_{0,exh}d_{turb}^2} \tag{3.59}$$

Turbine Blade Tip Mach Number:

$$M_{turb} = \frac{2\pi}{60}\cdot\frac{N_r d_{turb}}{\sqrt{\gamma_{exh}R_{exh}}} = \frac{2\pi N_{tc} d_{turb}}{60\cdot\sqrt{\gamma_{exh}R_{exh}T_{0,exh}}} \tag{3.60}$$

For the turbine, the specific gas constant for the exhaust flow has a value of $289\ \mathrm{J\ kg^{-1}K^{-1}}$ and the specific heat ratio of the exhaust gas is 1.35.

A similar approach is followed to convert the compressor corrected mass flow rate and corrected speed parameter to the compressor mass flow coefficient $\emptyset_{comp}$ and the blade tip Mach Number M_{comp}:

Compressor Mass Flow Coefficient:

$$\emptyset_C = \frac{\dot{m}_{comp,corr}\sqrt{R_{air}T_{ref}}}{p_{ref} \cdot d_{comp}^2} \tag{3.61}$$

Compressor Blade Tip Mach Number:

$$M_{comp} = \frac{2\pi}{60} \cdot \frac{N_{comp,corr}d_{comp}}{\sqrt{\gamma_{air}R_{air}T_{ref}}} \tag{3.62}$$

Once the flow and speed parameters have been converted to dimensionless quantities, the non-dimensional turbine and compressor maps can be plotted as shown in Figures 3-12 and 3-13 respectively. (Refer back to Figures 3-7 and 3-8 for the turbine and compressor maps with dimensions.)

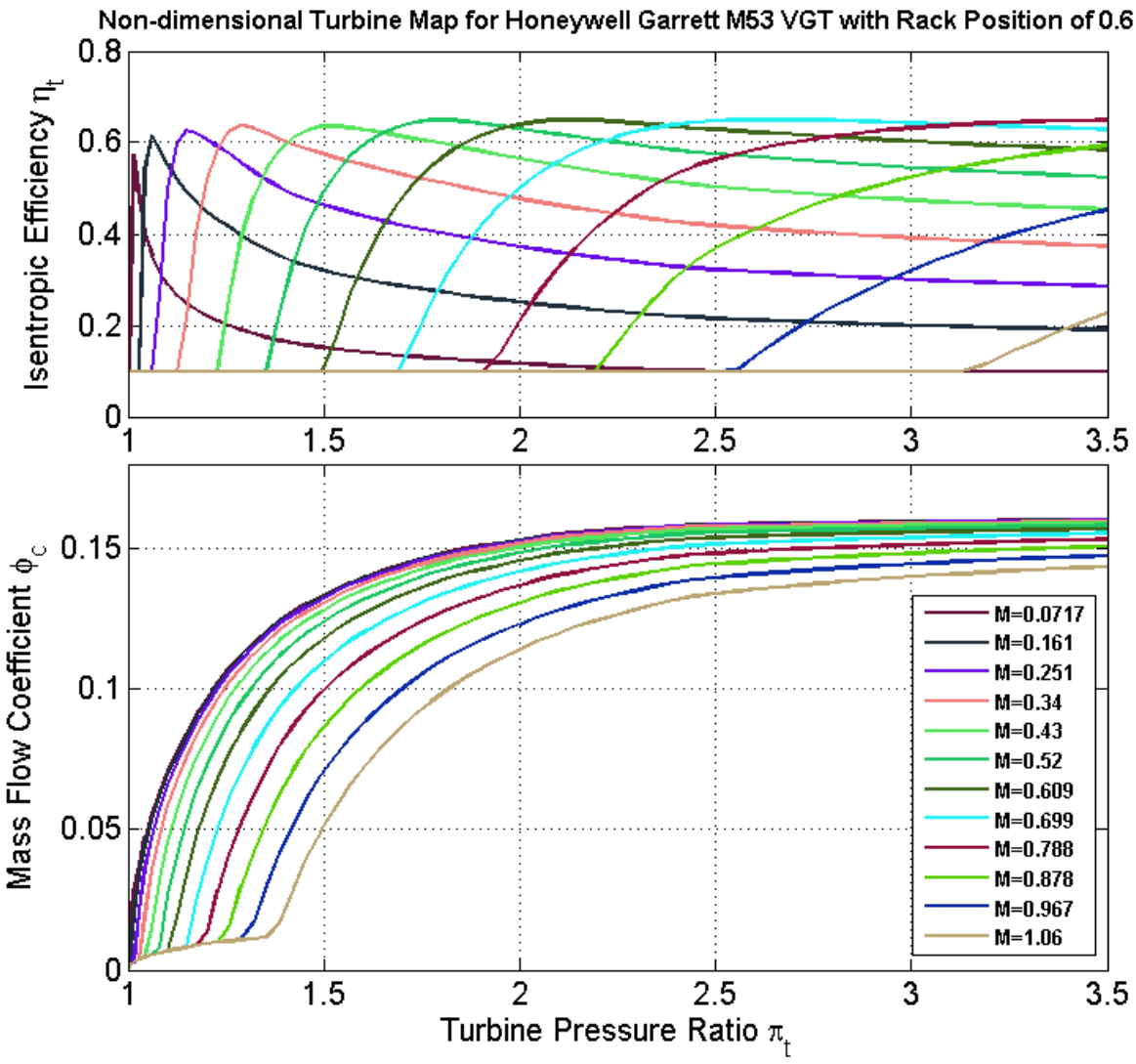

Figure 3-12: Non-dimensional Turbine Map for the Honeywell Garrett M53 VGT Family of Geometrically Similar Turbochargers at a Rack Position of 0.6 (T60 Family of Speed Lines).

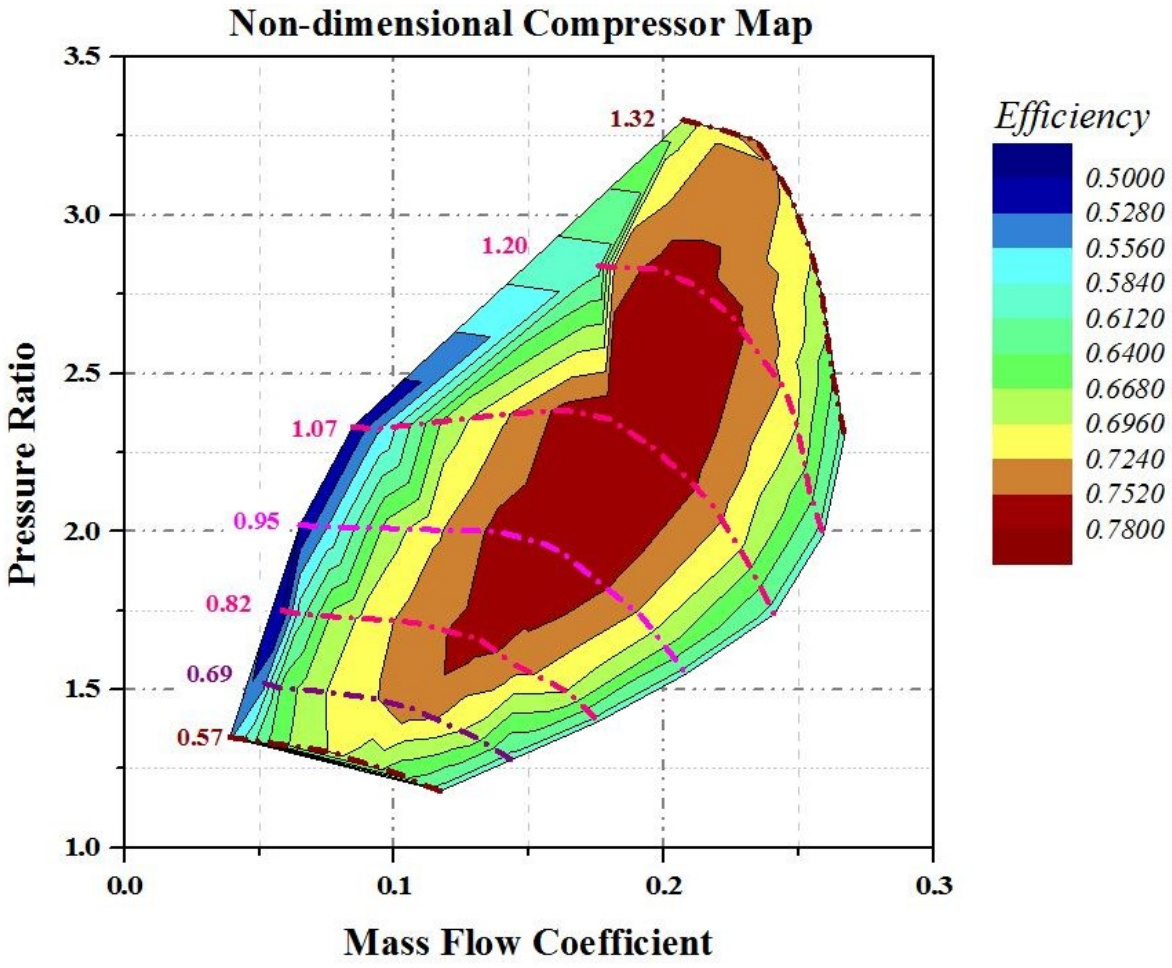

Figure 3-13: Non-dimensional Compressor Map for the Honeywell Garrett M53 VGT Family of Turbochargers. The isolines from 0.57 to 1.32 represent the blade tip Mach Numbers.

In Bell et al. [177], the desired compressor specifications are evaluated first, following which the matching turbine specifications are determined. For turbocharger matching of LTC engines, it might make more sense to evaluate the turbine requirements first due to the low exhaust enthalpy observed in LTC strategies, which limits the useful work that can be extracted by the turbine. Moreover, the turbine performance is heavily influenced by the variable valve timing strategies as well as the high EGR fractions required to keep the peak pressure rise rate within the acceptable limit of 10 bar/degree. Thus, for this research, the turbine parameters were calculated first.

The required turbine and compressor wheel diameters are calculated as follows:

1. First, the desired operating point at which the turbine is to be matched is selected. This desired operating point should ideally be the most frequently attained point during normal driving conditions. At this point, the cycle-averaged exhaust mass flow rate, the cycle-averaged turbine pressure ratio (or expansion ratio), and the cycle averaged exhaust temperature from EES (or GT-Power) simulations are calculated.
2. The maximum isentropic efficiency value in the non-dimensional turbine map is chosen for the pressure ratio calculated in Step 1, and the corresponding mass flow coefficient value is identified. Note that the mass flow coefficient and the isentropic efficiency η_T should be obtained from the pair of curves that correspond to the same blade tip Mach Number.
3. The value of mass flow coefficient evaluated in Step 2, the cycle-averaged exhaust mass flow rate, the cycle-averaged turbine pressure ratio Π_T, and the cycle-averaged exhaust temperature are substituted into Equation 3.59, and the new turbine wheel diameter is obtained.
4. Using the blade tip Mach Number obtained in Step 2 and the calculated turbine wheel diameter, the turbocharger speed can be evaluated using Equation 3.60. From the turbocharger speed, the torque produced by the turbine can be calculated using:

$$\tau_T = \frac{\eta_{s,t}\dot{m}_{exh}c_{p,exh}T_{0,exh}}{\omega_{TC}} \cdot \left(1 - \Pi_T^{\frac{\gamma_{exh}-1}{\gamma_{exh}}}\right) \tag{3.63}$$

5. A torque balance is established between the turbine and the compressor: $\boldsymbol{\tau_T = \tau_C}$. The torque generated in the compressor is given by:

$$\tau_C = \frac{\dot{m}_{int}c_{p,int}T_{int}}{\eta_{s,c}\omega_{TC}} \cdot \left(\Pi_C^{\frac{\gamma_{air}-1}{\gamma_{air}}} - 1\right) \tag{3.64}$$

6. A guess value for the compressor isentropic efficiency is chosen and substituted into the compressor torque equation to find the compressor pressure ratio. The required intake temperature and intake mass flow rate at the selected operating point should already be known.

7. The compressor mass flow coefficient is then selected for the calculated value of compressor pressure ratio and the efficiency guess value. From the mass flow coefficient Equation 3.61, the compressor wheel diameter may be evaluated.
8. The blade tip Mach Number for the compressor is then calculated by substituting this new value of the compressor wheel diameter into Equation 3.62. If there is a mismatch between the calculated Mach Number and the region in the non-dimensional compressor map where the operating point falls, a new guess value for the isentropic efficiency is selected and Steps 6 and 7 are repeated to recalculate the compressor wheel diameter until a correct value of the wheel diameter is obtained.

3.8 Chapter Summary

This chapter covered in detail the characteristics of different engine simulation modeling techniques: the zero-dimensional filling-and-emptying method, one-dimensional gas dynamics, and three-dimensional CFD coupled with combustion chemistry. For each technique, the differential equations representing the system and the solution procedure were covered. The chapter also presented a turbocharger scaling method based on dimensional analysis. In the next chapter, Chapter 4, the models discussed in this chapter are validated with experimental data before proceeding with the simulation studies. Chapter 7 presents the results of the turbocharger scaling to establish a new turbocharger design for the Divided Exhaust Period concept.

CHAPTER 4: MODEL VALIDATION

Before the GT-Power, KIVA and EES models were used to perform the simulation studies described in the upcoming chapters, they were validated with data obtained from multi-cylinder engine experiments as well as simulation data from earlier work. This chapter describes the model validation procedures for each of the aforementioned simulation models. Section 4.1 describes the coupled KIVA and GT-Power simulation validation procedure as well as presents the validation results, followed by Section 4.2 which discusses the validation procedure and results of the EES filling-and-emptying model.

4.1 KIVA and GT-Power Model Validation

The flowchart in Figure 4-1 shows the approach used in validating the KIVA-3V and GT-Power models.

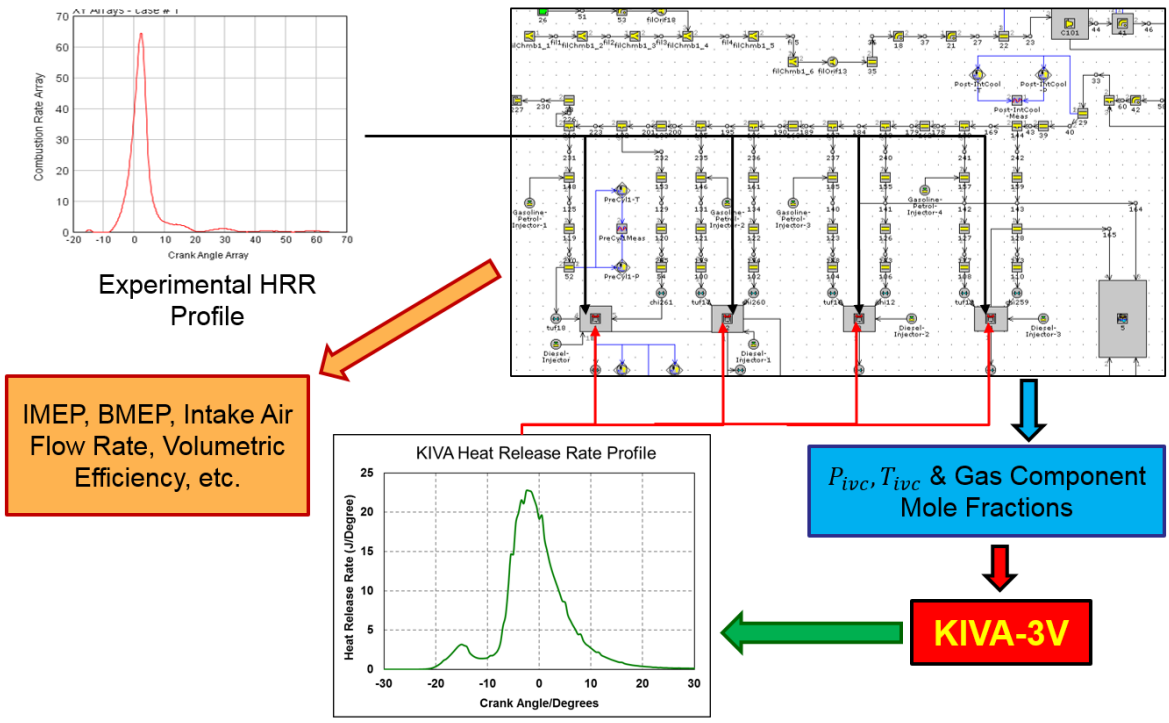

Figure 4-1: GT-Power and KIVA-3V Model Validation Approach

Heat release data calculated from experimental in-cylinder pressure data was fed as input into the GT-Power model to calculate the pressure and temperature of the intake charge at IVC. The IVC temperature and pressure were then used to calculate the chemical composition of the intake charge,

specifically the mole fractions of nitrogen, oxygen and iso-octane, and if EGR was used, the mole fractions of carbon dioxide, carbon monoxide and water as well. The mole fractions of the gaseous components, along with the IVC temperature and pressure, and the experimental injection profile were used as inputs for the KIVA simulation to obtain the predicted heat release rate (HRR) curves.

The HRR curves were then fed back into the GT-Power model to obtain the engine performance parameters such as IMEP, BMEP, intake air flow rate and volumetric efficiency. It is important to note that the heat transfer coefficient of the working gas in the cylinder, calculated by the Woschni model [147] in GT-Power, was tuned to match the heat transfer at EVO obtained from the KIVA simulation, similar to the approach used in [161].

4.1.1 Model Validation for Stock Piston Geometry

The stock piston with the re-entrant bowl geometry (given in Figure 3-10a in Chapter 3) and a compression ratio of 16.7 was validated the low load operating points of 1 Bar BMEP, 2.6 Bar BMEP and 4 Bar BMEP. This piston geometry was used for the Early Exhaust Valve Opening (EEVO) and cylinder deactivation studies. Table 4-1 gives the experimental parameters for the aforementioned three low load operating points.

Table 4-1. Experimental Data Points for Stock Piston Geometry Validation

	1 Bar BMEP	**2.6 Bar BMEP**	**4 Bar BMEP**
Intake Manifold Pressure (Bar)	1.006	1.02	1.06
Fuel Energy (J)	275.1	393	563.3
Engine Speed (rev/min)	1,500		
Gasoline Quantity (mg/cyl/cyc)	3.525	6.321	10.5
Diesel Quantity (mg/cyl/cyc)	2.619	2.482	2.1
Gasoline Start of Injection (deg.)	-227.4		
Diesel Start of Injection (deg.)	-40	-42	-45
Diesel Fuel Rail Pressure (Bar)	400		480
EGR Fraction (%)	49.9	44.9	0

The experimental heat release rate curves for the 1, 2.6 and 4 Bar BMEP operating points were fed into the GT-Power model along with the fueling quantity, boost pressure and EGR fraction to obtain the in-cylinder pressure and temperature values at IVC, which were then fed into a MATLAB code to calculate the mole fractions of the gaseous components at IVC. Table 4-2 gives the values of the IVC pressure, IVC temperature and mole fractions for each of the low load points. It is important to note that in order to match the pressure traces in KIVA for the 1 Bar BMEP and 2.6 Bar BMEP load points, carbon monoxide had to be included, along with additional iso-octane so that the unburnt fuel and partially oxidized fuel in the EGR was also accounted for in the heat release.

Table 4-2. KIVA Inputs at Intake Valve Closure for Low Load Points

Load Point (Bar BMEP)	**1**	**2.6**	**4**
IVC Pressure (Bar)	1.17	1.20	1.28
IVC Temperature (K)	370	402	356
Gas Species Mole Fractions			
Iso-octane	0.002123	0.003428	0.004726
Nitrogen	0.777467	0.773816	0.786267
Oxygen	0.168388	0.158294	0.209008
Carbon Dioxide	0.021709	0.029695	0
Water Vapor	0.027274	0.033909	0
Carbon Monoxide	0.003039	8.58×10^{-4}	0

Since the n-heptane (representing the diesel fuel) was directly injected into the cylinder, injection profiles had to be specified into KIVA-3V to model the in-cylinder fuel injection process. The engine uses Bosch CRIP2-MI Common Rail Injectors for diesel injection, so the injection profiles for each load point were obtained by linearly interpolating and scaling the injection profiles for the CRIP2-MI obtained from injector characterization experiments. Figure 4-2 shows the injection profiles used for the 1, 2.6 and 4 Bar BMEP load points.

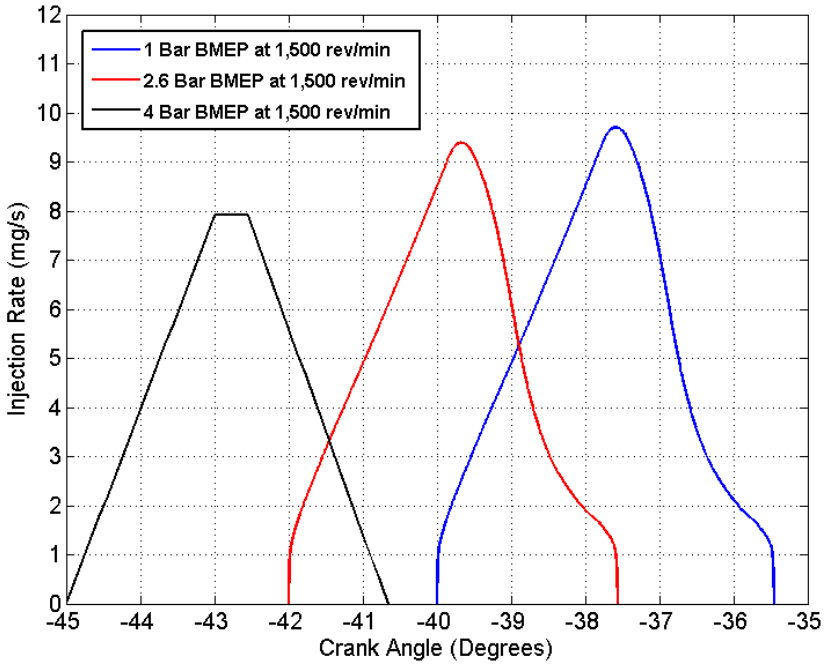

Figure 4-2: Injection Rate Profiles for the 1, 2.6 and 4 Bar BMEP load points

Table 4-3 gives the values of the combustion chamber boundary temperatures used as the boundary conditions for calculating the heat losses in KIVA-3V for the 1, 2.6 and 4 Bar BMEP load points. The values of 390 K for the cylinder liner temperature and 440 K for the cylinder wall and head temperatures are typical values used for low load simulations.

Table 4-3: Combustion Chamber Temperature Boundary Conditions for KIVA-3V

Parameter	Value
Cylinder Liner Temperature (K)	390
Cylinder Head Temperature (K)	440
Cylinder Wall Temperature (K)	440

The pressure traces and heat release rate curves obtained from KIVA were then compared with pressure traces and apparent heat release rate curves from experiments. As shown in Figures 4-3, 4-4 and 4-5, KIVA successfully captured the experimental pressure traces.

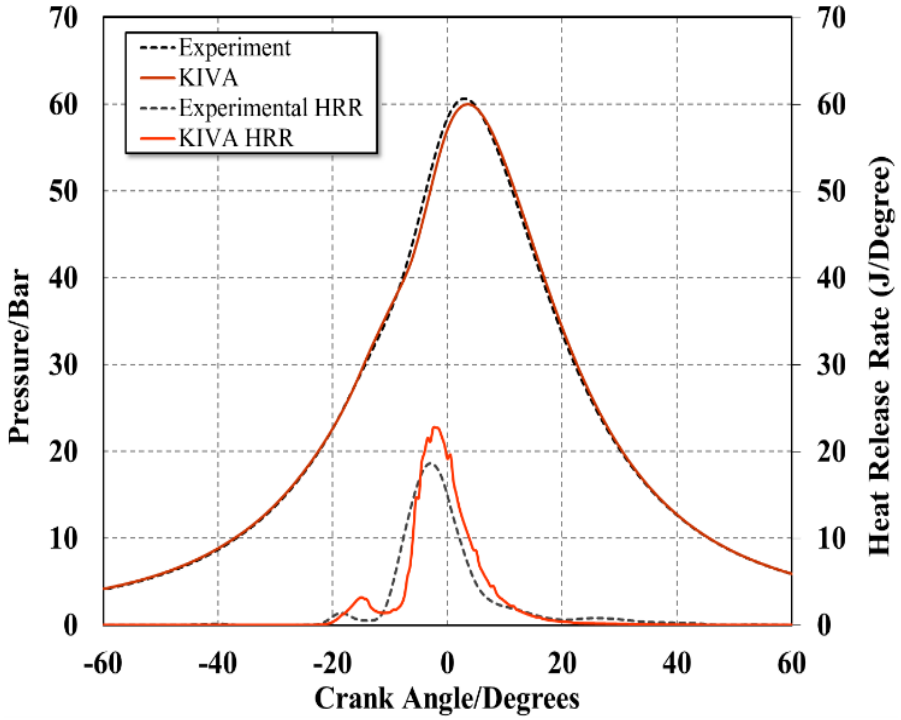

Figure 4-3: Pressure Trace and Heat Release Rate Curves from experiments and KIVA-3V simulations for 1 Bar BMEP at $1,500\ \text{rev} \cdot \text{min}^{-1}$.

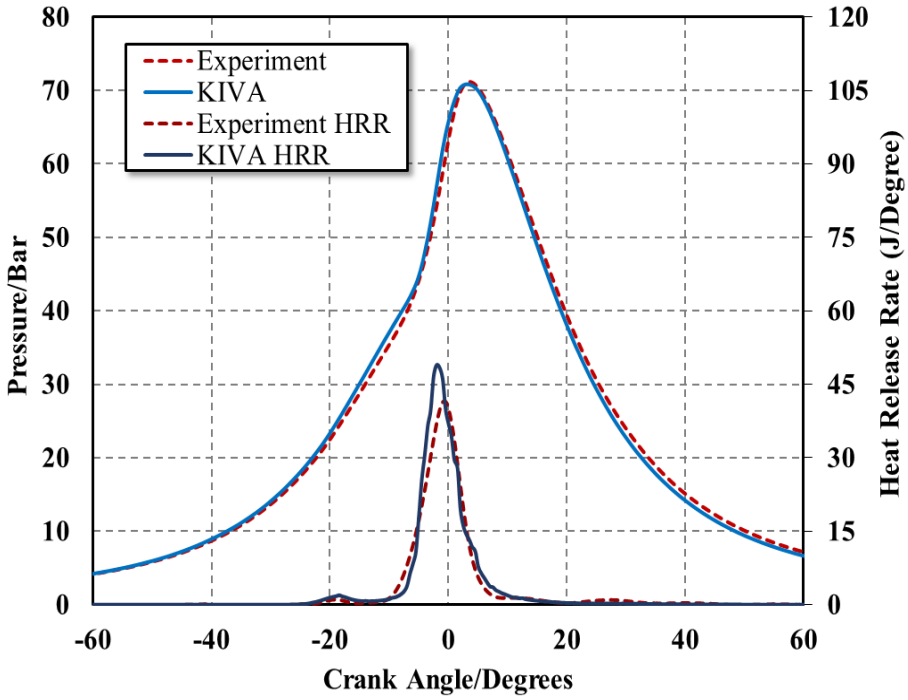

Figure 4-4: Pressure Trace and Heat Release Rate Curves from experiments and KIVA-3V simulations for 2.6 Bar BMEP at $1,500\ \text{rev} \cdot \text{min}^{-1}$.

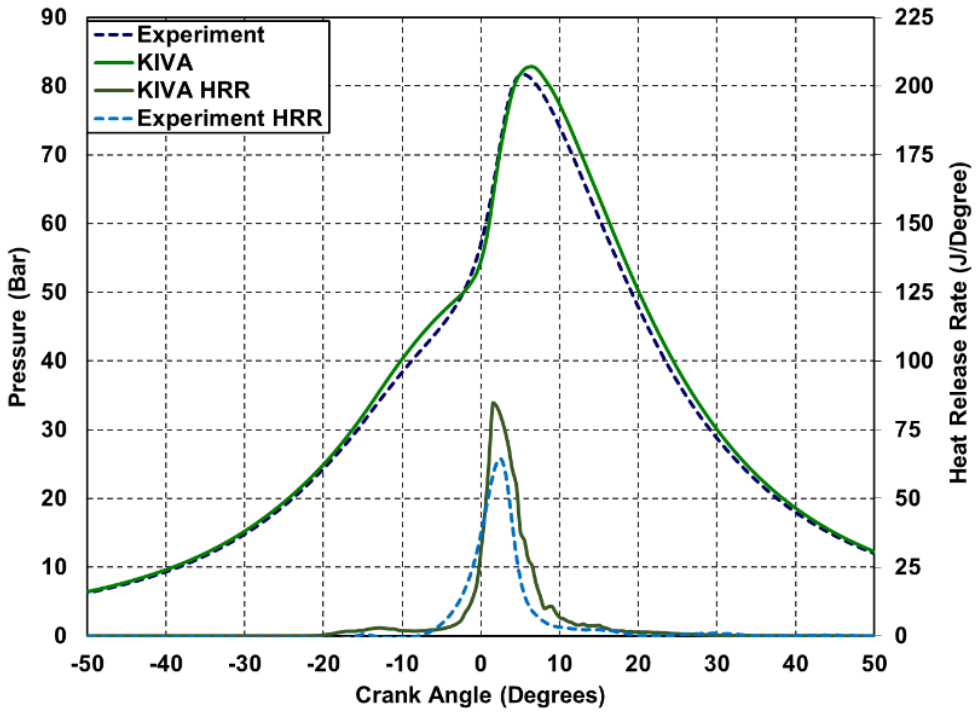

Figure 4-5: Pressure Trace and Heat Release Rate Curves from experiments and KIVA-3V simulations for 4 Bar BMEP at $1,500\ \mathbf{rev \cdot min^{-1}}$.

4.1.2 Model Validation for RCCI Piston Geometry

As described in the previous chapter, the RCCI piston was flat bottomed, and the compression ratio of the engine was reduced to 15.1 when this piston was used. The KIVA-3V model for the RCCI piston geometry was validated against experimental data for the 8 Bar BMEP at $3{,}000\ rev \cdot min^{-1}$ operating point, and Table 4-4 gives the experimental parameters.

Some of the experimental parameters had to be adjusted so that the simulation pressure trace would be accurately matched with the experimental pressure trace. In an actual experiment, since there would be up to a 5% uncertainty in the fuel flow rate and the boost pressure measurements, these parameters were adjusted until the simulation results matched the experimental results. Moreover, in KIVA-3V, the chemical kinetics is sensitive to the IVC temperature, and since the chemical reaction rate constants for each of the reactions in the chemical mechanism were tuned for a particular case [167], it was necessary to adjust the value of IVC temperature to allow the earlier tuned constants to match the experimental pressure trace. The

reaction rate constants could be retuned for each operating point, but that would require too much effort and is out of the scope of this research.

Table 4-4. 8 Bar BMEP at $3,000\ \mathrm{rev \cdot min^{-1}}$ Operating Point Experimental Parameters

	Experiment	Adjusted Value for Simulation
Intake Manifold Pressure (Bar)	1.572	1.62
IVC Pressure (Bar)	1.9	2.04
IVC Temperature (K)	357	390
Fuel Energy (J)	930.4	930.4
Engine Speed (rev/min)	3,000	
Gasoline Quantity (mg/cyl/cyc)	19.3	18.34
Diesel Quantity (mg/cyl/cyc)	2.6	2.44
Gasoline Start of Injection (deg.)	-227.4	
Diesel Pilot Start of Injection (deg.)	-54	
Diesel Main Start of Injection (deg.)	-20.7	
Pilot Injection Fuel Split (%)	60	
Main Injection Fuel Split (%)	40	
Diesel Fuel Rail Pressure (Bar)	500	
EGR Fraction (%)	0	5.45

Table 4-5 gives the values of the combustion chamber boundary temperatures used as the boundary conditions for calculating the heat losses in KIVA-3V for the 8 Bar BMEP operating point. These values were chosen through trial and error until the expansion stroke of the KIVA pressure trace matched the expansion stroke of the experimental pressure trace.

Table 4-5: Combustion Chamber Temperature Boundary Conditions for KIVA-3V at 8 Bar BMEP

Parameter	Value
Cylinder Liner Temperature (K)	465
Cylinder Head Temperature (K)	465
Cylinder Wall Temperature (K)	440

Figure 4-6 shows the injection profiles used for the 8 Bar BMEP load point. Note that this load point requires the use of two injections of diesel fuel: the pilot injection at 54 degrees BTDC for fuel conditioning, and the main injection at 20 degrees BTDC. The fuel split is 60:40 between the two injections.

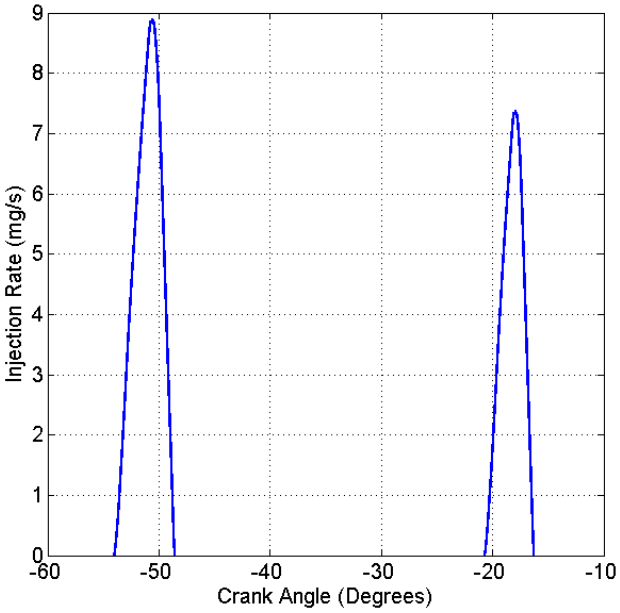

Figure 4-6: Diesel Fuel Injection Profile for 8 Bar BMEP Load Point

As Figure 4-7 shows, the adjusted parameters enabled the KIVA simulation to accurately capture the experimental pressure trace.

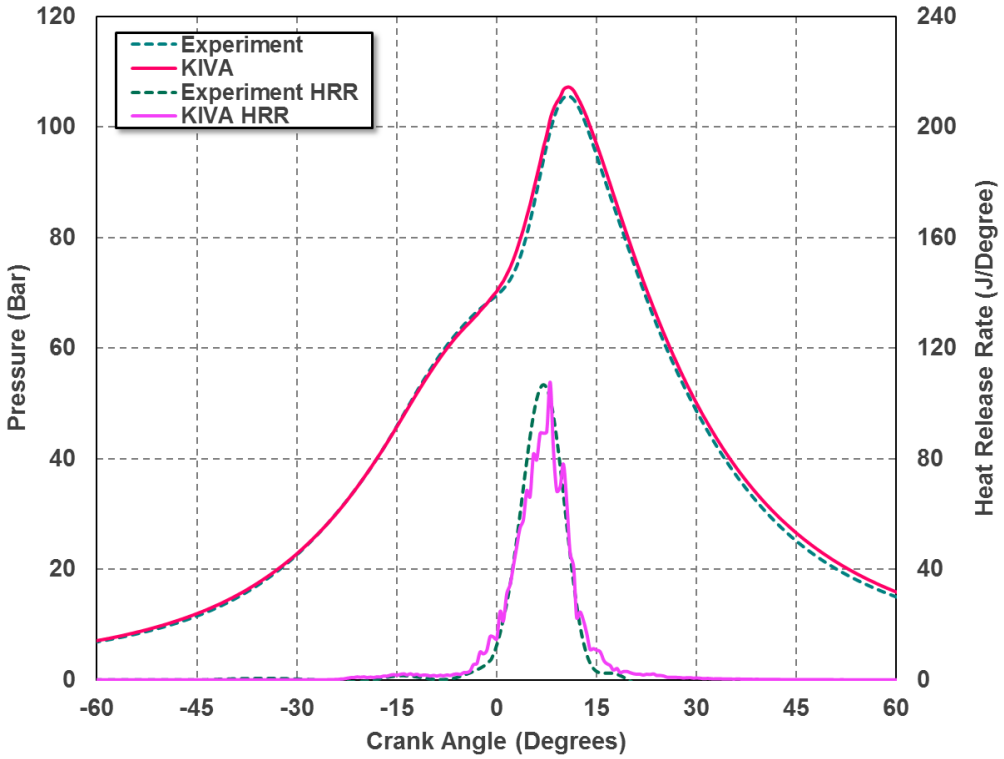

Figure 4-7: Pressure Trace and Heat Release Rate Curves from experiments and KIVA-3V simulations for 8 Bar BMEP at $3,000\ \text{rev} \cdot \text{min}^{-1}$.

4.1.3 GT-Power Engine System Model Validation

The heat release rate profiles and combustion efficiency values obtained from the KIVA simulations (shown in Figures 4-3, 4-4, 4-5 and 4-7) were then fed back into the GT-Power model to obtain the engine performance parameters such as BMEP, exhaust gas temperatures, intake air flow rates and turbocharger speed. The in-cylinder heat transfer coefficient evaluated by the Woschni model in GT-Power had to be adjusted through the use of a heat transfer multiplier to match the heat losses evaluated by KIVA at EVO, similar to the method used in [161]. The GT-Power evaluated engine performance parameters for the low load operating points are given in Table 4-3, while the 8 Bar BMEP operating point values are given in Table 4-4. From these tables, it can be seen that the GT-Power model captured the engine performance quantities with acceptable accuracy.

Table 4-6. Comparison between Simulations and Experiments for Low Load Points

Quantity	1 Bar BMEP		2.6 Bar BMEP		4 Bar BMEP	
	Expt.	Simul.	Expt.	Simul.	Expt.	Simul.
BMEP (Bar)	1.1	1.06	2.65	2.42	4.00	4.15
Intake Air Flow Rate (kg/h)	41.11	41.86	45.07	45.24	89.8	93.9
Exhaust Gas Temp. (K)	440.2	448.2	501.2	491.2	N/A	500.2

Table 4-7. Comparison between Simulations and Experiments for 8 Bar BMEP at $3,000\ \mathrm{rev \cdot min^{-1}}$

	Simulation	Experiment
BMEP (Bar)	8.15	8
Intake Air Flow Rate (kg/h)	304.18	305.22
Turbocharger Speed (rev/min)	133,932	129,250
Turbine Inlet Temperature (K)	647	612

4.1.4 GT-Power Diesel Oxidation Catalyst Model Validation

A different set of RCCI operating points for which experimental emissions data pre- and post-catalyst was available was used to calibrate the GT-Power DOC aftertreatment model. Table 4-8 shows RCCI data points used for calibrating the GT-Power DOC model.

Table 4-8. RCCI experimental data for DOC model validation

Load (Bar)	1	2	3	4
Operating conditions				
Exhaust Gas Temp. (K)	419	445	480	516
Air Flow Rate(kg/hr)	88	87	87	89
DI(mg/inj)	3.864	4.278	4.264	3.396
PFI(mg/inj)	2.812	4.178	6.7	9.49
Engine Speed (rev/min)	1,500			
Emissions				
Pre-DOC UHC (ppm)	1,192	1,006	1,108	1,091
Post-DOC UHC (ppm)	1,128	1,182	1,019	147
NO (ppm)	5.5	8.56	4.81	6.26
CO (ppm)	7,005	5,820	2,458	1,432
H_2O (%)	2.3	3.07	4.05	4.69
CO_2(%)	2.8	2.54	3.98	4.7
O_2(%)	16.96	15.35	14.3	13

The developer supplied "DOC_Sampara_and_Bissett" example model was used as the starting point for validation. This model already has default values for exhaust temperatures, gas concentration, flow rate and catalyst Pt-dispersion. Firstly, warm-up behavior was verified with a test where only air (O_2 + N_2) was directed through the catalyst, and the geometrical and thermal inputs were checked. Exhaust temperature, gas concentration and flow rates for the above mentioned RCCI steady state cases were available from experiments. Using the pre- and post-catalyst UHC concentrations, the Pt-dispersion was adjusted until the model output matched the experiments.

Post-DOC UHC from the 1, 2 and 4 Bar RCCI cases matched the experiments with the default Pt-dispersion from the baseline model but the UHC emissions for the 3 Bar case were not captured accurately by the model. Hence the 3 Bar RCCI case was taken to calibrate the GT-Power model further as this was in the DOC light-off temperature range. The Pt-dispersion factor was changed to 1.45% to fit the experiments for all the RCCI cases. Figure 4-8 shows the results obtained from experiments and the GT-Power model for RCCI steady state cases after calibration.

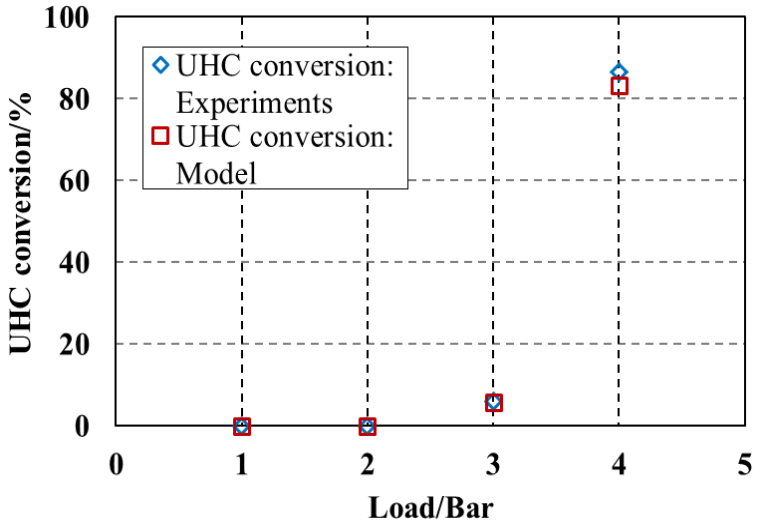

Figure 4-8. Validation of UHC conversion in GT-Power model with experimental data

The GT-Power DOC model was further calibrated using CDC test cases from experiments to increase confidence in the model. Table 4-9 shows CDC data used for calibrating the DOC model.

Table 4-9. CDC experimental data for DOC calibration

Load (bar)	1	2	3	4
Operating conditions				
Exhaust Gas Temp (K)	464	522	570	608
Air flow(kg/hr)	53.5	54	61	68
DI(mg/inj)	13.3	10.88	8.01	5.43
Engine Speed (rev/min)	1500			
Emissions				
Pre-DOC UHC (ppm)	203	144	95	75
Post-DOC UHC (ppm)	123	3.5	1.05	1.32
NO (ppm)	40	57	106	148
CO (ppm)	757	560	381	273
H_2O (%)	3.34	4.48	5.81	6.69
CO_2(%)	3.695	5.51	6.65	7.59
O_2(%)	19.25	12.6	10.75	9.45

A Pt-dispersion factor of 3.1% was used to match the CDC experimental UHC conversion. This was slightly higher than that used for the RCCI cases due to the difference in exhaust gas compositions between RCCI and CDC cases. CDC experiments were run much earlier than RCCI experiments. As Pt-dispersion reduces with catalyst age [178], RCCI cases had a lower Pt-dispersion factor. Figure 4-9 shows the results obtained from experiments and the GT-Power model for CDC steady state cases after calibration.

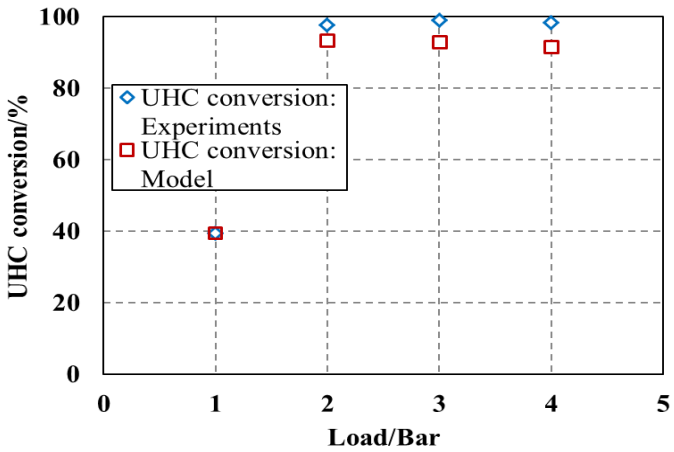

Figure 4-9. DOC calibration of results from CDC experiments

4.2 Zero-dimensional Filling-and-Emptying Model Validation

The zero-dimensional filling-and-emptying model in EES was validated against a single-cylinder version of the GT-Power model for the General Motors Z19DTH 1.9L engine. The 8 Bar BMEP at 3,000 $rev \cdot min^{-1}$ operating point was used to validate the EES model. The HRR curve for the 8 Bar BMEP operating point (shown in Figure 4-5) was curve fit to the Wiebe function given by Equation 3.9.

As shown by the p-V plot in Figure 4-10, the model results match with the GT-Power results with great accuracy.

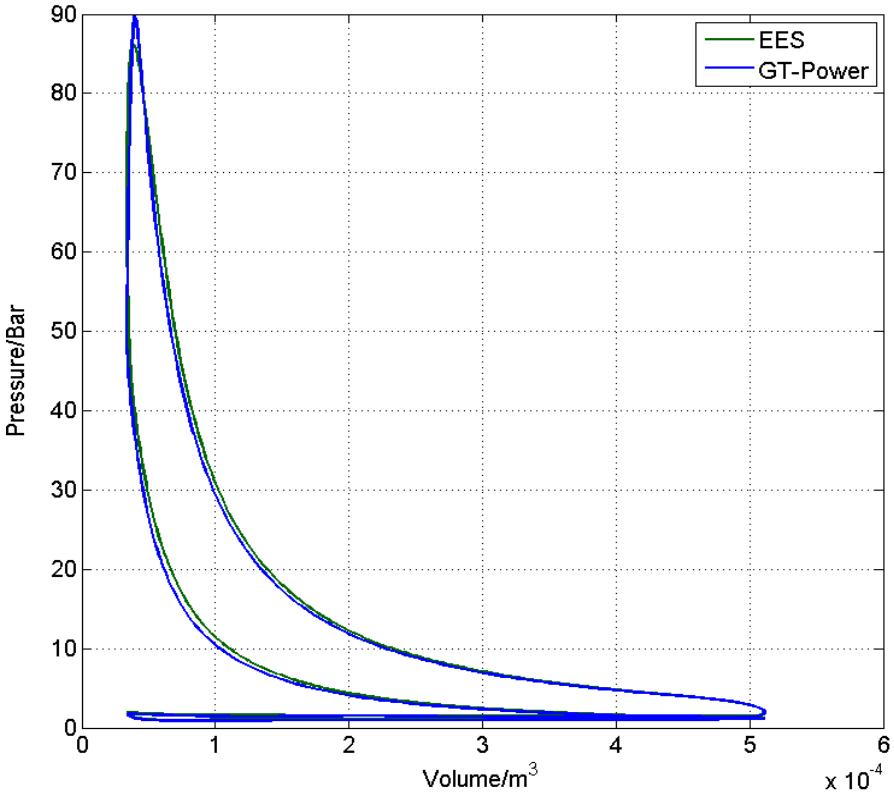

Figure 4-10: p-V plot for comparison of EES Code and GT-Power Results.

The flow through the exhaust ports are given in Figure(s) 4-11. 4-11a shows the Mach Number evolution over crank angle from EVO to EVC, while 4-11b shows the actual mass flow rate in kg/s. The model once again matches the GT-Power results very well. But, because the momentum equation was not considered in the model, the pressure wave effects seen in GT-Power results were not captured. This is however not a problem, because one of the main objectives of the model is to separate out gas dynamic effects seen in GT-Power so that a thermodynamic analysis can be performed to determine the operating conditions/parameters with the best thermal efficiency before optimizing those operating conditions in GT-Power.

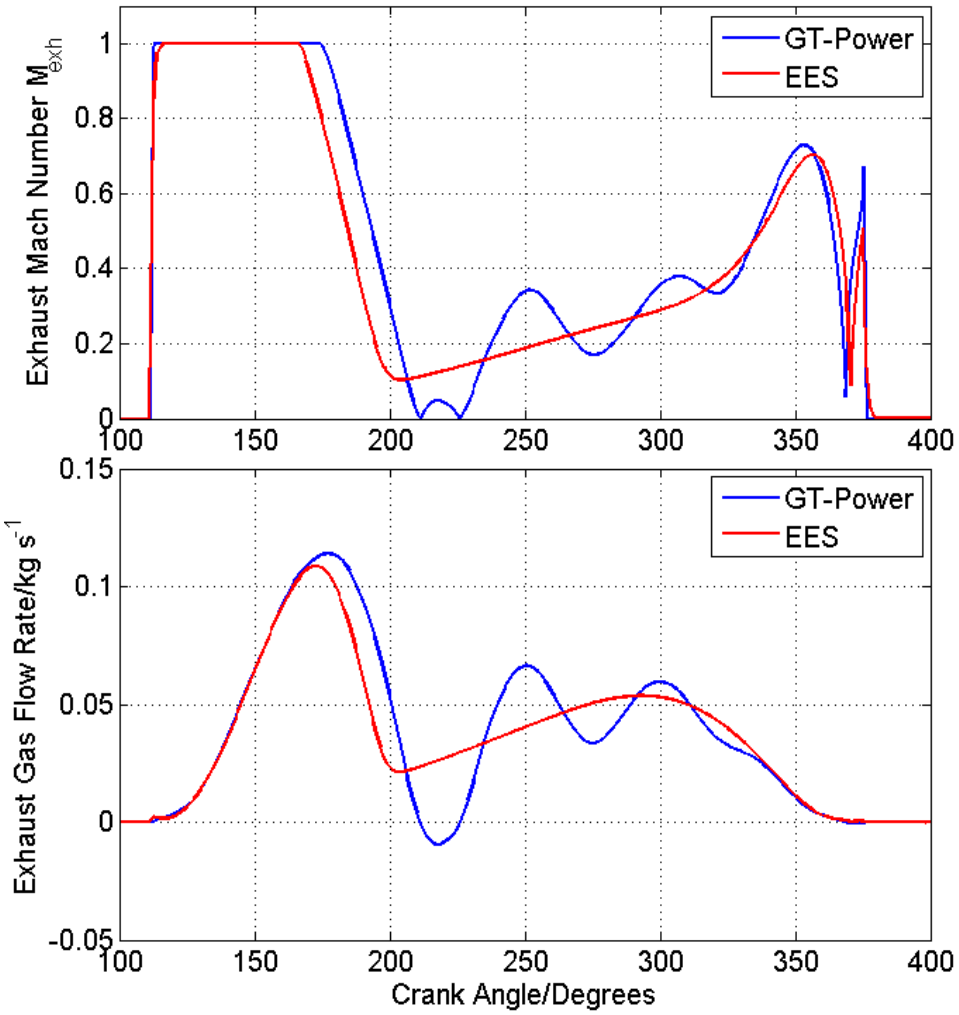

Figure 4-11: Exhaust Port Flow Results Comparison (4-11a (Top): Mach Number; 4-11b (Bottom): Exhaust Mass Flow Rate (in kg/s))

The results for the exhaust manifold pressure are given in Figure 4-12. Similar to the Mach Number and exhaust flow rate results for the exhaust ports, the pressure profile in the exhaust manifold is captured by the 0-D code, but without the pressure wave effects seen in GT-Power. The pressures are also slightly higher because the exhaust manifold is modeled as a constant volume adiabatic reservoir to allow us to determine the maximum possible potential pressure work that can be recovered by the turbine.

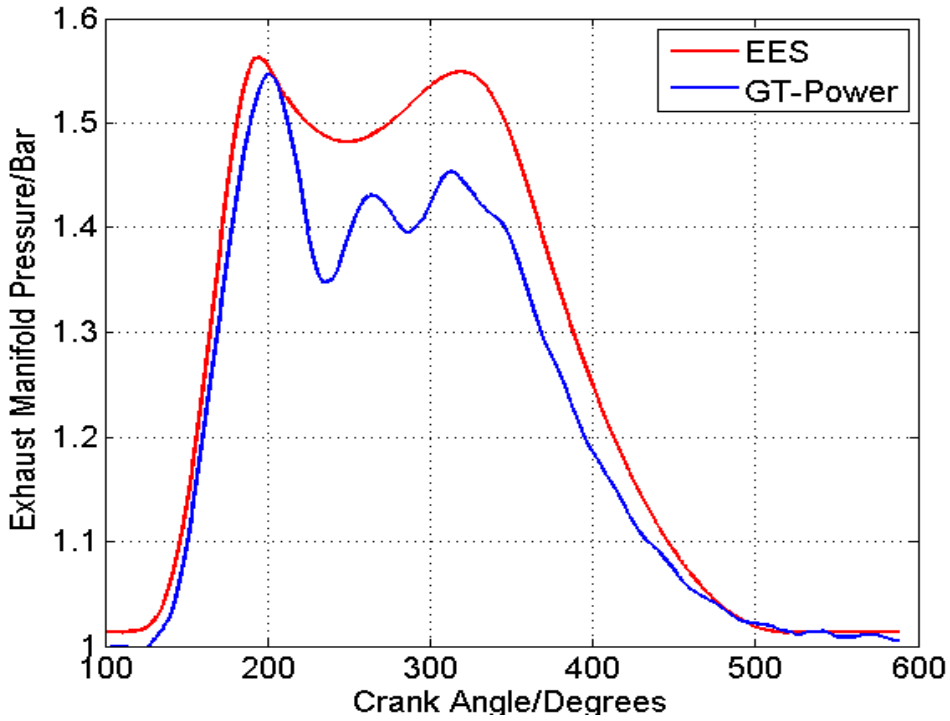

Figure 4-12: Exhaust Manifold Pressure Results

Table 4-10 gives the thermodynamic property parameter comparison between the 2 codes. As can be seen, the results are captured with acceptable fidelity by the 0-D code.

Table 4-10 Thermodynamic Parameter Comparison between GT-Power and EES

	GT-Power	**0-D Code**
Average Exhaust Pressure/Bar	1.146	1.183
Trapped Mass/mg	618.03	628.9
IVC Pres./Bar	1.367	1.415
IVC Temp./K	346.01	354.6
Heat Loss at EVO/J	98.99	112.7

Table 4-11 gives the engine performance parameters between the two codes. Once again, the results are captured with adequate fidelity. The pumping work is similar because of the similarity in backpressure difference between the two codes.

Table 4-11 Engine Performance Parameter Comparison between GT-Power and EES

	GT-Power	0-D Code
Gross IMEP/Bar	9.59	9.65
Net IMEP/Bar	9.07	9.14
PMEP/Bar	-0.52	-0.51
Gross Thermal Efficiency (%)	49.4	49.5
Net Thermal Efficiency (%)	47	46.9

4.3 Model Validation Conclusions

In this chapter the various engine simulation models were properly calibrated and validated with experimental data to ensure that they were suitable for the simulation studies in the upcoming chapters. Validation of the models sometimes required certain changes to the experimental parameters used as model inputs, such as a change in the fueling rates and the intercooler wall temperatures. These parameters had to be adjusted depending on the accuracy and quality of the experimental measurements available. Because the intake air flow rate in experiments and the in-cylinder pressure are measured with a Laminar Flow Element (LFE) and a high sampling rate pressure transducer, respectively, these measurements are by nature highly accurate, and so it was decided that matching the intake air flow rate and in-cylinder pressure trace was very crucial for model validation, and that uncertainties up to 10% in other measurements, such as fuel flow rate were acceptable.

CHAPTER 5: LOW LOAD OPTIMIZATION USING VARIABLE VALVE ACTUATION STRATEGIES

As discussed in Chapter 2, one of the major challenges pertaining to mitigating the high UHC and CO emissions at low load RCCI operation are the low exhaust gas temperatures that are insufficient to activate the DOC. Hence it is vital to investigate operation strategies that will increase the exhaust gas temperatures for DOC light-off. This chapter explores the use of three different VVA strategies: Early Exhaust Valve Opening (EEVO) using a fully flexible VVA system, EEVO using a cam phaser, and cylinder deactivation, and evaluates the effectiveness of these strategies in raising the exhaust gas temperatures for DOC light-off. Section 5.1 describes the motivation for the VVA study by showing that methods such as varying the combustion phasing and post-injection are not effective in raising the exhaust gas temperatures, followed by Section 5.2, which presents the results of the EEVO simulation study using a fully flexible VVA system. Section 5.3 then compares the effectiveness of a cam phaser with that of a fully flexible VVA system in raising the exhaust gas temperatures. Section 5.4 investigates cylinder deactivation and finally Section 5.5 compares the effectiveness of each of these strategies in raising the exhaust gas temperatures, as well as the impact of each strategy on fuel economy and emissions.

5.1 Motivation for Variable Valve Actuation Techniques to Raise Exhaust Gas Temperature

Implementing variable valve actuation and cylinder deactivation requires a modification of the valvetrain mechanism to include more complex controls. Before devising a simulation study to investigate the use of variable valve actuation and cylinder deactivation to increase the exhaust gas temperature, it was necessary to evaluate the effectiveness of other potential strategies to increase the exhaust gas temperature. This section evaluates two such strategies that could potentially increase the exhaust gas temperature to achieve DOC light-off: combustion phasing and post-injection.

5.1.1 Combustion Phasing Simulation Study

With RCCI, the exhaust gas temperature may potentially be varied through the modification of the global fuel reactivity by adjusting the ratio of the high reactivity fuel to the low reactivity fuel, such that combustion phasing is varied [179]. Since the combustion efficiency is influenced by combustion phasing,

the exhaust gas temperatures at the end of combustion will vary as well, and an appropriate phasing could potentially give an exhaust temperature value sufficient for DOC light-off, without having to worry about implementing VVA strategies. Therefore, before devising a simulation study to investigate the use of VVA for improved low-load system performance, it was decided that the effect of combustion phasing through the variation of global fuel reactivity on the exhaust gas temperature be studied.

A series of coupled GT-Power and KIVA-3V simulations was conducted to investigate whether adjustment of the combustion phasing via variation of global fuel reactivity could be used to raise the exhaust gas temperature to that of the DOC light-off temperature for a near-idle load point of 1 Bar BMEP at 1,500 $\mathrm{rev} \cdot \mathrm{min}^{-1}$. The ratio of high reactivity fuel to low reactivity fuel was varied from 10% iso-octane/90% n-heptane to 90% iso-octane/10% n-heptane, with intervals of 5% between ratios, while keeping the total fuel energy constant. To quantify the global reactivity of the fuel for each iso-octane/n-heptane ratio, the global Primary Reference Fuel (PRF) Octane Number Ψ_{PRF} was used. The global PRF Octane Number is defined by Equation 5.1:

$$\Psi_{PRF} = \frac{m_{C_8H_{18}} \cdot 100 + m_{C_7H_{16}} \cdot 0}{m_{C_8H_{18}} + m_{C_7H_{16}}} \tag{5.1}$$

where $m_{C_8H_{18}}$ is the mass of port-fuel injected iso-octane with an octane rating of 100 and $m_{C_7H_{16}}$ is the mass of direct-injected n-heptane with an octane rating of 0. Figure 5-1 shows the variation of Ψ_{PRF} with the iso-octane/n-heptane ratio. The higher the ratio of the lower reactivity iso-octane to the higher reactivity n-heptane, the higher the global PRF Octane Number, which results in a less reactive fuel.

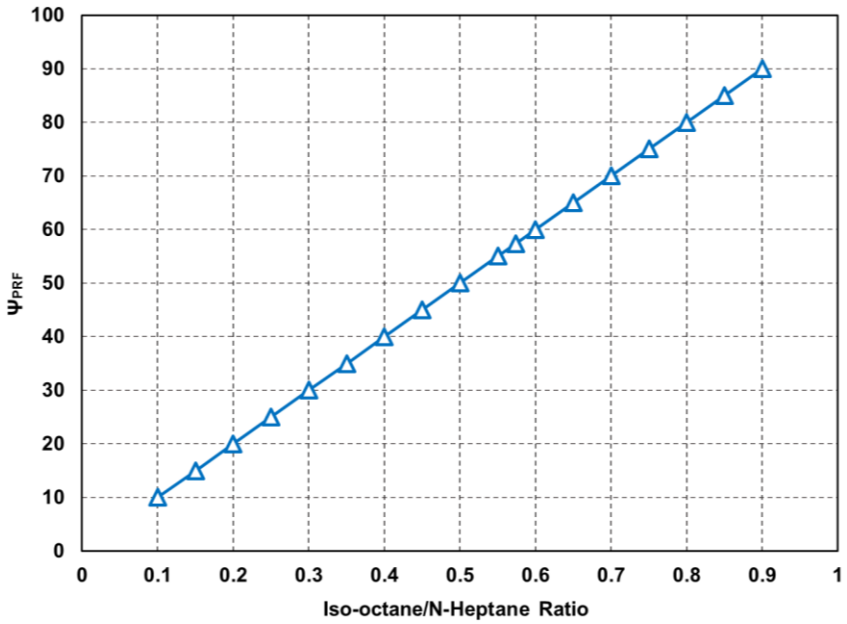

Figure 5-1: Plot of Global PRF Octane Number Ψ_{PRF} as a function of the Iso-octane/N-Heptane Ratio. The higher the ratio of Iso-octane to N-Heptane, the lower the fuel reactivity.

Figure 5-2 shows the pressure traces and heat release rate curves for different values of Ψ_{PRF}. At a higher Ψ_{PRF}, due to the larger quantity of the lower reactivity iso-octane in the fuel blend, the global fuel reactivity is lower, leading to a more retarded combustion phasing and therefore a less rapid heat release. At iso-octane/n-heptane ratios of 75% and above, the global fuel reactivity was too low for auto-ignition to occur, and hence no combustion was observed for $\Psi_{PRF} > 75$.

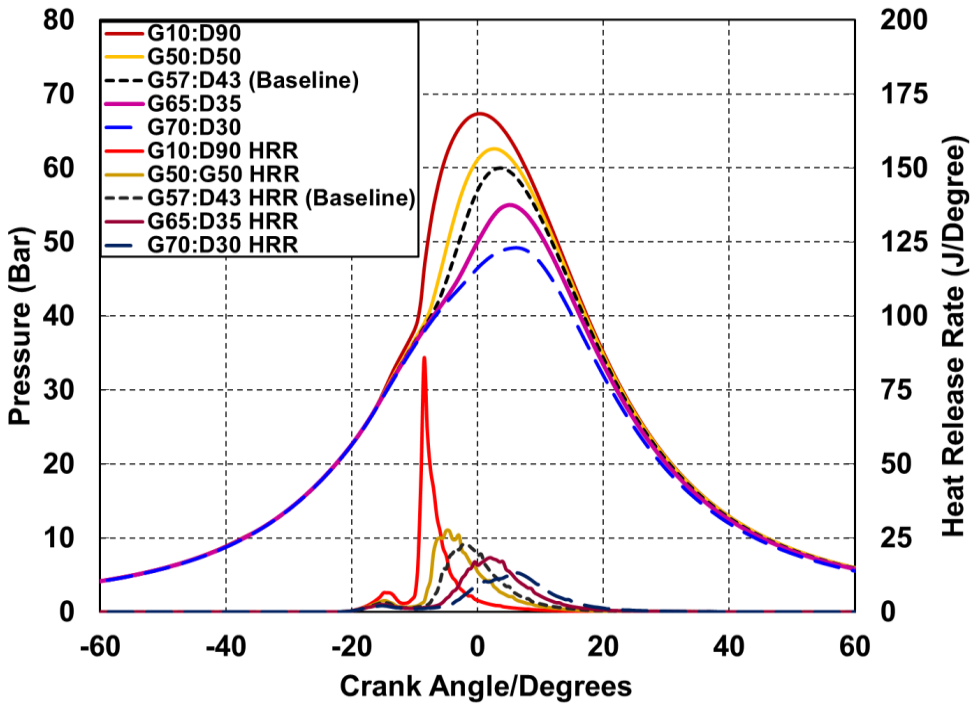

Figure 5-2. Pressure traces and heat release rate curves for different iso-octane/n-heptane fueling ratios. The format Gx:Dy denotes the percentages of iso-octane and n-heptane in the fuel mixture, with x being the percentage of iso-octane and y the percentage of n-heptane.

With increasing global fuel reactivity, the combustion efficiency increased, as shown in Figure 5-3a. However, due to the more rapid combustion process at a higher global fuel reactivity, the Peak Pressure Rise Rate (PPRR) increased with a decrease in Ψ_{PRF}, and this increase follows a roughly linear relationship as shown in Figure 5-3b.

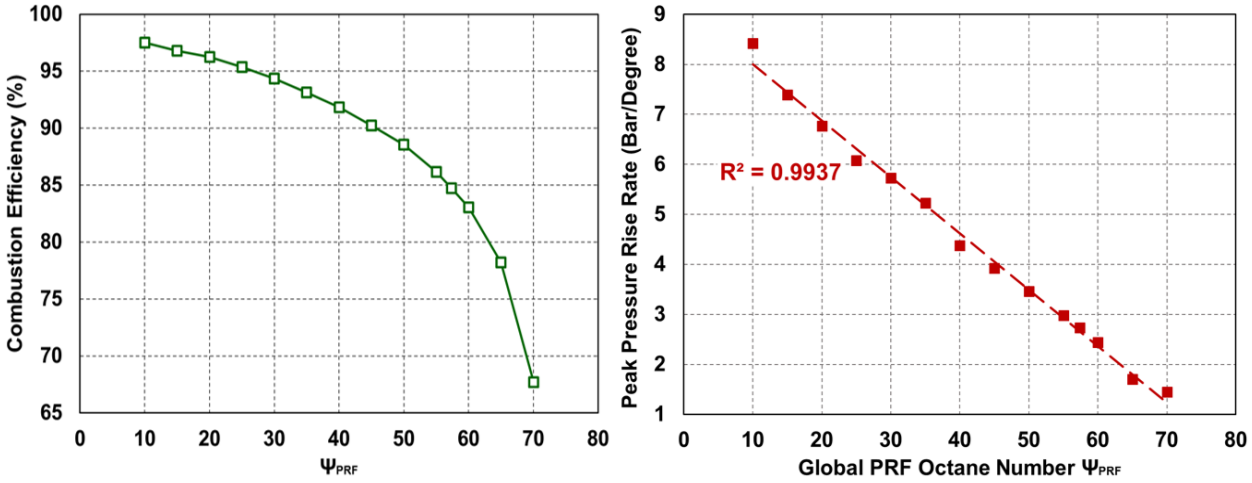

Figure 5-3: Combustion Efficiency (Left, 5-3a) and Peak Pressure Rise Rate (Right, 5-3b) as a function of the global PRF Octane Number Ψ_{PRF}.

For all the iso-octane/n-heptane fueling ratios, the exhaust gas temperatures before the DOC were below the light-off temperature of 457 K [180], as shown in Figure 5-4a. As a result, the UHC conversion efficiency values were almost zero and the CO conversion efficiency was only between 11% and 60%, as shown in Figure 5-4b. Even though the cylinder-out UHC and CO emissions were reduced at lower values of Ψ_{PRF} due to improved combustion efficiency (as shown in Figure 5-3a), the low exhaust gas temperatures that were insufficient to light off the DOC show that varying the combustion phasing via changes in the gasoline/diesel ratio is not an effective method to mitigate CO and UHC emissions at low load operation. Moreover, the earlier combustion phasing through a higher global reactivity gives high peak pressure rise rates, thereby increasing combustion noise. Hence, it is of interest to investigate other strategies that can raise the exhaust gas temperatures.

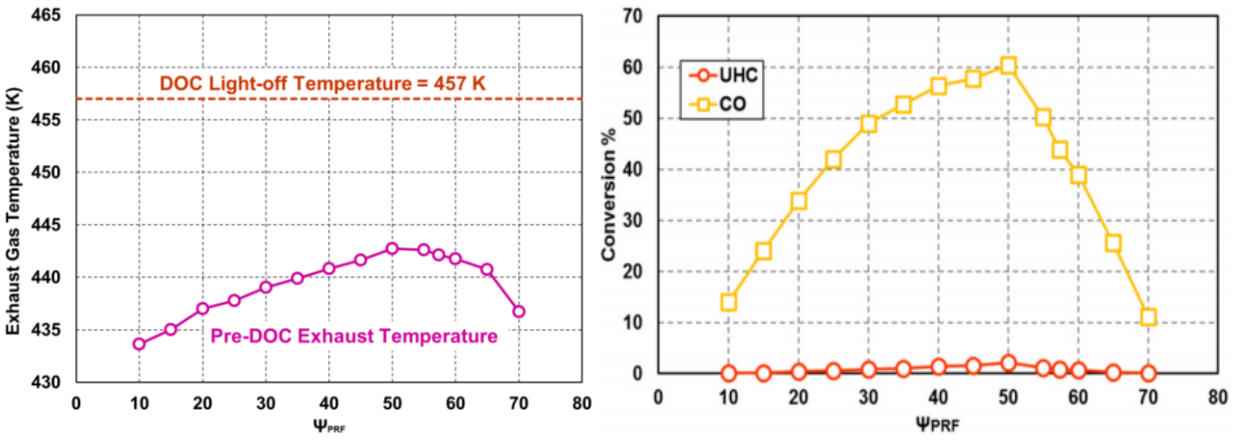

Figure 5-4: (Left, 5-4a) Pre-DOC Exhaust Temperature for the combustion phasing study. (Right, 5-4b): Catalyst UHC and CO conversion efficiency for the combustion phasing study.

5.1.2 Post-injection of Additional High Reactivity Diesel Fuel

Post-injection, which is the subsequent injection of fuel into the combustion chamber during the expansion stroke following the main injection, is another potential method to improve the DOC performance. Because this additional fuel is introduced later into the expansion stroke, the combustion of this fuel is largely used to raise the exhaust gas temperature, which in turn can potentially lead to a rapid DOC light-off [181, 182] and hence significantly increase the UHC and CO conversion efficiency. But, because the late injection of fuel means minimal conversion to useful work in the cylinder, the fuel economy will deteriorate.

For the post-injection study, for guidance the mass of additional diesel fuel to be injected into the cylinder after the main injection (sufficient to raise the exhaust gas temperature to the catalyst light-off temperature of 457 K) was calculated using a simple thermodynamic calculation. Assuming that the thermodynamic properties of exhaust gas are the same as that of air at an elevated temperature:

$$\left(\dot{m}_e + \dot{m}_f\right) \cdot h_{457} - \dot{m}_e h_{442} = \dot{m}_f \cdot q_{LHV,C_7H_{16}} \tag{5.2}$$

where $\dot{m}_e$ and $\dot{m}_f$ are the flow rates of the exhaust gas and the additional diesel fuel, respectively. h_{457} is the desired enthalpy of the exhaust gas at the DOC light-off temperature of 457 K, h_{442} is the exhaust gas enthalpy at the baseline case of 442 K exhaust temperature (enthalpies of air at the temperatures of 442 K

and 457 K are calculated based on NIST-JANAF table references [183]), and $q_{LHV,C_7H_{16}}$ is the lower heating value of n-heptane, with a value of $44.917\ \mathrm{MJ\ kg^{-1}}$ [184, 185], which is representative of diesel fuel.

Equation 5.2 assumes that all the additional post-injected diesel fuel is used to increase the exhaust gas temperature to the desired value, and that none of the energy from this additional fuel is converted to work or is lost to the surroundings as heat. This equation also assumes complete combustion of the fuel. In reality, combustion would be incomplete, and work from the additional fuel and losses to surroundings due to heat transfer must be accounted for. Incorporating these losses into the equation would result in a higher fuel mass than that calculated for this study. However, Equation 5.2 is a useful starting point to get an initial estimate of the fuel required, giving one the idealized lower limit of fueling needed to raise the exhaust temperature to 457 K.

From Equation 5.2, the lower limit of additional fuel flow rate required would be $4.11\ \mathrm{mg \cdot s^{-1}}$, for all cylinders (0.082 mg/cycle/cylinder), which is about 1.34% of the fueling rate (see Table 4.). To explore this using the CFD code, this additional fuel was injected using a second injection into the cylinder at injection timings from 10 degrees ATDC to 90 degrees ATDC, with 10 degree intervals between the timings. However, the combustion temperatures reached were not sufficient to combust the additional fuel for all the injection timings, and hence the exhaust gas temperatures were not increased sufficiently. This happened because the combustion efficiency at the 1 Bar BMEP load point was already very low (~ 85%), and as a result, the temperatures reached at the end of combustion of the main fuel was not high enough for the additional fuel to burn. In practice, other methods would need to be adopted to ensure clean combustion of the late-injected fuel.

5.2 Early Exhaust Valve Opening Using a Fully Flexible Variable Valvetrain System

5.2.1 Simulation Methodology

For the EEVO study using a fully flexible VVT system, the EGR cooler was removed from the high pressure EGR loop, since high exhaust gas temperatures were desired. The EVO timing was varied between 100 to 40 degrees ATDC, with intervals of 20 degrees between timings. Assuming a fully flexible

valvetrain system, EEVO timing valve lift profiles were obtained by varying the dwell time of the intake valves at the maximum valve lift of 8 mm. Figure 5-5 shows the early and stock exhaust valve lift profiles.

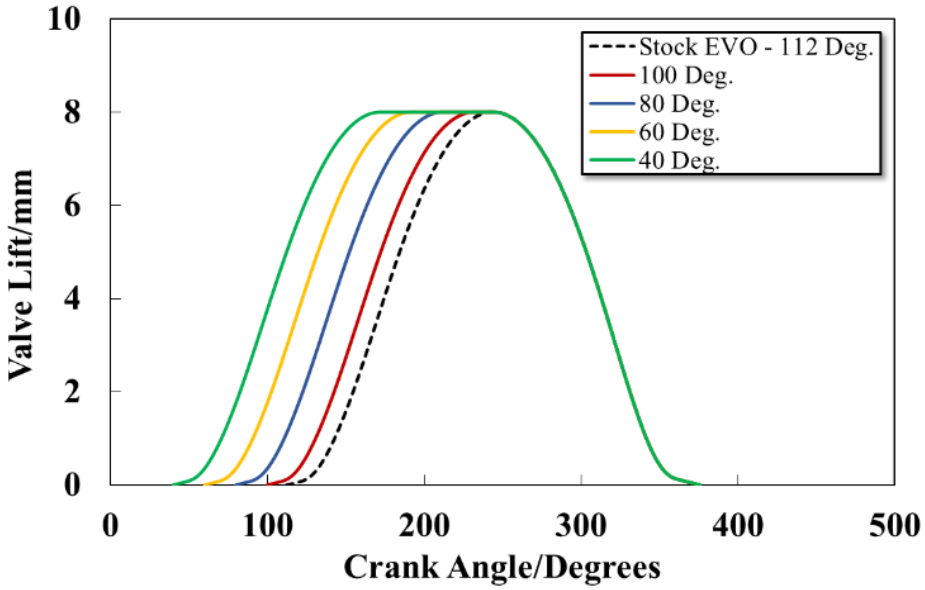

Figure 5-5. Valve lift profiles considered in the simulations

The flowchart in Figure 5-6 shows the methodology for the study. The valve lift profiles shown in Figure 5-5 were fed into the GT-Power model, along with the heat release rate profile for the baseline case with stock valve timing of 112 degrees ATDC. The EGR fraction required to keep the IVC pressure and temperature constant was calculated for each EVO timing. (The required EGR values are given in Figure 5-9b, and the corresponding change in equivalence ratio is given in Figure 5-13b.) The resulting IVC pressures and temperatures are given in Table 5-1. (Case 1 refers to the 1 Bar BMEP at 1,500 rev/min operating point, while Case 2 refers to the 2.6 Bar BMEP at 1,500 rev/min operating point. For more information on the operating point parameters, please refer to Section 4.1.1 in Chapter 4.)

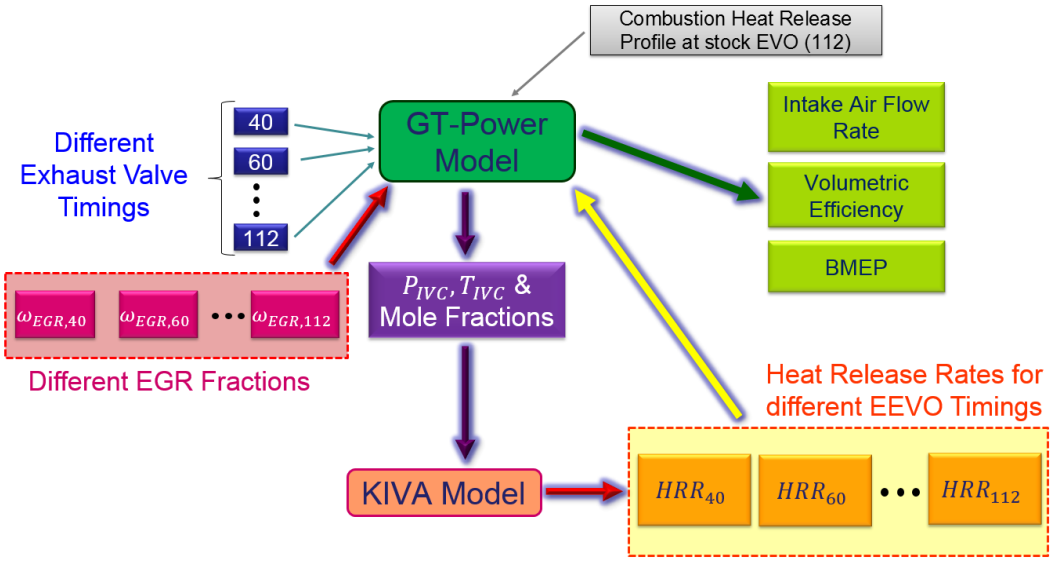

Figure 5-6. Schematic of solution methodology

Table 5-1. IVC Conditions for Cases 1 and 2

	Case 1	Case 2
IVC Pressure/Bar	1.17	1.2
IVC Temperature/K	391	412

The IVC pressure, IVC temperature and EGR fraction were used to calculate the mole fractions of the gas components in the intake charge, which were fed into KIVA to obtain the heat release rates for each EVO timing. The heat release rates were then fed back into the GT-Power model to obtain the engine performance parameters, such as the intake air flow rate, volumetric efficiency and BMEP. The following sub-section 5.1.2 presents and discusses the results.

5.2.2 EEVO Study Results

Figures 5-7 and 5-8 show the pressure traces and heat release rate curves for case 1 (1 Bar BMEP load point) and case 2 (2.6 Bar BMEP load point), respectively, for different EVO timings. As can be seen from the pressure traces, advancing the EVO timing advances the combustion timing, and increases the

peak pressure reached, albeit only slightly for case 1. A more significant change in combustion phasing is observed for case 2.

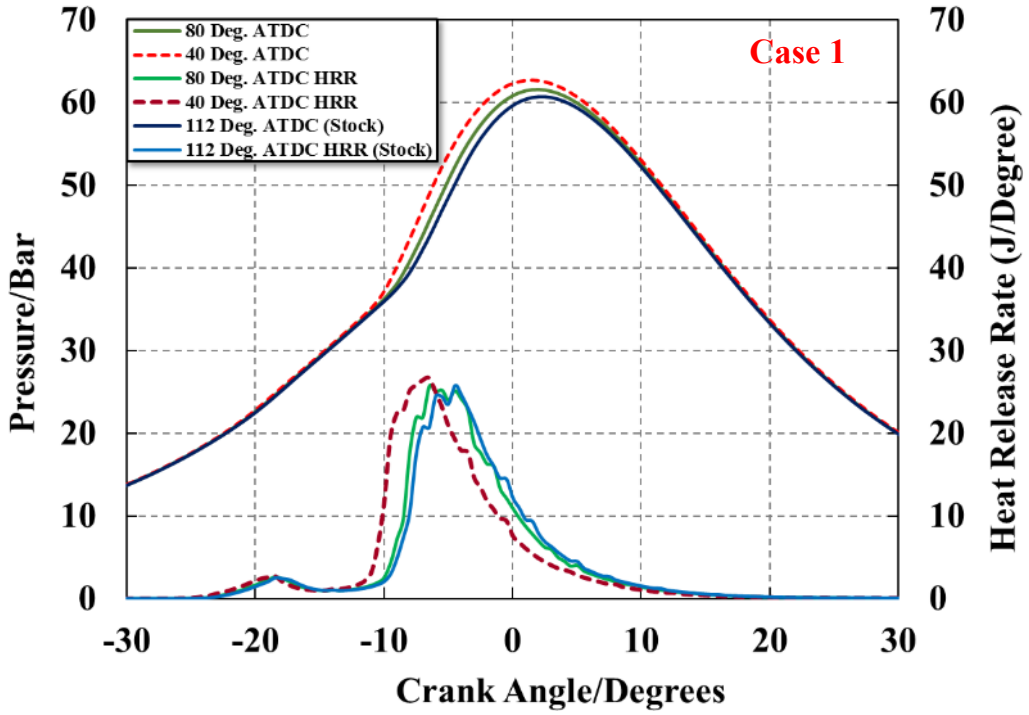

Figure 5-7. Pressure Traces and Heat Release Rate Curves for Case 1

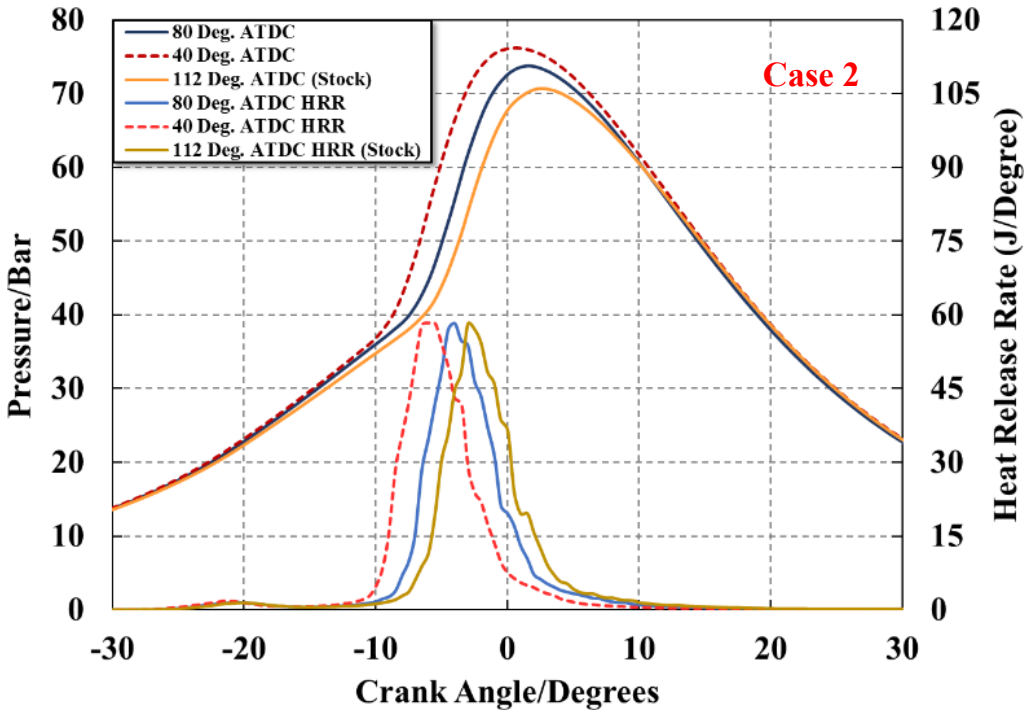

Figure 5-8. Pressure Traces and Heat Release Rate Curves for case 2

Figure 5-9a shows the exhaust gas temperatures in the exhaust manifold at the turbine inlet, the DOC inlet (turbine outlet) and at the end of the EGR loop for both load points. As expected, opening the exhaust valve early gives rise to higher exhaust gas temperatures, but the increase in exhaust gas temperature is more pronounced and significant between the EVO timings of 40 deg. ATDC and 60 deg. ATDC than it is between the other valve timings. The exhaust gas temperatures are also higher for case 2 as compared to case 1, since case 2 is at a higher load point.

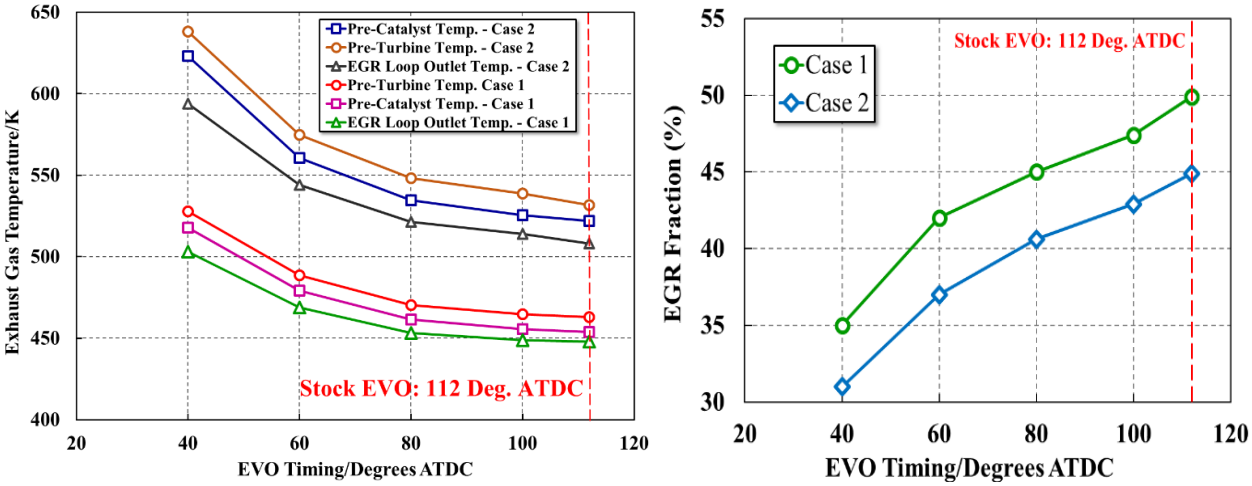

Figure 5-9a. (Left) Exhaust Gas Temperatures at different locations for both cases; Figure 5-9b. (Right) Required EGR Fractions as a Function of EVO Timing.

Due to higher exhaust gas temperatures at advanced EVO timings, a lower EGR fraction is required to keep the IVC temperature constant. Hence, the quantity of fresh air inducted into the cylinders is increased, as indicated in Figure 5-10a, thereby improving volumetric efficiency for the same intake pressure. A lower EGR fraction also means that the exhaust gas mass flow rate through the catalyst is increased, as shown in Figure 5-10b.

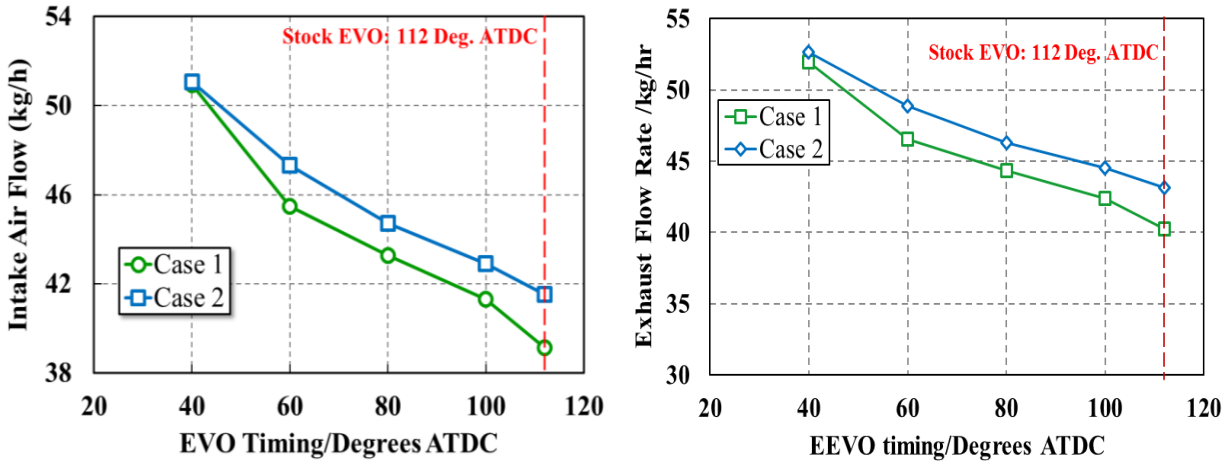

Figure 5-10a. (Left) Intake Air Flow Rate for different EVO Timings; Figure 5-10b. (Right) Exhaust gas flow rate for different EVO Timings

Opening the exhaust valve earlier reduces the work output of the engine system as shown in Figure 5-11. The BMEP drops as the EVO timing is advanced because the expansion stroke is cut short with the exhaust gases leaving the cylinders earlier than with the stock arrangement. Once again, the reduction in the BMEP is more significant between 40 and 60 degrees ATDC, since the magnitude of the pressure drop during the earlier part of the expansion stroke is much greater than during the latter part of the expansion stroke, resulting in a greater work potential being lost. As a result of the reduced work output, the brake specific fuel consumption (BSFC) increased from 554 g/kWh at the stock valve timing to 607 g/kWh at 80 degrees ATDC for case 1, and increased from 264 g/kWh at stock EVO timing to 283 g/kWh at 80 degrees ATDC for case 2.

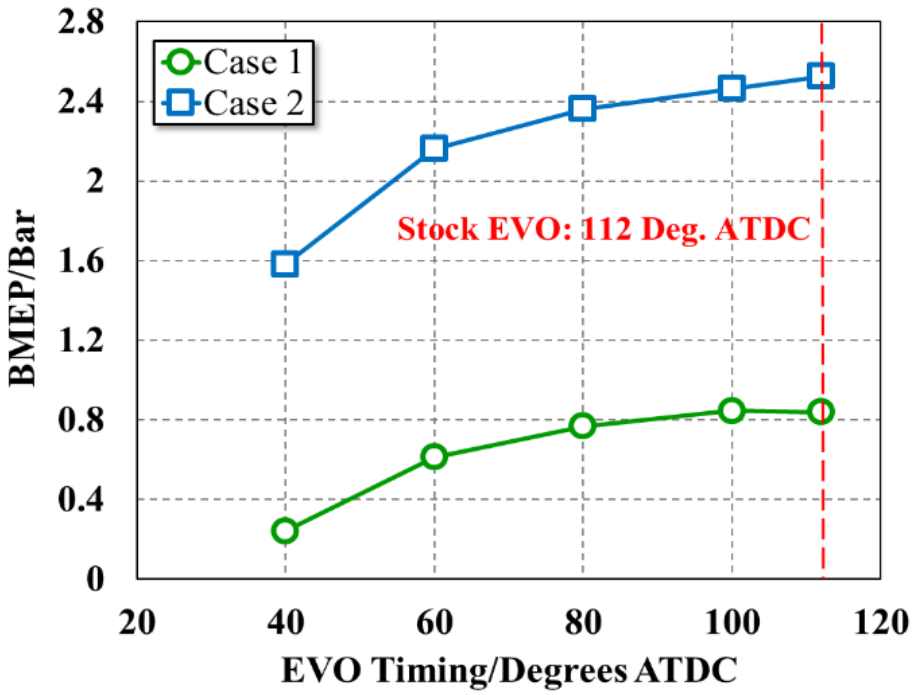

Figure 5-11. BMEP as a function of EVO timing for both cases

Figures 5-12a and 5-12b show the cylinder-out NOx and soot emissions respectively for different EVO timings. NOx emissions increase with advancing EVO timing due to improved combustion efficiencies that lead to higher in-cylinder temperatures favoring NOx formation. NOx emissions are higher for case 2 than they are for case 1 due to higher combustion temperatures reached at the higher load point

in case 2. Though Figure 5-12a shows a more drastic increase in NOx emissions for case 2, NOx values are still very low, with a maximum of 35 ppm for 40 degrees ATDC. Soot emissions are extremely low as well, but unlike NOx, they show a decrease with advancing EVO timing.

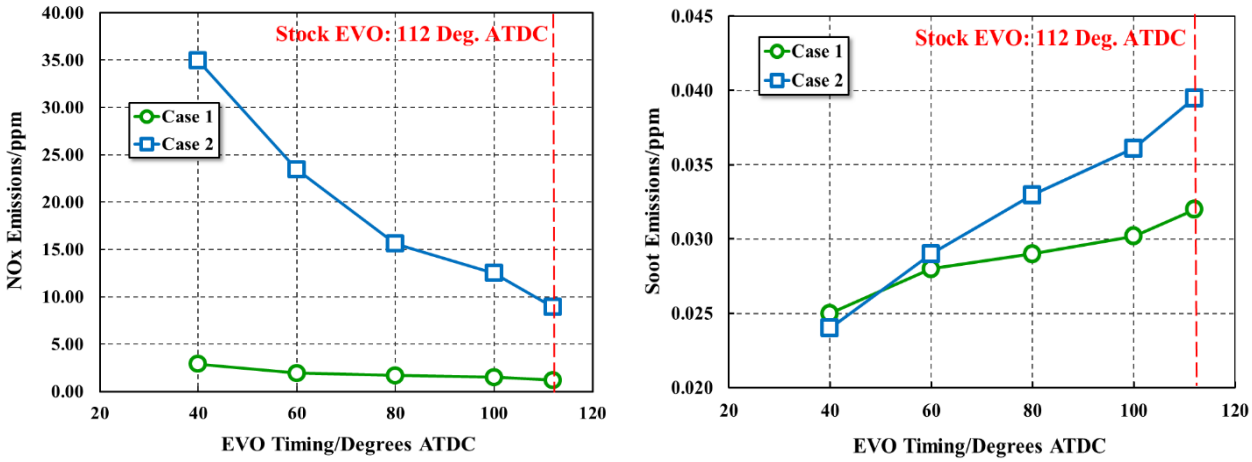

Figure 5-12. NOx (Left, 5-12a) and Soot (Right, 5-12b) Emissions for both cases

Figure 5-13a shows the cylinder-out UHC and CO emissions for both cases. There does not appear to be a trend for either case when it comes to UHC, but the CO emissions decrease with advancing EVO timing for case 2, albeit slightly. To account for the lack of a visible trend for the UHC and CO emissions, one needs to evaluate the change in the fuel-air equivalence ratio $\emptyset$ with EVO timing, as well as the modified fuel-to-charge equivalence ratio $\emptyset'$, which is defined by the following equation:

$$\emptyset' = \emptyset \cdot (1 - \omega_{EGR})$$

where ω_{EGR} is the EGR fraction. This modified equivalence ratio, which takes into account the dilution effect of EGR, is a measure of the specific energy content of the charge and is a rough indicator of the combustion temperatures reached for a given intake pressure [186, 187].

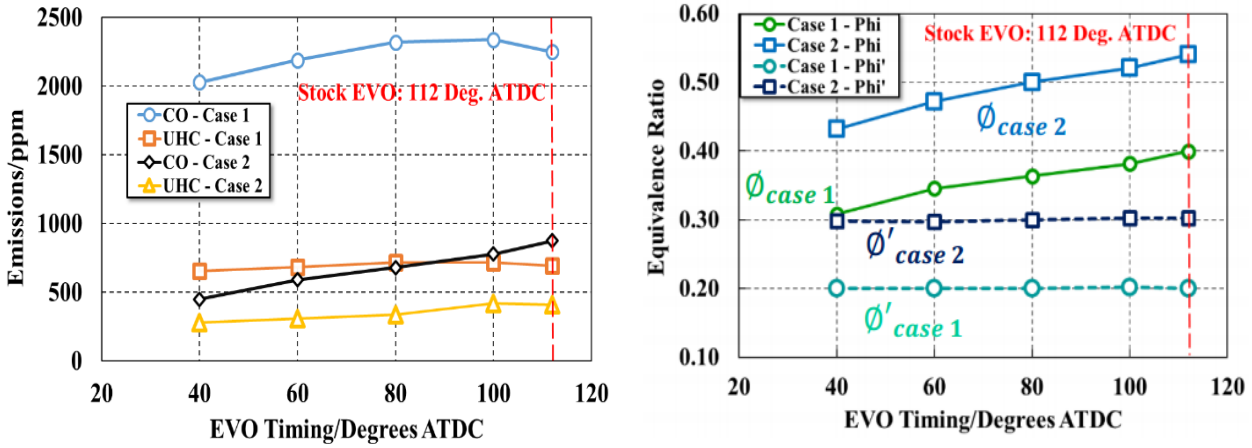

Figure 5-13a. (Left) CO and UHC Cylinder-Out Emissions for both cases; Figure 5-13b (Right) Fuel-to-air and Fuel-to-charge Equivalence Ratio at IVC for both cases

Both the fuel-to-air and fuel-to-charge equivalence ratios are plotted with respect to EVO timing in Figure 5-13b. The values of $\emptyset$ are already very low for these low-load cases, and only exhibit small changes with advancing EVO timing. Moreover, $\emptyset'$ remains constant at 0.2 for case 1 and 0.3 for case 2 irrespective of the EVO timing. This means that the energy content of the intake charge remains the same across the EVO sweep, thereby leading to relatively minor and insignificant discrepancies in the temperatures reached after combustion at all EVO timings for a particular case. This in turn contributes to the UHC and CO phenomena observed in Figure 5-13a.

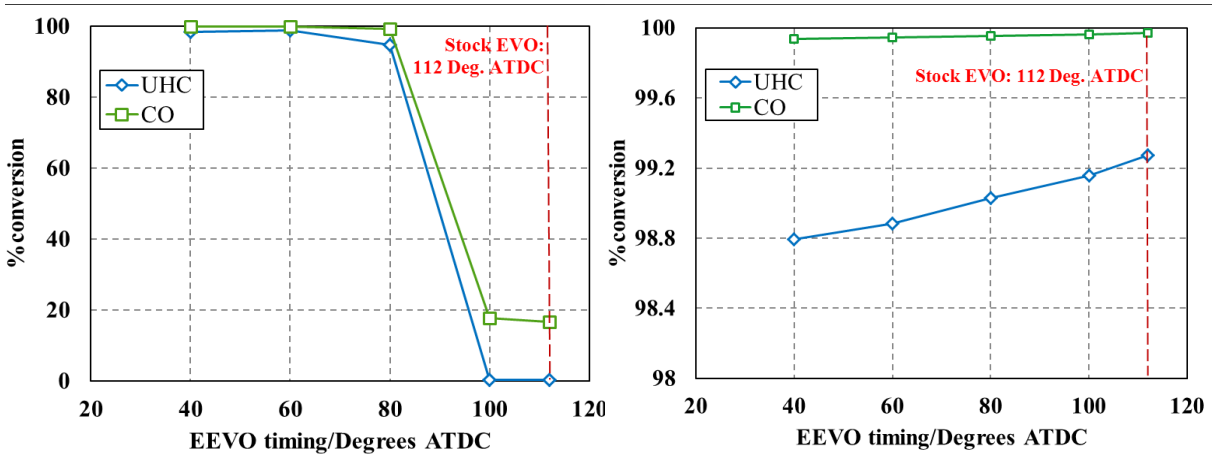

Figure 5-14. DOC performance for Case 1 (5-14a, Left) and Case 2 (5-14b, Right; Note Scale Change for 5-14b)

The main advantage of the EEVO strategy for LTC engines lies in the exhaust temperature being high enough to activate the DOC. With the high exhaust temperatures, the catalyst light off time is reduced and the conversion efficiency of the catalyst is significantly enhanced, resulting in near complete conversion of the UHC and CO emissions. As shown in Figure 5-14a, opening the exhaust valve at the stock valve timing of 112 degrees ATDC, and 100 degrees ATDC results in only about 18% conversion of CO and virtually zero conversion of UHC. This is because the temperatures of 454 K and 456 K are below the light-off temperature of 457 K. As the EVO timing is advanced further to 80 degrees ATDC, the exhaust gas temperature is larger than the activation temperature and the UHC oxidation approaches 95% and the CO oxidation is close to 100%.

For case 2, the conversion efficiencies for CO approached 100% and the conversion efficiencies for UHC were between 98.8% and 99.3% for all EVO timings, as the pre-catalyst exhaust temperatures were significantly higher than the light-off temperature, as shown in Figure 5-14b (note scale change). It is interesting to note the very small decrease in conversion efficiency for the UHC with advanced EVO timing. Since a lower EGR fraction is used for a more advanced EVO timing, a larger mass flow rate of the exhaust gas is directed through the catalyst (shown in Figure 5-10b), thereby slightly reducing the conversion efficiency. The decrease is minor however, as the conversion is more sensitive to exhaust temperature than mass flow rate.

5.3 Comparison of Fully Flexible Valvetrain with Cam Phaser

Although the fully flexible valvetrain (covered in the previous section) offers tremendous freedom in valve control, it is complex, expensive and prone to failures due to complicated control strategies involved in real world operation. To overcome the challenges posed by a fully flexible VVT system, a cam-phaser, could be used [53]. While the cam-phaser does not offer the control autonomy and flexibility of the fully flexible VVT, it is much easier to manufacture and install on an engine, and its control mechanisms are much less complex. It was therefore decided to compare the engine performance, specifically pumping work and BSFC between the two systems for the 80 degrees ATDC EVO operating point for case 1 (the threshold point in the fully flexible VVT study where the catalyst light-off temperature was reached). Figure

5-15 shows the valve lift profile for the 80 degrees ATDC case with the cam-phaser, the stock EVO, the fully flexible 80 deg. EVO and intake valve profiles as reference points.

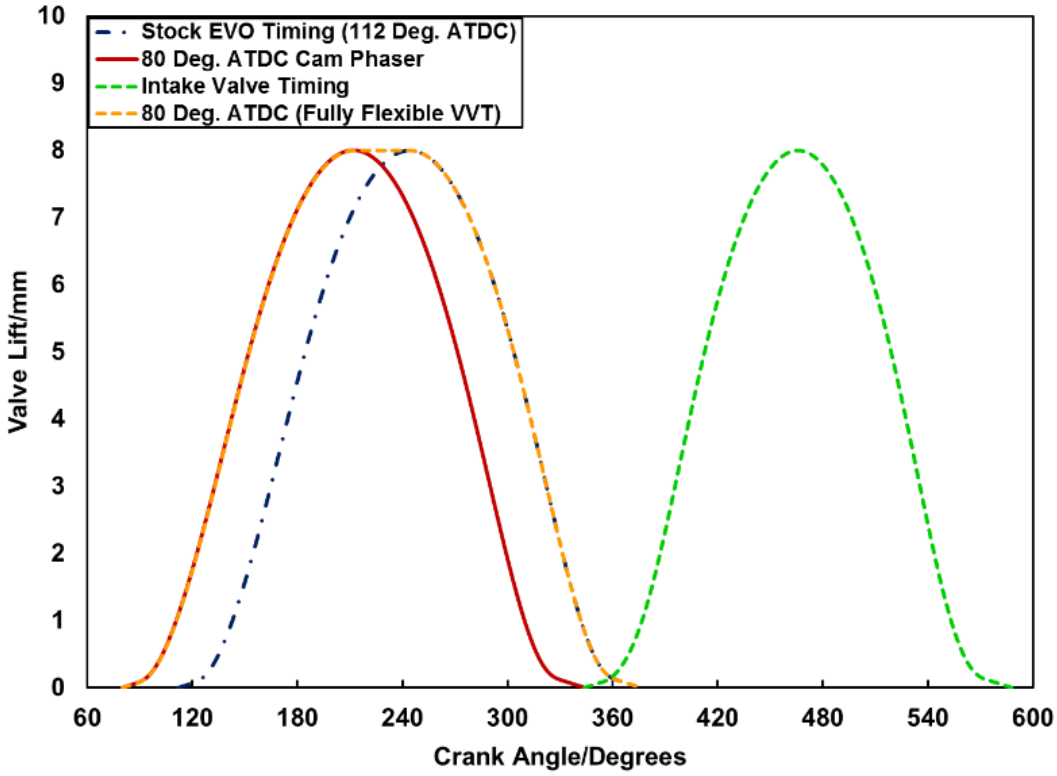

Figure 5-15. Intake Valve, Stock EVO, 80 Deg. ATDC Cam Phaser and Fully Flexible Profiles

Figure 5-16 shows the flowchart of the methodology used for the VVT system comparison study. The heat release rate for the 80 degrees ATDC cam phaser timing, and the combustion heat release profile for the 80 degrees ATDC timing from the fully flexible VVT study were used in the GT-Power model to obtain the in-cylinder pressure and temperature at IVC. One important thing to note is that, because of the lack of valve overlap for the cam phaser case, external EGR was not used. Rather, EGR was accomplished internally due to the zero valve overlap, and the EGR fraction was obtained as an output from GT-Power. This resulted in an EGR fraction of 22%, and the IVC pressure and IVC temperature were then used to calculate the gas component mole fractions in the intake charge at IVC. Because hot EGR was desired to raise the combustion temperatures, the EGR cooler was bypassed for the fully flexible VVT strategy. Table 5-2 shows the IVC pressures and temperatures used for the KIVA simulation.

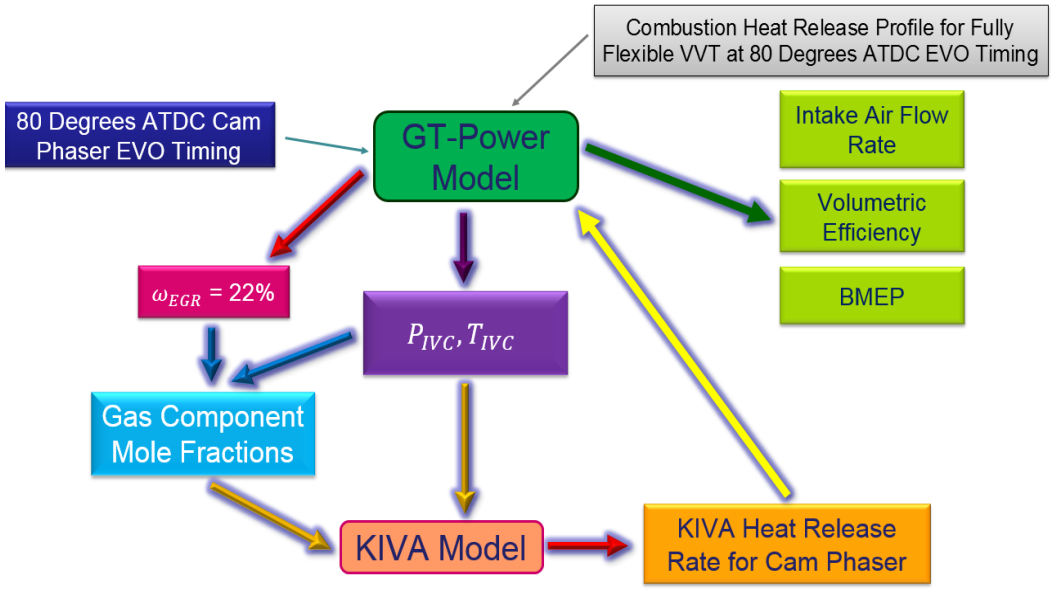

Figure 5-16. Methodology for VVT comparison study

Table 5-2 IVC conditions for VVT comparison study

	Fully Flexible VVT	**Cam Phaser**
IVC Pressure (Bar)	1.17	1.15
IVC Temperature (K)	390	388

The IVC pressure, IVC temperature and the mole fractions were then used as inputs in the KIVA CFD model to obtain the heat release rate, which was then fed back into GT-Power to obtain the engine performance parameters, such as BMEP, intake air flow rate, etc. As described in the general procedure section, the heat transfer coefficient of the in-cylinder gas calculated by the Woschni model [147] in GT-Power, was tuned to match the heat transfer at EVO obtained from KIVA, similar to the approach used in [161].

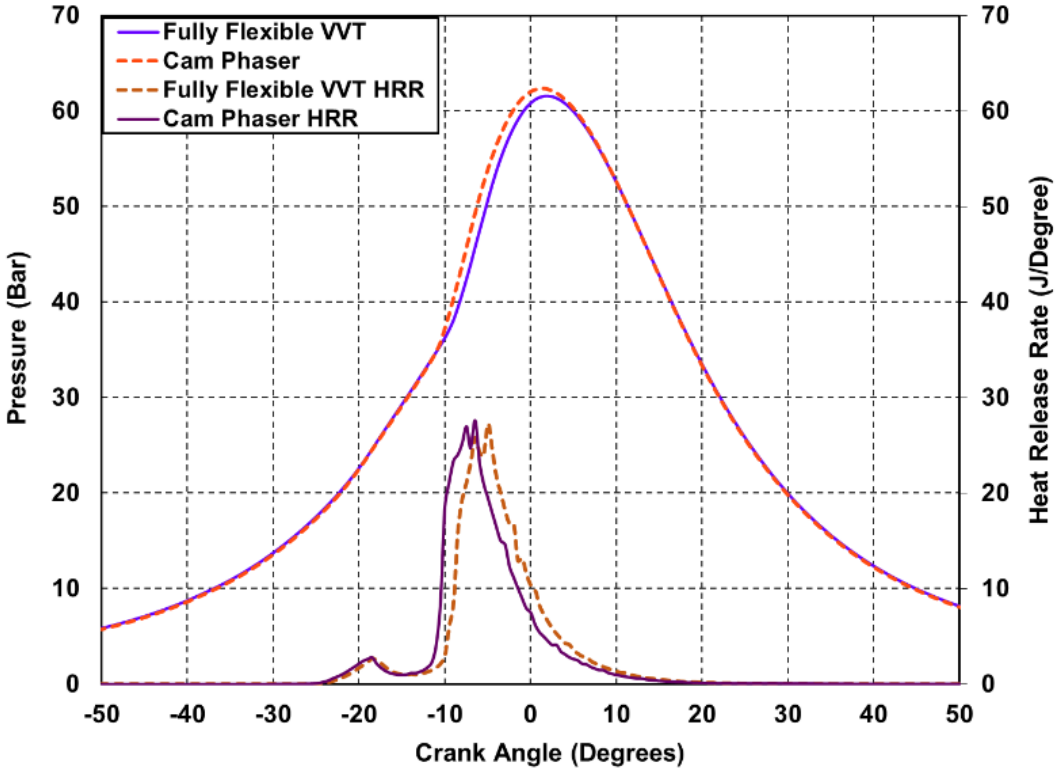

Figure 5-17. Pressure Traces and Heat Release Rate Curves for VVT Comparison Study

As Figure 5-17 shows, for the cam phaser case, the combustion phasing was slightly advanced and a higher peak pressure was reached. The combustion efficiency values for both cases were similar: 90.2% for the cam phaser case and 90.5% for the fully flexible VVT case.

Table 5-3. Emissions for VVT Comparison Study (values in ppm)

	Fully Flexible VVT	Cam Phaser
NOx	0.006	0.020
Soot	0.023	0.029
UHC	814	728
CO	2,320	1,900

Table 5-3 shows the emissions for both VVT strategies. Due to the low combustion temperatures reached and the highly lean equivalence ratios, the NO_x and soot emissions are very low as expected, while the UHC and CO emissions for both VVT strategies appear to be similar. The UHC and CO emissions

trends can once again be explained by calculating the fuel-to-charge equivalence ratio $\emptyset'$, using the procedure explained in section 5.1.2.

Table 5-4. Equivalence Ratio Comparison for VVT Comparison Study

	Fully Flexible VVT	Cam Phaser
$\emptyset$	0.36	0.26
$\emptyset'$	0.2	0.2

As Table 5-4 shows, the fuel-to-charge equivalence ratio for both VVT strategies was the same, indicating that the energy content of the charge for both strategies was similar. This resulted in relatively minor and insignificant discrepancies in the temperatures reached at the end of combustion for both VVT strategies, contributing to the emissions phenomena observed in Table 5-3.

Table 5-5. Engine performance comparison for VVT study

	Baseline Case	Fully Flexible VVT	Cam Phaser
BMEP (Bar)	0.84	0.77	0.44
PMEP (Bar)	0.15	0.17	0.48
Intake Air Flow Rate (kg/h)	39.15	43.27	64.12
Pre-DOC Exhaust Temperature (K)	453.8	463.3	472.45
EGR Fraction (%)	49.9	45	22
DOC Exhaust Flow Rate (kg/h)	40.21	44.02	65.22
BSFC ($g\ kWh^{-1}$)	553	607	1,053

Table 5-5 shows the engine system performance parameters for both the VVT strategies and the baseline case (with stock valve timing of 112 degrees ATDC). The net IMEP is much lower for the cam phaser, because of the increased pumping work resulting from the recompression of the exhaust gas. In the cam phaser case, the valve overlap between the exhaust and intake valves has been reduced from 32 degrees to 0 degrees (essentially no overlap). As a result, a greater quantity of hot exhaust gas is trapped as residual, resulting in increased heat loss during the compression stroke as shown in Figure 5-18. The increased heat loss contributes to a larger pumping work for the cam phaser case; this phenomenon is similar to what Borgqvist et al. [33] observed for gasoline PPC.

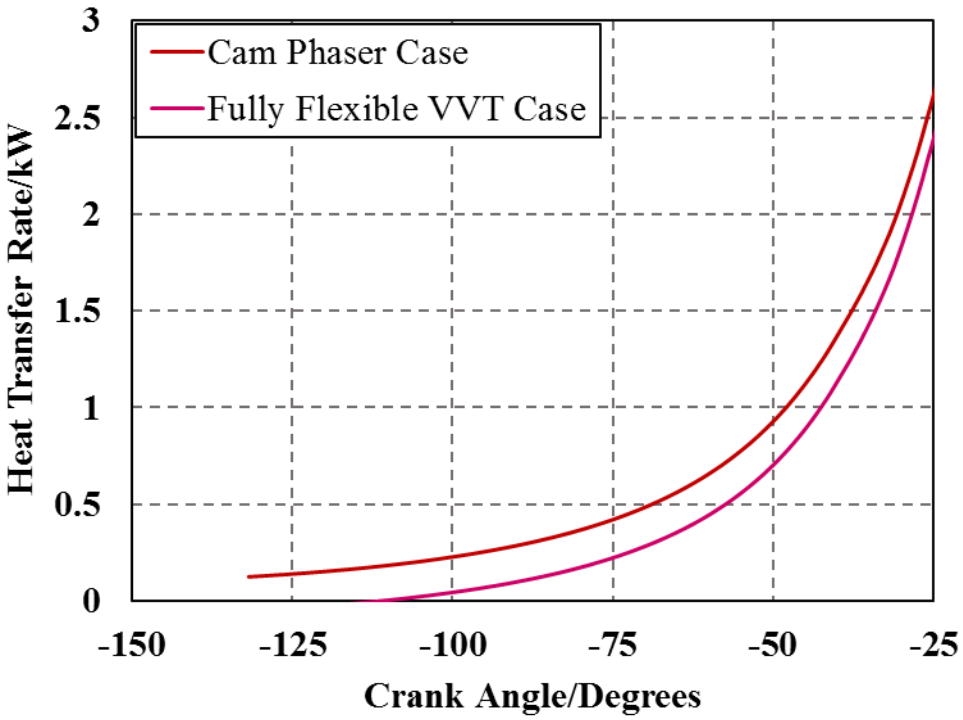

Figure 5-18. Heat Transfer Rate during the Compression Stroke before SOC.

The lower EGR fraction for the cam phaser case resulted in a significantly improved volumetric efficiency, and a greater quantity of intake air was drawn into the cylinders for this case. The lower EGR fraction also resulted in a higher exhaust gas flow rate through the catalyst, as a smaller proportion of exhaust gas was recycled.

Both the fully flexible VVT and cam phaser strategies gave pre-DOC exhaust gas temperatures that were higher than the DOC light-off temperature. However, by cutting short the expansion stroke when opening the exhaust valves at 80 degrees ATDC instead of the stock valve timing of 112 degrees ATDC, the fuel economy deteriorated for both VVT strategies. Moreover, the increased pumping work from the cam phaser resulted in a significant deterioration in fuel economy, as noted by the BSFC value of 1,053 g kWh^{-1} for the cam phaser case. Compared with the baseline value of 553 g kWh^{-1} for the stock valve timing of 112 degrees ATDC, this is a 90.4% deterioration in fuel economy, versus a 9.6% deterioration for the fully flexible case.

Table 5-6. DOC performance comparison for VVT comparison study

	Fully Flexible VVT	Cam Phaser
UHC Conversion (%)	94.9	89.7
CO Conversion (%)	99.6	98.1

As Table 5-6 shows, due to the exhaust gas temperatures being higher than the DOC light-off temperature for both strategies, the conversion efficiencies of UHC and CO were high. However, the UHC and CO conversion efficiencies were lower for the cam phaser than they were for the fully flexible VVT. This is due to the higher exhaust gas flow rate through the catalyst for the cam phaser strategy, which was a consequence of the lower EGR fraction for that strategy.

5.4 Cylinder Deactivation Study

Sections 5.2 and 5.3 both showed that EEVO using either the fully flexible VVT or the cam phaser was able to achieve exhaust gas temperatures high enough for DOC light-off. However, because the expansion stroke duration was cut short by opening the exhaust valves early, the work output from the engine was decreased, leading to a significant deterioration in fuel economy. To address the fuel economy penalty posed by the post-injection and EEVO strategies, cylinder deactivation may be implemented [114]. By running a fewer number of cylinders at a higher load point while motoring the other cylinders with their intake and exhaust valves closed, the required fueling can be reduced, significantly improving fuel economy. Moreover, the higher exhaust gas temperatures at the higher load point will lead to a more rapid catalyst light-off and improved DOC efficiency. The lower exhaust gas flow rates from the smaller number of fired cylinders may further improve the DOC efficiency. This section describes the methodology and results of the cylinder deactivation study for the 1 Bar BMEP at 1,500 rev/min load point.

5.4.1 Methodology for Cylinder Deactivation Study

For the cylinder deactivation study, three of the four cylinders were motored while only cylinder 1 was fired. Actuators were added to the intake and exhaust valves for cylinders 2, 3 and 4 to keep them closed for the duration of the entire simulation so that pumping work would be reduced. Actuators were

also used to cut off the fuel supply to the motoring cylinders. Figure 5-19 shows the modifications made to the GT-Power model to include the cylinder deactivation circuit.

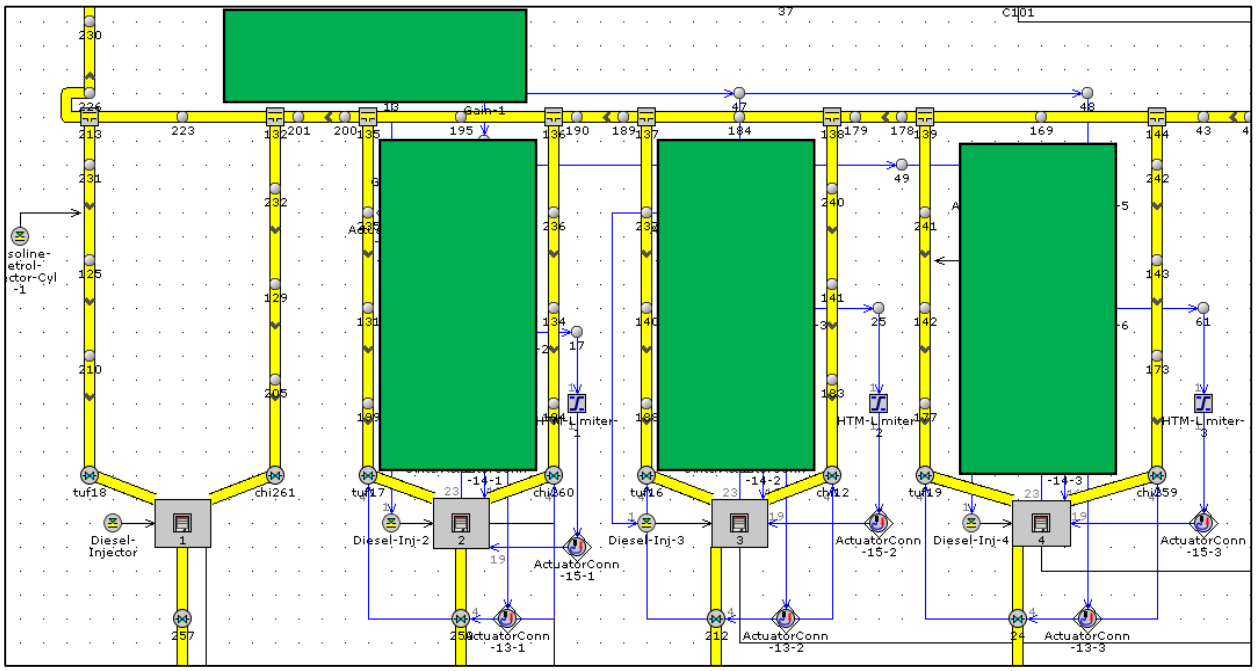

Figure 5-19. Modifications to cylinders 2, 3 and 4 in the GT-Power model to include the cylinder deactivation circuit. Major modifications include actuators to keep the motored cylinder valves closed and cut fueling off to the motored cylinders, as highlighted by the shaded green boxes.

The heat release rate curve for the 4 Bar BMEP at 1,500 rev/min operating point (shown in Figure 4-5), and the corresponding gasoline and diesel fueling quantities were fed as inputs to cylinder 1, and the engine performance quantities such as BMEP, intake air flow rate and BSFC were evaluated. Sub-section 5.4.2 describes and analyzes the results.

5.4.2 Cylinder Deactivation Study Results

Table 5-7 shows the engine performance parameters for the cylinder deactivation case. (The case with all cylinders firing is given as a reference for comparison.)

Table 5-7. Engine performance parameters for cylinder deactivation study

	All Cylinders Firing	Only Cylinder 1 Firing
BMEP (Bar)	4.15	0.68
PMEP (Bar)	0.24	0.05
Intake Air Flow Rate (kg/h)	93.9	22.8
Pre-DOC Exhaust Temperature. (K)	500.15	472.45
DOC Exhaust Flow Rate (kg/h)	96.18	23.34

The gross IMEP for the cylinder deactivation case was around 1/3rd of the gross IMEP for the 4 Bar BMEP case (with all cylinders firing) due to in-cylinder variability effects, which are a consequence of the discrepancies in the air-fuel ratio among cylinders. These discrepancies occur as a result of gas dynamic effects in the intake manifold. The BMEP of 0.68 Bar for the cylinder deactivation case was less than 1/4th of the BMEP value for the 4 Bar BMEP case because of the friction work, which was primarily dependent on engine speed. The friction mean effective pressure (FMEP) was the same for all cases at 1.04 Bar.

Table 5-8 shows the cylinder-out emissions. With the high combustion efficiency of 94%, the cylinder-out CO and UHC emissions were already low to begin with, and the low combustion temperatures and lean equivalence ratio gave low NO_x and soot emissions as well.

Table 5-8. Cylinder-out emissions for cylinder deactivation study

UHC (ppm)	566
CO (ppm)	709
NOx (ppm)	0.059
Soot (ppm)	0.025

With only one cylinder firing, the pumping work was significantly reduced due to the intake and exhaust valves being closed for all the motoring cylinders, and the intake and exhaust flow rates through the engine were decreased as well. The pre-DOC exhaust temperature of 472.45 K was lower than that for the case in which all cylinders were firing (500.15 K), due to higher heat transfer at the reduced flow rate for the cylinder deactivation case. However, since 472.45 K was marginally higher than the light-off temperature of 457 K, UHC and CO conversion by the catalyst was not a problem, as Table 5-9 shows. The higher exhaust gas temperature for the cylinder deactivation case as compared with the baseline case can

be explained by the fact that cylinder 1 in the cylinder deactivation case was running at a much higher load point (4 Bar BMEP equivalent fueling) than in the baseline case.

Table 5-9. DOC performance for cylinder deactivation study

	All Cylinders Firing	Only Cylinder 1 Firing	Baseline Case
UHC Conversion (%)	79.8	99.6	0
CO Conversion (%)	93.4	99.9	18

Compared with the 4 Bar BMEP case in which all cylinders were firing, the cylinder deactivation case showed a much higher UHC conversion, and a slightly higher CO conversion. This is due to the lower exhaust gas mass flow rate through the catalyst as only one cylinder was firing. The lower exhaust gas flow rate for the cylinder deactivation case also gave a higher UHC and CO conversion efficiency than both the VVT cases where the exhaust valves were opened early at 80 degrees ATDC, while also giving better fuel economy.

5.5 Comparison of VVT Strategies with Cylinder Deactivation for Low Load RCCI Operation

The results from sections 5.2 to 5.4 show that at near-idle load conditions, cylinder deactivation is the most favorable strategy to achieve best engine performance and DOC efficiency for low load RCCI operation. Although all three strategies covered in this chapter showed that the exhaust gas temperatures could be raised to sufficiently high enough values for DOC activation, the much lower exhaust gas flow rates arising from cylinder deactivation as compared to both the EEVO strategies gave the highest DOC conversion efficiencies, and the low fuel consumption due to firing a fewer number of cylinders gave the best fuel economy. In fact, the BSFC for cylinder deactivation was only 351 g kWh^{-1} compared to the fully flexible VVT case of 607 g kWh^{-1} and 1,053 g kWh^{-1} for the cam phaser case.

However, in practice, cylinder 1 cannot be continuously operating while the other cylinders are motored, as this would lead to Noise, Vibration and Harshness (NVH) issues, and the lack of balance among the cylinders would result in additional stresses on the engine that could lead to damage. Hence, cylinder deactivation using 1 cylinder should be simulated as a transient event that fires all 4 cylinders, one cylinder

at a time based on an optimized firing order. An alternative deactivation strategy would be to fire cylinders 1 and 4 simultaneously or cylinders 2 and 3 simultaneously at 2 Bar BMEP equivalent fueling per cylinder. These investigations could be part of future studies.

CHAPTER 6: MEDIUM LOAD/HIGH LOAD SETUP

The previous chapter investigated operating strategies to optimize the combustion process and engine performance while reducing emissions during low load operation. In this chapter, strategies for system simulation of high load operation are investigated. The 8 Bar BMEP load point at $3{,}000\ \mathrm{rev} \cdot \mathrm{min}^{-1}$ and 18 Bar IMEP load point at $2{,}000\ \mathrm{rev} \cdot \mathrm{min}^{-1}$ were the medium load and high load operating points, respectively.

The 8 Bar BMEP load point was already investigated in Chapter 3, as it was one of the experimental data points used to validate and calibrate the GT-Power and KIVA-3V models. Before any modifications were made to the stock engine configuration, the high load operating point of 18 Bar IMEP was first simulated in KIVA-3V to obtain the heat release rate. The conditions at IVC for this operating point were obtained from previous simulation studies conducted by Wu et al. [109] and are given in Table 6-1.

Table 6-1: IVC and Engine Conditions for the 18 Bar IMEP Case

Engine Speed ($\mathrm{rev} \cdot \mathrm{min}^{-1}$)	2,000
IVC Pressure (Bar)	2.4
IVC Temperature (K)	370
EGR Fraction (%)	35
Gasoline Quantity (mg/cyl/cyc)	39.06
Diesel Quantity (mg/cyl/cyc)	2.94
Gasoline Start of Injection (Deg.)	-227.4
No. of Diesel Injections	1
Diesel Start of Injection (Deg.)	-48

These values gave a pressure trace with a peak pressure of 123.82 bar and a peak pressure rise rate of 9.5 bar/degree, less than the maximum threshold of 10 bar/degree. Figure 6-1 shows the pressure trace and heat release rate from KIVA.

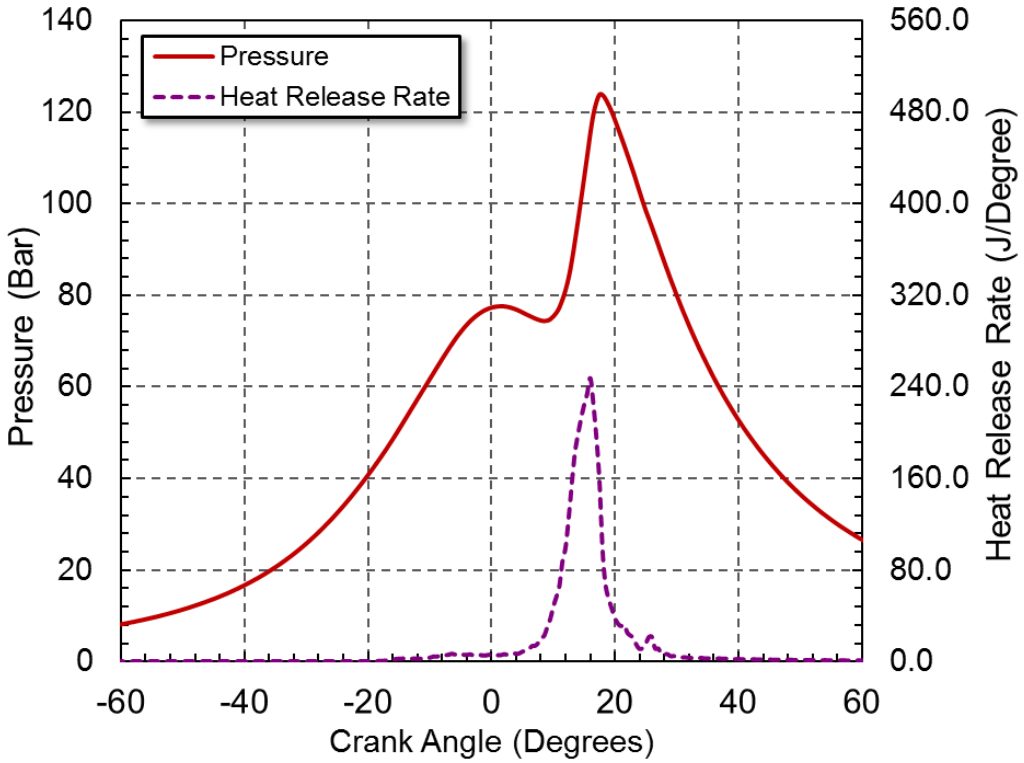

Figure 6-1: KIVA-3V Pressure Trace and Heat Release Rate Curve for the 18 Bar IMEP at $2,000\ \mathbf{rev \cdot min^{-1}}$ operating point.

The heat release rate was then fed into a "bare-bones" GT-Power model of the 1.9-Liter engine in which all the controllers/targeting controller templates were removed, and signal active dials were incorporated in their place to manually fine tune the values of the parameters, such as turbocharger rack position and EGR valve diameter at the steady state operating points. An additional Low Pressure (LP) EGR circuit was also incorporated into the engine model to allow the use of LP-EGR and/or hybrid dual loop EGR strategies over the load range. Figure 6-2 shows the modified GT-Power model with the LP EGR circuit, while Figure 6-3 shows the signal active dial templates used in the model.

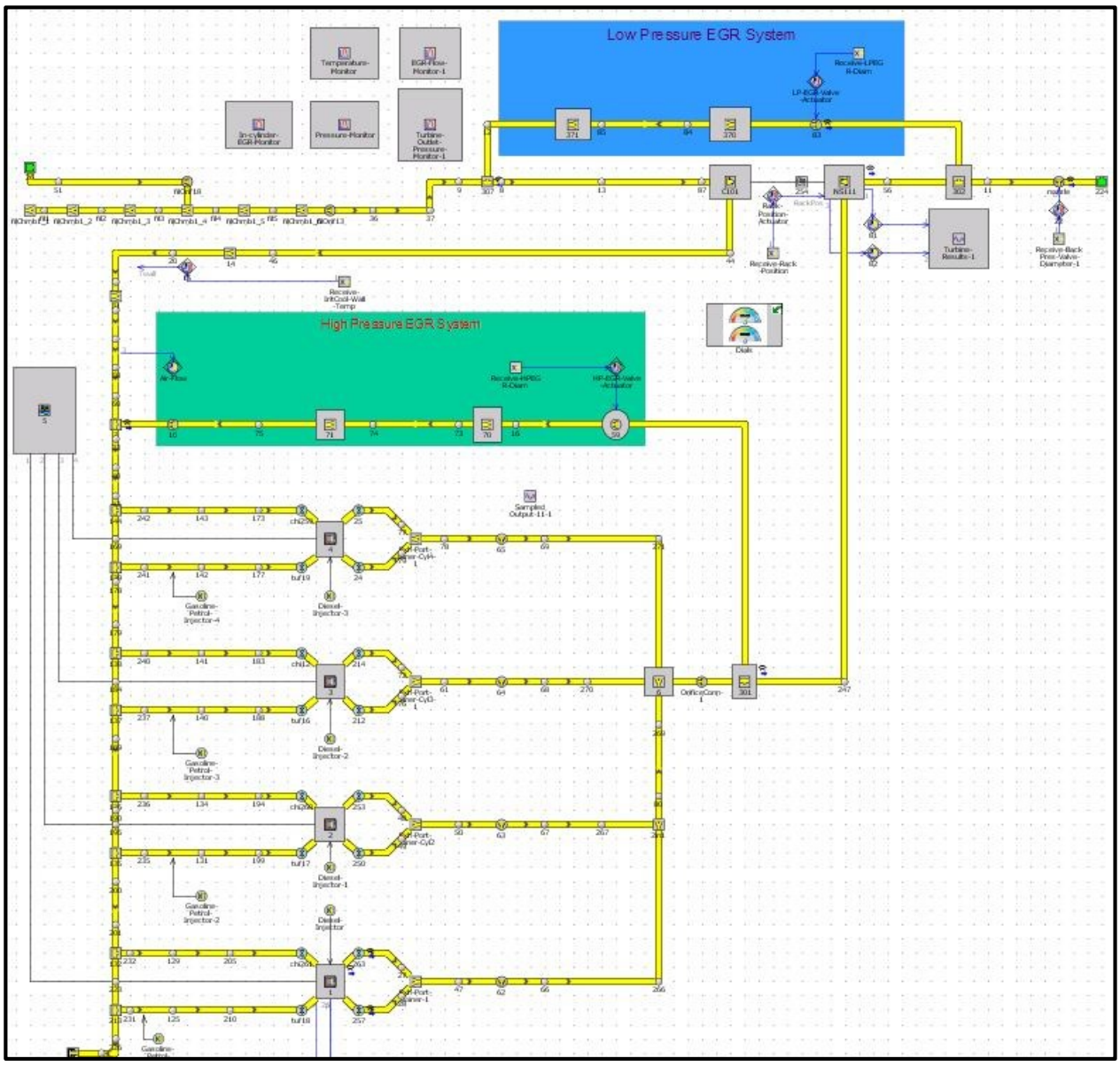

Figure 6-2: "Bare bones" GT-Power Model with controller templates removed and LP EGR Loop Added.

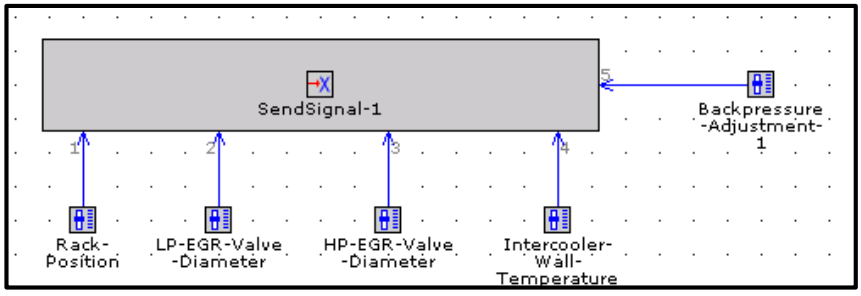

Figure 6-3: Signal Active Dials for Open-loop control in real time

In most studies involving LTC concepts Negative Valve Overlap (NVO) was used predominantly to implement EGR internally. As discussed earlier, EGR is necessary for charge dilution in LTC concepts as load is increased so that the PPRR is kept low for combustion stability. NVO, however, causes the pumping penalty to worsen due to heat losses from the residual gases during recompression of the charge, worsening the fuel economy. To overcome the pumping penalty, Yun et al. [23] proposed using a Positive Valve Overlap (PVO) strategy, which allowed them to obtain an optimal residual gas fraction and optimal combustion phasing. To make up for the residual gas deficit, EGR was introduced into the cylinder through an external EGR loop.

For this research, the PVO strategy of Yun et al. [23] was implemented to minimize the pumping penalty, and EGR was supplied through an external circuit. Due to the low exhaust enthalpy prevalent in RCCI, it was necessary to maximize the extraction of enthalpy from the exhaust by the turbine, so only LP-EGR was used, allowing all of the exhaust gas to flow through the turbine. Moreover, it was not possible to use HP-EGR as the pressure difference between the intake and the turbine inlet would not be sufficient to drive such a high EGR flow rate; the rack position would have to be set to the "most-closed" setting for building up the backpressure, which will also have a detrimental effect on the turbine efficiency.

To achieve the EGR fraction of 35%, the throttle diameter at the LP-EGR inlet had to be reduced from 36 mm to 32 mm to provide sufficient backpressure for EGR flow. Table 6-2 shows the values of the rack position and EGR valve diameter along with the desired boost pressure and external EGR fraction required to achieve the IVC conditions. Table 6-3 gives the engine and turbocharger performance results from GT-Power.

Table 6-2: Model Parameters to achieve the IVC Conditions for the 18 Bar IMEP load point

VGT Rack Position	0.387
HP EGR Valve Diameter (mm)	0
LP EGR Valve Diameter (mm)	21.5
CAC-2 Wall Temp. (K)	343
LP-EGR Throttle Diameter (mm)	32
Woschni Heat Transfer Multiplier	0.4758

Table 6-3: Engine Performance Parameters for the 18 Bar IMEP load point

Exhaust Manifold Pressure (Bar)	2
Intake Manifold Pressure (Bar)	1.95
Intake Air Flow Rate ($kg \cdot h^{-1}$)	152.9
Total EGR Flow Rate ($kg \cdot h^{-1}$)	79.6
Gross IMEP (Bar)	18.26
Net IMEP (Bar)	18.09
PMEP (Bar)	-0.17
BMEP (Bar)	17.35

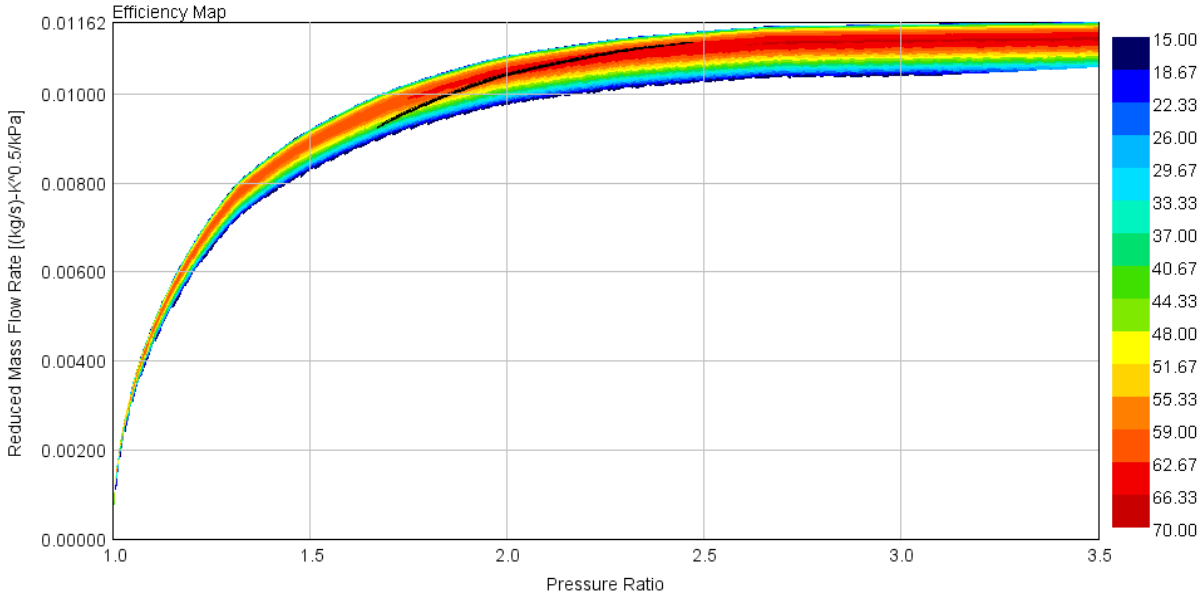

Figure 6-4: Operating points on turbine map for 18 Bar IMEP (black line)

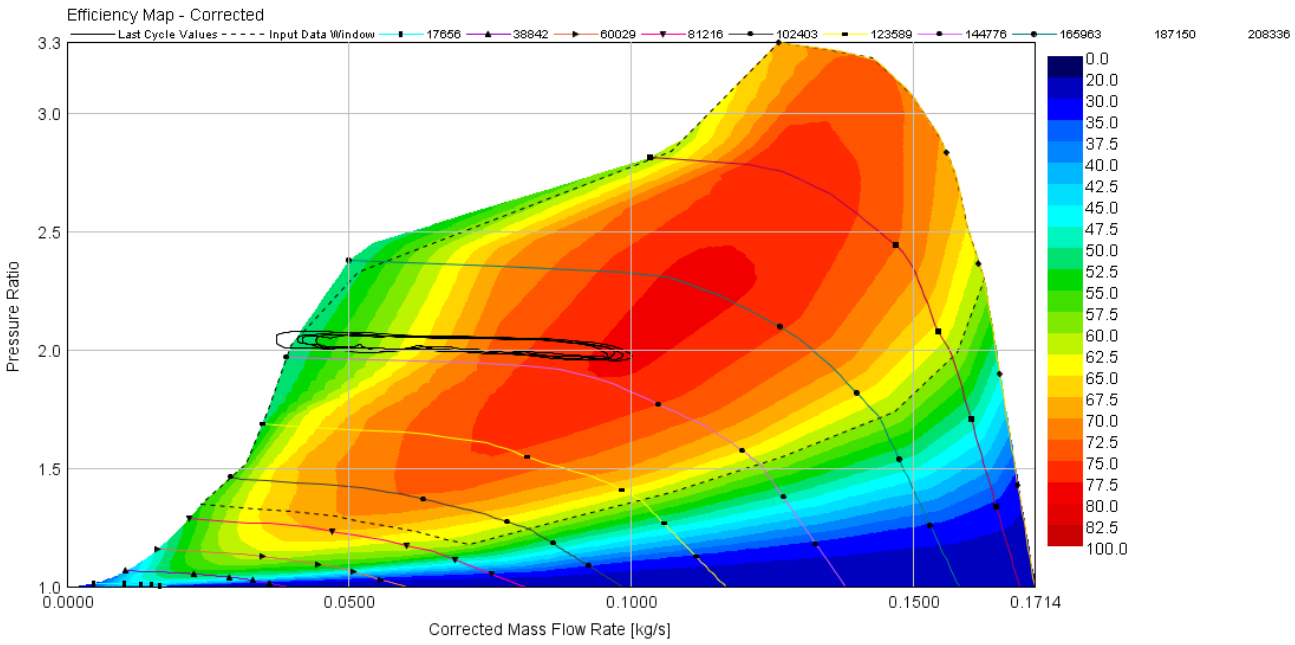

Figure 6-5: Compressor Map showing the operating points during a cycle for the 18 Bar IMEP load point (black lines).

Figures 6-4 and 6-5 show the operating points of the turbine and compressor effectively during an engine cycle at the 18 Bar IMEP operating point. It can be observed that the turbocharger is not operating at its best efficiency at high load; the turbine efficiency is 58%, while the compressor efficiency is 68%, giving an overall turbocharger efficiency of only 39%. Moreover, as the compressor map shows, at certain points during the cycle, the compressor is moving into the surge region, which indicates that the turbocharger may be oversized for high load, medium speed operation and that a smaller turbocharger may be needed. The pumping work is also negative, at -0.17 Bar.

To further improve the fuel economy, the pumping penalty can be reduced by improving the turbocharger efficiency such that the intake-exhaust pressure difference can be decreased. This can be achieved by selecting a smaller turbocharger that shifts the operating point on the compressor map to a more efficient island so that the backpressure may be reduced. In addition, the gas exchange process may be enhanced through a redesign of the exhaust manifold with a concept known as the Divided Exhaust Period (DEP). This is covered in the next chapter.

CHAPTER 7: SIMULATION OF THE DIVIDED EXHAUST PERIOD CONCEPT IN A MULTI-CYLINDER RCCI ENGINE

This chapter covers the details of the simulation study on the Divided Exhaust Period (DEP) concept for multi-cylinder RCCI operation. Section 7.1 provides the motivation for the DEP concept by investigating the drawbacks of using the stock exhaust manifold configuration. Section 7.2 gives an overview of the methodology used in the DEP study, followed by Section 7.3 which describes the changes made to the EES code written for the stock configuration to include the blowdown and scavenging manifolds. Section 7.4 discusses the DEP simulation with stock exhaust valve area, and compares the results obtained with those of the stock exhaust manifold configuration. Following this, Section 7.5 presents the results for the optimization studies of the exhaust valve area for DEP done using EES. Section 7.6 then covers the setup of the DEP concept in GT-Power, as well as the optimization of the scavenging valve timing and turbocharger for the DEP concept at medium and high load operation, following which Section 7.7 presents the results of the DEP concept for low load operation. Finally, Section 7.8 concludes the chapter by comparing the results obtained DEP implementation on RCCI with other DEP studies in literature.

7.1 Motivation for Divided Exhaust Period Concept – Reduce Pumping Losses

As discussed in Chapter 2, due to the low exhaust gas enthalpy observed in LTC strategies, it is necessary to generate a high exhaust backpressure in turbocharged LTC engines to obtain high turbine pressure ratios for efficient turbocharger operation. This contributes to increased pumping losses, in turn leading to a deterioration in fuel economy. As the log(p)-log(V) diagram in Figure 7-1 and Table 7-1 show, the stock engine configuration gives a negative pumping work for both the 8 Bar BMEP and the 18 Bar IMEP operating points that were investigated in Chapter 5.

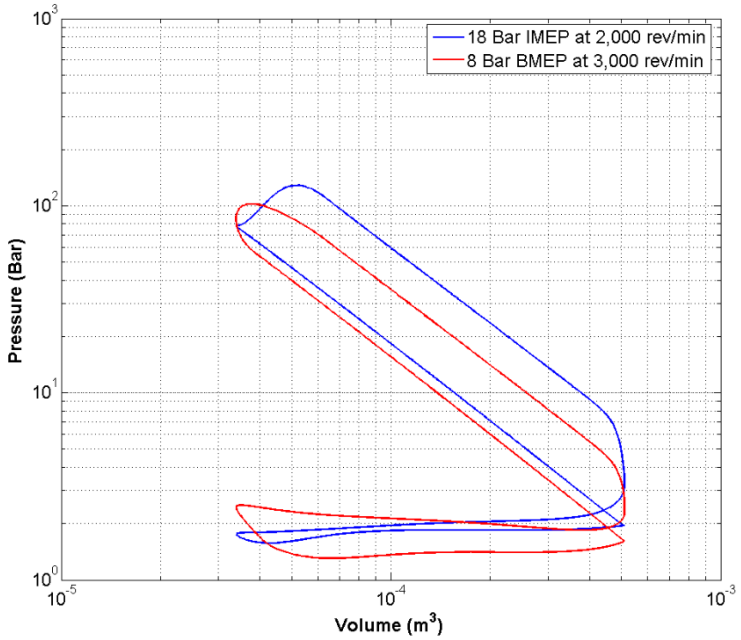

Figure 7-1: p-V Diagram for both the 8 Bar BMEP and 18 Bar IMEP operating points. (Results are from EES)

Table 7-1: Pumping Mean Effective Pressure for the Two Operating Points

Load Point	PMEP (Bar)
8 Bar BMEP	-0.53
18 Bar IMEP	-0.17

To understand at a fundamental level why the increased backpressure is detrimental to the gas exchange process, it is necessary to examine the pressure history of the cylinder, the intake manifold and the exhaust manifold during the exhaust valve open period. Figure 7-2 shows the pressure history plots from the EES simulations of the stock engine configuration for the 8 Bar BMEP and 18 Bar IMEP operating points.

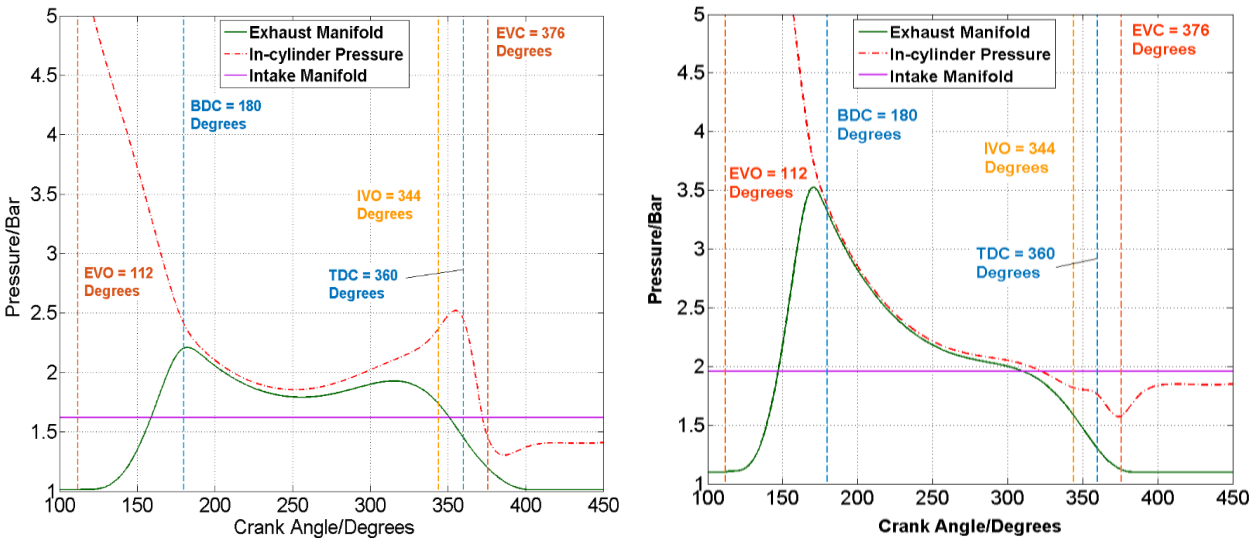

Figure 7-2: In-cylinder, exhaust manifold and intake manifold pressure history plots for the 8 Bar BMEP and 18 Bar IMEP EES simulations. (7-2a, Left): Pressure History for the 8 Bar BMEP at $3,000\ \text{rev} \cdot \text{min}^{-1}$. (7-2b, Right): Pressure History for the 18 Bar IMEP at $2,000\ \text{rev} \cdot \text{min}^{-1}$.

As the plot for the 8 Bar BMEP case shows, when the exhaust valves are first opened at 112 degrees ATDC, the initial higher energy gas is evacuated from the cylinder first into the exhaust manifold, resulting in a rapid decrease in the in-cylinder pressure and a rapid rise in the exhaust manifold pressure until both pressures are almost equal. As the piston reaches BDC and changes travel direction, the remaining gas in the cylinder undergoes compression while cylinder evacuation is still taking place. This results in the rate of pressure drop in the cylinder decreasing significantly at first, and the in-cylinder pressure reaching a minimum of about 1.75 bar before starting to increase again for the 8 Bar BMEP case. The in-cylinder pressure then continues to increase until TDC is reached, at which point the piston motion changes direction once more. From BDC to TDC, it can be observed that the in-cylinder pressure is always greater than the exhaust manifold pressure, resulting in an unfavorable pressure difference that hinders the evacuation process during the exhaust stroke. Also, when the intake valves open at 344 degrees ATDC, the intake manifold pressure is lower than the in-cylinder and exhaust manifold pressures until the piston reaches TDC, producing a negative pressure gradient that the intake air has to overcome before entering the cylinder.

A similar phenomenon is observed for the 18 Bar IMEP case, although at the lower engine speed, the in-cylinder pressure does not reach a minimum before starting to rise again as in the 8 Bar BMEP case, but the rate of pressure drop rapidly decreases as the piston moves upwards from BDC to TDC, giving rise to the in-cylinder pressure being greater than the exhaust pressure, albeit by a smaller amount than in the 8 Bar BMEP case. As the intake valves open, the pressure difference is more favorable than in the 8 Bar BMEP case, but the exhaust pressure/in-cylinder pressure difference being negative contributes to a negative PMEP for an engine cycle.

One way to overcome the negative/unfavorable pressure gradient is to redesign the exhaust system such that the piston is working against an environment with a lower downstream pressure than the pressure in the cylinder for a longer portion of the exhaust stroke. The Divided Exhaust Period (DEP) concept can accomplish this by distributing the exhaust flow into two separate exhaust manifolds: the blowdown manifold which is connected to the turbocharger turbine, and the scavenging manifold which bypasses the turbine and is connected to the turbine outlet. By bypassing the turbine, the scavenging manifold is closer to ambient pressure, so a positive pressure difference between the cylinder and the exhaust system can be maintained over a longer duration than in a conventional engine, thereby reducing the pumping work, and in some cases, even giving a positive pumping work. The exhaust gas distribution between the two manifolds, and hence the backpressure can be varied by using different valve timings for the blowdown and scavenging valves [116]. This way, the scavenging valve essentially functions as a wastegate by directing the excess exhaust gas to the turbine outlet. Unlike a conventional wastegate however, there are no additional throttling losses in the exhaust manifolds as the valve timing already determines the exhaust gas distribution at the cylinder. Even though a supercharger may be required to supplement the boost pressure at certain operating conditions due to the lower exhaust flow rates through the turbocharger turbine, the supercharger would not need to work as hard as in the case with a wastegate-controlled FGT due to the lack of throttling losses.

The objective of this chapter is to compare the system performance of the DEP concept to that of the stock exhaust manifold configuration at three different engine operation conditions: a low load, medium

speed operating point, a medium load, high speed operating point and a high load, medium speed operating point. Particular emphasis is placed on the impact of the DEP concept on fuel consumption and the boosting system efficiency when evaluating system performance. The following section provides an overview of the procedure used for the DEP simulation study.

7.2 Overview of DEP Simulation Study Methodology

Figure 7-3 shows a flowchart summarizing the methodology used for the DEP simulation study. First, the KIVA-3V heat release profiles for the three different operating points were curve fit to the Wiebe function to simulate the combustion process in the EES model. Simulations of the DEP concept were then executed in EES to determine the system parameters, such as exhaust valve diameter and valve timings that gave optimal thermodynamic efficiency. Based on the EES results, the turbocharger was scaled using the procedure described in Chapter 3, and the GT-Power model of the stock engine configuration was modified to incorporate the newly scaled turbocharger along with the aforementioned optimized system parameters. GT-Power simulations were performed to further optimize the parameters that could not be optimized in the EES simulations, such as the turbocharger and supercharger efficiencies, charge-air-cooler wall temperatures and the EGR valve diameters to obtain the required IVC conditions.

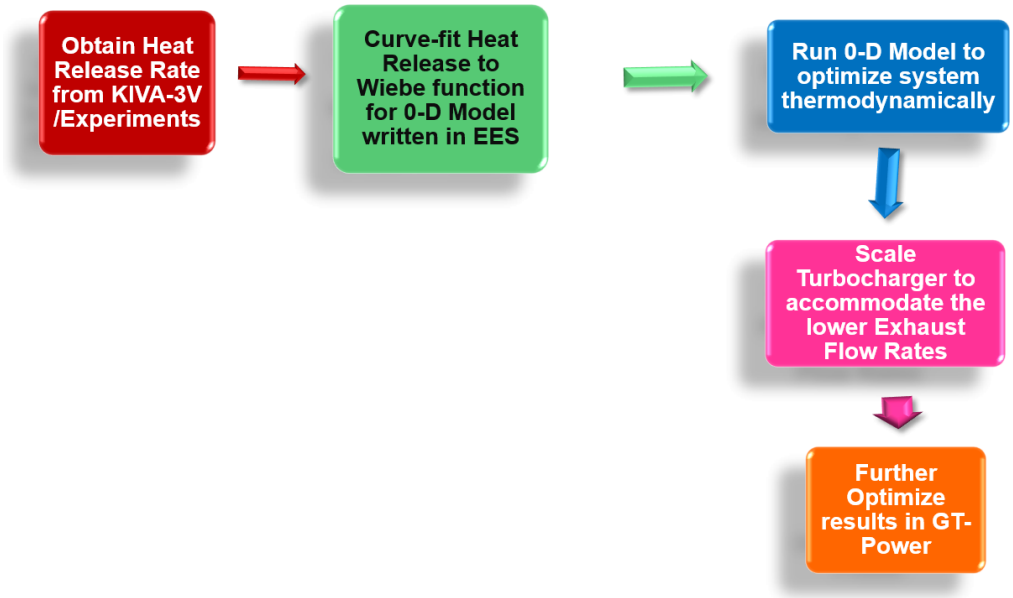

Figure 7-3: Flowchart showing the methodology for DEP simulations

7.3 Modification of EES Code for DEP Filling-and-emptying Simulations

To simulate the DEP concept in EES, the code was first modified to replace the stock exhaust manifold with the blowdown and scavenging manifolds and separate exhaust valve timings corresponding to the manifolds the exhaust valves were connected to. This was done through the introduction of the procedures given in Table 7-2:

Table 7-2: List of new procedures incorporated into EES code for DEP simulations

Procedure Name	Procedure Description
VALVELIFTBLOWDOWN	Computes the Valve Lift and Discharge Coefficient for the Blowdown Valve
VALVELIFTSCAVENGE	Computes the Valve Lift and Discharge Coefficient for the Scavenging Valve
FLOW_BLOWDOWN	Computes the Mass Flow Rate in the Blowdown Port
FLOW_SCAVENGE	Computes the Mass Flow Rate in the Scavenging Port
EXH_DENSITY_BLOWDOWN	Computes the static exhaust gas density at Blowdown Port
EXH_DENSITY_SCAVENGE	Computes the static exhaust gas density at Scavenging Port
MACH_BLOWDOWN	Computes the Mach Number of the Blowdown Port Flow
MACH_SCAVENGE	Computes the Mach Number of the Scavenging Port Flow
STATICBLOWDOWN	Computes the Static Temperature and Enthalpy at Blowdown Port
STATICSCAVENGE	Computes the Static Temperature and Enthalpy at Scavenging Port
BLOWDOWN_THROATVELOCITY	Computes the throat velocity at Blowdown Port
SCAVENGE_THROATVELOCITY	Computes the throat velocity at Scavenging Port
SCAVENGEFLOW	Simulates the exhaust exit leaving scavenging manifold

The VALVELIFTBLOWDOWN procedure is similar to the VALVELIFTEXHAUST procedure in the code for the stock engine configuration. The only difference here is the different expression for the τ_{bd} parameter in the valve lift profile curve fit equation due to the earlier valve closing timing for the blowdown valve. As in the case for the exhaust valve lift profile, the polynomial equation for the blowdown valve lift profile was obtained by curve fitting the valve lift profile in MATLAB using the least squares method. Details of the code modifications are given in Appendix B.

The VALVELIFTSCAVENGE procedure for the scavenging valve also follows a similar structure to the VALVELIFTBLOWDOWN procedure, with the τ_{sc} parameter for the scavenging valve lift profile polynomial equation adjusted for the later opening time of the scavenging valve, as seen in Appendix B.

With 2 exhaust manifolds now present, the exhaust flow through the blowdown and scavenging ports into the blowdown and scavenging manifolds is now simulated through the use of 2 procedures: FLOW_BLOWDOWN and FLOW_SCAVENGE, whose structure is similar to the FLOW_EXHAUST.

The MASSFLOW and ENERGYFLOW procedures in the stock engine configuration code were replaced by the MASSFLOW_DEP and ENERGYFLOW_DEP procedures, which now incorporate the mass and energy flows due to the independent actuation of the exhaust valves, resulting in overlap between the blowdown and scavenging valves, and in overlap between the scavenging and intake valves, as seen in Appendix B.

7.4 DEP Simulations with Stock Exhaust Valve Area

Initial simulations of the DEP concept were performed using the stock exhaust valves and the stock exhaust manifold volume of 309.25 cm^3 each for both the blowdown and scavenging manifolds. The reason for choosing the stock exhaust valve and manifold dimensions was to ensure a controlled comparison of the concept with the conventional engine configuration. Figure 7-4b and Table 7-3 show the blowdown and scavenging valve lift curves used for the simulations; these profiles are similar to the profiles used by Moller et al. [116], shown in Figure 7-4a.

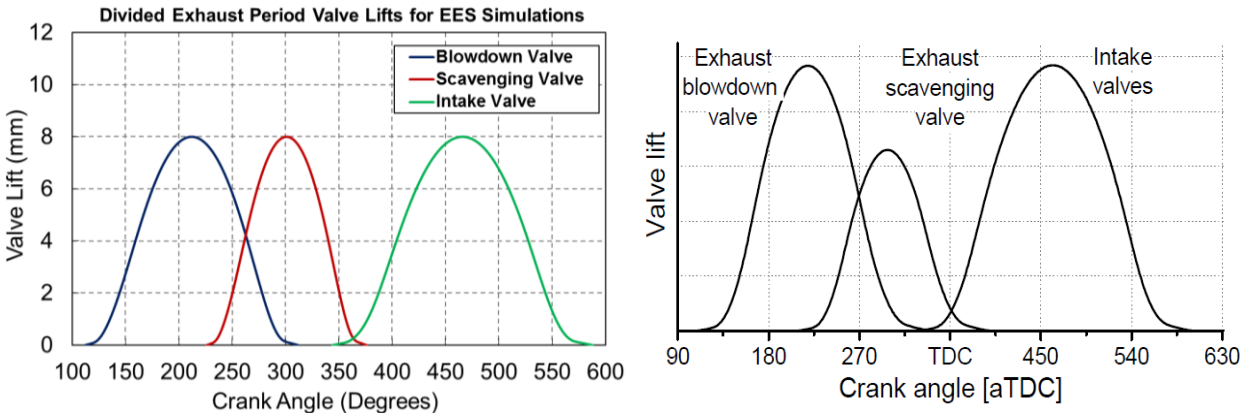

Figure 7-4: (7-4a, Left) Valve Lift Profiles used for the initial DEP Simulations. These profiles are similar to the profiles used by Moller et al. [116] (Right, 7-4b); the only difference between the two sets of profiles is that the maximum scavenging valve lift is the same as the maximum blowdown valve lift of 8 mm for the EES simulations.

A valve open duration of 200 degrees, which is slightly longer than the cylinder firing order phasing of 180 degrees, was chosen for the blowdown valve to minimize pulse interference between the exhaust pulses from different cylinders to maximize pulse turbocharging.

Table 7-3: Blowdown, Scavenging and Intake Valve Opening Timings for DEP

Valve Type	Valve Opening Timing (Deg. ATDC)	Valve Closing Timing (Deg. ATDC)	Valve Open Duration (Degrees)
Blowdown	112	312	200
Scavenging	226	376	150
Intake	344	588	244

Comparing the log(p)-log(V) plots shown in Figure 7-5, it can be observed that the area of the pumping loop for the DEP concept is smaller than that for the stock engine configuration, indicating an improvement in the pumping work for both the 8 Bar BMEP and the 18 Bar IMEP operating points. Table 7-4 gives the PMEP values and the percent change in PMEP at both operating points. PMEP changed by 20.8% from -0.53 Bar to -0.42 Bar at the 8 Bar BMEP operating point and by 55.9% from -0.17 Bar to -0.075 Bar at the 18 Bar IMEP operating point.

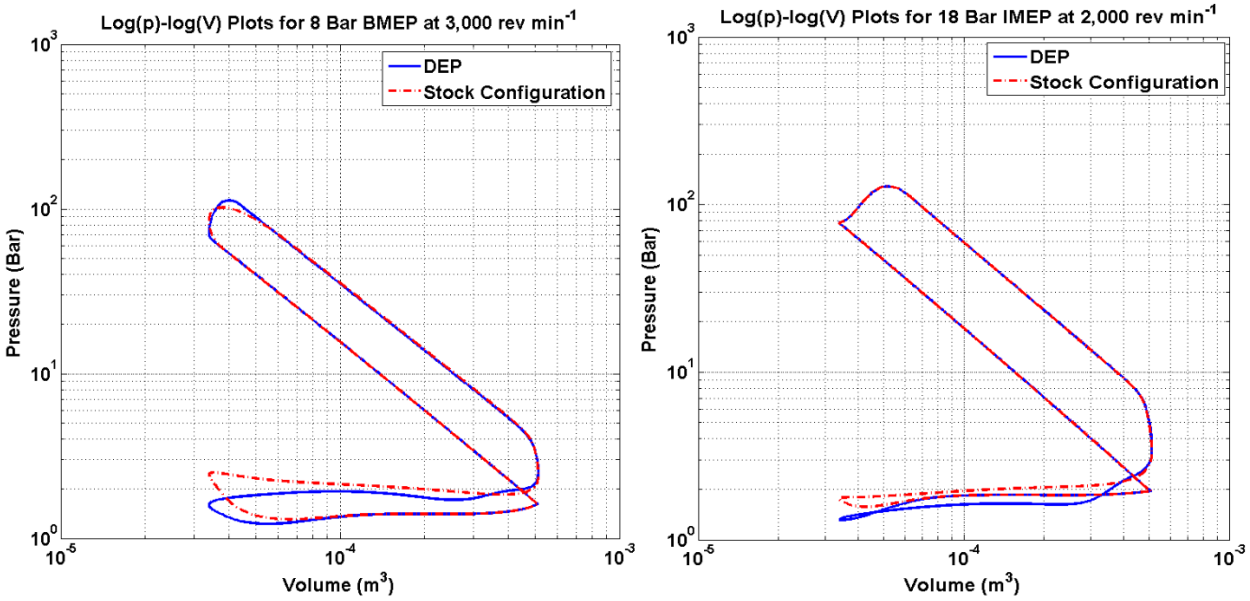

Figure 7-5: (7-5a, Left): Log(p)-log(V) plot of the stock and DEP configurations for the 8 Bar BMEP case. (Right, 7-5b): Log(p)-log(V) plot of the stock and DEP configurations for the 8 Bar BMEP case.

Table 7-4: PMEP Comparison between DEP and Stock Configuration

Load Point	PMEP (Bar)		Percent Change in PMEP
	Stock Configuration	DEP	
8 Bar BMEP	-0.53	-0.42	20.8
18 Bar IMEP	-0.17	-0.075	55.9

Once again, the pressure history plots (shown in Figures 7-6 and 7-7) for the DEP simulations of the 8 Bar BMEP and the 18 Bar IMEP operating points can help explain the decrease in the PMEP observed. Unlike in the stock engine configuration, where both exhaust valves open at 112 degrees ATDC and close at 376 degrees ATDC, the scavenging valve opens later at 226 degrees ATDC, directing the exhaust gas through the scavenging port into the scavenging manifold where the pressure is atmospheric at valve opening. As a result, there is a positive pressure gradient between the cylinder and the scavenging manifold when the scavenging valve opens, which in turn creates a path with lower flow resistance than in the stock configuration, giving rise to a less negative pumping work.

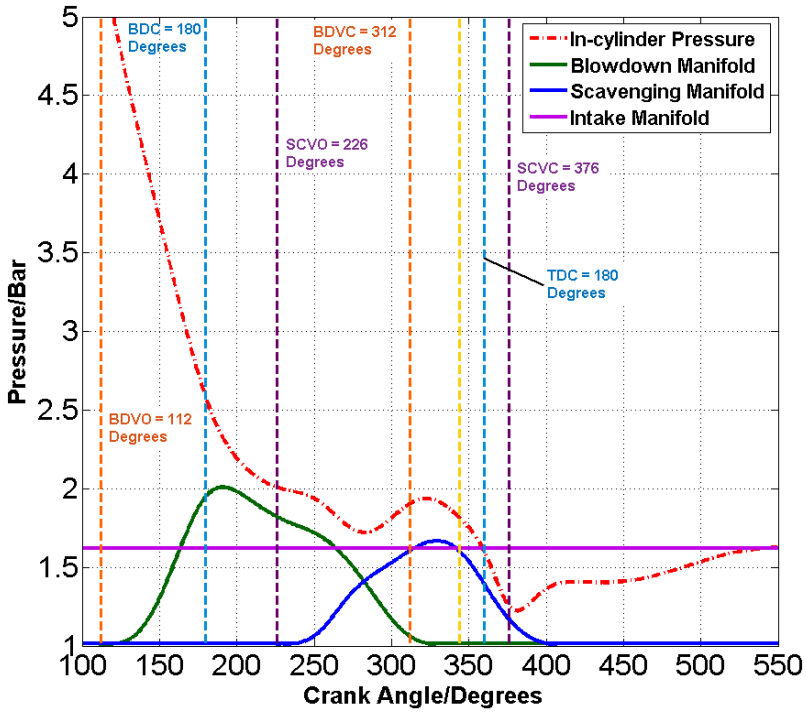

Figure 7-6: In-cylinder, blowdown manifold, scavenging manifold, and intake manifold pressure history for the EES Simulation of the Divided Exhaust Period (DEP) Concept at the 8 Bar BMEP load point. The exhaust valve diameter is the stock diameter of 21.92 mm.

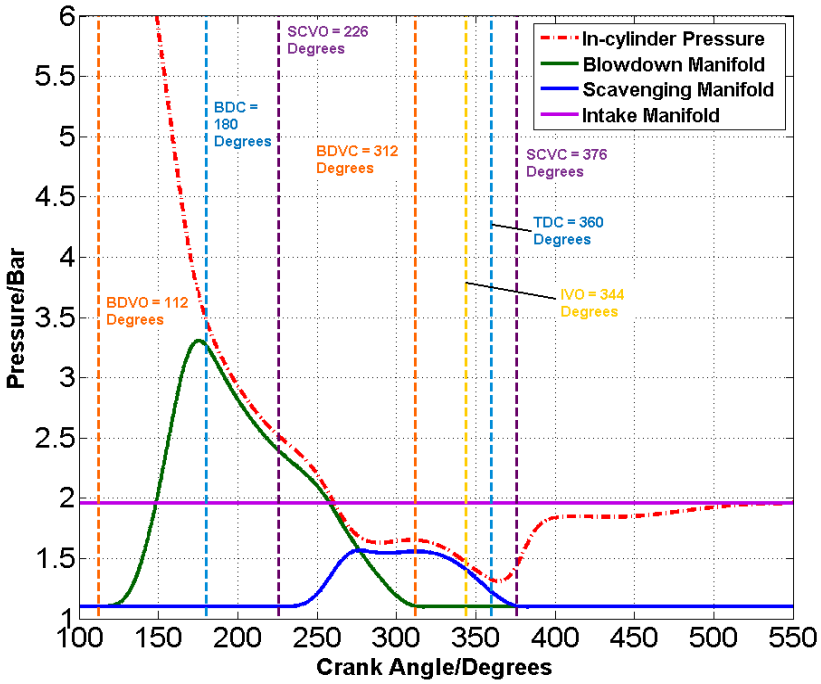

Figure 7-7: In-cylinder, blowdown manifold, scavenging manifold, and intake manifold pressure history for the EES Simulation of the Divided Exhaust Period (DEP) Concept at the 18 Bar IMEP load point. The exhaust valve diameter is the stock diameter of 21.92 mm.

7.5 Optimization of DEP System Parameters using EES

The results in Section 7.4 show that the DEP concept can significantly reduce pumping work by directing the exhaust flow to two separate manifolds that are each at a lower downstream pressure than the in-cylinder pressure at exhaust valve opening. However, these results were obtained using the stock exhaust valve areas. The system performance could be further improved by using a different exhaust valve area that is optimized for the 1.9-Liter engine. This section presents the results of the optimization studies performed using EES for the aforementioned system parameters.

7.5.1 Exhaust Valve Area Optimization

From the studies performed by Moller et al. [116] and Gundmalm et al. [121], the conventional design principle of making the exhaust valve area smaller than the intake valve area is not ideal for the DEP concept. This is especially true at higher engine speeds, as the restricted valve area can prolong the choking duration at the exhaust ports, exacerbating the pumping penalty. Thus, a larger exhaust valve area must be used to reduce the choking duration. However, the extent to which the exhaust valve area can be increased

is limited by the cylinder head and the cylinder head gasket geometries. This occurs mainly because of the limit to which the cylinder head gasket width can be reduced. As the CAD drawings of the cylinder head in Figure 7-8 show, the minimum value to which the gasket width can be reduced that will prevent leakage is 3 mm. With this reduced width, the total exhaust valve area may be increased up to 30% while keeping the intake valve area constant.

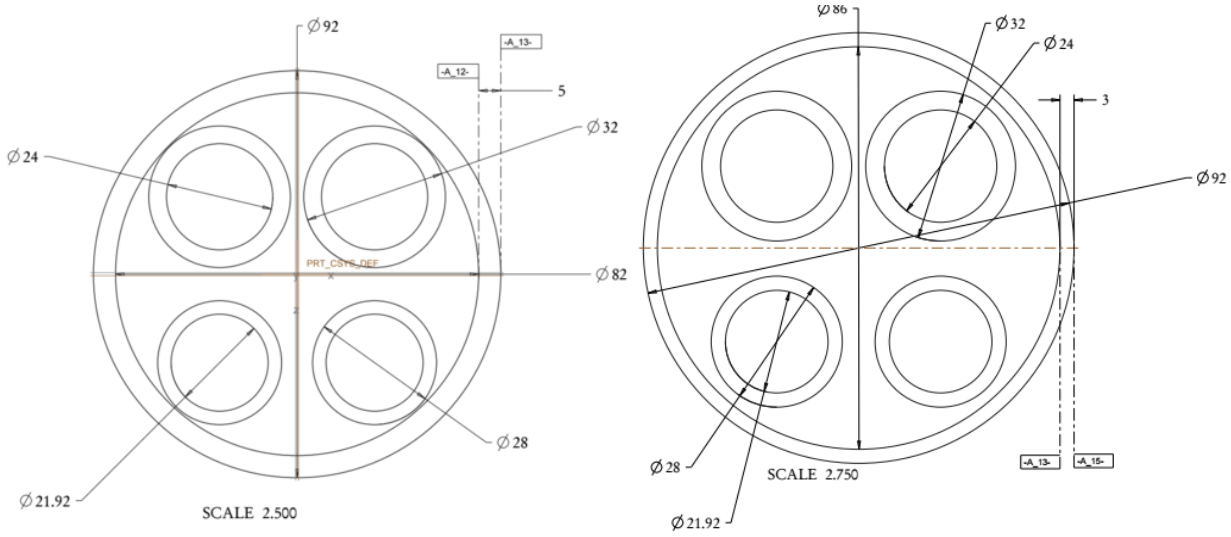

Figure 7-8: 2D CAD Sketch of the cylinder head geometry for the General Motors 1.9L Engine. (7-8a, Left): Stock Cylinder Head and Gasket Dimensions. Current gasket width is 5 mm, and the physical diameters of the intake and exhaust valves are 32 and 28 mm respectively, while their effective diameters are 24 mm and 21.92 mm respectively. (7-8b, Right): Cylinder head with modified gasket width. The gasket width can be reduced down to 3 mm; this is the minimum value that will prevent leakage. With this new width, the exhaust valve area can be increased up to 30% while the intake valve area is kept the same.

To understand the impact of the exhaust valve area on the flow in the exhaust ports and the pumping work, a parametric sweep of the exhaust valve area increase from 0 % to 30% was performed in EES with intervals of 5%, for both the 8 Bar BMEP and 18 Bar IMEP load points. To account for the effect of area change on the flow characteristics at the exhaust ports, the discharge coefficients were adjusted as well. The reader is requested to consult Appendix B for the polynomial coefficients in the discharge coefficient curve fit equation corresponding to each exhaust valve area.

Figures 7-9 and 7-10 show the variation of PMEP as a function of exhaust valve area increase for both the 8 Bar BMEP and 18 Bar IMEP load points respectively. For both figures, the increase in valve area for the stock engine configuration is also plotted to isolate the pumping work improvement caused by the DEP concept so that the effect of area increase can be more clearly observed. As the plots show, the PMEP becomes more positive as the exhaust valve area is increased: at a 30% increase in exhaust valve area, the PMEP increased from -0.42 Bar to -0.30 Bar at the 8 Bar BMEP load point, while the PMEP increased from -0.075 Bar to 0.02 Bar for the 18 Bar IMEP operating point. The decrease in pumping penalty was more significant at the 8 Bar BMEP point which is at a higher speed of $3{,}000\ \text{rev} \cdot \text{min}^{-1}$.

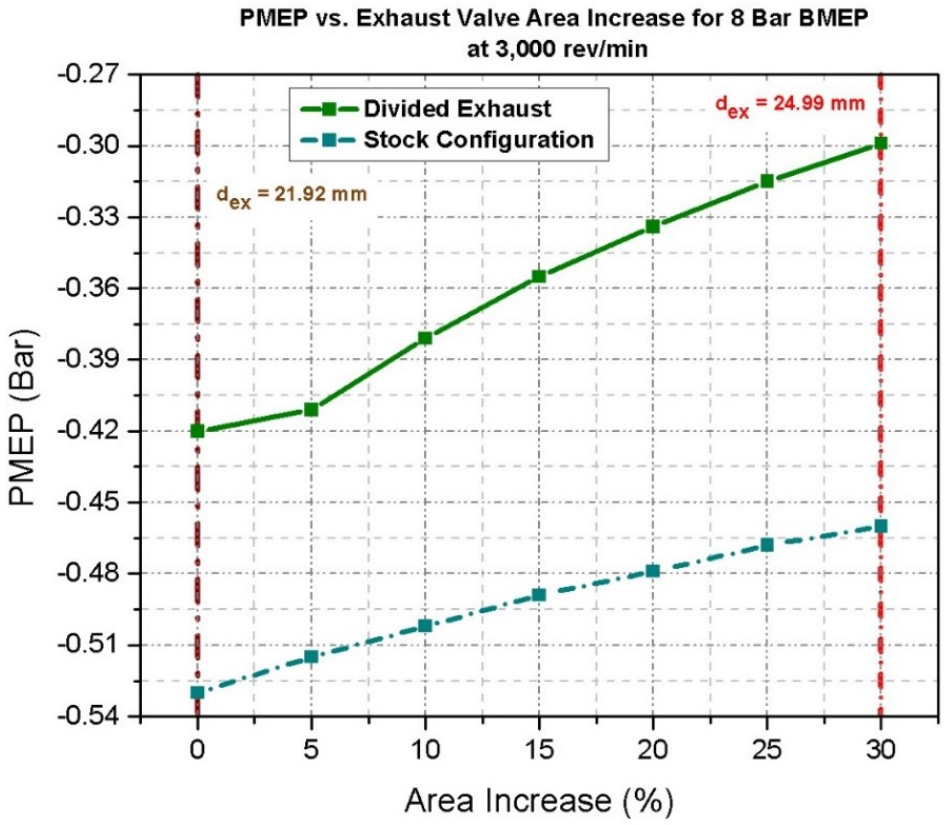

Figure 7-9: Pumping Mean Effective Pressure as a function of Exhaust Valve Area increase for the 8 Bar BMEP at $3{,}000\ \text{rev} \cdot \text{min}^{-1}$ operating point. Stock exhaust valve diameter is 21.92 mm, and a 30% increase in valve diameter corresponds to 24.99 mm. The improvement in pumping work for the stock exhaust configuration is also shown here to separate out the impact of the DEP concept.

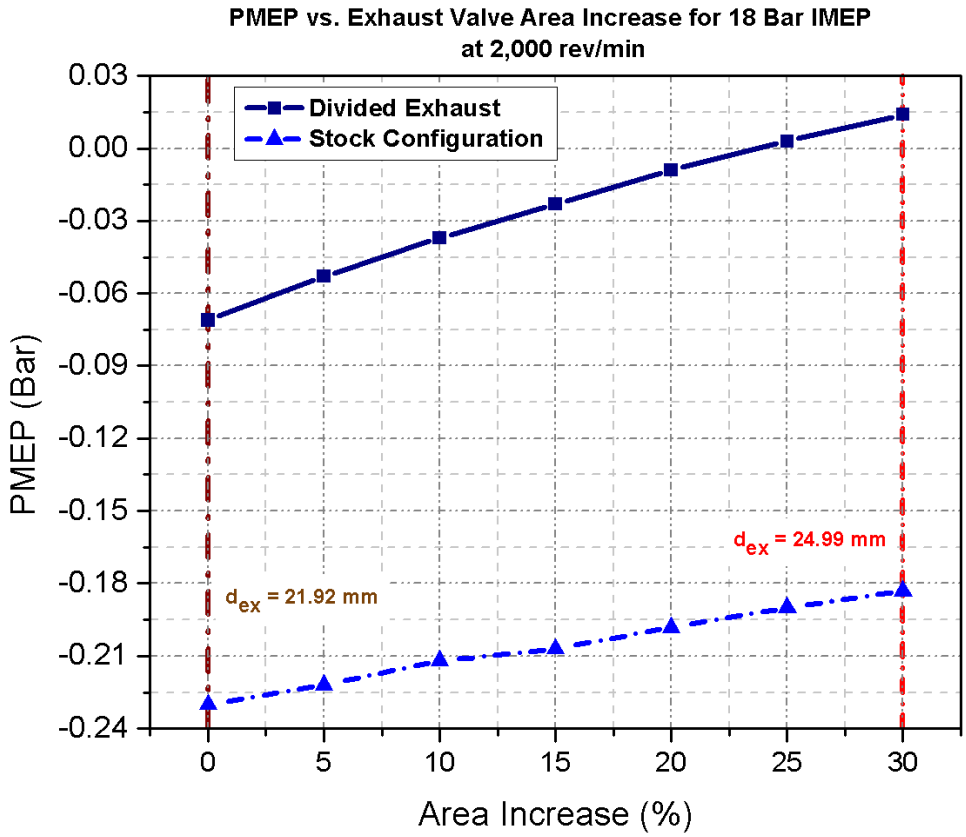

Figure 7-10: Pumping Mean Effective Pressure as a function of Exhaust Valve Area increase for the 18 Bar IMEP at $2,000\ \text{rev} \cdot \text{min}^{-1}$ operating point. Stock exhaust valve diameter is 21.92 mm, and a 30% increase in valve diameter corresponds to 24.99 mm. The improvement in pumping work for the stock exhaust configuration is also shown here to separate out the impact of the DEP concept.

To explain the decrease in pumping penalty for an increase exhaust valve area, it is necessary to examine the flow characteristics at the blowdown and scavenging valve ports. As the Exhaust Port Mach Number plot in Figure 7-11 shows, for the 8 Bar BMEP case, the choking duration is reduced for both the blowdown and scavenging valves, and the overall Mach Number throughout the valve open period for both valves is smaller. With a smaller choking duration, the exhaust gas can be more efficiently and easily evacuated, leading to a more efficient gas exchange process and thus a lowered pumping penalty.

A similar phenomenon is observed for the 18 Bar IMEP Mach Number plot shown in Figure 7-12. However, the choking duration is decreased by a smaller amount since the engine speed is lower for this operating point than for the 8 Bar BMEP operating point.

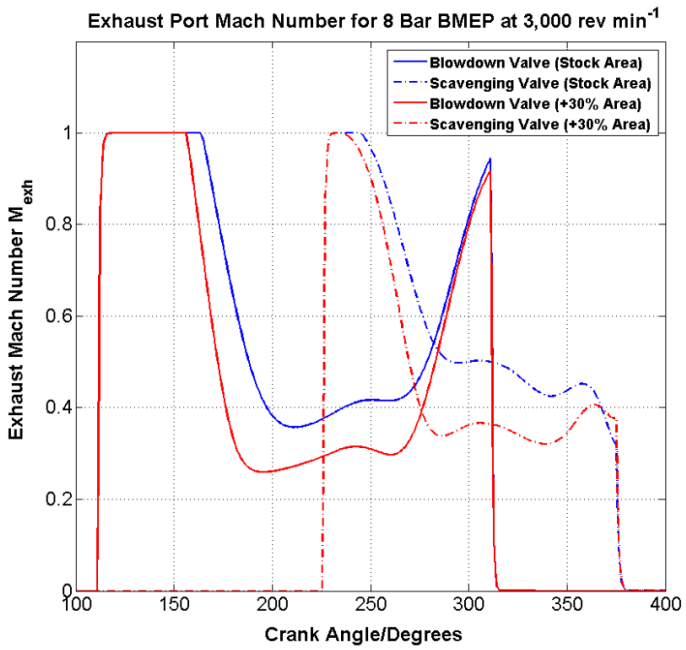

Figure 7-11: Exhaust Flow Mach Number at Blowdown and Scavenging Valves for the 8 Bar BMEP at $3,000\ \text{rev} \cdot \text{min}^{-1}$ operating point for both the stock exhaust valve area and the 30% larger exhaust valve area. Note that with a larger valve area, the choking duration is reduced for both valves.

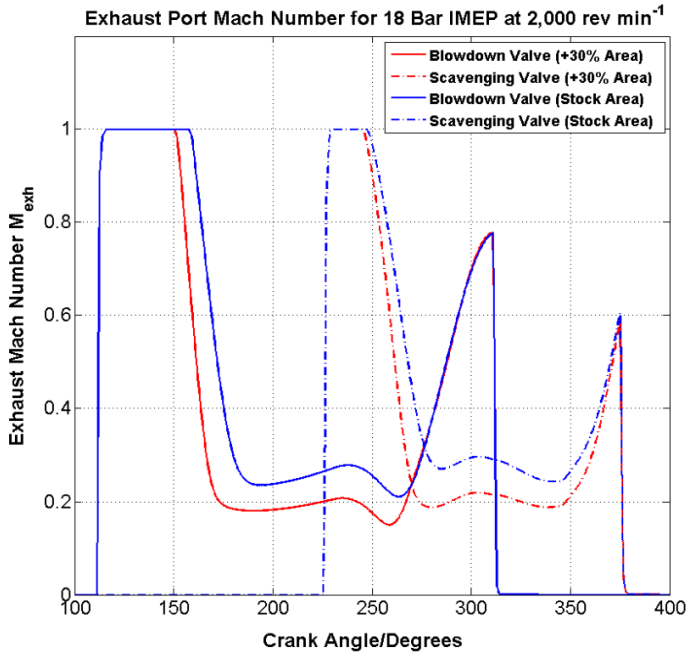

Figure 7-12: Exhaust Flow Mach Number at Blowdown and Scavenging Valves for the 18 Bar IMEP at $2,000\ \text{rev} \cdot \text{min}^{-1}$ operating point for both the stock exhaust valve area and the 30% larger exhaust valve area. The reduction in choking duration is less than what is observed for the 8 Bar BMEP point.

Despite the improvement in the pumping work, the mass flow rate through the turbine was only modestly increased with an increase in exhaust valve area. To understand why, it is necessary to consult the valve discharge coefficient plot in Figure 7-13.

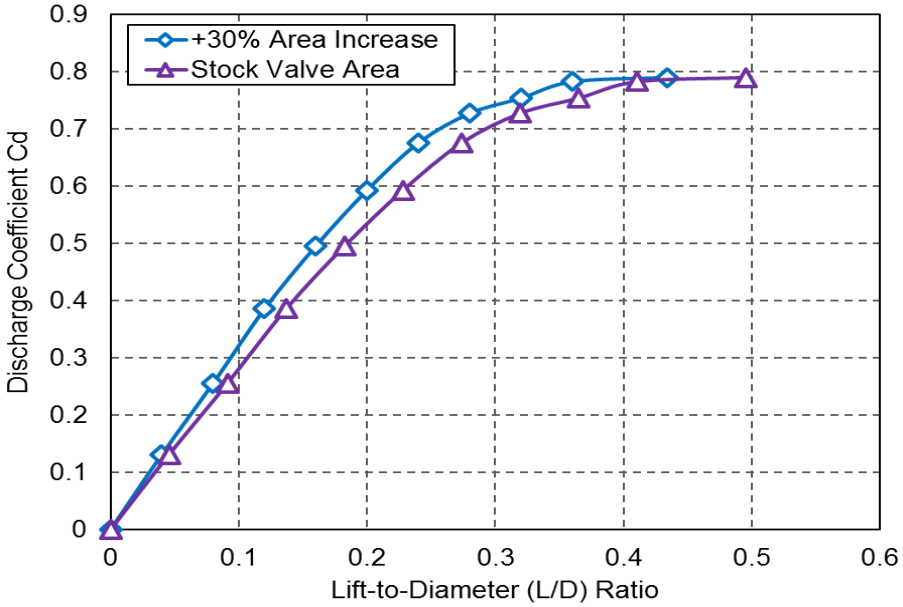

Figure 7-13: Exhaust Valve Discharge Coefficient as a function of valve lift-to-diameter (L/D) ratio for both the stock exhaust valve area and the 30% increased valve area.

The valve discharge coefficient starts to plateau as the lift-to-diameter ratio increases beyond 0.25. Thus, even with a 30% increase in exhaust valve area, if the valve lift and duration for the blowdown and scavenging valves are kept the same, the discharge coefficient does not change much, resulting in similar ratios of effective flow areas for the blowdown and scavenging valves, which in turn means that the mass flow rate through the turbine does not increase significantly. In order to direct a greater flow quantity through the turbine, the duration of the scavenge valve opening has to be decreased so that the cycle-averaged discharge coefficient and thereby the effective flow area of the scavenging valve during the cycle is reduced. The next sub-section investigates the use of scavenging valve timing variation to modulate the exhaust flow distribution.

7.5.2 Control of Exhaust Flow Distribution by Changing Scavenging Valve Opening Timing

Roth et al. [118] showed in their simulations and experiments of BorgWarner's Valve Event Modulated Boost (VEMB) system that varying the scavenging valve opening timing was able to provide substantial boost modulation by controlling the exhaust flow distribution between the blowdown and scavenging manifolds. By retarding the scavenging valve opening (SCVO) timing, a greater proportion of the exhaust could be directed towards the blowdown manifold, allowing the turbocharger to provide more boost. It was therefore decided to perform a parametric sweep of the SCVO timing to understand the effect it had on the exhaust flow distribution, and determine whether SCVO timing would be an effective control knob for adjusting the exhaust backpressure and flow rate for the turbine in an RCCI engine.

For the SCVO timing studies, the blowdown valve lift profile and the scavenging valve closing (SCVC) timing were kept constant, while the SCVO timing was varied from 226 Degrees to 286 Degrees in 10 Degree intervals. Figure 7-14 shows the valve lift profiles used for the SCVO sweep.

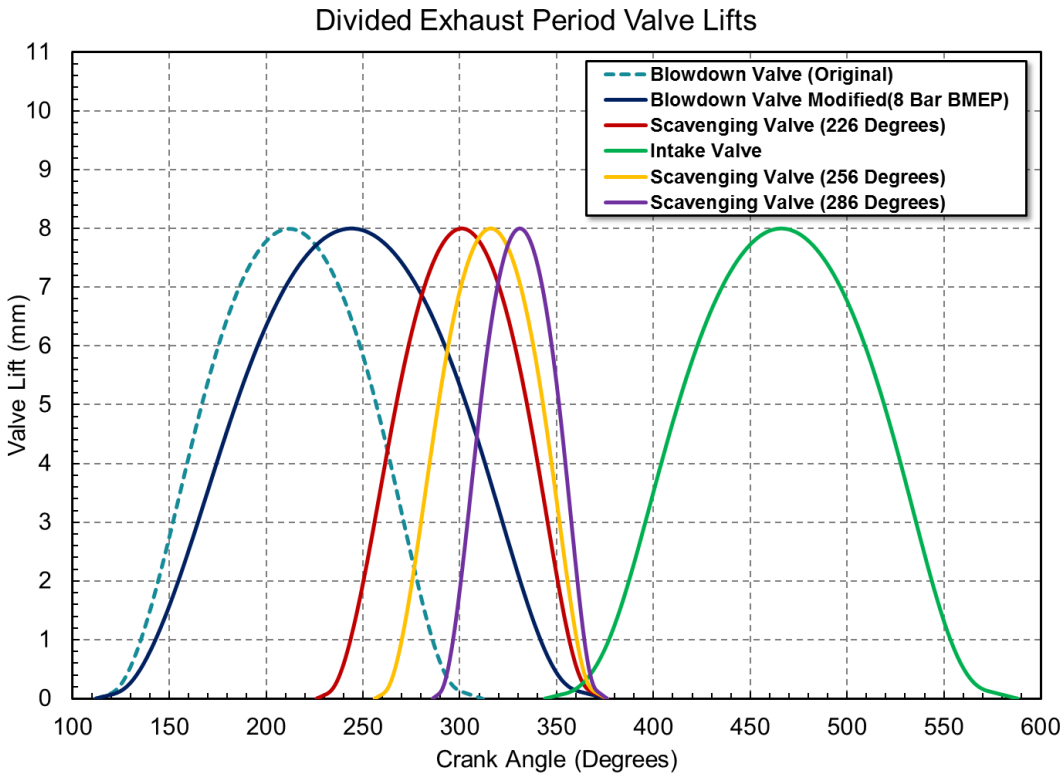

Figure 7-14: Valve Lift Profiles for the SCVO Timing Parametric Study.

Figure 7-15 shows the change in exhaust flow proportion through the turbine as a function of SCVO timing for both the 8 Bar BMEP and 18 Bar IMEP cases. With the 8 Bar BMEP case, the exhaust flow proportion could not be sufficiently modulated with a more retarded SCVO timing beyond 264 degrees ATDC. Thus it was decided to change the blowdown valve lift profile for the 8 Bar BMEP case to the stock exhaust valve lift profile with EVO timing of 112 degrees ATDC and EVC timing of 376 degrees ATDC (shown by the solid dark blue curve in Figure 7-14). By using the stock EVO profile for the blowdown valve, the exhaust flow distribution range could be extended, as shown in Figure 7-16.

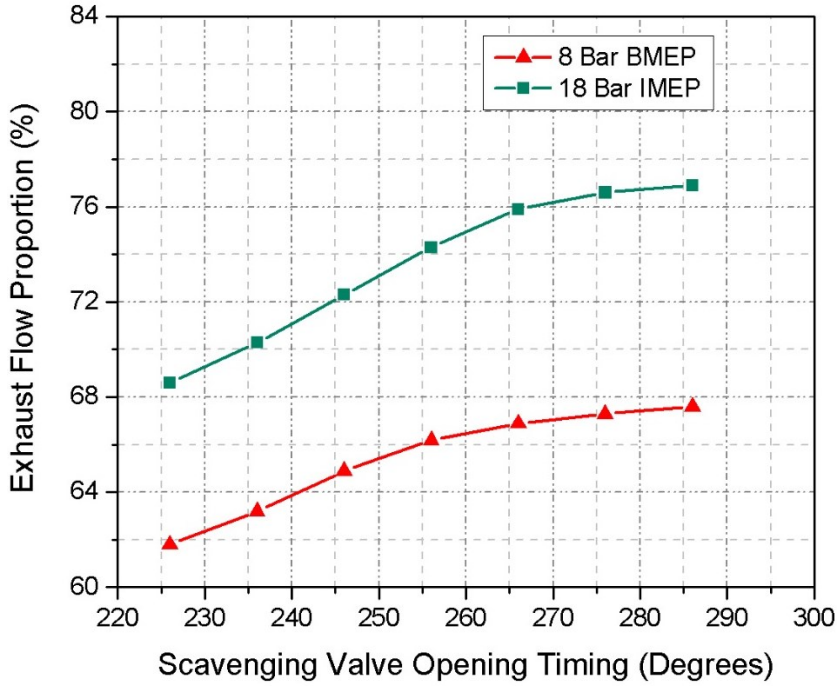

Figure 7-15: Exhaust Flow Proportion through the blowdown manifold/turbine as a function of SCVO Timing for the original blowdown valve open duration of 200 degrees (BDVO = 112 Degrees ATDC and BDVC = 312 Degrees ATDC)

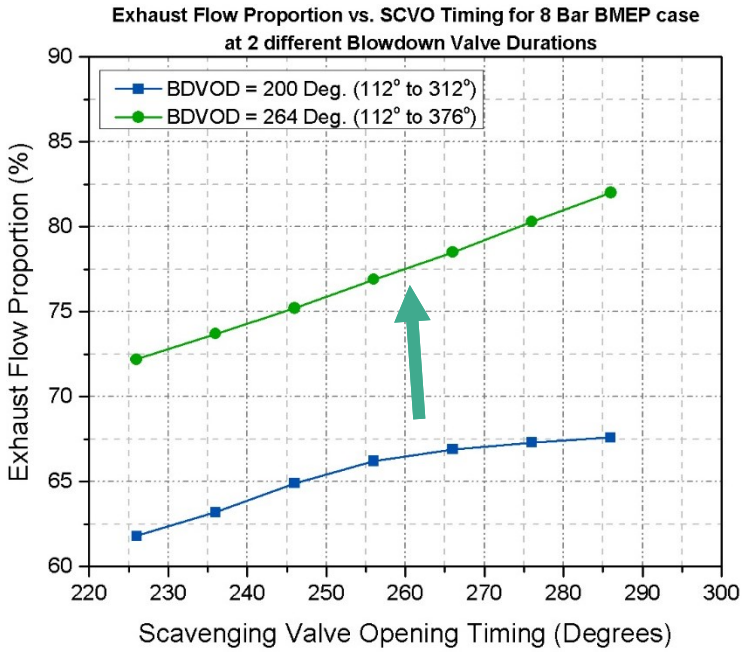

Figure 7-16: Exhaust Flow Proportion through the blowdown manifold/turbine as a function of SCVO Timing for two different blowdown valve open durations (BDVOD) – this is for the 8 Bar BMEP load point. By using the stock exhaust valve lift profile for the blowdown valve, the flow proportion is substantially increased and the distribution can be better modulated with a change in SCVO timing.

From the SCVO timing study, it was decided that the stock exhaust valve lift profile would be used for the blowdown valve operation at the 8 Bar BMEP load point and the 200 degrees BDVOD profile would be used for the 18 Bar IMEP load point. The SCVO timing cannot be finalized at this point, because the actual scavenging valve lift strategy would depend heavily on the compressor performance (both turbocharger and supercharger) and the impact of the compressor performance on fuel economy. Thus, for determining the scavenging valve operating strategy, 1-D system simulations in GT-Power must be executed.

7.5.3 Turbocharger Scaling

The turbocharger scaling procedure described in Chapter 3 was used to determine the geometrical requirements of the new turbocharger for the DEP concept. The scaling procedure was performed using the 8 Bar BMEP point as the reference due to the higher intake and exhaust flow rates at that point, which are a consequence of the higher engine speed of $3{,}000\ \mathrm{rev} \cdot \mathrm{min}^{-1}$. Moreover, since the 8 Bar BMEP point is

a more frequently encountered operating condition during a typical driving cycle, it made sense to choose that point for optimization and further investigation. The T60 map (at a rack position of 0.6) was chosen as the template for the scaling since the isentropic efficiencies at the rack position of 0.6 were the highest.

As the scavenging valve timing determines the exhaust flow rate through the turbine, the scaling was performed for each SCVO timing to determine the influence of the scavenging valve behavior on the optimal turbine and compressor wheel diameters. For each SCVO timing, the blowdown manifold pressure was used to calculate the turbine pressure ratio, and the maximum isentropic efficiency for each corresponding pressure ratio was obtained from the non-dimensional T60 map. The corresponding values for the mass flow coefficient were then evaluated, and the mass flow coefficient, blowdown manifold pressure, blowdown manifold temperature and blowdown mass flow rate were fed into Equation 3.59 (see Chapter 3) to find the turbine wheel diameter for each SCVO timing. Figure 7-17 gives the mass flow coefficient and turbine isentropic efficiency as well as the turbine wheel diameter for different SCVO timings, while Figure 7-18 gives the centrifugal compressor isentropic efficiency, centrifugal compressor pressure ratio, and the compressor wheel diameter as functions of SCVO timing. Note that for the compressor wheel diameter evaluation, only SCVO timings of 256 Degrees ATDC and later were considered because, at earlier SCVO timings, the compressor efficiencies and pressure ratios were too low and these points lay well into the choked flow region of the map where accurate values of efficiency were unavailable.

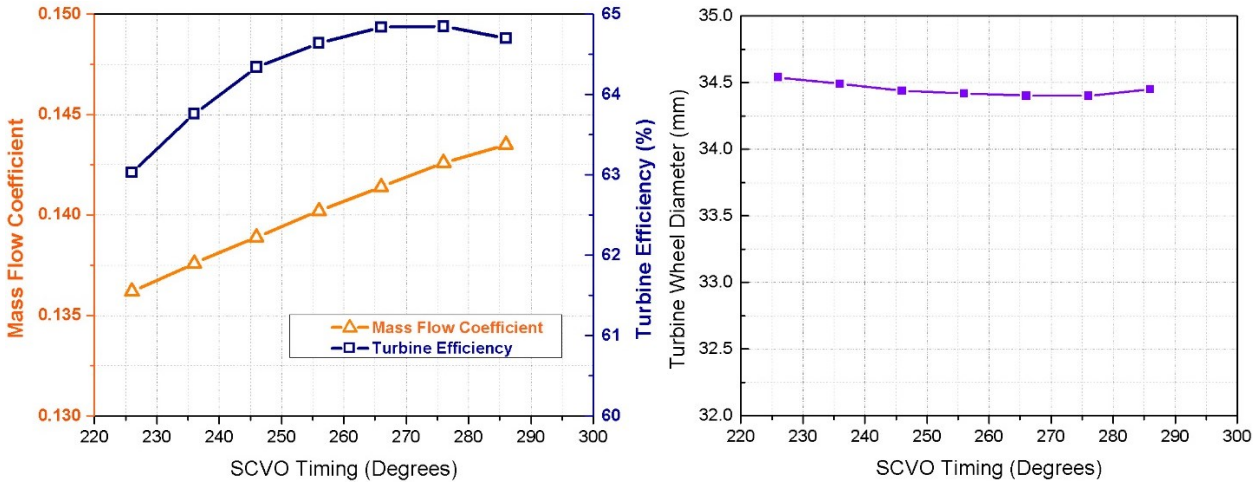

Figure 7-17: (7-17a, Left): Variation of Turbine Mass Flow Coefficient and Isentropic Efficiency with SCVO Timing. (7-17b, Right): Variation of Turbine Wheel Diameter with SCVO Timing.

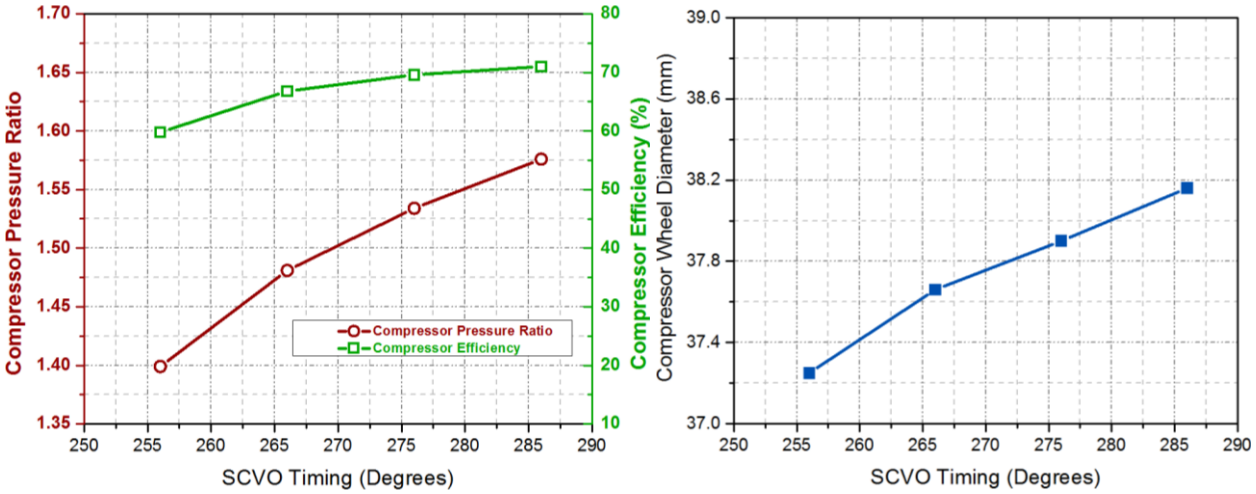

Figure 7-18: (7-18a, Left): Variation of Centrifugal Compressor Pressure Ratio and Isentropic Efficiency with SCVO Timing. (7-18b, Right): Variation of Centrifugal Compressor Wheel Diameter with SCVO Timing.

As the results show, the valve timing did not have a significant effect on the turbine or compressor wheel diameters. Based on these results, the new turbine and compressor wheel diameters were calculated by taking the mean of the wheel diameters given in Figures 7-17b and 7-18b. These values were determined to be 34.45 mm and 37.74 mm respectively. The new turbine wheel diameter is 13.6% smaller than the stock turbine wheel diameter of 39.87 mm while the new compressor wheel diameter is 10% smaller than the stock compressor wheel diameter of 41.92 mm.

7.6 GT-Power Modeling of the Divided Exhaust Period

The GT-Power model for the DEP concept is shown in Figure 7-19. The stock exhaust manifold was removed, and two separate exhaust manifolds were constructed: the blowdown manifold (highlighted in orange) and the scavenging manifold (highlighted in blue). The blowdown manifold was connected to the turbine inlet and was designed in a 4-2-1 configuration for efficient utilization of pulse turbocharging. The stock VGT was replaced with the smaller FGT whose turbine and compressor wheel diameter selection was discussed in the previous section.

As the preliminary studies in EES show, a boost deficit is to be expected due to the reduction in the exhaust gas mass flow rate through the turbine, which limits the power supplied to the centrifugal compressor. Therefore, an Eaton TVS-R410 Roots-type Supercharger was incorporated into the model as a 2nd stage compressor to make up for the deficit. The compressor map for the TVS-R410 was fed into the compressor template representing the blower, and a reduction gear component was used to represent the pulley/belt drive connection between the cranktrain and the supercharger. A 2nd charge air cooler was added downstream of the turbocharger compressor and upstream of the TVS-410 to cool the intake charge before it enters the supercharger. The compressor housing, seals and rotors of the TVS-410 are not built to withstand high temperatures, so the intake charge has to be cooled to an acceptable temperature before it enters the TVS-R410 to protect its components, necessitating the use of the 2nd charge air cooler. A clutch was added to the system to allow the supercharger to disengage from the cranktrain when not needed, and a supercharger bypass valve was also incorporated.

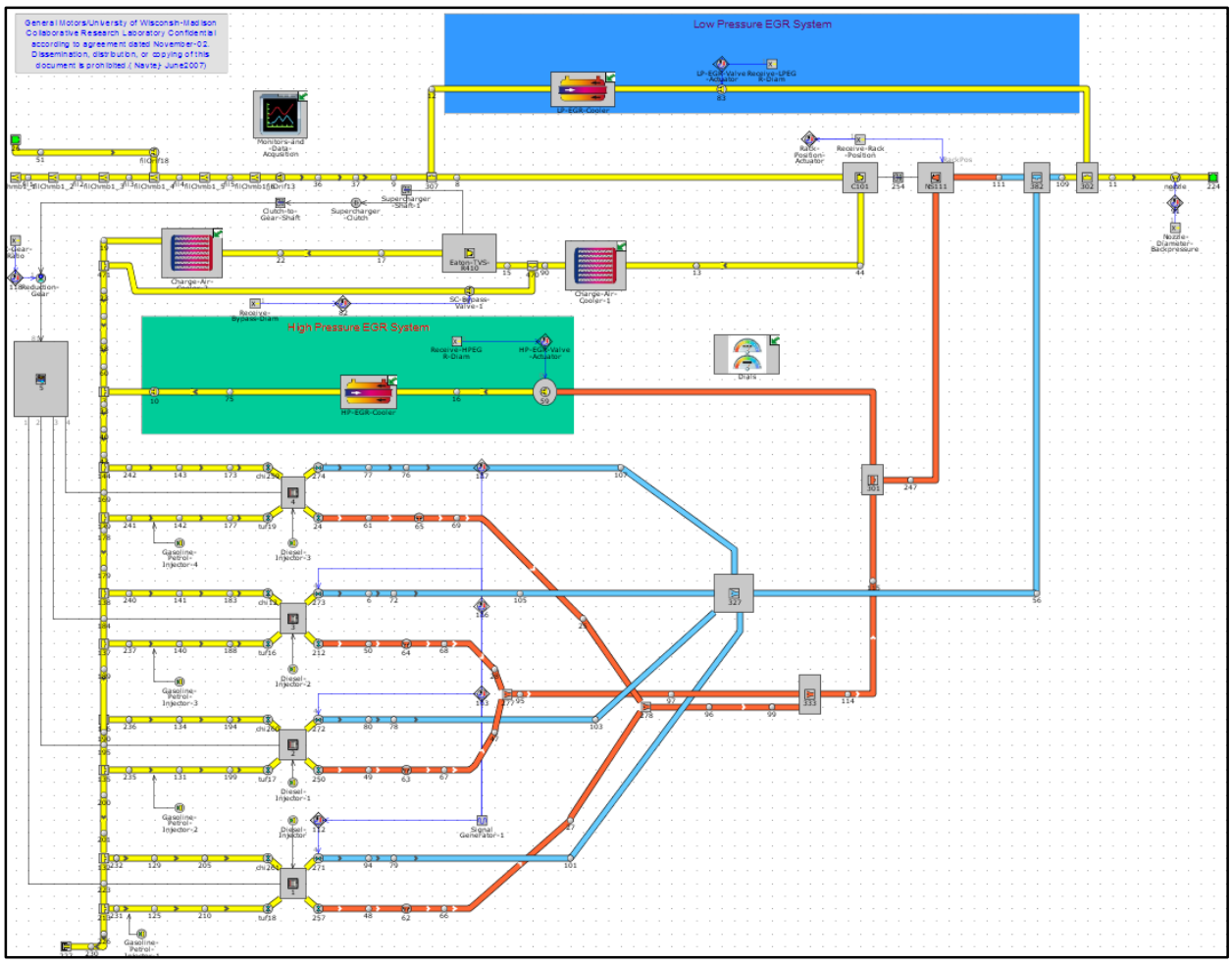

Figure 7-19: GT-Power Model of Stock Engine Configuration modified for Divided Exhaust Period (DEP). The orange flow components represent the blowdown manifold which is connected to the turbocharger turbine inlet while the blue flow components depict the scavenging manifold which bypasses the turbine. An Eaton TVS-R410 Roots Blower was added as a 2nd stage compressor to make up for any potential boost deficit, and a charge air cooler was added between the two compressor stages. The turbocharger has been scaled based on the work of Bell et al. [177].

Based on the exhaust valve area study described in Section 7.5, the largest possible exhaust valve diameter of 24.99 mm (physical valve diameter of 32 mm) was chosen as this would give the least choked flow duration possible. The stock exhaust valve lift profile was used for the blowdown valve at the 8 Bar BMEP load point while the 200-degree duration blowdown valve lift profile (112 Degrees ATDC to 312 Degrees ATDC) was used for the 18 Bar IMEP load point. Similar to the SCVO study in EES, the SCVO timing was varied from 226 Degrees ATDC to 286 Degrees ATDC with 10 degree intervals. The objective of the GT-Power study was to investigate the effect of SCVO timing on the turbocharger and supercharger

performance, and how the performance of the two compressors in turn would affect the pumping work, the BMEP and the BSFC.

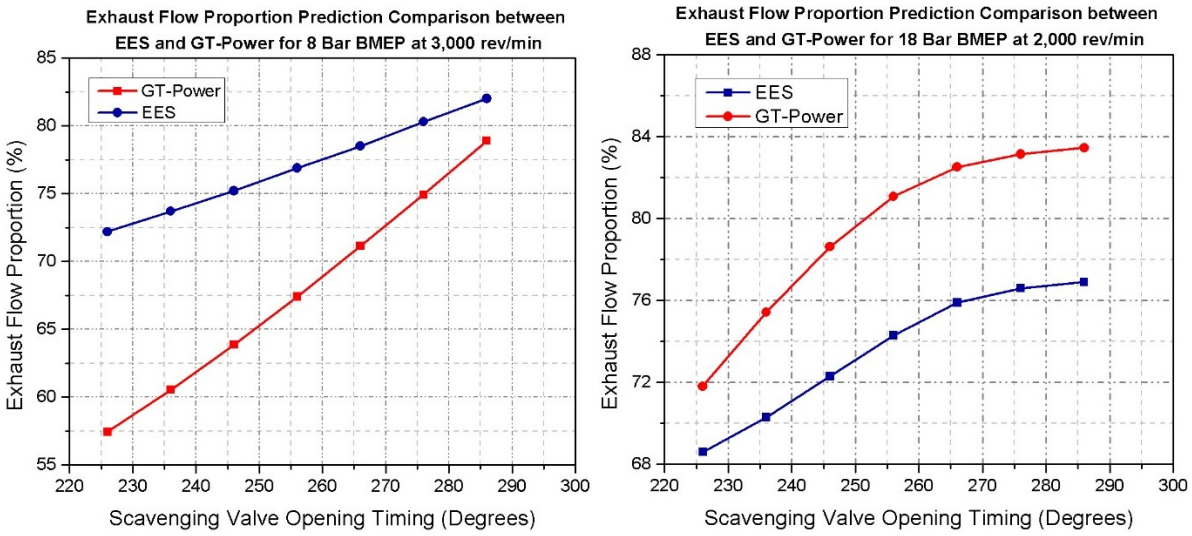

Figure 7-20: Exhaust Flow Distribution Comparison between GT-Power and EES models for: (Left, 7-20a) 8 Bar BMEP load point and (Right, 7-20b): 18 Bar IMEP load point.

The exhaust flow proportion predicted by GT-Power and the zero-dimensional model in EES is different, but this is to be expected due to the gas dynamics effects that are captured by GT-Power that affect the flow characteristics. Moreover, the influence of other cylinders was not considered in the EES model as only a single cylinder was simulated. Nevertheless, the zero-dimensional model was used as a guide to determine the first guess values for the new turbocharger design and to plan further studies, so this discrepancy was acceptable.

From the size of the pumping loops shown in Figure 7-21 for different SCVO timings, they were all smaller than the pumping loop (or more positive in the 18 Bar IMEP case) for the stock engine configuration, indicating that there is indeed a pumping benefit with the DEP concept. With a more retarded SCVO timing, the area of the pumping loop became more negative, giving rise to a more negative PMEP, as shown in Figure 7-22.

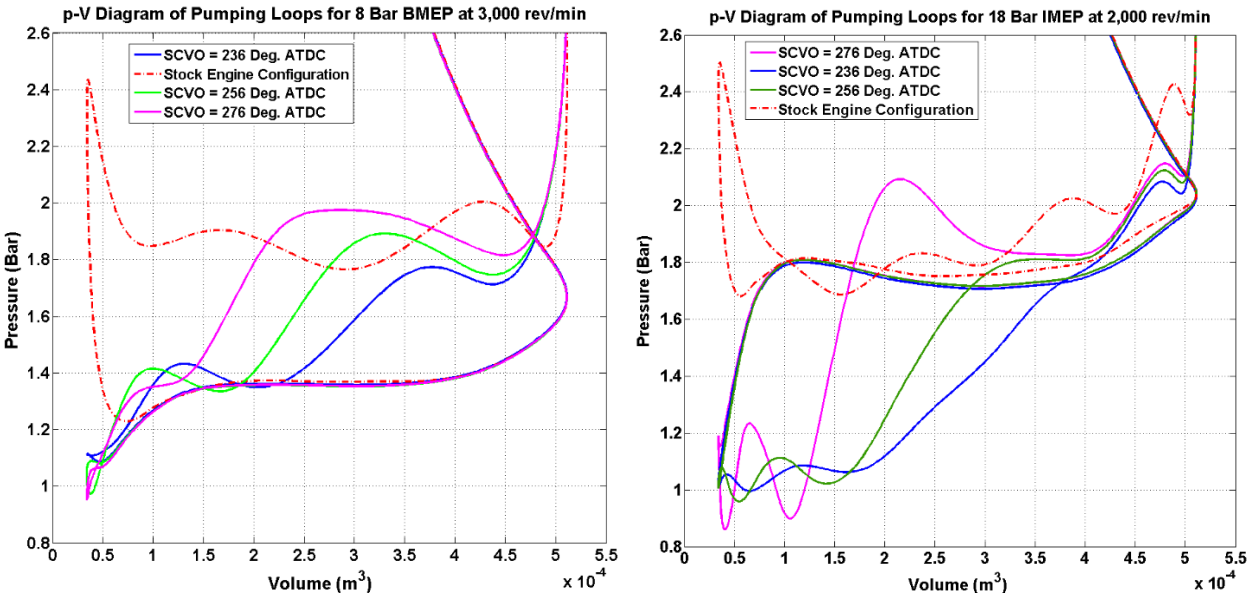

Figure 7-21: p-V diagrams showing the pumping loops for the DEP and stock configurations for both the 8 Bar BMEP and 18 Bar IMEP cases. (Left, 7-21a): 8 Bar BMEP. Right (7-21b): 18 Bar IMEP.

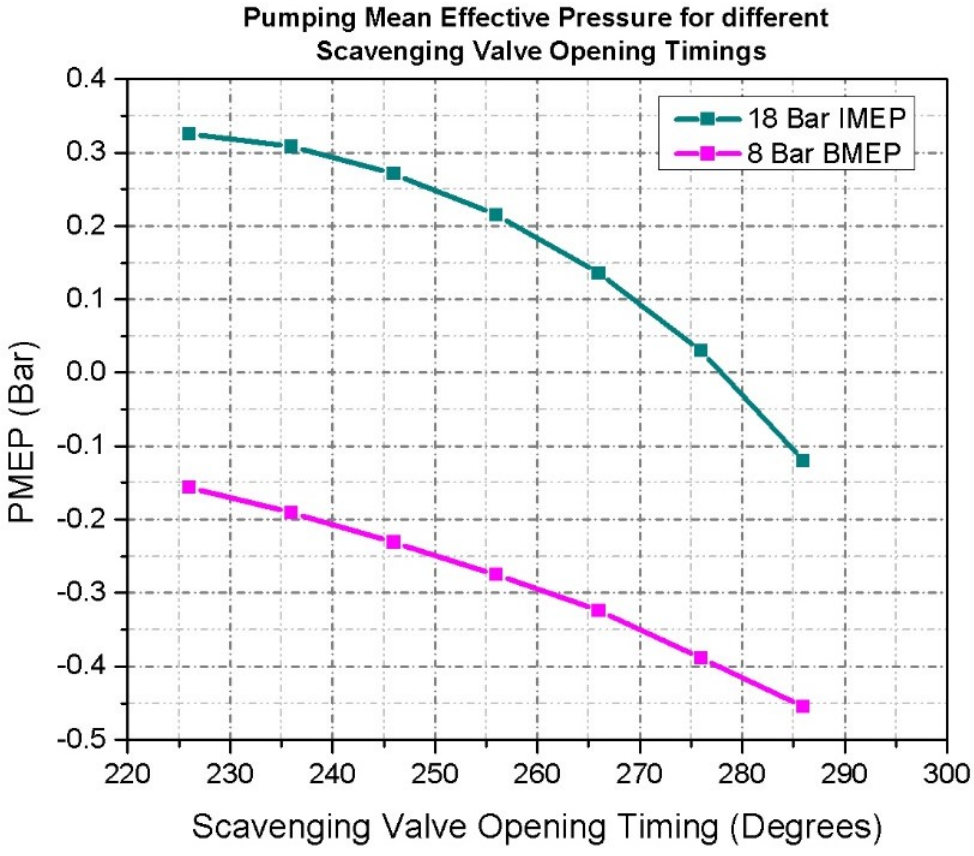

Figure 7-22: PMEP as a function of SCVO timing for 8 Bar BMEP and 18 Bar IMEP

The pumping penalty increase with a more retarded SCVO timing can once again be explained by analyzing the manifold and cylinder pressure history plots. Figures 7-23 and 7-24 show the pressure history plots at an SCVO timing of 236 Degrees ATDC and 276 Degrees ATDC respectively for the 8 Bar BMEP point. Once the piston moves away from the BDC position (at 180 Degrees) and the pressure difference between the blowdown manifold and the cylinder has approached zero, the in-cylinder pressure starts to increase as the in-cylinder volume decreases due to the movement of the piston. If the scavenging valve is opened earlier (i.e., at 236 Degrees ATDC), the pressure in the cylinder drops rapidly as the gas now has a 2^{nd} path (of lower flow resistance) to the scavenging manifold, which is close to atmospheric pressure. Opening the scavenging valve later (i.e., at 276 Degrees) causes the cylinder pressure to rise to almost 2 Bar. With a larger pressure difference between the cylinder and the blowdown manifold for a later SCVO timing, the backflow of exhaust into the cylinder from the blowdown manifold increases, causing a deterioration in the efficiency of the gas exchange process. The engine backpressure also rises as there is a larger proportion of the exhaust flowing through the blowdown manifold when the open duration of the scavenging valve, and hence the effective flow area of the scavenging valve is reduced.

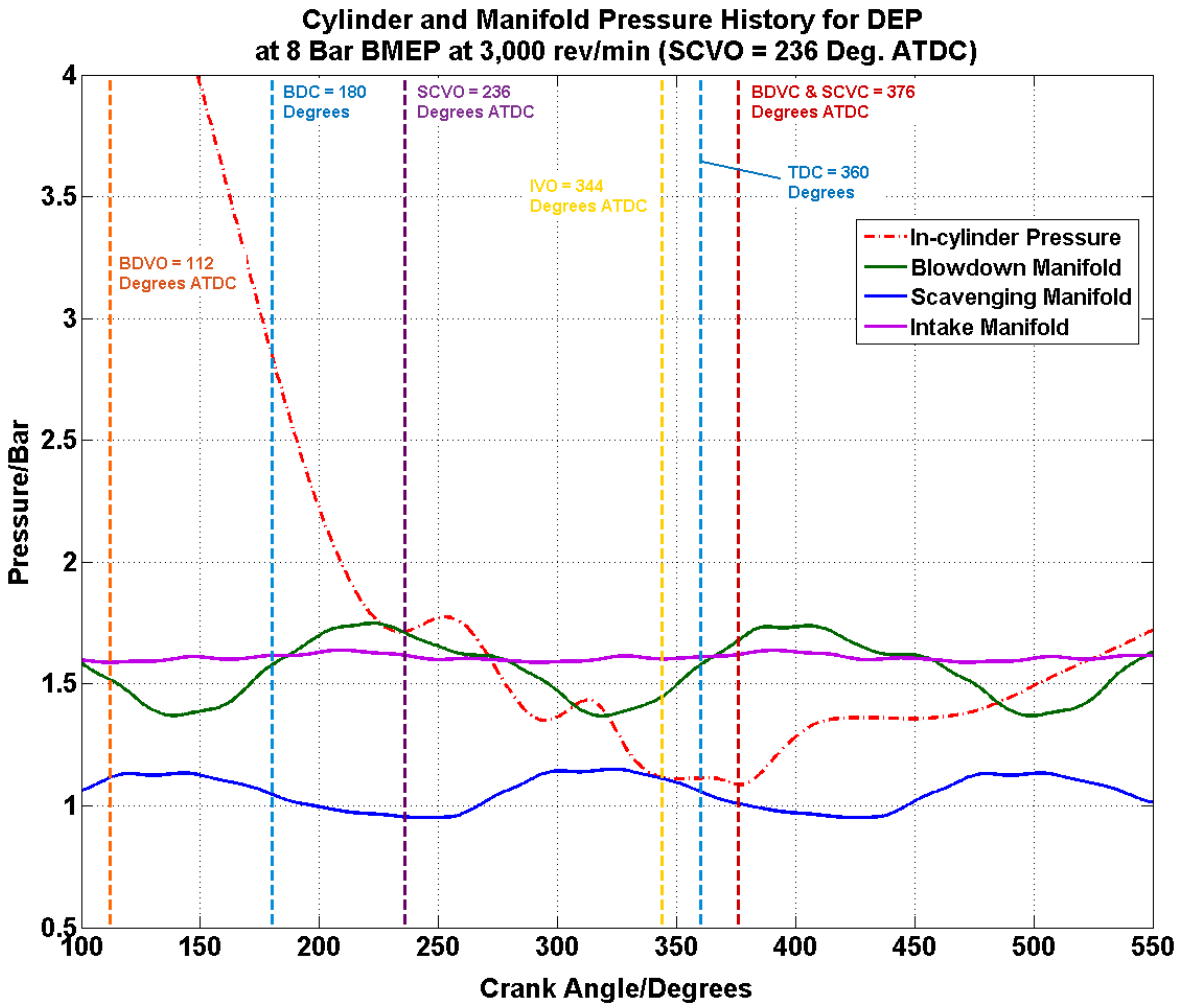

Figure 7-23: In-cylinder, blowdown manifold, scavenging manifold, and intake manifold pressure history for the GT-Power Simulation of the Divided Exhaust Period (DEP) Concept at the 8 Bar BMEP load point for an SCVO Timing of 236 Degrees ATDC.

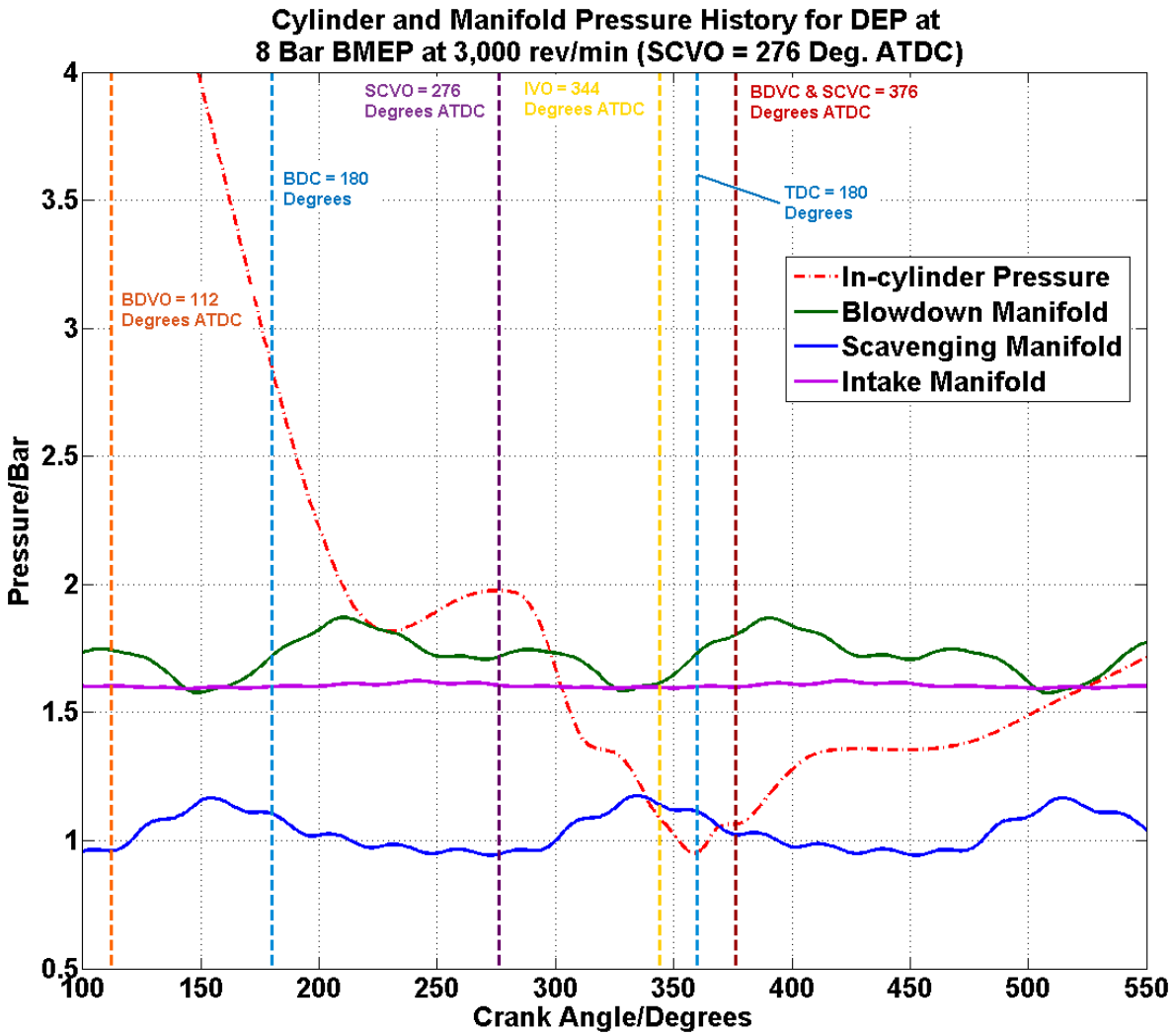

Figure 7-24: In-cylinder, blowdown manifold, scavenging manifold, and intake manifold pressure history for the GT-Power Simulation of the Divided Exhaust Period (DEP) Concept at the 8 Bar BMEP load point for an SCVO Timing of 276 Degrees ATDC.

A similar phenomenon is observed for the 18 Bar IMEP operating point as well. The difference with the 18 Bar IMEP case as compared to the 8 Bar BMEP case is that for the 8 Bar operating point, both the blowdown valve and the scavenging valve close at the same crank angle of 376 Degrees ATDC, which results in the blowdown manifold pressure being greater than the intake manifold pressure for a longer duration of the cycle. This in turn causes the intake air to work against an unfavorable pressure gradient resulting in a deteriorated pumping penalty. When the blowdown valve closes at 312 Degrees ATDC for the 18 Bar IMEP case, the path to the blowdown manifold is closed and only a path to the scavenging

manifold is open. This prevents the blowdown manifold pressure from rising above the intake manifold pressure until the blowdown pulse from another cylinder arrives, ensuring that a favorable pressure gradient exists between the intake manifold and the cylinder for a longer duration than in the 8 Bar BMEP case.

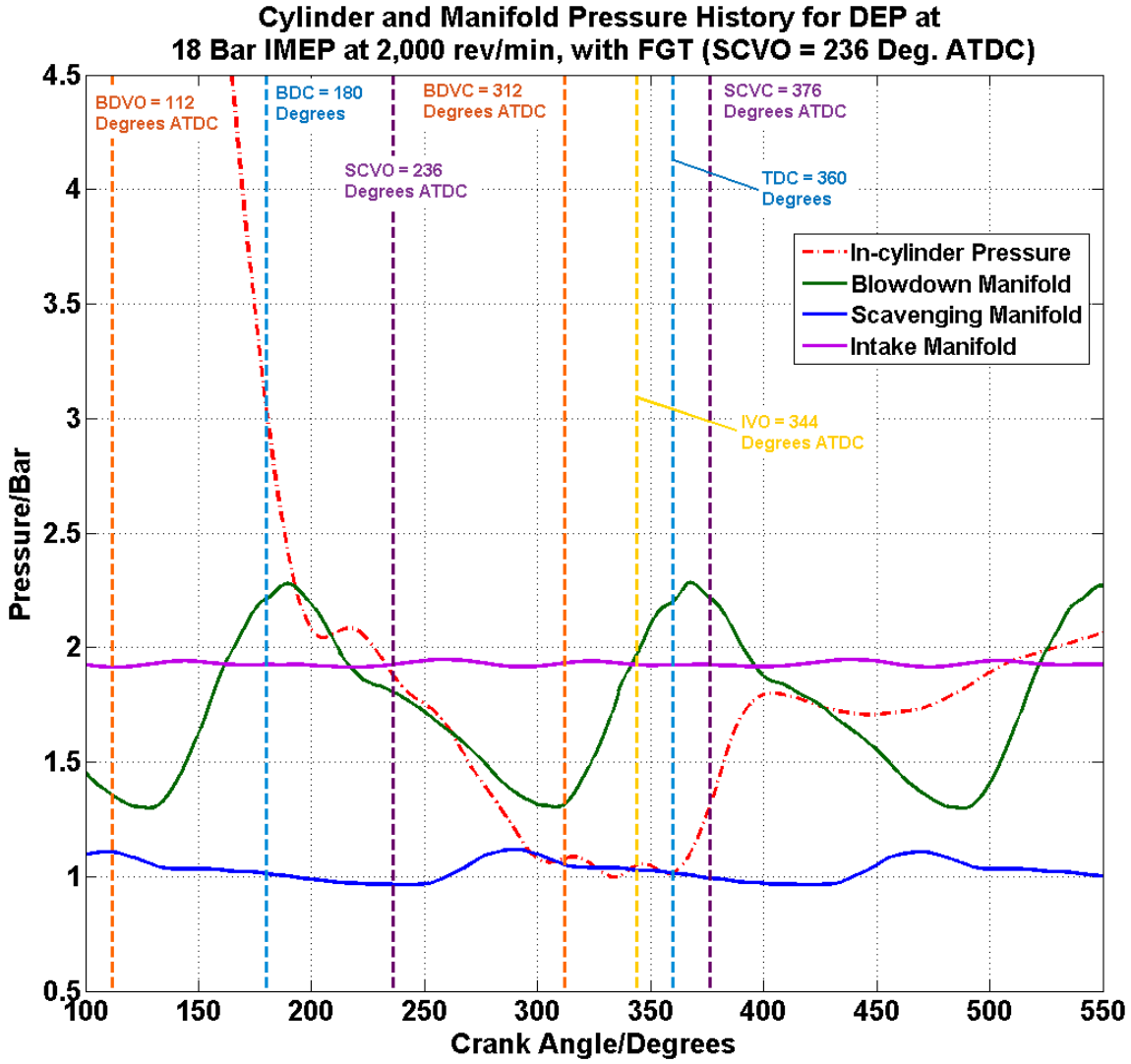

Figure 7-25: In-cylinder, blowdown manifold, scavenging manifold, and intake manifold pressure history for the GT-Power Simulation of the Divided Exhaust Period (DEP) Concept at the 18 Bar IMEP load point for an SCVO Timing of 236 Degrees ATDC.

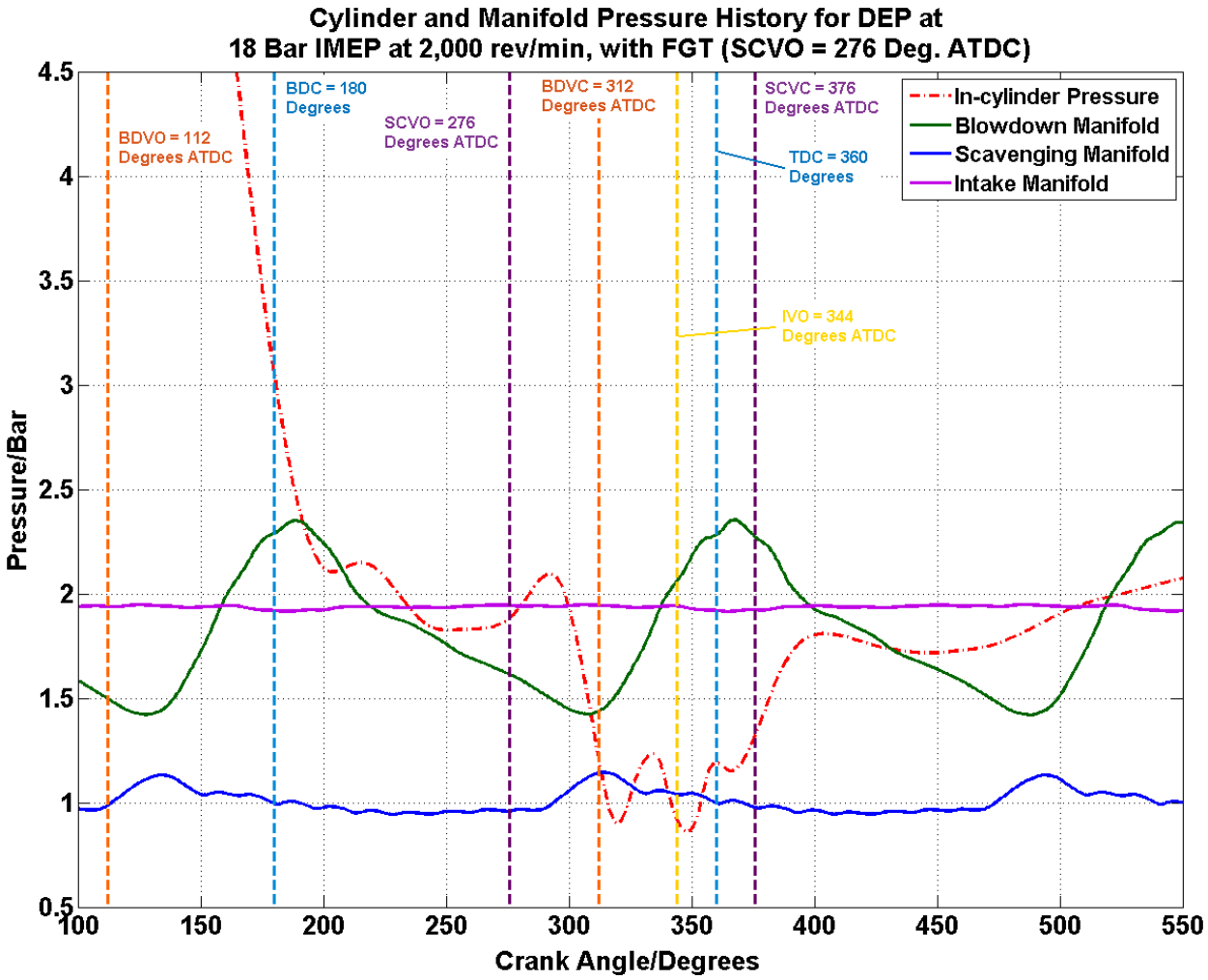

Figure 7-26: In-cylinder, blowdown manifold, scavenging manifold, and intake manifold pressure history for the GT-Power Simulation of the Divided Exhaust Period (DEP) Concept at the 18 Bar IMEP load point for an SCVO Timing of 276 Degrees ATDC.

Figure 7-27 shows the cycle-averaged blowdown manifold pressure, the cycle-averaged centrifugal compressor outlet pressure and the cycle-averaged scavenging manifold pressure for both the 8 Bar BMEP and 18 Bar IMEP operating points. With a more retarded SCVO timing, there is a greater exhaust flow through the blowdown manifold, resulting in an increase in the blowdown manifold pressure and in turn the pressure ratio across the turbine. With a higher pressure ratio across the turbine, more enthalpy is available to drive the turbine, resulting in more power being transferred to the centrifugal compressor, which in turn causes the LP-stage compressor outlet pressure to increase.

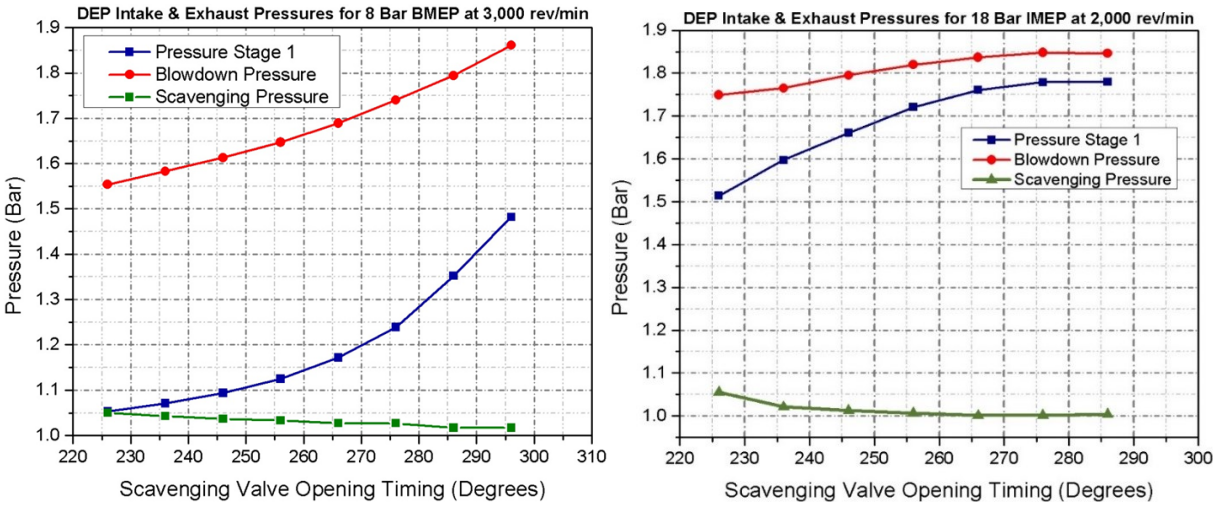

Figure 7-27: Cycle-averaged Stage 1 (centrifugal compressor outlet), blowdown manifold and scavenging manifold pressures for the: (7-27a, Left): 8 Bar BMEP and (7-27b, Right): 18 Bar IMEP operating points.

With more power available to the turbocharger, the supercharger does not have to rotate at a high speed as the SCVO timing is retarded. Therefore, the pulley ratio between the cranktrain and the supercharger was reduced, and this resulted in a lower power consumption by the supercharger while the power consumption by the centrifugal compressor increased, as shown in Figure 7-28.

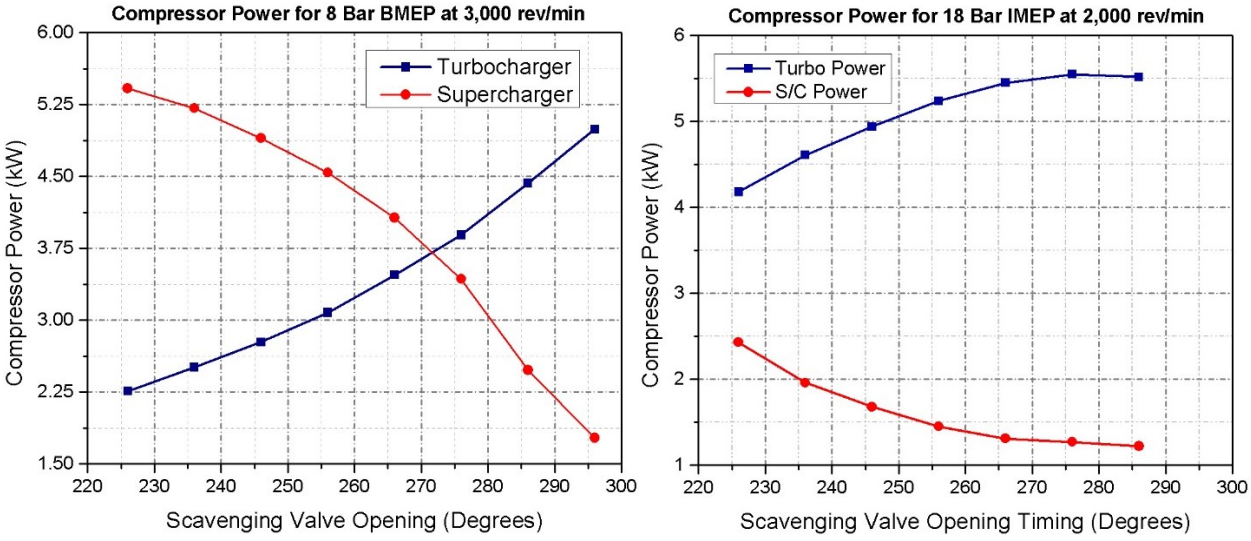

Figure 7-28: Compressor Power Input for the Turbocharger compressor and supercharger as functions of SCVO timing for the: (7-28a, Left): 8 Bar BMEP and (7-28b, Right): 18 Bar IMEP operating points.

As the blowdown manifold pressure increased with a more retarded SCVO timing, the pressure ratio across the turbine and the mass flow rate through the turbine increased, resulting in an improvement in the isentropic efficiency of the turbine. The compressor isentropic efficiency also increased with the higher pressure ratios across the compressor and higher intake mass flow rate with a more retarded SCVO timing. The improved compressor efficiency, along with the improved turbine efficiency, led to an improvement in the overall turbocharger efficiency, as indicated by the purple line. For the 8 Bar BMEP case, there was a drastic improvement in compressor efficiency compared to the 18 Bar IMEP case, because the operating point moved away from the choked flow region in the compressor map for the 8 Bar BMEP case with a more retarded SCVO timing. The compressor efficiency plateaued out in the 18 Bar IMEP case as the compressor was already operating very close to its maximum efficiency of 78%.

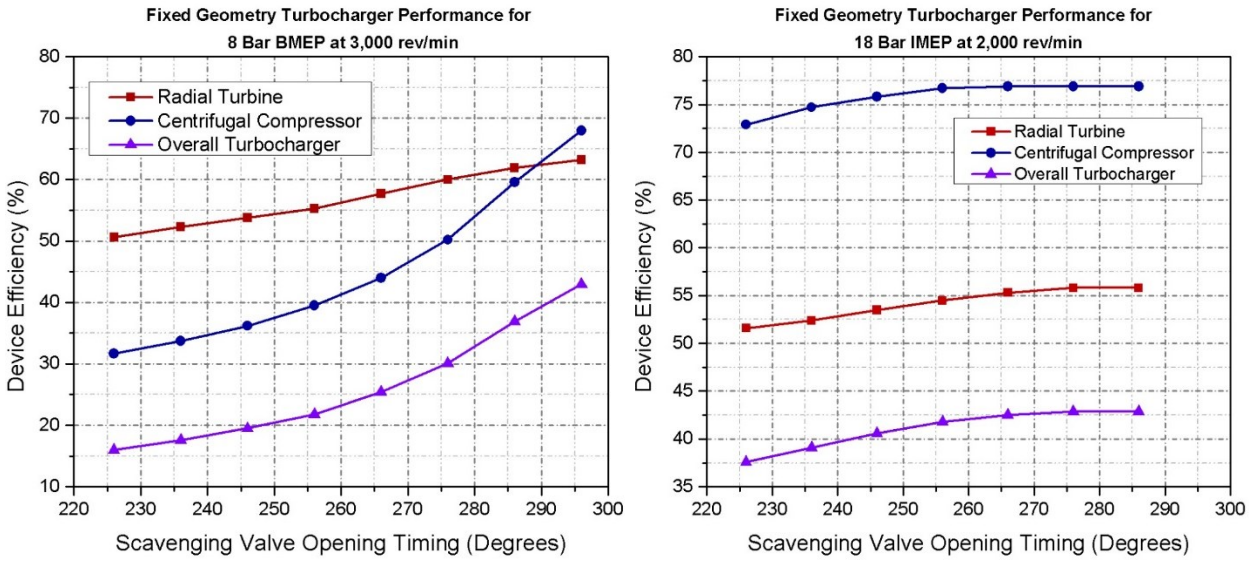

Figure 7-29: Turbine, compressor and overall turbocharger efficiencies as functions of SCVO timing for the: (7-29a, Left): 8 Bar BMEP and (7-29b, Right): 18 Bar IMEP operating points.

Because of the improved overall turbocharger efficiency and the increase in the power available to the turbocharger compressor with retarded SCVO timing, the required supercharger speed was lower, and this meant that required supercharger to cranktrain pulley ratio could be reduced. Figure 7-30 shows the pulley ratio as a function of SCVO timing. The pulley ratio drop was more drastic for the 8 Bar BMEP case

as the exhaust energy proportion increased with a more retarded SCVO timing, while for the 18 Bar IMEP case, the ratio plateaued out since the exhaust energy available also plateaued out.

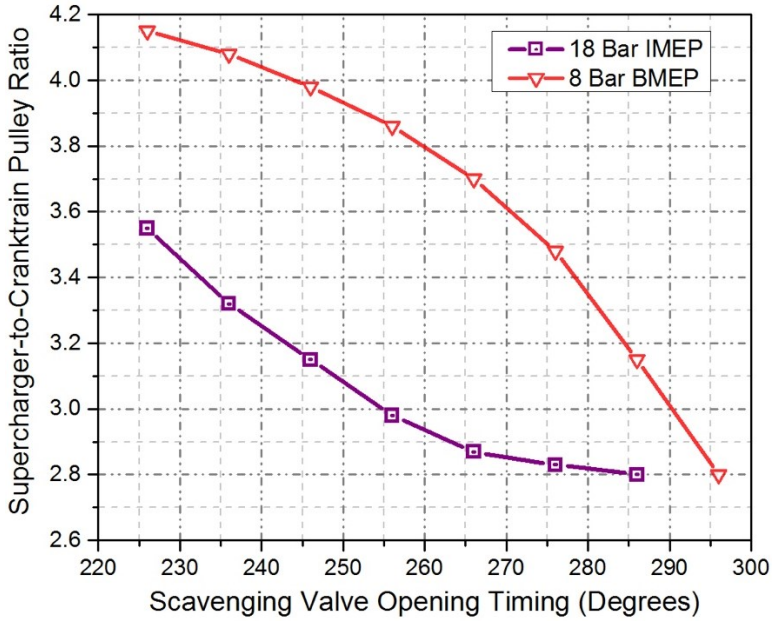

Figure 7-30: Supercharger-to-Cranktrain Pulley Ratio as a function of SCVO Timing

Figures 7-32 and 7-33 show the $IMEP_n$, BMEP, ISFC and BSFC for the 8 Bar BMEP and the 18 Bar IMEP operating points respectively. As was shown earlier, the pumping work is less negative at advanced SCVO timings, and so the net IMEP is greater while the ISFC is lower for more advanced SCVO timings. In spite of the pumping benefit however, the exhaust enthalpy available to the turbine is not sufficient to provide the required boost due to the lower mass flow rates through the turbine and the lower expansion ratio, and the supercharger has to make up for the deficit. Because of this, the parasitic losses are higher than the pumping benefit, resulting in lower values of BMEP and higher values of BSFC when the divided exhaust period is used. This is especially true for the 8 Bar BMEP case which is at a higher engine speed of 3,000 $rev \cdot min^{-1}$. At the higher engine speeds, the power drawn by the supercharger from the cranktrain is even higher, giving rise to higher FMEP values as shown in Figure 7-31.

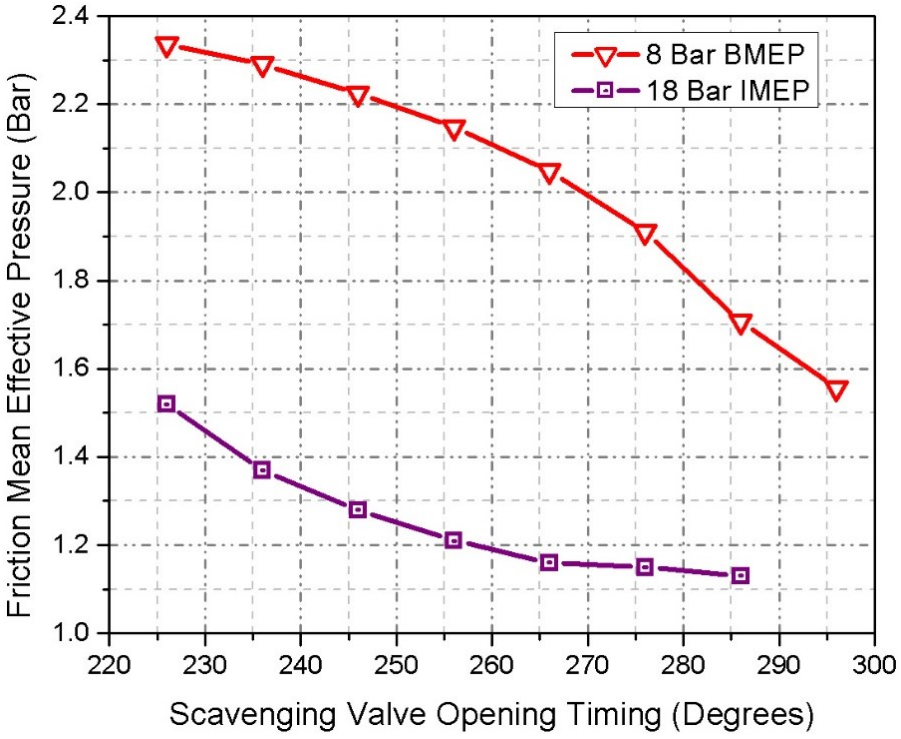

Figure 7-31: FMEP as a function of SCVO Timing.

When the exhaust flow proportion through the turbine increases with a more retarded SCVO timing for the 8 Bar BMEP case, due to the reduction in required pulley ratio and hence the power drawn by the supercharger, the BMEP starts to increase and the BSFC starts to drop. The maximum values of BMEP (7.75 Bar) and minimum values of BSFC (203 g/kWh) are still lower and higher respectively compared to the stock engine configuration (8.15 Bar and 198 g/kWh) however, primarily due to the additional parasitic load from the supercharger that contributes to the FMEP.

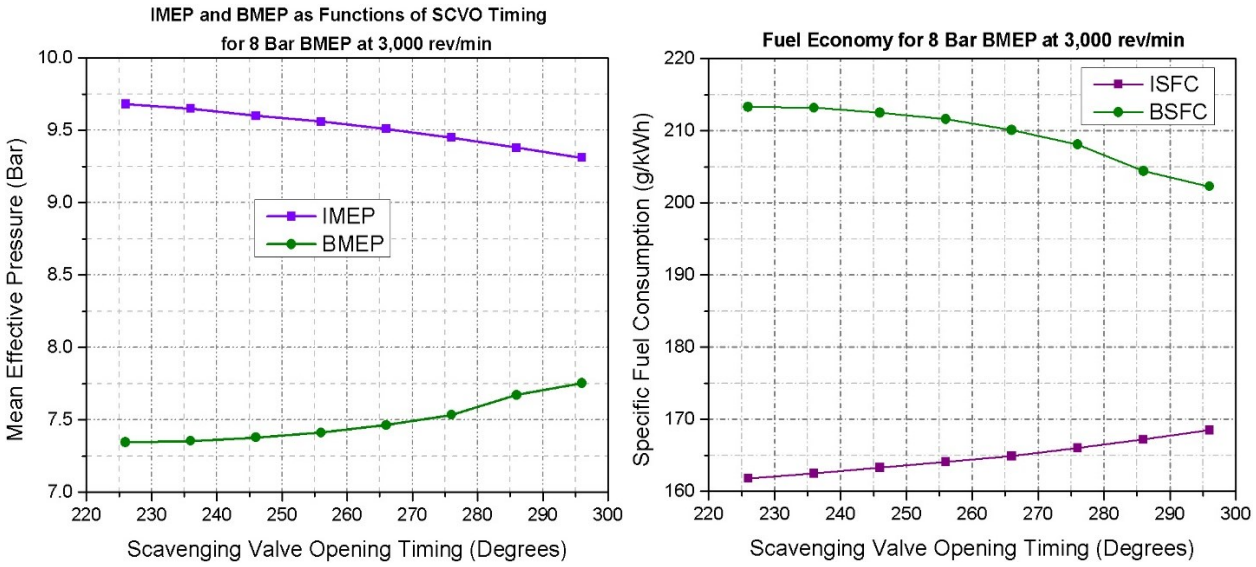

Figure 7-32: (Left, 7-32a) Mean Effective Pressure and (Right, 7-32b) Specific Fuel Consumption as a function of SCVO timing for the 8 Bar BMEP at $3,000\ \text{rev} \cdot \text{min}^{-1}$ load point.

For the 18 Bar IMEP case, a similar trend as that for the 8 Bar BMEP is observed for both the BMEP and BSFC up until the SCVO timing of 256 Degrees ATDC. The BMEP reaches a peak value of 17.29 Bar at 256 Degrees ATDC while the BSFC reaches a trough value of $185.2\ \text{g} \cdot \text{kWh}^{-1}$ at the same SCVO timing. This happens because until 256 Degrees ATDC, the reduction in parasitic losses by running the supercharger at a lower speed is greater than the pumping penalty increase from the increased blowdown manifold backpressure. Beyond 256 Degrees ATDC, the required pulley ratio starts to plateau, which in turn causes the FMEP to approach a constant value as well while the pumping penalty (as shown in Figure 7-22) continues to increase at a greater rate. As a consequence, the pumping penalty beyond 256 Degrees ATDC is greater than the benefit of lower parasitic losses, causing the BMEP to decrease and the BSFC to increase.

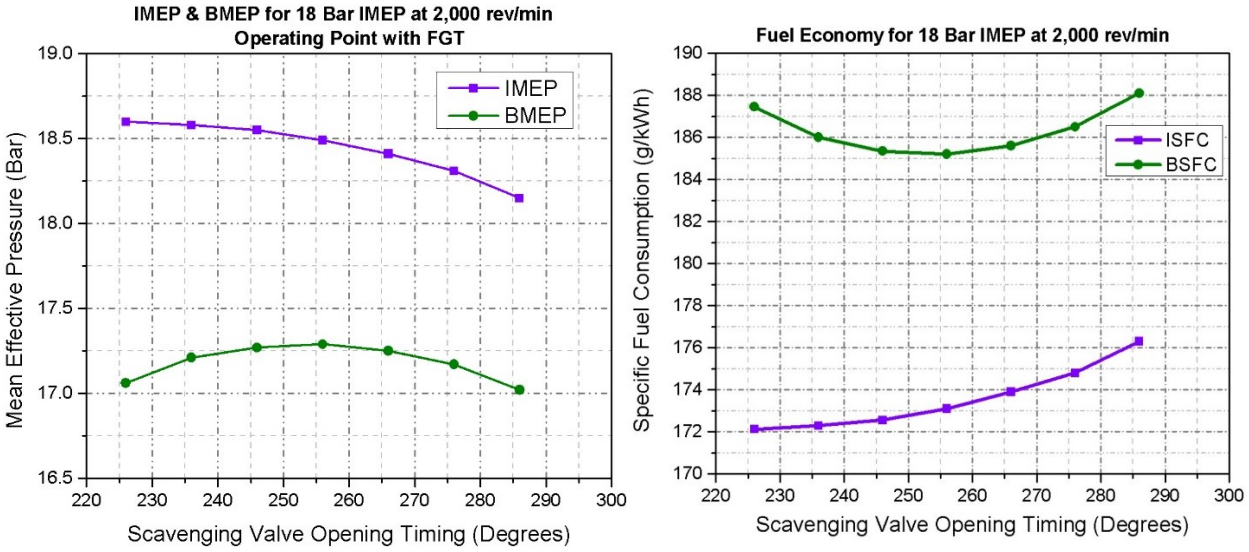

Figure 7-33: (Left, 7-33a) Mean Effective Pressure and (Right, 7-33b) Specific Fuel Consumption as a function of SCVO timing for the 18 Bar IMEP at $2,000\ rev \cdot min^{-1}$ load point.

7.6.1 Comparison of the Divided Exhaust Period Concept with a Conventional Wastegate

In existing literature, the Divided Exhaust Period has been described as a "more efficient wastegate" than a conventional pneumatic wastegate, but none of these studies have actually compared the two concepts to prove why the DEP concept is more efficient. Since the DEP concept requires a significant redesign of the exhaust manifold and the installation of a VVA system which can be very expensive, it is necessary to justify the added costs of implementing the DEP concept over using the cheaper and easier-to-install pneumatic wastegate whose purpose is to determine the portion of the exhaust flow that is directed to the turbine. Thus, a simulation study was performed to identify the benefits and determine the performance improvement if a wastegate were to be used.

For the conventional wastegate study, the VGT in the stock engine configuration was replaced by the scaled FGT whose wheel dimensions are given in Section 7.5.3. A signal active dial and actuator were connected to the fixed geometry turbine for adjusting the wastegate diameter. The wastegate diameter was adjusted such that the exhaust flow proportion through the turbine matched the corresponding exhaust flow proportion through the blowdown manifold for three different SCVO timings. The wastegate simulation

was performed for only the 18 Bar IMEP point, because at 8 Bar BMEP, the intake manifold pressure is too low to force the wastegate actuator to open.

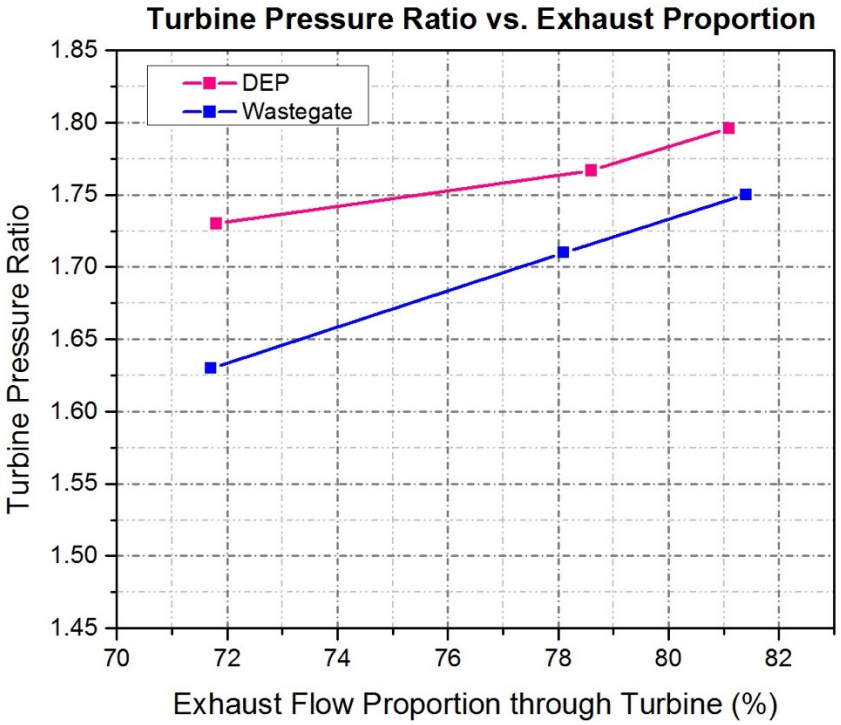

Figure 7-34: Comparison of Turbine Pressure Ratio between Divided Exhaust Period and Conventional Wastegate

As Figure 7-34 shows, the pressure ratio across the turbine is higher for the DEP concept than it is for the conventional wastegate. This happens because, in the DEP concept the high energy blowdown pulse has already been evacuated from the cylinder during the blowdown valve open duration, and due to the lack of a wastegate, does not experience any further throttling losses in the turbine housing (where the wastegate is usually located). On the other hand, with a conventional wastegate, all the exhaust gas passes through both the exhaust valves, and in addition to this throttling loss, experiences another throttling loss at the wastegate when some of the flow bypasses the turbine and expands through the wastegate opening. This additional throttling loss reduces the exhaust energy further, thereby causing an additional pressure drop at the turbine inlet.

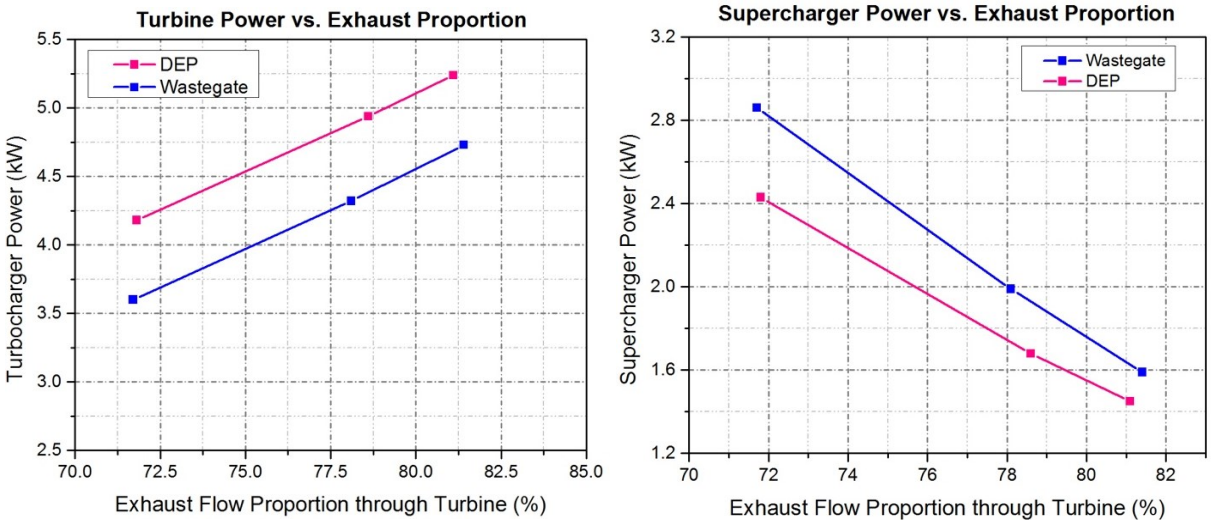

Figure 7-35: (Left, 7-35a) Turbocharger Power and (Right, 7-35b) Supercharger Power comparison between DEP and conventional wastegate.

Figure 7-35 shows the turbocharger and supercharger power for both the DEP and conventional wastegate. Due to the lower pressure ratio across the turbine, the turbine isentropic efficiency and the work extracted by the turbine are lower for the conventional wastegate, thereby necessitating the supercharger to work harder than the turbocharger, resulting in a higher power draw by the supercharger in the conventional wastegate configuration.

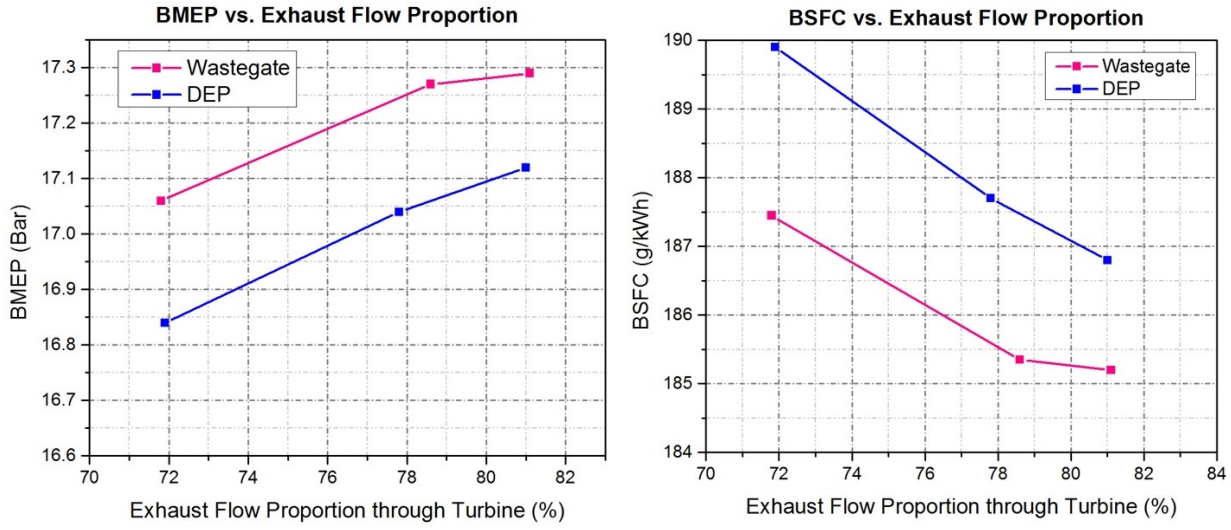

Figure 7-36: (Left, 7-36a) BMEP and (Right, 7-36b) BSFC comparison between DEP and conventional wastegate

7.6.2 Replacement of the Fixed Geometry Turbocharger with a Variable Geometry Turbocharger

From the results shown in Section 7.6.1, it can be seen that the fixed geometry turbocharger is not ideal for the DEP concept as applied to RCCI and other LTC strategies because only a limited degree of control over the turbine performance is possible. This happens due to the fact that the FGT is optimized at only one operating point, and since the SCVO timing affects both the blowdown mass flow rate and the blowdown manifold pressure simultaneously, it is a challenge to adapt both the flow rate and pressure ratio to a fixed geometry turbine housing. Furthermore, due to the low exhaust enthalpy, a higher than usual turbine inlet pressure is required to improve the turbine isentropic efficiency, and regulating the flow distribution between the blowdown and scavenging manifolds alone was not sufficient to raise the turbine inlet pressure to desired values without drastically deteriorating the pumping penalty.

As mentioned in Chapter 2, the dimensions of the turbine housing/volute need to be varied for a wide range of load and speed conditions; this necessitates the use of a VGT to obtain an optimal aspect ratio for better system performance and improved fuel economy at each operating point. By adjusting the aspect ratio along with valve timing, a finer control of the backpressure can be obtained, allowing a more efficient extraction of work from the turbine. If the VGT is able to supply all the generated boost, the supercharger may be disconnected from the cranktrain and be bypassed completely if sufficient exhaust energy may be recovered, allowing a further improvement in fuel economy by eliminating parasitic losses.

For the VGT study, the FGT in the DEP engine model was replaced by a VGT with the new turbine and compressor wheel diameters of 34.45 mm and 37.74 mm respectively. The stock Honeywell Garrett M53 VGT maps were scaled using the aforementioned diameters and fed into the "TurbineMapVGT" template. A rack position actuator and SignalActiveDial were connected to the VGT template to allow adjustment of the rack position during the simulation runtime. If the rack position allowed the VGT alone to supply the required boost pressure, the supercharger was disconnected from the cranktrain using the clutch and the supercharger bypass valve was fully opened. The VGT rack position was only changed for the high load 18 Bar IMEP point for different SCVO timings. For the 8 Bar BMEP point, the rack position of 0.6 was assumed to be the ideal rack position for the VGT, since the FGT was scaled using this rack

position from the stock VGT. Moreover, the blowdown manifold pressure would have to be increased to very high values of 2 Bar or greater by operating the VGT at a more closed rack position when the exhaust enthalpy was low at the 8 Bar BMEP load point; this would only worsen the pumping penalty even though the supercharger does not need to work as hard due to extremely high backpressures.

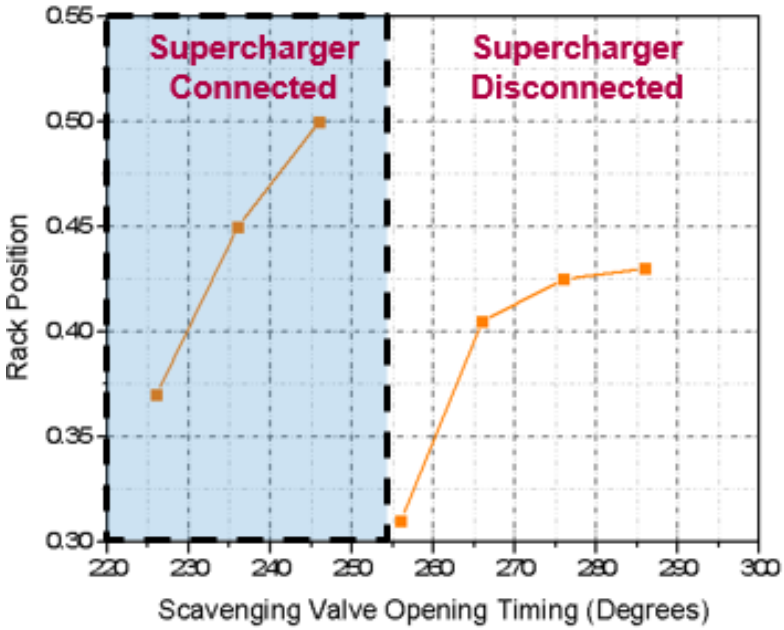

Figure 7-37: Change in required VGT Rack Position for different SCVO Timings

Figure 7-37 shows the rack position as a function of SCVO timing. As the SCVO timing is retarded until 246 degrees, the rack position is increased from 0.37 to 0.5. This is done because more exhaust energy is available to drive the turbine, and there is a need to increase the turbine inlet nozzle area for preventing an excessive buildup of backpressure, since elevated backpressures can deteriorate the pumping penalty. At a 256 degree SCVO timing, there is sufficient exhaust enthalpy to drive the VGT and so the supercharger was disconnected from the cranktrain at that valve timing and more retarded valve timings. The rack position had to be lowered to 0.3 once the supercharger was disconnected to increase the backpressure slightly so that the pressure ratio across the turbine and hence the turbine isentropic efficiency could be increased. The rack position was then increased again, but overall, the values remained lower than when the supercharger was connected.

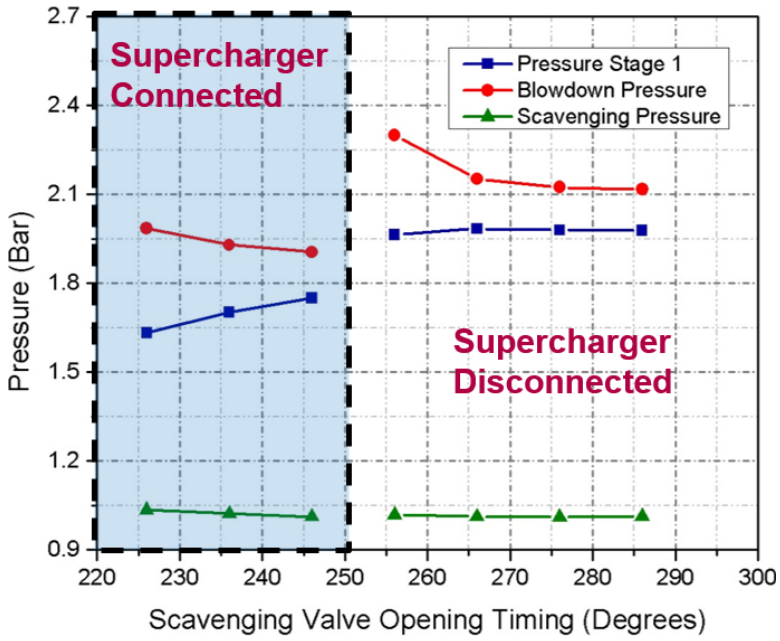

Figure 7-38: Cycle-averaged Stage 1 (centrifugal compressor outlet), blowdown manifold and scavenging manifold pressures for the 18 Bar IMEP at $2,000\ rev \cdot min^{-1}$ load point.

Figure 7-38 shows the centrifugal compressor outlet (stage 1) pressure, blowdown manifold pressure and the scavenging manifold pressure when the VGT was used. As expected, there is a significant jump in the blowdown manifold pressure once the supercharger is disconnected because of the restricted turbine inlet area caused by the decrease in the rack position. The blowdown manifold pressure then decreases with a more retarded SCVO timing as the inlet area becomes less restricted with an increase in the rack position. With a higher pressure ratio across the turbine due to the elevated blowdown manifold pressure, the centrifugal compressor outlet pressure increases as well since more power is being supplied from the turbine to the compressor. Once the supercharger has been disconnected, the compressor outlet pressure is now constant as the system now only has one compressor stage which is sufficient to provide the required boost pressure of 1.93 Bar.

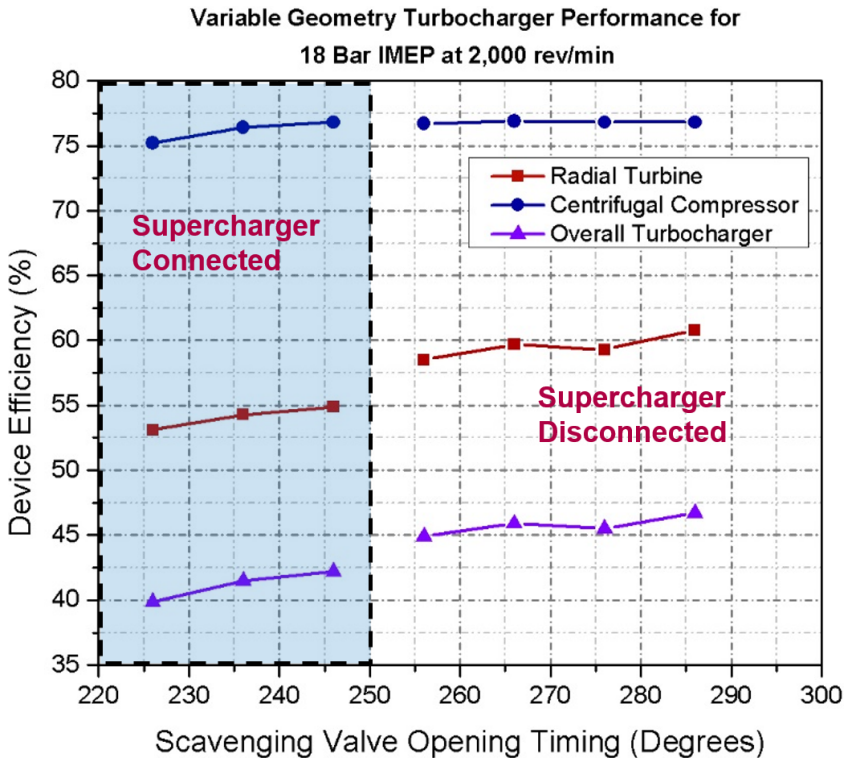

Figure 7-39: Turbine, centrifugal compressor and overall VGT efficiency for the 18 Bar IMEP load point

Once the supercharger is disconnected and the rack position is reduced to increase the turbine inlet pressure, there is an increase in the turbine isentropic efficiency from 55% to 58%, as Figure 7-39 shows. The compressor isentropic efficiency does not change much because the compressor is already operating very close to its maximum efficiency of 78%. But because of the sudden jump in turbine efficiency the overall turbocharger efficiency increases from 42.5% to 45% as the supercharger is disconnected.

Figure 7-40 shows the $IMEP_n$, BMEP, ISFC and BSFC comparison between the FGT and VGT cases for the 18 Bar IMEP load point. As the plots show, the BMEP is higher for the VGT over the FGT for all SCVO timings. This illustrates that the additional control over the turbine inlet pressure by restricting the turbine inlet area enhances the exhaust enthalpy utilization by the turbine and thus reduces the power demand by the supercharger, lowering the parasitic losses. Once the supercharger is disconnected from the cranktrain at 256 Degrees ATDC and beyond, the BMEP shows a significant increase due to no more parasitic losses from the supercharger. The BMEP reaches a peak value of 17.53 Bar at 266 Degrees ATDC

SCVO timing, while the BSFC reaches the lowest value of 181.6 g/kWh at the same point. This is a 1% increase in the BMEP and a 1% improvement in BSFC over the stock engine configuration. Beyond this point, the BMEP drops and the BSFC increases as the pumping penalty increases with a more retarded SCVO timing.

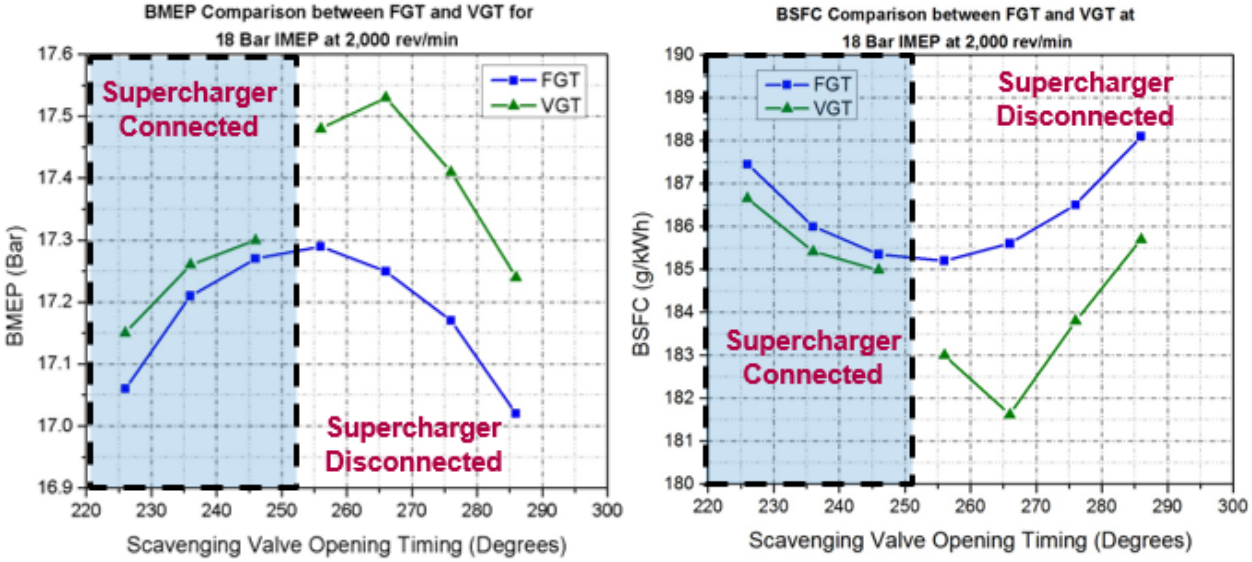

Figure 7-40: (Left, 7-40a) Mean Effective Pressure and (Right, 7-40b) Specific Fuel Consumption as a function of SCVO timing for the 18 Bar IMEP at $2,000\ \text{rev} \cdot \text{min}^{-1}$ load point.

7.7 Impact of Divided Exhaust Period on Low-Load Operation

One other benefit that the DEP concept offers over a wastegate and a conventional exhaust manifold is the ability to route all the exhaust flow through the scavenging manifold so that the flow completely bypasses the turbine and heads directly to the aftertreatment system. Since the exhaust gas enthalpy at low load operation is not sufficient for the turbine to extract any useful work, the turbine essentially acts as a heat sink and hence causes the exhaust gas temperature to drop. If the temperature drops to a low enough value by the time the flow reaches the DOC, the DOC will not light-off and its UHC and CO conversion efficiency will be poor. By only opening the scavenging valve while keeping the blowdown valve closed during low load operation, all the exhaust flow is directed to the DOC without having to lose any energy in the turbine, ensuring that the exhaust temperature is still equal to or greater than the DOC light-off

temperature. This section investigates the low load valve operation strategy for DEP, and compares the effect that opening the scavenging valve alone at low load has with that of a conventional exhaust system.

For this study, the 2.6 Bar BMEP (for 15.1 Compression Ratio) at $1{,}500\ \text{rev} \cdot \text{min}^{-1}$ operating point was chosen. The operation parameters for this point are given in Table 7-5.

Table 7-5: Intake Pressure and Fueling Parameters for the 2.6 Bar BMEP load point

Intake Manifold Pressure (Bar)	1.09
Gasoline Quantity (mg/cyl/cyc)	6.321
Diesel Quantity (mg/cyl/cyc)	2.482

Even though the stock engine configuration requires a boost pressure of 1.09 Bar at this load point, this value is so close to atmospheric that very little boost is being supplied by the turbocharger. So it was assumed that bypassing the turbine completely for the DEP configuration would not have a significant effect on the combustion.

GT-Power simulations for both the stock and DEP configurations were conducted by feeding in the experimental heat release rate curve for the 2.6 Bar BMEP operating point into the cylinder templates for both configurations. The HRR curve is given in Figure 7-41 below.

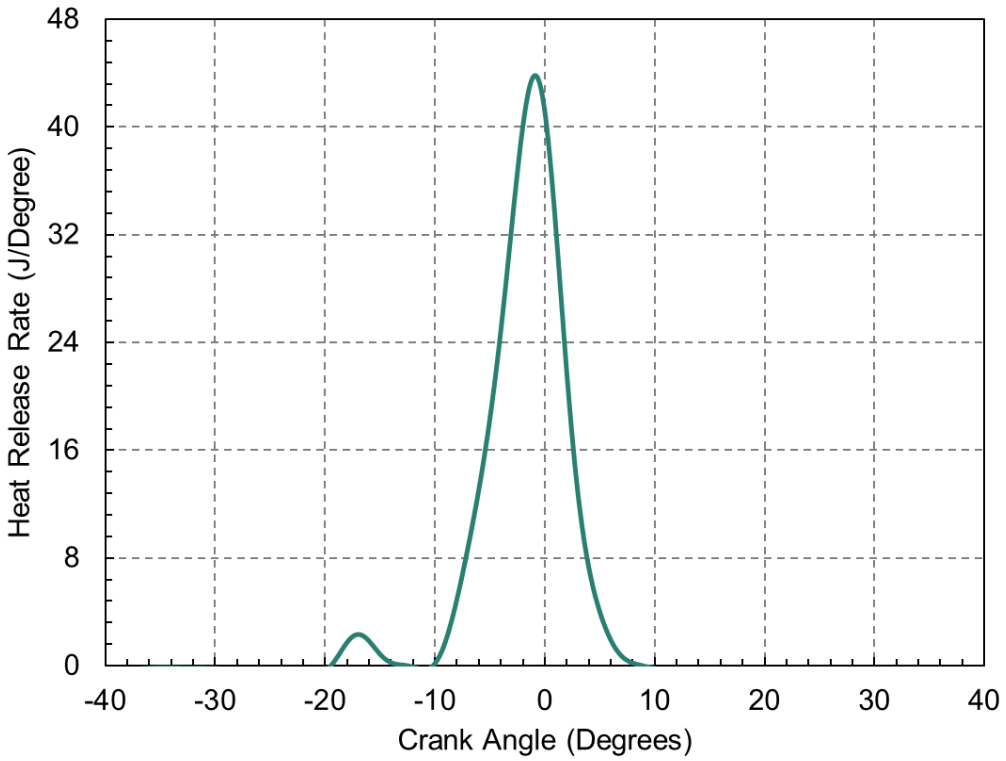

Figure 7-41: HRR Curve for 2.6 Bar BMEP at $1,500\ \text{rev} \cdot \text{min}^{-1}$ (15.1 Compression Ratio)

An additional compressor bypass valve was added parallel to the turbocharger compressor in the DEP configuration model to reroute the intake air flow directly into the cylinders without having to pass through the centrifugal compressor.

The target boost pressure for the turbocharger in the conventional engine configuration was set to 1.09 Bar, but the turbocharger in the DEP configuration could not be completely deactivated and would continue to rotate in the simulation even though there was no flow through the turbine and the compressor. To overcome this problem, the overblown compressor model of Casey et al. [188] was activated in the centrifugal compressor template for the DEP configuration. For faster convergence, the initial turbocharger speed in the DEP model was set to $5{,}000\ \text{rev} \cdot \text{min}^{-1}$ to allow the turbocharger speed to reach zero more rapidly.

Figure 7-42 shows the Mach Number for the gas flows for one of the exhaust ports for the stock engine configuration and the scavenging port for the DEP configuration. The choking duration is longer for the DEP configuration and the overall Mach Number is also higher throughout the valve open period, which

is to be expected since the effective flow area is much smaller since only one of the exhaust valves is open. However, for the stock exhaust configuration, flow reversal is observed at 175 Degrees ATDC and the exhaust gas flows back into the cylinder from the exhaust manifold until 185 Degrees ATDC.

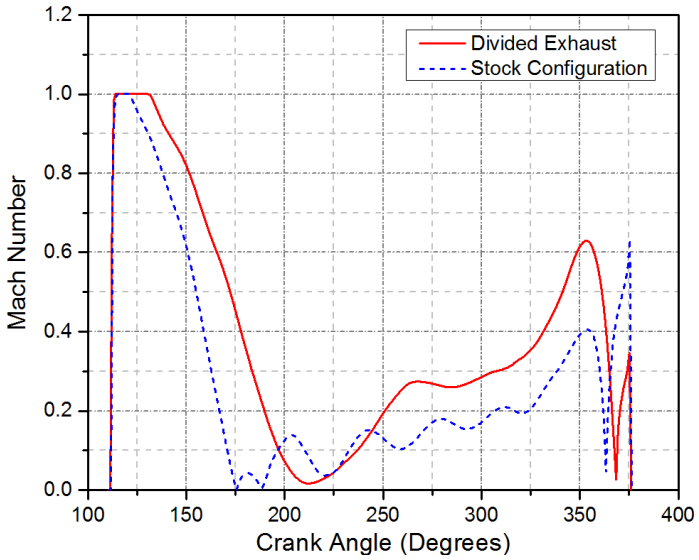

Figure 7-42: Exhaust Port and Scavenging Port Mach Number for the 2.6 Bar BMEP load point

Table 7-6: Engine Performance Parameters for both the stock engine and Divided Exhaust Configurations at the 2.6 Bar BMEP

	Stock Configuration	Divided Exhaust
$IMEP_g$ (Bar)	**3.53**	**3.43**
$IMEP_n$ (Bar)	3.31	3.3
PMEP (Bar)	**-0.22**	**-0.13**
BMEP (Bar)	2.81	2.8
BSFC (g/kWh)	236.5	237

Table 7-6 shows the engine performance parameters of $IMEP_g$, $IMEP_n$, PMEP, BMEP and BSFC for the stock engine configuration and the DEP configuration. The gross IMEP is higher for the stock configuration than it is for the DEP configuration, and this has to do with the higher intake air flow rate into the engine due to the higher intake manifold pressure supplied by the turbocharger. However, compared with the stock configuration, the PMEP for the DEP is 40% less negative, and because of this, the higher gross IMEP benefit from the stock configuration is offset by the larger pumping penalty, giving rise to

similar values of BMEP and BSFC for both configurations. (If the air-fuel ratio were to be maintained at the same value as that for the stock configuration, the required fuel flow rate would actually be lower for the DEP configuration, and if the combustion efficiency were the same for both cases with the reduced fueling rate, the BSFC could actually be lower than in the stock engine configuration.)

The flow reversal observed in Figure 7-42 and the improvement in pumping work can once again be explained by studying the pressure history plots for both configurations in Figures 7-43 and 7-44. With the stock configuration, the exhaust manifold pressure averages around 1.25 Bar and is higher than the intake manifold pressure of 1.09 Bar throughout the cycle, especially during the valve overlap period. This is because, even though the intake manifold pressure is only slightly above atmospheric, the turbocharger is still providing this additional boost in the stock configuration, and the turbine therefore has to increase the backpressure in the exhaust manifold to power the compressor. As a result, there is an unfavorable pressure gradient over a longer duration that the engine has to work against, giving rise to a more negative pumping penalty for the stock configuration.

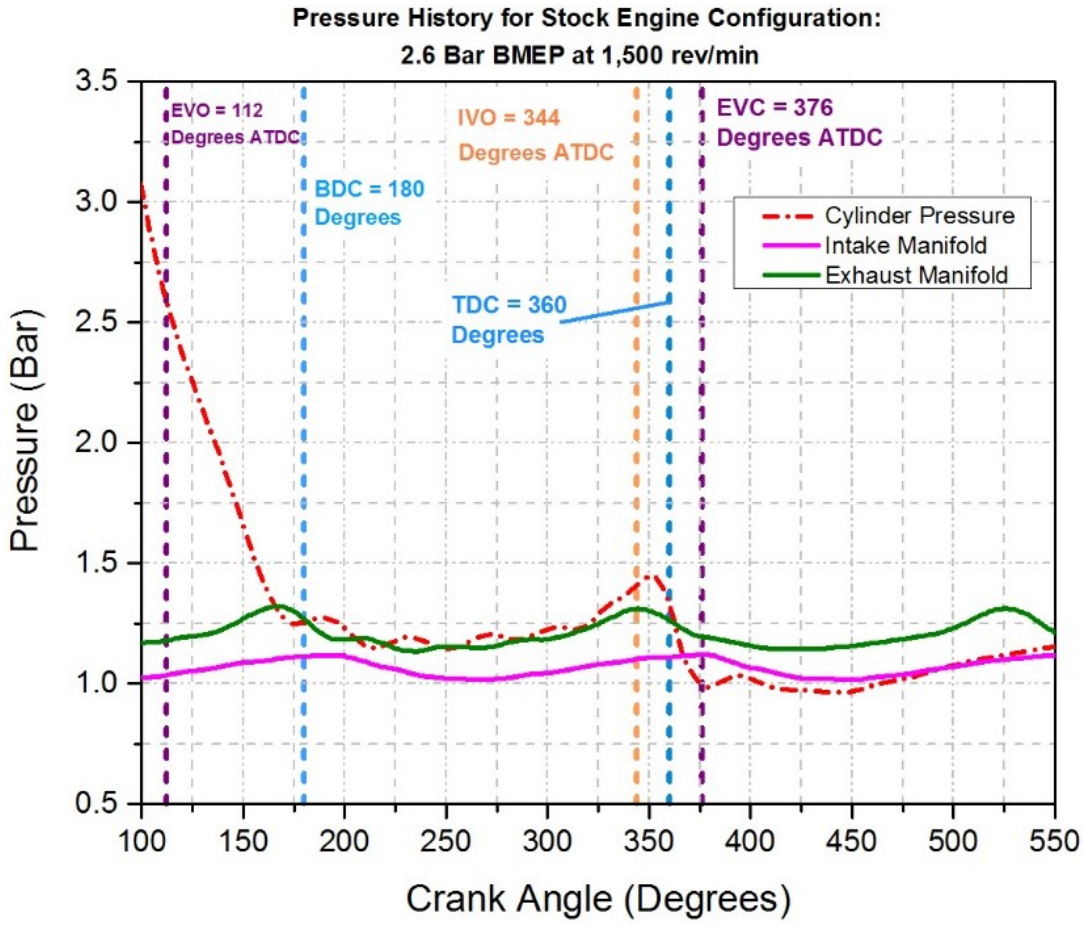

Figure 7-43: In-cylinder, exhaust manifold, and intake manifold pressure history for the GT-Power Simulation of the stock engine at the 2.6 Bar BMEP load point.

For the DEP configuration, with the turbocharger bypassed, the engine essentially behaves as a naturally aspirated engine, so the intake and scavenging manifold pressures hover around 1 Bar. With a smaller pressure difference across the engine, the intake air does not encounter as much flow resistance as the stock configuration, giving rise to a more positive PMEP.

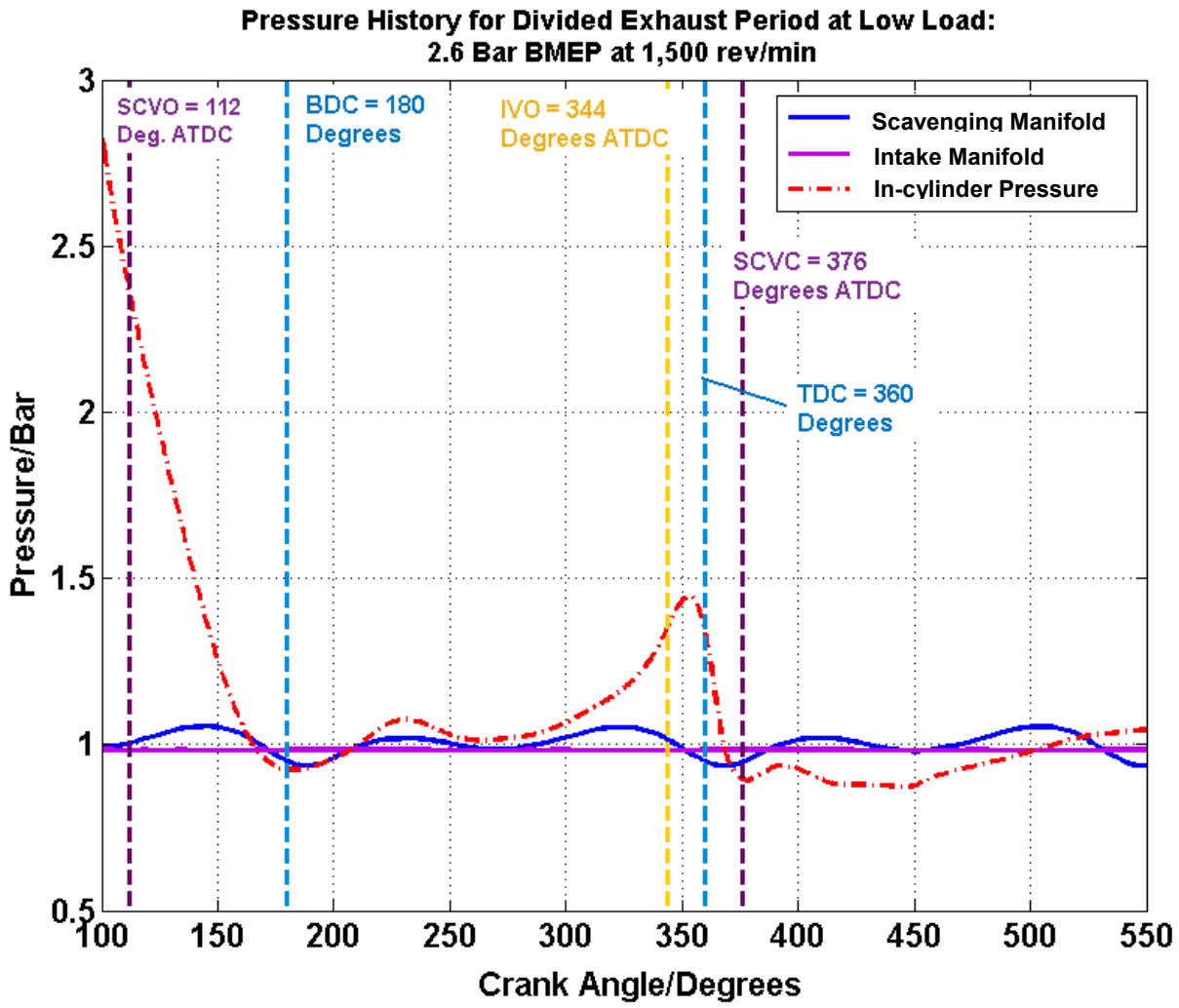

Figure 7-44: In-cylinder, scavenging manifold, and intake manifold pressure history for the GT-Power Simulation of the Divided Exhaust Period (DEP) Concept at the 2.6 Bar BMEP load point with only the scavenging valve open.

Table 7-7 shows the turbine inlet and outlet temperatures, and the exhaust gas flow rate through the DOC for both configurations. Due to the extraction of enthalpy from the turbine, there is a 17 K drop in the exhaust gas temperature for the stock configuration, while there is only 3 K drop for the DEP configuration. In both cases, the exhaust gas temperature is higher than the DOC light-off temperature of 457 K, so the DOC will light-off and will thus have a high UHC and CO conversion efficiency for both configurations. However, due to the lack of boost in the DEP configuration, the exhaust gas flow rate is

lower through the DOC, and as was shown in Chapter 5, with the lower flow rate, the DEP configuration is expected to give a higher conversion efficiency for the DOC than the stock engine configuration.

Table 7-7: Turbine Inlet and Outlet Temperatures, and Exhaust Gas Mass Flow Rate for both the stock engine and DEP configurations at the 2.6 Bar BMEP load point.

	Stock Configuration	Divided Exhaust
Turbine Inlet (Or Scavenging Manifold for DEP) Temperature (K)	479	479
Turbine Outlet Temperature (K)	462	476
Exhaust Gas Flow Rate (kg/h)	97.5	89.2

7.8 Comparison of RCCI Divided Exhaust Period Results with Results from other DEP Studies in Literature

To evaluate the impact of the DEP on RCCI (and LTC) engine performance, it is of interest to compare the results obtained with other studies in literature. Since no other study so far has investigated the use of DEP to low temperature combustion concepts such as RCCI, the only literature available for comparison are the papers on conventional engine DEP studies reviewed in Chapter 2. This section attempts to more thoroughly explain the phenomena observed for RCCI performance by consulting the results from conventional engine DEP literature, and finding any similarities and differences between the conventional engine studies and the RCCI study.

Initial zero-dimensional EES results confirmed the phenomena observed by all the conventional engine studies that the pumping penalty was significantly reduced by implementing the DEP concept, since the separate exhaust valve timings and the separate exhaust manifolds make an effort to ensure that the exhaust gas in the cylinder is exposed to a positive pressure gradient for as long a duration as possible for a more efficient exhaust evacuation process. The results also showed that increasing the exhaust valve area was beneficial since the choking duration could be minimized with a less restricted flow area in the blowdown and scavenging ports.

Simulating the DEP concept in GT-Power proved to be a challenge however, mainly due to the well-known problem of low exhaust enthalpy available to the turbocharger. Because of this, the FGT was

not sufficient to supply the required boost pressure and a boost deficit existed, which had to be compensated through the use of a mechanical supercharger as a 2nd stage compressor. The SI engine studies performed by Moller [116], Roth [118] and Hu [120] did not have this problem because there is a limit in the boost pressure that can be supplied to SI engines to prevent knocking. Compression ignition engines on the other hand require high boost pressures to increase the load limit; there is also a necessity to run as lean as possible to improve the thermal efficiency by increasing the value of the specific heat ratio [189], while for SI engines, the stoichiometric air-fuel ratio has to be maintained.

Because of the limited quantity of boost that could be provided, and the possibility to vary the combustion phasing by spark timing, Roth et al. [118] were able to attain BSFC improvements of up to 2.5% and 4% over the load range by significantly reducing the pumping penalty. For the RCCI points, the parasitic losses from the supercharger were usually greater than the pumping benefit from DEP, causing a rise in the BSFC, especially for the 8 Bar BMEP operating point where BSFC rose by 2.5% (compared to the baseline engine) for the most fuel efficient SCVO timing.

One possible reason why the turbocharger alone was not able to supply the required boost pressure and intake flow rate at the 8 Bar BMEP point is the range of the stock turbocharger map. With the original turbocharger, the 1.62 Bar boost pressure point (with a $305.22\ \mathrm{kg \cdot h^{-1}}$) flow rate is very close to the low speed lines and the choke region. This happens most likely due to the fact that the blowdown energy available at 8 Bar BMEP is too low, and as a result, the turbocharger speed may not be fast enough for the centrifugal compressor to operate at high isentropic efficiencies, which in turn gives a poor boost response. Recall that the scaling procedure of Bell et al. [177] assumes that the A/R ratio of the turbine and compressor housings are constant, but in reality, a different turbine and compressor housing may be required for LTC engines. This explains why using a VGT instead of an FGT for the high load 18 Bar IMEP point was able to show a 1% improvement in BSFC over the stock engine configuration, as the VGT allowed control over the A/R ratio and thus the turbocharger efficiency, and also removed the need for a second stage compressor, eliminating parasitic losses. Therefore, another turbocharger map with a different turbine and compressor housing geometry that is more efficient at the 8 Bar BMEP point could have been selected and

used for scaling. (Since turbocharger maps are often proprietary and hard to come by, the only available Honeywell Garrett M53 maps were used for scaling.)

At high load, sometimes it may be required to increase the turbine outlet pressure through the use of a throttle to drive LP EGR, which could potentially lead to a lower turbine efficiency and higher pumping work. To overcome this problem, Roth et al.'s [119] idea of scavenge-sourced EGR could have been used. Scavenge-sourced EGR could however, not be implemented at the 18 Bar IMEP point, because a very high EGR fraction of 35% was required for that point, and the proportion of exhaust directed to the scavenging manifold at the minimum BSFC timing (256 Degrees ATDC SCVO Timing) was only 19%.

Perhaps the closest study to the present RCCI study was the work done by Gundmalm et al. on a heavy-duty diesel engine [121–123], since these experiments and simulations were performed for a compression-ignition engine and also investigated the impact of external EGR on engine performance. It was shown in this research that using EGR strongly impacted the choice of valve timing strategies due to the need to adjust the exhaust system pressure for EGR flow. Figure 7-45 shows the BSFC change (compared with the base engine) at a number of operating points on the engine load-speed map for the DEP concept, with and without LP-EGR. Without EGR, the BSFC reductions using the DEP concept were on the order of 1.2% or more at high load for low and medium engine speeds; in fact, as the speed decreased for the non-EGR cases, the BSFC reduction was even greater. With LP-EGR, the BSFC reductions were not that significant at medium and high loads. The authors believed that this phenomenon was a consequence of the need for higher exhaust manifold pressures in the LP-EGR case to perform both turbine work and to have sufficient backpressure to drive the LP-EGR flow.

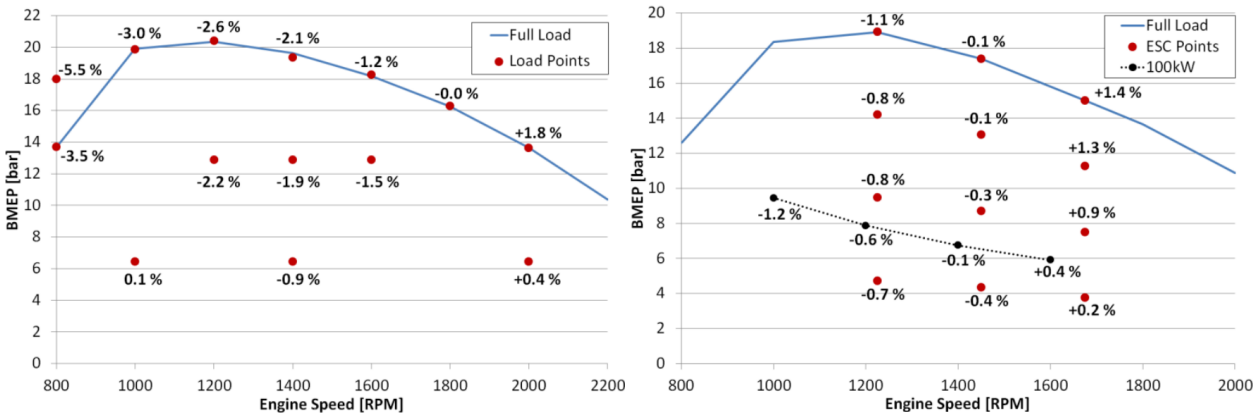

Figure 7-45: BSFC Change in the Engine Operating Map for DEP engine vs. base engine for: (Left, 7-45a) Non-EGR case and (Right, 7-45b) LP-EGR case. (Source: [123])

Similar results to the Gundmalm study [123] were observed for the RCCI study, in that the BSFC increased slightly with DEP at high load and medium speed (compared to the stock engine configuration) when the FGT was used at the most fuel-efficient SCVO timing. Unlike what the authors identified however, the PMEP using the DEP for RCCI was +0.15 Bar, which was 0.31 Bar greater than in the stock engine configuration. The main reason for the decline in BSFC was the parasitic loss from the supercharger, which negated the pumping penalty reduction benefit. If the VGT were used instead of the FGT, the supercharger could be removed and a 1% benefit in BSFC was observed, similar to the 0.8% benefit observed at an analogous point (but with the FGT) for the heavy duty diesel engine. More details from the Gundmalm [123] study are required however, such as the exact EGR fraction used at that 0.8% improvement point to fully compare the results between the two studies, but the specific details were not available in the paper.

Since the 18 Bar IMEP point at 2,000 rev/min is not the maximum load that can be attained at this speed for the General Motors 1.9L engine according to the stock engine map, a greater BSFC reduction might be expected at a higher load for the medium speed cases if one speculates/extrapolates the results from an analogous region on the heavy duty diesel engine map.

To deal with higher blowdown flow rates, Gundmalm suggested using larger blowdown than scavenging valves when LP EGR was used [122]. For the General Motors 1.9L engine, this may not be feasible because increasing the blowdown valve area by a larger amount than the scavenging valve area

could reduce the bridge spacing between the blowdown valve and the intake valves, as well as the bridge spacing between the blowdown valve and the scavenging valves. Reducing the bridge spacing is detrimental to the structural integrity due to high thermal and mechanical stress concentrations that could cause cracks in the cylinder head and damage the engine.

In conclusion, the Divided Exhaust Period concept shows mixed results when applied to an LTC strategy such as RCCI. The lower flow rates through the turbocharger turbine limit the quantity of boost that can be achieved and a 2nd compressor stage is needed to make up the deficit which can potentially deteriorate the fuel economy. More investigation is needed at other operating points in the engine map to identify if DEP can provide a fuel economy benefit at those points before deciding on adopting this concept in a production engine running on LTC strategies such as RCCI.

CHAPTER 8: CONCLUSIONS AND FUTURE WORK

In the present research different strategies to optimize the air handling system of a multi-cylinder light duty engine running on reactivity controlled compression ignition (RCCI) were explored. The objectives were threefold: improve combustion stability and mitigate UHC and CO emissions at low loads, determine and evaluate the system level requirements for high load RCCI operation, and use VVA as well as manifold redesign techniques to mitigate the pumping penalty at medium and high loads. This chapter lists the main conclusions of this research project, and investigates potential ideas for future work.

8.1 Summary of Major Conclusions

1. Air Handling System Optimization for Low Load Operation

Optimization of the air handling system for low load operation was necessary to improve the combustion efficiency and Diesel Oxidation Catalyst (DOC) conversion efficiency to mitigate UHC and CO emissions at low load. This was done by investigating strategies that could raise exhaust gas temperatures to light-off the DOC for a more efficient low load UHC and CO conversion. Since varying the combustion phasing through the adjustment of the gasoline-to-diesel ratio and post-injection of additional fuel could not raise the exhaust gas temperature, VVA strategies such as Early Exhaust Valve Opening (EEVO) and cylinder deactivation were studied. Below are the major findings of the EEVO and cylinder deactivation studies:

i) Advancing the EVO timing through the use of VVA increases the exhaust gas temperature, thereby reducing the fraction of EGR needed to attain the same IVC temperature and pressure, which, in turn, improves volumetric efficiency.

ii) The higher exhaust gas temperatures at advanced EVO timings are especially beneficial in improving the aftertreatment efficiency at low load operation, since the exhaust gas temperatures are high enough to light-off the catalyst. Advancing the EVO timing from 112 degrees ATDC to 80 degrees ATDC improves the UHC and CO conversion by the DOC from 0% and 18% respectively to almost 100% for 1 Bar BMEP at 1,500 rev/min.

iii) A drawback of opening the exhaust valves early is a lower work output per engine cycle due to the reduced expansion stroke duration, which causes the fuel economy to deteriorate. The BSFC increased from 554 g/kWh at the stock exhaust valve timing to 607 g/kWh at 80 degrees ATDC for 1 Bar BMEP at 1,500 rev/min, a 9.6% deterioration in fuel economy.

iv) EEVO using a cam phaser also yielded an exhaust gas temperature higher than the DOC light-off temperature of 457 K, and did not require the use of external EGR because EGR could be accomplished internally through zero valve overlap. However, the cam phaser gave even poorer volumetric efficiency and a much higher pumping penalty compared than the fully flexible VVA case at 80 degrees ATDC. Compared with the stock EVO timing, the EEVO using a cam phaser gave a BSFC of 1,053 g/kWh, a 90% increase. The increase in pumping penalty over the stock valve timings was due to heat losses from the recompression of the trapped residual gases during the compression stroke.

v) Cylinder deactivation with only one cylinder firing at a 4 Bar BMEP equivalent fueling rate proved to be the best strategy for raising the exhaust gas temperature at 1 Bar BMEP, because of the superior fuel economy of 351 g/kWh. The lower BSFC is due to the firing cylinder operating at a load point with a higher combustion efficiency, and the reduction in pumping penalty as the intake and exhaust valves of the motoring cylinders were closed.

vi) Cylinder deactivation also offered the best UHC and CO conversion efficiencies among the three strategies investigated, because in addition to raising the exhaust gas temperature to a value higher than the DOC light-off temperature, the exhaust flow rate through the DOC was also much lower with only one cylinder firing. As a result of the lower exhaust flow rates, the UHC and CO conversion efficiencies were close to 100%.

2. Determination of Engine System Level Requirements for High Load Operation

System level requirements were determined for multi-cylinder RCCI operation at a high load operating point of 18 Bar IMEP at 2,000 rev/min through the use of coupled GT-Power/KIVA-3V simulations. For this operating point, an EGR fraction of 35% was implemented through the use of a newly

incorporated low pressure (LP) EGR circuit. A throttle was added to the turbocharger turbine outlet/LP-EGR circuit inlet to raise the backpressure for driving EGR flow.

At such a high load operating point, it was not possible to use the stock high pressure (HP) EGR circuit due to the insufficient backpressure between the turbine inlet and the compressor outlet. Moreover, using HP EGR would reduce the exhaust flow through the turbine as a portion of the exhaust flow bypasses the turbine. Since the entire exhaust flow is not available for utilization by the turbine, the turbocharger would not be able to supply the desired boost pressure.

Even with LP-EGR, the cycle-averaged isentropic efficiency for the turbocharger compressor only reached 68.2% (less than the maximum isentropic efficiency of 78%), and at certain portions of the cycle, the compressor went into the surge region, indicating that the turbocharger was not properly sized for RCCI.

3. Exhaust Manifold Redesign using the Divided Exhaust Period Concept

A major challenge for turbocharged engines running on LTC strategies such as RCCI is the significant pumping penalty caused by high exhaust backpressures at the turbocharger turbine inlet. High backpressures are necessary for the turbine to extract as much work as possible because of the low exhaust enthalpy prevalent in LTC strategies such as RCCI. To overcome this backpressure problem, the Divided Exhaust Period (DEP) concept was proposed for the exhaust manifold redesign. In this concept, the stock exhaust manifold was removed, and was replaced with two separate exhaust manifolds: the blowdown manifold, which was connected directly to the turbocharger turbine, and the scavenging manifold, which bypassed the turbine and was connected to the turbine outlet. By using a VVA system to separately actuate each exhaust valve, the exhaust flow could be distributed between the two manifolds, lowering the overall engine backpressure, which in turn reduced the pumping penalty. The exhaust flow distribution between the two manifolds was primarily dependent on the individual timing of each exhaust valve. Below are the following conclusions from the DEP simulation study:

i) DEP helped reduce the pumping penalty at both the 8 Bar BMEP at 18 Bar IMEP load points, with the penalty reduction greater at the 8 Bar BMEP point since that point was at a higher speed.

ii) The conventional trade-off between intake and exhaust valve area does not apply to the DEP concept; larger exhaust valves would be beneficial as flow through a larger valve area can decrease the choking duration, especially at higher speeds and loads, which can also be beneficial for pumping work. There is however, a limit on the exhaust valve area due to geometrical and mechanical constraints.

iii) Since a smaller portion of the exhaust gas flows through the turbocharger turbine due to division of flow between the exhaust manifolds, a smaller fixed geometry turbocharger (FGT) was used to handle the lower blowdown flow rates. The turbocharger dimensions were selected using dimensional analysis techniques, and were optimized at the 8 Bar BMEP load point. The scaling results gave a turbocharger with turbine and compressor wheel diameters that were 13.6% and 10% smaller respectively than the stock turbine and compressor wheel diameters.

iv) Because of the low exhaust enthalpy problem prevalent in RCCI, the FGT alone could not supply the required boost and therefore this resulted in adding a supercharger to the system as a 2^{nd} stage compressor. While the supercharger was able to provide the pumping benefit, the parasitic losses of the supercharger outweighed the pumping benefit it gave. Because of the parasitic losses, the BSFC was higher than that for the stock engine configuration at both the 8 Bar BMEP and 18 Bar IMEP load points.

v) Retarding the scavenging valve opening timing allowed a greater proportion of the exhaust gases to be evacuated into the blowdown manifold which increased the exhaust back pressure, and mass flow rate through the turbine. This in turn increased the turbocharger compressor power, and in turn the 1^{st} stage compressor outlet pressure.

vi) By using a variable geometry turbocharger (VGT) instead of an FGT, an additional degree of freedom in regulating the exhaust backpressure was now available in addition to the scavenging valve opening timing. This happens because when the rack position of the VGT vanes are changed, the A/R ratio is adjusted as well, which also impacts the turbocharger performance. By properly controlling the backpressure through a late opening of the scavenging valve (266 Degrees ATDC)

and a smaller rack position of 0.33 at the 18 Bar IMEP load point, the BSFC was improved by 1% over the stock engine configuration.

vii) DEP has also proven to be beneficial for low load operation. Since boosting is minimal at low loads, the turbocharger only acts as a heat sink in a conventional engine, lowering the exhaust gas temperature to values that might be too low to light-off the DOC. With the DEP concept, the turbine can be completely bypassed by only opening the scavenging valve while the blowdown valve is kept closed. Since the turbine is bypassed, there is minimal exhaust backpressure which reduces the pumping penalty, and heat losses are minimized. This in turn ensures that the exhaust gas temperature is high enough to light-off the DOC. Furthermore, because the pumping penalty is minimized by bypassing the turbine, the BSFC may drop as well.

8.2 Future Work

As mentioned in Chapter 5, one of the major issues with cylinder deactivation is Noise, Vibration and Harshness (NVH) and a lack of balance between cylinders that could cause engine damage. It is therefore vital to carry out NVH studies between various cylinder deactivation strategies such as 2-cylinder firing and 1-cylinder firing strategies and determine from a mechanical/NVH standpoint which would be a more feasible strategy. Moreover, cylinder deactivation in real world implementation is actually a transient process, so the cylinder deactivation process in GT-Power should be simulated by firing all cylinders one cylinder at a time based on an optimal firing order.

While the Divided Exhaust Period (DEP) concept has shown that the pumping penalty can be minimized by lowering the average backpressure through the distribution of exhaust gas among two manifolds, the low exhaust enthalpy meant that a supercharger had to be used as a 2^{nd} stage compressor to overcome the boost deficit, which resulted in parasitic losses that were greater than the pumping benefit. To overcome this problem, the supercharger may be actuated by means of an electric motor rather than the cranktrain [190–193]. An electric motor has the advantages of high transmission efficiencies with minimal losses in the shafts and electrical connections. In addition, with the supercharger decoupled from the cranktrain, the electric motor may rotate the supercharger rotors at a higher speed and this may allow the

supercharger to operate in a more efficient region on its map. In a hybrid vehicle application, the electrical energy for the supercharger may be supplied from generators and supercapacitors [194, 195] that store energy from regenerative braking (Shown in Figure 8-1), which can help reduce the BSFC.

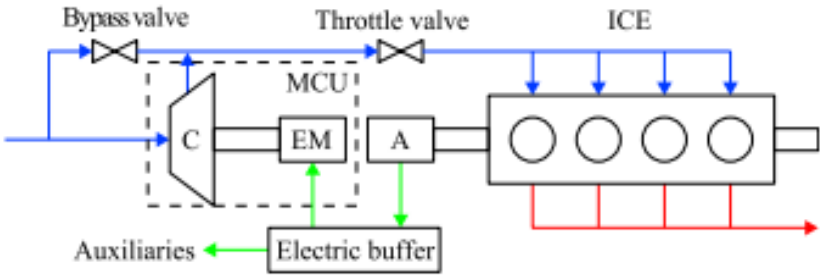

Figure 8-1: Electric supercharger in a hybrid vehicle architecture. Source: [195]

To improve the turbocharger efficiency and maximize turbine work extraction, a novel technique referred to as Active Control Turbocharging (ACT) may be used [196–204]. In this concept, the turbine inlet area of a VGT is made to vary cyclically by applying a sinusoidal signal to the VGT rack position (Shown in Figure 8-2). The frequency of this sinusoidal signal is dependent on engine speed. Using an appropriate signal amplitude and phase angle, the rack position may be actuated such that the enthalpy from the exhaust pulses is more efficiently extracted, giving rise to an increase in turbine power output, and in turn an increase in the centrifugal compressor power input. This will allow for an increase in the boost pressure and an improvement in engine torque, especially torque at low speed, which in turn can reduce the BSFC.

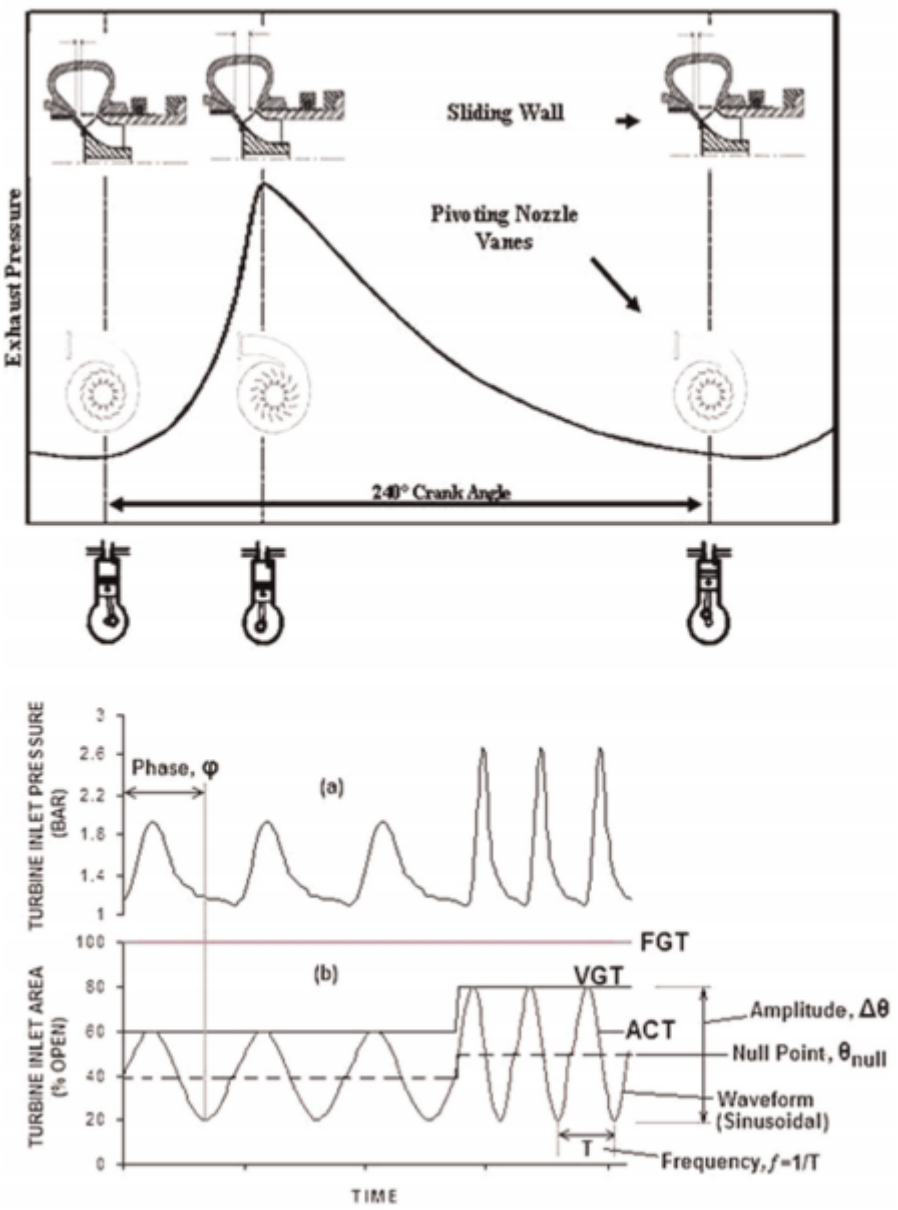

Figure 8-2: Active Control Turbocharging Concept. Source: [203]

Another strategy to maximize turbine work extraction and improve turbocharger efficiency would be to use a mixed flow turbine [205–210] instead of conventional axial or radial flow turbines. In a mixed flow turbine rotor, the leading edge of the turbine blade is swept downwards, creating a non-zero inlet angle for the exhaust gas as shown in Figure 8-3 [211]. Mixed flow turbines have been shown to be more efficient at lower blade-speed ratios than radial or axial turbines (as shown in Figure 8-4), whose efficiencies peak at a blade-speed ratio of 0.7. LTC concepts such as RCCI which use high EGR fractions to keep the peak

pressure rise rate within acceptable limits would probably benefit from a mixed flow turbine, since high EGR fractions move the turbine operating point to lower blade-speed ratios [212, 213]. Moreover, the mixed flow turbine rotor has a lower moment of inertia, which can be beneficial in improving transient response.

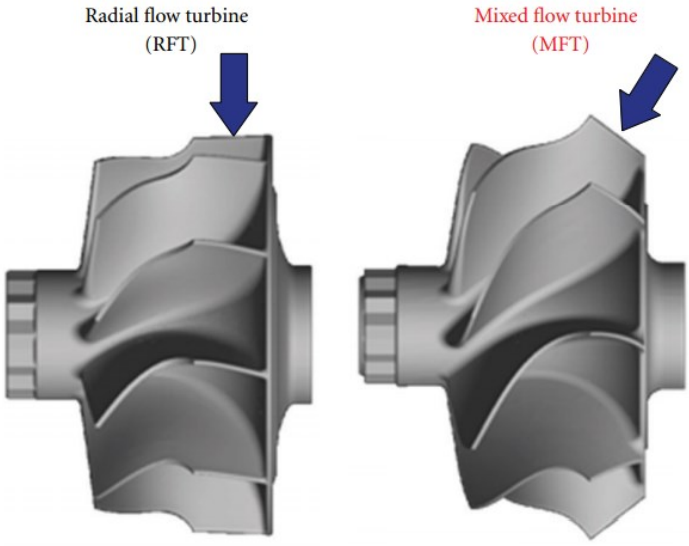

Figure 8-3: Mixed flow vs. radial flow turbine blade geometry. Source: [211]

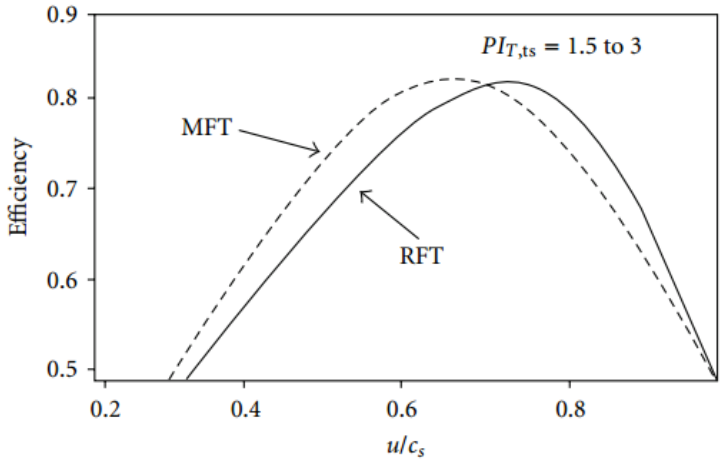

Figure 8-4: Turbine Isentropic Efficiency as a function of Blade Speed Ratio for Radial and Mixed Flow Turbines. Source: [211]

Finally, before RCCI as a combustion concept is implemented in a production engine, it is also important to evaluate the transient operation of a multi-cylinder engine in which the engine load and speed are continuously changing. Real world engine operation involves transient conditions, during which the

pollutant emissions typically exceed their acceptable values owing to the non-linear and non-steady conditions prevalent during transient operation [93]. Moreover, due to rapid changes in operating conditions during transients, undesirable phenomena (such as turbocharger lag) may occur due to physical constraints of the air handling components, thereby inhibiting the rate at which the desired system state can be reached. High EGR fractions used in LTC concepts such as RCCI also make said combustion strategies more susceptible to delays in EGR response and coupling between the exhaust gas flow rate and turbine inlet pressure [214, 215]. To address the aforementioned operational challenges of increased emissions and system response delays, the air handling system must be extensively studied and the components optimized for improved transient response.

REFERENCES AND BIBLIOGRAPHY

[1] B. Isler, "Transportation Systems," in *Handbook of Energy Efficiency and Renewable Energy*, D. Y. Goswami and F. Kreith, Eds. Boca Raton, FL: CRC Press, 2007, pp. 8-1-34.

[2] J. Yang, "Four-stroke Gasoline HCCI Engines with Thermal Management," in *HCCI and CAI Engines for the Automotive Industry*, 1 edition., H. Zhao, Ed. Boca Raton FL; Cambridge, England: Woodhead Publishing, 2007, pp. 77–102.

[3] J. Heywood, *Internal Combustion Engine Fundamentals*. McGraw-Hill Education, 1988.

[4] R. J. Farrauto, "Industrial Catalysis: A Practical Guide," in *Kent and Riegel's Handbook of Industrial Chemistry and Biotechnology*, J. A. Kent, Ed. Springer US, 2007, pp. 271–304.

[5] A. Gupta, "Advanced Technologies for Clean and Efficient Energy Conversion in Power Systems," in *Thermal Engineering in Power Systems*, 1st ed., R. Amano and B. Sundén, Eds. WIT Press, 2008, pp. 37–70.

[6] D.-I. P. Eckert and D.-I. S. Rakowski, "Pollutant Formation," in *Combustion Engines Development*, G. P. Merker, C. Schwarz, and R. Teichmann, Eds. Springer Berlin Heidelberg, 2012, pp. 193–223.

[7] O. I. Smith, "Fundamentals of soot formation in flames with application to diesel engine particulate emissions," *Progress in Energy and Combustion Science*, vol. 7, no. 4, pp. 275–291, 1981.

[8] M. Zheng, G. T. Reader, and J. G. Hawley, "Diesel Engine Exhaust Gas Recirculation—A Review on Advanced and Novel Concepts," *Energy Conversion and Management*, vol. 45, no. 6, pp. 883–900, Apr. 2004.

[9] J. Hoard, M. Abarham, D. Styles, J. M. Giuliano, C. S. Sluder, and J. M. E. Storey, "Diesel EGR Cooler Fouling," SAE International, Warrendale, PA, SAE Technical Paper 2008-01–2475, Oct. 2008.

[10] N. Miyoshi, S. 'ichi Matsumoto, K. Katoh, T. Tanaka, J. Harada, N. Takahashi, K. Yokota, M. Sugiura, and K. Kasahara, "Development of New Concept Three-Way Catalyst for Automotive Lean-Burn Engines," SAE International, Warrendale, PA, SAE Technical Paper 950809, Feb. 1995.

[11] Y. He, "Development and Application of a Lean NOX Trap Model," SAE International, Warrendale, PA, SAE Technical Paper 2006-01–0686, Apr. 2006.

[12] Y.-W. Kim, J. Sun, I. Kolmanovsky, and J. Koncsol, "A Phenomenological Control Oriented Lean NOx Trap Model," SAE International, Warrendale, PA, SAE Technical Paper 2003-01–1164, Mar. 2003.

[13] J. Gieshoff, M. Pfeifer, A. Schäfer-Sindlinger, P. C. Spurk, G. Garr, T. Leprince, and M. Crocker, "Advanced Urea SCR Catalysts for Automotive Applications," SAE International, Warrendale, PA, SAE Technical Paper 2001-01–0514, Mar. 2001.

[14] O. A. Haralampous, I. P. Kandylas, G. C. Koltsakis, and Z. C. Samaras, "Diesel Particulate Filter Pressure Drop Part 1: Modelling and Experimental Validation," *International Journal of Engine Research*, vol. 5, no. 2, pp. 149–162, Apr. 2004.

[15] F. Jun, G. Jinke, Y. Wenhua, Y. Mingguo, and T. Weixin, "Study on the Exhaust Back-pressure Threshold-value MAP for the Diesel Particulate Filter Regeneration," in *2011 Third International Conference on Measuring Technology and Mechatronics Automation (ICMTMA)*, 2011, vol. 3, pp. 557–560.

[16] C. G. Li, F. Mao, S. B. Swartzmiller, S. A. Wallin, and R. R. Ziebarth, "Properties and Performance of Diesel Particulate Filters of an Advanced Ceramic Material," SAE International, Warrendale, PA, SAE Technical Paper 2004-01–0955, Mar. 2004.

[17] A. G. Konstandopoulos, M. Kostoglou, E. Skaperdas, E. Papaioannou, D. Zarvalis, and E. Kladopoulou, "Fundamental Studies of Diesel Particulate Filters: Transient Loading, Regeneration and Aging," SAE International, Warrendale, PA, SAE Technical Paper 2000-01–1016, Mar. 2000.

[18] J. E. Dec, "Advanced compression-ignition engines—understanding the in-cylinder processes," *Proceedings of the Combustion Institute*, vol. 32, no. 2, pp. 2727–2742, 2009.

[19] R. H. Thring, "Homogeneous-Charge Compression-Ignition (HCCI) Engines," SAE International, Warrendale, PA, SAE Technical Paper 892068, Sep. 1989.

[20] P. M. Najt and D. E. Foster, "Compression-Ignited Homogeneous Charge Combustion," SAE International, Warrendale, PA, SAE Technical Paper 830264, Feb. 1983.

[21] T. Tsurushima, E. Kunishima, Y. Asaumi, Y. Aoyagi, and Y. Enomoto, "The Effect of Knock on Heat Loss in Homogeneous Charge Compression Ignition Engines," SAE International, Warrendale, PA, SAE Technical Paper 2002-01–0108, Mar. 2002.

[22] T. Urushihara, K. Yamaguchi, K. Yoshizawa, and T. Itoh, "A Study of a Gasoline-fueled Compression Ignition Engine ∼ Expansion of HCCI Operation Range Using SI Combustion as a Trigger of Compression Ignition ∼," SAE International, Warrendale, PA, SAE Technical Paper 2005-01–0180, Apr. 2005.

[23] H. Yun, N. Wermuth, and P. Najt, "Extending the High Load Operating Limit of a Naturally-Aspirated Gasoline HCCI Combustion Engine," SAE International, Warrendale, PA, SAE Technical Paper 2010-01–0847, Apr. 2010.

[24] H. Persson, A. Hultqvist, B. Johansson, and A. Remón, "Investigation of the Early Flame Development in Spark Assisted HCCI Combustion Using High Speed Chemiluminescence Imaging," SAE International, Warrendale, PA, SAE Technical Paper 2007-01–0212, Apr. 2007.

[25] J. B. Martz, H. Kwak, H. G. Im, G. A. Lavoie, and D. N. Assanis, "Combustion regime of a reacting front propagating into an auto-igniting mixture," *Proceedings of the Combustion Institute*, vol. 33, no. 2, pp. 3001–3006, 2011.

[26] Y. Iwabuchi, K. Kawai, T. Shoji, and Y. Takeda, "Trial of New Concept Diesel Combustion System - Premixed Compression-Ignited Combustion -," SAE International, Warrendale, PA, SAE Technical Paper 1999-01–0185, Mar. 1999.

[27] K. Okude, K. Mori, S. Shiino, and T. Moriya, "Premixed Compression Ignition (PCI) Combustion for Simultaneous Reduction of NOx and Soot in Diesel Engine," SAE International, Warrendale, PA, SAE Technical Paper 2004-01–1907, Jun. 2004.

[28] S. Kimura, O. Aoki, Y. Kitahara, and E. Aiyoshizawa, "Ultra-Clean Combustion Technology Combining a Low-Temperature and Premixed Combustion Concept for Meeting Future Emission Standards," SAE International, Warrendale, PA, SAE Technical Paper 2001-01–0200, Mar. 2001.

[29] H. Yanagihara, "Ignition timing control at Toyota UNIBUS combustion system," presented at the IFP. International congress, 2002, pp. 35–42.

[30] C. Noehre, M. Andersson, B. Johansson, and A. Hultqvist, "Characterization of Partially Premixed Combustion," SAE International, Warrendale, PA, SAE Technical Paper 2006-01–3412, Oct. 2006.

[31] G. T. Kalghatgi, P. Risberg, and H.-E. Ångström, "Advantages of Fuels with High Resistance to Auto-ignition in Late-injection, Low-temperature, Compression Ignition Combustion," SAE International, Warrendale, PA, SAE Technical Paper 2006-01–3385, Oct. 2006.

[32] H. Solaka, U. Aronsson, M. Tuner, and B. Johansson, "Investigation of Partially Premixed Combustion Characteristics in Low Load Range with Regards to Fuel Octane Number in a Light-Duty Diesel Engine," SAE International, Warrendale, PA, SAE Technical Paper 2012-01–0684, Apr. 2012.

[33] P. Borgqvist, P. Tunestal, and B. Johansson, "Gasoline Partially Premixed Combustion in a Light Duty Engine at Low Load and Idle Operating Conditions," SAE International, Warrendale, PA, SAE Technical Paper 2012-01–0687, Apr. 2012.

[34] P. W. Bessonette, C. H. Schleyer, K. P. Duffy, W. L. Hardy, and M. P. Liechty, "Effects of Fuel Property Changes on Heavy-Duty HCCI Combustion," SAE International, Warrendale, PA, SAE Technical Paper 2007-01–0191, Apr. 2007.

[35] K. Inagaki, T. Fuyuto, K. Nishikawa, K. Nakakita, and I. Sakata, "Dual-Fuel PCI Combustion Controlled by In-Cylinder Stratification of Ignitability," SAE International, Warrendale, PA, SAE Technical Paper 2006-01–0028, Apr. 2006.

[36] S. L. Kokjohn, R. M. Hanson, D. A. Splitter, and R. D. Reitz, "Experiments and Modeling of Dual-Fuel HCCI and PCCI Combustion Using In-Cylinder Fuel Blending," SAE International, Warrendale, PA, SAE Technical Paper 2009-01–2647, Nov. 2009.

[37] R. M. Hanson, S. L. Kokjohn, D. A. Splitter, and R. D. Reitz, "An Experimental Investigation of Fuel Reactivity Controlled PCCI Combustion in a Heavy-Duty Engine," SAE International, Warrendale, PA, SAE Technical Paper 2010-01–0864, Apr. 2010.

[38] S. L. Kokjohn, R. M. Hanson, D. A. Splitter, and R. D. Reitz, "Fuel reactivity controlled compression ignition (RCCI): a pathway to controlled high-efficiency clean combustion," *International Journal of Engine Research*, vol. 12, no. 3, pp. 209–226, Jun. 2011.

[39] D. Splitter, S. Kokjohn, K. Rein, R. Hanson, S. Sanders, and R. D. Reitz, "An Optical Investigation of Ignition Processes in Fuel Reactivity Controlled PCCI Combustion," SAE International, Warrendale, PA, SAE Technical Paper 2010-01–0345, Apr. 2010.

[40] R. M. Hanson, "Experimental Investigation of Transient RCCI Combustion in a Light Duty Diesel Engine," THE UNIVERSITY OF WISCONSIN - MADISON, 2013.

[41] T. Kuboyama, Y. Moriyoshi, K. Hatamura, J. Takanashi, Y. Urata, and T. Yamada, "Improvement of thermal efficiency of a four-cylinder gasoline homogeneous charge compression ignition engine via blowdown supercharging," *International Journal of Engine Research*, vol. 13, no. 3, pp. 226–237, Jun. 2012.

[42] V. Y. Prikhodko, S. J. Curran, T. L. Barone, S. A. Lewis, J. M. Storey, K. Cho, R. M. Wagner, and J. E. Parks, "Emission Characteristics of a Diesel Engine Operating with In-Cylinder Gasoline and Diesel Fuel Blending," SAE International, Warrendale, PA, SAE Technical Paper 2010-01–2266, Oct. 2010.

[43] J.-J. Zheng, J.-H. Wang, B. Wang, and Z.-H. Huang, "Effect of the compression ratio on the performance and combustion of a natural-gas direct-injection engine," *Proceedings of the Institution of Mechanical Engineers, Part D: Journal of Automobile Engineering*, vol. 223, no. 1, pp. 85–98, Jan. 2009.

[44] S. Curran, V. Prikhodko, K. Cho, C. S. Sluder, J. Parks, R. Wagner, S. Kokjohn, and R. D. Reitz, "In-Cylinder Fuel Blending of Gasoline/Diesel for Improved Efficiency and Lowest Possible Emissions on a Multi-Cylinder Light-Duty Diesel Engine," SAE International, Warrendale, PA, SAE Technical Paper 2010-01–2206, Oct. 2010.

[45] J. Bittle, J. Zheng, X. Sue, and T. Jacobs, "Cylinder-to-cylinder variation sources in diesel low temperature combustion and the influence they have on emissions," presented at the Spring Technical Meeting of the Central States of the Combustion Institute, Dayton, OH, 2012.

[46] J.-O. Olsson, P. Tunestål, G. Haraldsson, and B. Johansson, "A Turbo Charged Dual Fuel HCCI Engine," Warrendale, PA, SAE Technical Paper 2001-01–1896, May 2001.

[47] P. Shingne, D. N. Assanis, A. Babajimopoulos, P. Keller, D. Roth, and M. Becker, "Turbocharger matching for a 4-cylinder gasoline HCCI engine using a 1D engine simulation," SAE Technical Paper, Warrendale, PA, 2010-01–2143, 2010.

[48] S. Mamalis, V. Nair, P. Andruskiewicz, D. Assanis, A. Babajimopoulos, N. Wermuth, and P. Najt, "Comparison of Different Boosting Strategies for Homogeneous Charge Compression Ignition Engines-A Modeling Study," *SAE International Journal of Engines*, vol. 3, no. 1, pp. 296–308, 2010.

[49] R. D. Reitz and G. Duraisamy, "Review of high efficiency and clean reactivity controlled compression ignition (RCCI) combustion in internal combustion engines," *Progress in Energy and Combustion Science*.

[50] J. Wang, "Hybrid Robust Air-Path Control for Diesel Engines Operating Conventional and Low Temperature Combustion Modes," *IEEE Transactions on Control Systems Technology*, vol. 16, no. 6, pp. 1138–1151, Nov. 2008.

[51] O. H. M. Ghazal, Y. S. H. Najjar, and K. J. M. Al-Khishali, "Modeling the Effect of Variable Timing of the Exhaust Valves on SI Engine Emissions for Greener Vehicles," *Energy and Power Engineering*, vol. 5, no. 3, pp. 181–189, 2013.

[52] H. Hong, G. B. Parvate-Patil, and B. Gordon, "Review and analysis of variable valve timing strategies—eight ways to approach," *Proceedings of the Institution of Mechanical Engineers, Part D: Journal of Automobile Engineering*, vol. 218, no. 10, pp. 1179–1200, Oct. 2004.

[53] H.-H. Liao, “Control and Robustness Analysis of Homogeneous Charge Compression Ignition Using Exhaust Recompression,” Stanford University, 2011.

[54] C. Brüstle and D. Schwarzenthal, “VarioCam Plus - A Highlight of the Porsche 911 Turbo Engine,” SAE International, Warrendale, PA, SAE Technical Paper 2001-01–0245, Mar. 2001.

[55] R. Flierl and M. Klüting, “The Third Generation of Valvetrains - New Fully Variable Valvetrains for Throttle-Free Load Control,” SAE International, Warrendale, PA, SAE Technical Paper 2000-01–1227, Mar. 2000.

[56] D. Cope and A. Wright, “Electromagnetic Fully Flexible Valve Actuator,” SAE International, Warrendale, PA, SAE Technical Paper 2006-01–0044, Apr. 2006.

[57] J. Martinez-Frias, S. M. Aceves, D. Flowers, J. R. Smith, and R. Dibble, “HCCI Engine Control by Thermal Management,” SAE International, Warrendale, PA, SAE Technical Paper 2000-01–2869, Oct. 2000.

[58] J. Willand, R.-G. Nieberding, G. Vent, and C. Enderle, “The Knocking Syndrome - Its Cure and Its Potential,” SAE International, Warrendale, PA, SAE Technical Paper 982483, Oct. 1998.

[59] H. Zhao, “Four-stroke CAI Engines with Residual Gas Trapping,” in *HCCI and CAI Engines for the Automotive Industry*, 1 edition., Boca Raton FL; Cambridge, England: Woodhead Publishing, 2007, p. 106.

[60] A. Fuerhapter, W. F. Piock, and G. K. Fraidl, “CSI - Controlled Auto Ignition - the Best Solution for the Fuel Consumption - Versus Emission Trade-Off?,” SAE International, Warrendale, PA, SAE Technical Paper 2003-01–0754, Mar. 2003.

[61] P. Borgqvist, P. Tunestal, and B. Johansson, “Comparison of Negative Valve Overlap (NVO) and Rebreathing Valve Strategies on a Gasoline PPC Engine at Low Load and Idle Operating Conditions,” SAE International, Warrendale, PA, SAE Technical Paper 2013-01–0902, Apr. 2013.

[62] C. J. Chiang and A. G. Stefanopoulou, “Stability Analysis in Homogeneous Charge Compression Ignition (HCCI) Engines With High Dilution,” *IEEE Transactions on Control Systems Technology*, vol. 15, no. 2, pp. 209–219, Mar. 2007.

[63] K. Hatamura, “A Study on HCCI(Homogeneous Charge Compression Ignition) Gasoline Engine Supercharged by Exhaust Blow Down Pressure,” SAE International, Warrendale, PA, SAE Technical Paper 2007-01–1873, Jul. 2007.

[64] T. Kuboyama, Y. Moriyoshi, K. Hatamura, J. Takanashi, Y. Urata, and T. Yamada, “Extension of an operating load range of a four-cylinder gasoline homogeneous charge compression ignition engine via a blowdown supercharge system, aiming at in-cylinder thermal stratification,” *International Journal of Engine Research*, p. 1468087412437826, 2012.

[65] M. Sideris, *Methods for Monitoring and Diagnosing the Efficiency of Catalytic Converters: A Patent-oriented Survey*. Elsevier Science, 1998.

[66] M. Izadi Najafabadi and N. Abdul Aziz, “Homogeneous Charge Compression Ignition Combustion: Challenges and Proposed Solutions,” *Journal of Combustion*, vol. 2013, p. e783789, Aug. 2013.

[67] P. M. Laing, "Development of an Alternator-Powered Electrically-Heated Catalyst System," SAE International, Warrendale, PA, SAE Technical Paper 941042, Mar. 1994.

[68] L. S. Socha, D. F. Thompson, and P. A. Weber, "Optimization of Extruded Electrically Heated Catalysts," SAE International, Warrendale, PA, SAE Technical Paper 940468, Mar. 1994.

[69] R. C. Cornelison and W. A. Whittenberger, "Catalytic converter system," EP0456919 A2, 21-Nov-1991.

[70] S. D. Burch, T. F. Potter, M. A. Keyser, M. J. Brady, and K. F. Michaels, "Reducing Cold-Start Emissions by Catalytic Converter Thermal Management," SAE International, Warrendale, PA, SAE Technical Paper 950409, Feb. 1995.

[71] V. Y. Prikhodko, S. J. Curran, J. E. Parks, and R. M. Wagner, "Effectiveness of Diesel Oxidation Catalyst in Reducing HC and CO Emissions from Reactivity Controlled Compression Ignition," SAE International, Warrendale, PA, SAE Technical Paper 2013-01–0515, Apr. 2013.

[72] S. R. Katare and P. M. Laing, "Hydrogen in Diesel Exhaust: Effect on Diesel Oxidation Catalyst Flow Reactor Experiments and Model Predictions," SAE International, Warrendale, PA, SAE Technical Paper 2009-01–1268, Apr. 2009.

[73] B. Lecointe and G. Monnier, "Downsizing a gasoline engine using turbocharging with direct injection," SAE International, Warrendale, PA, SAE Technical Paper 2003-01–0542, 2003.

[74] B. Lee, "Dual -stage boosting systems: Modeling of configurations, matching and boost control options," UNIVERSITY OF MICHIGAN, 2009.

[75] C. Capiluppi, "Three-dimensional Simulation of a Turbocharger for Motorsport Applications," University of Parma, 2012.

[76] S. Bennett, *Modern Diesel Technology: Diesel Engines*. Cengage Learning, 2009.

[77] N. C. Baines, *Fundamentals of Turbocharging*. White River Junction, Vt.: Concepts ETI, Inc., 2005.

[78] N. Watson and M. S. Janota, *Turbocharging the Internal Combustion Engine*. Wiley, 1982.

[79] K. J. Fogarty, "Turbocharger Turbines: An Experimental Study on the Effects of Wastegate Size and Flow Passage Design," The Ohio State University, 2013.

[80] S. Bennett, *Modern Diesel Technology: Light Duty Diesels*. Cengage Learning, 2011.

[81] T. Andreas, "Wastegate Actuator Modeling and Model-Based Boost Pressure Control," presented at the IFAC Workshop on Engine and Powertrain Control, Simulation and Modeling, Paris, France, 2009, pp. 87–94.

[82] M. J. Nunney, *Light and Heavy Vehicle Technology*. Routledge, 2007.

[83] Q. Xin, *Diesel Engine System Design*. Elsevier, 2011.

[84] Y. JINNAI, H. ARIMIZU, N. TASHIRO, M. TOJO, T. YOKOYAMA, and N. HAYASHI, "A Variable Geometry (VG) Turbocharger for Passenger Cars to Meet European Union Emission Regulations," *Mitsubishi Heavy Industries Technical Review*, vol. 49, no. 2, p. 17, 2012.

[85] T. Gresh, *Compressor Performance: Aerodynamics for the User*. Newnes, 2001.

[86] W. D. Siuru Jr., "Automotive Superchargers and Turbochargers," in *Handbook of Turbomachinery*, 2nd ed., New York City, New York: Marcel Dekker Inc., 2003.

[87] L. Pohorelsky, Z. Zak, J. Macek, and O. Vitek, "Study of Pressure Wave Supercharger Potential using a 1-D and a 0-D Approach," *SAE International Journal of Engines*, vol. 4, no. 1, pp. 1331–1353, 2011.

[88] N. C. Baines, "Intake Boosting," in *Encyclopedia of Automotive Engineering*, vol. 1, Wiley, 2015.

[89] M. Mataczynski, J. Hoke, D. Paxson, and M. D. Polanka, "Design, Simulation, and Testing of a Pressure Wave Supercharger for a Small Internal Combustion Engine," SAE International, Warrendale, PA, SAE Technical Paper 2014-01–2136, 2014.

[90] P. Akbari, R. Nalim, and N. Mueller, "A review of wave rotor technology and its applications," *Journal of Engineering for Gas Turbines and Power*, vol. 128, no. 4, pp. 717–735, 2006.

[91] N. Watson, "Turbocharged Engines," in *Internal Combustion Engines*, San Diego, California: Academic Press, Inc., 1988.

[92] F. Schmitt, "Powerful Turbocharging System for Passenger Car Diesel Engines," BorgWarner Turbo Systems, 2014.

[93] C. D. Rakopoulos and E. G. Giakoumis, *Diesel Engine Transient Operation: Principles of Operation and Simulation Analysis*. Springer Science and Business Media, 2009.

[94] D.-I. P. Adomeit, M. S. S. Glück, D.-I. A. Sehr, and D.-I. S. Wedowswski, "Two-stage turbocharging — concept for high pressure charging on SI-engines," *MTZ Worldw*, vol. 71, no. 5, pp. 50–54, May 2010.

[95] F. Pfluger, "Regulated 2-Stage Turbocharging (R2S): A New Charging System for Commercial Diesel Engines," BorgWarner Turbo Systems, 2002.

[96] O. N. Varnier ., "Trends and Limits of Two-Stage Boosting Systems for Automotive Diesel Engines," Polytechnic University of Valencia, Valencia, Spain, 2012.

[97] C.-G. Cantemir, "Twin Turbo Strategy Operation," SAE International, Warrendale, PA, SAE Technical Paper 2001-01–0666, Mar. 2001.

[98] P. Wetzel, "Downspeeding a light duty diesel passenger car with a combined supercharger and turbocharger boosting system to improve vehicle drive cycle fuel economy," SAE International, Warrendale, PA, SAE Technical Paper 2013-01–0932, 2013.

[99] J. E. Dec and Y. Yang, "Boosted HCCI for high power without engine knock and with ultra-low NOx emissions-using conventional gasoline," *SAE International Journal of Engines*, vol. 3, no. 1, pp. 750–767, 2010.

[100] M. Christensen, B. Johansson, P. Amnéus, and F. Mauss, "Supercharged homogeneous charge compression ignition," *SAE Transactions, Journal of Engines*, vol. 107, 1998.

[101] M. Christensen and B. Johansson, "Supercharged homogeneous charge compression ignition (HCCI) with exhaust gas recirculation and pilot fuel," SAE International, Warrendale, PA, SAE Technical Paper 2000-01–1835, 2000.

[102] C. Wilhelmsson, P. Tunestal, and B. Johansson, "Operation strategy of a dual fuel HCCI engine with VGT," SAE International, Warrendale, PA, SAE Technical Paper 2007-01–1855, 2007.

[103] M. Martins and H. Zhao, "4-stroke multi-cylinder gasoline engine with controlled auto-ignition (CAI) combustion: a comparison between naturally aspirated and turbocharged operation," SAE International, Warrendale, PA, SAE Technical Paper 2008-36–0305, 2008.

[104] S. Mamalis, A. Babajimopoulos, O. Guralp, and P. Najt, "Optimal Use of Boosting Configurations and Valve Strategies for High Load HCCI-A Modeling Study," SAE International, Warrendale, PA, SAE Technical Paper 2012-01–1101, 2012.

[105] P. Shingne, D. Assanis, A. Babajimopoulos, A. Mond, and H. Yilmaz, "Application of a Supercharger in a Two-Stage Boosting System for a Gasoline HCCI Engine: A Simulation Study," in *ASME 2011 Internal Combustion Engine Division Fall Technical Conference*, 2011, pp. 547–556.

[106] I. Taritas, D. Kozarac, and M. Sjeric, "Numerical Study of Boosting Configurations and Valve Strategies for High Load HCCI Engine in Wide Range of Engine Speed," SAE International, Warrendale, PA, SAE Technical Paper 2014-01–1267, 2014.

[107] A. B. Dempsey and R. D. Reitz, "Computational optimization of reactivity controlled compression ignition in a heavy-duty engine with ultra low compression ratio," *SAE International Journal of Engines*, vol. 4, no. 2, pp. 2222–2239, 2011.

[108] U. Asad, R. Kumar, M. Zheng, and J. Tjong, "Ethanol-fueled low temperature combustion: A pathway to clean and efficient diesel engine cycles," *Applied Energy*, vol. 157, pp. 838–850, 2015.

[109] Y. Wu and R. D. Reitz, "Effects of exhaust gas recirculation and boost pressure on reactivity controlled compression ignition engine at high load operating conditions," *Journal of Energy Resources Technology*, vol. 137, no. 3, p. 32210, 2015.

[110] J. H. Lim and R. D. Reitz, "High load (21 bar IMEP) dual fuel RCCI combustion using dual direct injection," *Journal of Engineering for Gas Turbines and Power*, vol. 136, no. 10, p. 101514, 2014.

[111] S. V. Bohac and D. N. Assanis, "Effect of exhaust valve timing on gasoline engine performance and hydrocarbon emissions," *SAE transactions*, vol. 113, no. 4, pp. 2106–2116, 2004.

[112] G. B. Parvate-Patil, H. Hong, and B. Gordon, "Analysis of variable valve timing events and their effects on single cylinder diesel engine," *SAE transactions*, vol. 113, no. 3, pp. 1510–1519, 2004.

[113] L. Roberts, M. Magee, G. Shaver, A. Garg, J. McCarthy, E. Koeberlein, E. Holloway, R. Shute, D. Koeberlein, and D. Nielsen, "Modeling the impact of early exhaust valve opening on exhaust aftertreatment thermal management and efficiency for compression ignition engines," *International Journal of Engine Research*, vol. 16, no. 6, pp. 773–794, 2015.

[114] T. G. Leone and M. Pozar, "Fuel economy benefit of cylinder deactivation-sensitivity to vehicle application and operating constraints," SAE International, Warrendale, PA, SAE Technical Paper 2001-01–3591, 2001.

[115] X. Lu, C. Ding, A. Ramesh, G. Shaver, E. Holloway, J. McCarthy Jr, M. Ruth, E. Koeberlein, and D. Nielsen, "Impact of Cylinder Deactivation on Active Diesel Particulate Filter Regeneration at Highway Cruise Conditions," *Frontiers in Mechanical Engineering*, vol. 1, p. 9, 2015.

[116] C. Elmqvist Möller, P. Johansson, B. Grandin, and F. Lindström, "Divided exhaust period: a gas exchange system for turbocharged SI engines," in *SAE 2005 World Congress and Exhibition, April 2005, Detroit, MI, USA*, 2005.

[117] "Improvements in or relating to internal combustion engines," 12,227/22, 1924.

[118] D. B. Roth, P. Keller, and J. Sisson, "Valve-event modulated boost system," SAE Technical Paper, 2010.

[119] D. B. Roth and M. Becker, "Valve-event modulated boost system: Fuel consumption and performance with scavenge-sourced EGR," *SAE International Journal of Engines*, vol. 5, no. 2, pp. 538–546, 2012.

[120] B. Hu, S. Akehurst, C. Brace, C. Copeland, and J. Turner, "1-D Simulation Study of Divided Exhaust Period for a Highly Downsized Turbocharged SI Engine - Scavenge Valve Optimization," *SAE International Journal of Engines*, vol. 7, no. 3, pp. 1443–1452, Apr. 2014.

[121] S. Gundmalm, A. Cronhjort, and H.-E. \AAngström, "Divided exhaust period on heavy-duty diesel engines," in *THIESEL 2012 Conference on Thermo-and Fluid Dynamic Processes in Direct Injection Engines*, 2012.

[122] S. Gundmalm, A. Cronhjort, and H.-E. \AAngström, "Divided exhaust period: effects of changing the relation between intake, blow-down and scavenging valve area," in *SAE World Congress, April 16-18, 2013, Detroit, Michigan, USA*, 2013.

[123] S. Gundmalm, "Divided Exhaust Period on Heavy-Duty Diesel Engines," KTH Royal Institute of Technology, Stockholm, Sweden, 2013.

[124] A. M. Williams, A. T. Baker, and C. P. Garner, "Turbo-discharging: predicted improvements in engine fuel economy and performance," SAE International, Warrendale, PA, SAE Technical Paper 2011-01–0371, 2011.

[125] A. M. Williams, A. T. Baker, and R. Vijayakumar, "IC Engine Air System Uni-, Bi-, and Tri-Directional Energy Flow Optimisation: Turbocharging, Turbocompounding and Turbodischarging," in *ASME 2013 Internal Combustion Engine Division Fall Technical Conference*, 2013, p. V002T07A007–V002T07A007.

[126] A. M. Williams, A. T. Baker, C. P. Garner, and R. Vijayakumar, "Turbo-discharging turbocharged internal combustion engines," *Proceedings of the Institution of Mechanical Engineers, Part D: Journal of Automobile Engineering*, p. 954407012455986, 2012.

[127] R. S. Benson, J. H. Horlock, and D. E. Winterbone, *Thermodynamics and Gas Dynamics of Internal-Combustion Engines*. Oxford : New York: Oxford Univ Pr, 1982.

[128] C. D. Rakopoulos and E. G. Giakoumis, "Review of thermodynamic diesel engine simulations under transient operating conditions," SAE International, Warrendale, PA, SAE Technical Paper 2006-01–0884, 2006.

[129] C. D. Rakopoulos, E. G. Giakoumis, and C. N. Michos, "Quasi-linear versus filling and emptying modelling applied to the transient operation of a turbocharged diesel engine," *International Journal of Vehicle Design*, vol. 45, no. 1/2, p. 150, 2007.

[130] R. S. Benson, W. J. D. Annand, and P. C. Baruah, "A simulation model including intake and exhaust systems for a single cylinder four-stroke cycle spark ignition engine," *International Journal of Mechanical Sciences*, vol. 17, no. 2, pp. 97–124, Feb. 1975.

[131] R. S. Benson and P. C. Baruah, "Performance and Emission Predictions for a Multi-Cylinder Spark Ignition Engine," *Proceedings of the Institution of Mechanical Engineers*, vol. 191, no. 1, pp. 339–354, Jun. 1977.

[132] S. Stockar, M. Canova, Y. Guezennec, A. D. Torre, G. Montenegro, and A. Onorati, "Modeling wave action effects in internal combustion engine air path systems: comparison of numerical and system dynamics approaches," *International Journal of Engine Research*, vol. 14, no. 4, pp. 391–408, Aug. 2013.

[133] J. Anderson, *Modern Compressible Flow: With Historical Perspective*, 3 edition. Boston: McGraw-Hill Science/Engineering/Math, 2002.

[134] C. Borgnakke, P. Puzinauskas, and Y. Xiao, "Technical Report 1: Spark Ignition Engine Simulation Models," University of Michigan, Ann Arbor, Michigan, UM-MEAM-86-35, Feb. 1986.

[135] D. E. Foster, "An overview of zero-dimensional thermodynamic models for IC engine data analysis," SAE International, Warrendale, PA, SAE Technical Paper 852070, 1985.

[136] P. Kongsereeparp, B. Kashani, and M. D. Checkel, "A Stand-Alone Multi-Zone Model for Combustion in HCCI Engines," pp. 265–274, Jan. 2005.

[137] Y. Mo, "HCCI Heat Release Rate and Combustion Efficiency: A Couple KIVA Multi-zone Modeling Study," University of Michigan, Ann Arbor, Michigan, 2008.

[138] J. I. Ramos, "Comparisons between thermodynamic and one-dimensional combustion models of spark-ignition engines," *Applied Mathematical Modelling*, vol. 10, no. 6, pp. 409–422, Dec. 1986.

[139] R. Stone, *Introduction to Internal Combustion Engines*. Palgrave Macmillan, 2012.

[140] A. Babajimopoulos, D. N. Assanis, and S. B. Fiveland, "An approach for modeling the effects of gas exchange processes on HCCI combustion and its application in evaluating variable valve timing control strategies," SAE International, Warrendale, PA, SAE Technical Paper 2002-01–2829, 2002.

[141] A. Babajimopoulos, G. A. Lavoie, and D. N. Assanis, "Modeling HCCI combustion with high levels of residual gas fraction-a comparison of two VVA strategies," SAE International, Warrendale, PA, SAE Technical Paper 2003-01–3220, 2003.

[142] S.-C. Kong, C. D. Marriott, R. D. Reitz, and M. Christensen, "Modeling and experiments of HCCI engine combustion using detailed chemical kinetics with multidimensional CFD," SAE International, Warrendale, PA, SAE Technical Paper 2001-01–1026, 2001.

[143] A. Patel, S.-C. Kong, and R. D. Reitz, "Development and validation of a reduced reaction mechanism for HCCI engine simulations," SAE International, Warrendale, PA, SAE Technical Paper 2004-01–0558, 2004.

[144] "General Motors, Private Communication." 2012.

[145] J. I. Ghojel, "Review of the development and applications of the Wiebe function: a tribute to the contribution of Ivan Wiebe to engine research," *International Journal of Engine Research*, vol. 11, no. 4, pp. 297–312, 2010.

[146] C. R. Ferguson and A. T. Kirkpatrick, *Internal Combustion Engines: Applied Thermosciences*. John Wiley and Sons, 2015.

[147] G. Woschni, "A universally applicable equation for the instantaneous heat transfer coefficient in the internal combustion engine," SAE International, Warrendale, PA, SAE Technical Paper 670931, 1967.

[148] F. Payri, J. Benajes, J. Galindo, and J. R. Serrano, "Modelling of turbocharged diesel engines in transient operation. Part 2: wave action models for calculating the transient operation in a high speed direct injection engine," *Proceedings of the Institution of Mechanical Engineers, Part D: Journal of Automobile Engineering*, vol. 216, no. 6, pp. 479–493, 2002.

[149] S. Klein and G. Nellis, *Mastering EES*. Madison, WI: F-Chart Software.

[150] C. Hirsch, *Numerical Computation of Internal and External Flows: The Fundamentals of Computational Fluid Dynamics*. Butterworth-Heinemann, 2007.

[151] "GT-Suite Flow Theory Manual Version 2016." Gamma Technologies, 2015.

[152] R. Mauri, *Transport Phenomena in Multiphase Flows*. Springer, 2015.

[153] S. P. Sukhatme, *A Textbook on Heat Transfer*. Universities Press, 2005.

[154] F. Westin, "Simulation of Turbocharged SI-Engines - with focus on the Turbine," KTH School of Industrial Engineering and Management, Royal Institute of Technology, Stockholm, Sweden, 2005.

[155] C. S. Sampara, E. J. Bissett, M. Chmielewski, and D. Assanis, "Global Kinetics for Platinum Diesel Oxidation Catalysts," *Ind. Eng. Chem. Res.*, vol. 46, no. 24, pp. 7993–8003, Nov. 2007.

[156] S. K. Chen and P. F. Flynn, "Development of a single cylinder compression ignition research engine," SAE International, Warrendale, PA, SAE Technical Paper 650733, 1965.

[157] A. B. Dempsey, "Dual-Fuel Reactivity Controlled Compression Ignition (RCCI) with Alternative Fuels," THE UNIVERSITY OF WISCONSIN - MADISON, 2013.

[158] A. B. Dempsey, N. R. Walker, and R. Reitz, "Effect of piston bowl geometry on dual fuel reactivity controlled compression ignition (RCCI) in a light-duty engine operated with gasoline/diesel and methanol/diesel," *SAE International Journal of Engines*, vol. 6, no. 1, pp. 78–100, 2013.

[159] R. Hanson, S. Curran, R. Wagner, S. Kokjohn, D. Splitter, and R. Reitz, "Piston bowl optimization for RCCI combustion in a light-duty multi-cylinder engine," *SAE International Journal of Engines*, vol. 5, no. 2, pp. 286–299, 2012.

[160] D. Splitter, M. Wissink, S. Kokjohn, and R. D. Reitz, "Effect of compression ratio and piston geometry on RCCI load limits and efficiency," SAE International, Warrendale, PA, SAE Technical Paper 2012-01–0383, 2012.

[161] D. Splitter, M. Wissink, D. DelVescovo, and R. D. Reitz, "RCCI engine operation towards 60% thermal efficiency," SAE International, Warrendale, PA, SAE Technical Paper 2013-01–0279, 2013.

[162] N. Abani, A. Munnannur, and R. D. Reitz, "Reduction of Numerical Parameter Dependencies in Diesel Spray Models," *J. Eng. Gas Turbines Power*, vol. 130, no. 3, pp. 032809–032809, Apr. 2008.

[163] N. Abani, S. Kokjohn, S. W. Park, M. Bergin, A. Munnannur, W. Ning, Y. Sun, and R. D. Reitz, "An improved spray model for reducing numerical parameter dependencies in diesel engine CFD simulations," SAE International, Warrendale, PA, SAE Technical Paper 2008-01–0970, 2008.

[164] J. C. Beale and R. D. Reitz, "Modeling Spray Atomization with the Kelvin-Helmholtz/Rayleigh-Taylor Hybrid Model," *Atomization and Sprays*, vol. 9, no. 6, pp. 623–650, 1999.

[165] R. J. Kee, F. M. Rupley, and J. A. Miller, "Chemkin-Ii: A Fortran Chemical Kinetics Package for the Analysis of Gas-Phase Chemical Kinetics," Sandia National Labs., Livermore, CA (USA), SAND-89-8009, Sep. 1989.

[166] Z. Han and R. D. Reitz, "Turbulence Modeling of Internal Combustion Engines Using RNG κ-ε Models," *Combustion Science and Technology*, vol. 106, no. 4–6, pp. 267–295, Jan. 1995.

[167] H. Wang, M. Yao, and R. D. Reitz, "Development of a Reduced Primary Reference Fuel Mechanism for Internal Combustion Engine Combustion Simulations," *Energy Fuels*, vol. 27, no. 12, pp. 7843–7853, Dec. 2013.

[168] F. Perini, E. Galligani, and R. D. Reitz, "An Analytical Jacobian Approach to Sparse Reaction Kinetics for Computationally Efficient Combustion Modeling with Large Reaction Mechanisms," *Energy Fuels*, vol. 26, no. 8, pp. 4804–4822, Aug. 2012.

[169] F. Perini, "High-dimensional, unsupervised cell clustering for computationally efficient engine simulations with detailed combustion chemistry," *Fuel*, vol. 106, pp. 344–356, Apr. 2013.

[170] Z. Han and R. D. Reitz, "A temperature wall function formulation for variable-density turbulent flows with application to engine convective heat transfer modeling," *International Journal of Heat and Mass Transfer*, vol. 40, no. 3, pp. 613–625, Feb. 1997.

[171] Y. Sun, "Diesel combustion optimization and emissions reduction using adaptive injection strategies (AIS) with improved numerical models," University of Wisconsin-Madison, Madison, Wisconsin, 2007.

[172] H. Hiroyasu and T. Kadota, “Models for combustion and formation of nitric oxide and soot in direct injection diesel engines,” SAE International, Warrendale, PA, SAE Technical Paper 760129, 1976.

[173] S.-C. Kong, Y. Sun, and R. D. Rietz, “Modeling Diesel Spray Flame Liftoff, Sooting Tendency, and NOx Emissions Using Detailed Chemistry With Phenomenological Soot Model,” *J. Eng. Gas Turbines Power*, vol. 129, no. 1, pp. 245–251, Dec. 2005.

[174] Z. Han, A. Uludogan, G. J. Hampson, and R. D. Reitz, “Mechanism of soot and NOx emission reduction using multiple-injection in a diesel engine,” *SAE transactions*, vol. 105, pp. 837–852, 1996.

[175] J. Nagle and R. F. Strickland-Constable, “Oxidation of Carbon between 1,000 and 2,000 C,” in *Proceedings of the Fifth Conference on Carbon*, State College, Pennsylvania, 1963, vol. 2.

[176] S. L. Dixon and C. Hall, *Fluid Mechanics and Thermodynamics of Turbomachinery, Seventh Edition*, 7th ed. Amsterdam ; Boston: Butterworth-Heinemann, 2013.

[177] C. Bell, D. Zimmerle, T. Bradley, D. Olsen, and P. Young, “Scalable turbocharger performance maps for dynamic state-based engine models,” *International Journal of Engine Research*, p. 1468087415609855, 2015.

[178] M. Haneda, M. Sasaki, H. Hamada, and M. Ozawa, “Platinum-based catalyst for diesel hydrocarbon oxidation,” *Chinese Journal of Catalysis*, vol. 32, no. 5, pp. 777–781, 2011.

[179] D. Splitter, R. Hanson, S. Kokjohn, and R. D. Reitz, “Reactivity Controlled Compression Ignition (RCCI) Heavy-Duty Engine Operation at Mid-and High-Loads with Conventional and Alternative Fuels,” SAE International, Warrendale, PA, SAE Technical Paper 2011-01–0363, Apr. 2011.

[180] N. Kalva, “Aftertreatment Modeling of RCCI Engine during Transient Operation,” University of Wisconsin-Madison, Madison, Wisconsin, 2014.

[181] B. Challen and R. Baranescu, Eds., *Diesel Engine Reference Book*, 2 edition. Oxford, England ; Woburn, MA: Butterworth-Heinemann Ltd, 1999.

[182] S. Honardar, H. Busch, T. Schnorbus, C. Severin, A. F. Kolbeck, and T. Korfer, “Exhaust temperature management for diesel engines assessment of engine concepts and calibration strategies with regard to fuel penalty,” SAE International, Warrendale, PA, SAE Technical Paper 2011-24–0176, 2011.

[183] M. W. Chase Jr., “NIST- JANAF Thermochemical Tables 4th Edition,” National Institute of Standards and Technology, Gaithersburg, Maryland, Monograph 9, 1998.

[184] C. Borgnakke, *Fundamentals of Thermodynamics, 7th Edition*, 7th ed. John Wiley and Sons, Inc., 2008.

[185] S. Turns, *An Introduction to Combustion: Concepts and Applications*, 2nd ed. New York City, New York: McGraw-Hill Science/Engineering/Math, 2001.

[186] G. Lavoie, E. Ortiz-Soto, A. Babajimopoulos, J. B. Martz, and D. N. Assanis, “Thermodynamic sweet spot for high-efficiency, dilute, boosted gasoline engines,” *International Journal of Engine Research*, p. 1468087412455372, Aug. 2012.

[187] D. A. Splitter, “High efficiency RCCI combustion,” Ph.D., The University of Wisconsin - Madison, United States -- Wisconsin, 2012.

[188] M. V. Casey and M. Schlegel, “Estimation of the performance of turbocharger compressors at extremely low pressure ratios,” *Proceedings of the Institution of Mechanical Engineers, Part A: Journal of Power and Energy*, vol. 224, no. 2, pp. 239–250, 2010.

[189] J. Yi, “Design and Optimization of Gasoline Direct Injection Engines using Computational Fluid Dynamics,” in *Advanced Direct Injection Combustion Engine Technologies and Development: Gasoline and Gas Engines*, vol. 1, Cambridge, England: Woodhead Publishing, 2010.

[190] N. Chayopitak, R. Pupadubsin, S. Karukanan, P. Champa, P. Somsiri, and Y. Thinphowong, “Design of a 1.5 kW high speed switched reluctance motor for electric supercharger with optimal performance assessment,” in *Electrical Machines and Systems (ICEMS), 2012 15th International Conference on*, 2012, pp. 1–5.

[191] S. George, G. Morris, J. Dixon, D. Pearce, and G. Heslop, “Optimal boost control for an electrical supercharging application,” *SAE technical paper*, pp. 1–523, 2004.

[192] T. Noguchi, Y. Takata, Y. Yamashita, and S. Ibaraki, “160,000-r/min, 2.7-kW Electric Drive of Supercharger for Automobiles,” in *Power Electronics and Drives Systems, 2005. PEDS 2005. International Conference on*, 2005, vol. 2, pp. 1380–1385.

[193] T. Noguchi and M. Kano, “Development of 150000 r/min, 1.5 kW permanent-magnet motor for automotive supercharger,” in *Power Electronics and Drive Systems, 2007. PEDS’07. 7th International Conference on*, 2007, pp. 183–188.

[194] J. Wang, B. Taylor, Z. Sun, and D. Howe, “Experimental characterization of a supercapacitor-based electrical torque-boost system for downsized ICE vehicles,” *Vehicular Technology, IEEE Transactions on*, vol. 56, no. 6, pp. 3674–3681, 2007.

[195] N. Murgovski, S. Marinkov, D. Hilgersom, B. de Jager, M. Steinbuch, and J. Sjöberg, “Powertrain sizing of electrically supercharged internal combustion engine vehicles,” *IFAC-PapersOnLine*, vol. 48, no. 15, pp. 101–108, 2015.

[196] Y. Mérigot, S. Rajoo, and R. F. Martinez-Botas, “Active Control Turbocharger (ACT): A Method to Improve Energy Extraction From an Engine Exhaust Gas,” pp. 137–151, Jan. 2009.

[197] A. Pesiridis, “Issues in the integration of active control turbochargers with internal combustion engines,” *Int.J Automot. Technol.*, vol. 13, no. 6, pp. 873–884, Oct. 2012.

[198] A. Pesiridis, “The application of active control for turbocharger turbines,” *International Journal of Engine Research*, vol. 13, no. 4, pp. 385–398, Aug. 2012.

[199] A. Pesiridis and R. Martinez-Botas, “Active Control Turbocharger for Automotive Application: An Experimental Evaluation,” in *8th International Conference on Turbochargers and Turbocharging*, London, United Kingdom, 2006.

[200] A. Pesiridis and R. F. Martinez-Botas, “Experimental Evaluation of the Active Control Turbocharger Prototype Under Simulated Engine Conditions,” pp. 507–520, Oct. 2010.

[201] A. Pesiridis and R. F. Martinez-Botas, "Experimental testing of an active control turbocharger turbine inlet equipped with a sliding sleeve nozzle," *Proceedings of the Institution of Mechanical Engineers, Part D: Journal of Automobile Engineering*, p. 954407012464843, Dec. 2012.

[202] S. Rajoo and R. F. Martinez-Botas, "Improving energy extraction from pulsating exhaust flow by active operation of a turbocharger turbine," SAE International, Warrendale, PA, SAE Technical Paper 2007-01–1557, 2007.

[203] S. Rajoo, A. Pesiridis, and R. Martinez-Botas, "Novel method to improve engine exhaust energy extraction with active control turbocharger," *International Journal of Engine Research*, vol. 15, no. 2, pp. 236–249, Feb. 2014.

[204] A. Pesiridis, B. Dubois, and R. F. Martinez-Botas, "A One-Dimensional Investigation of the Effect of an Active Control Turbocharger on Internal Combustion Engine Performance," pp. 961–969, Jan. 2011.

[205] C. Arcoumanis, I. Hakeem, L. Khezzar, R. F. Martinez-Botas, and N. C. Baines, "Performance of a mixed flow turbocharger turbine under pulsating flow conditions," in *ASME 1995 International Gas Turbine and Aeroengine Congress and Exposition*, 1995, p. V002T04A011–V002T04A011.

[206] N. C. Baines, F. J. Wallace, and A. Whitfield, "Computer aided design of mixed flow turbines for turbochargers," *Journal of Engineering for Power*, vol. 101, no. 3, pp. 440–448, 1979.

[207] N. Karamanis and R. F. Martinez-Botas, "Mixed-flow turbines for automotive turbochargers: steady and unsteady performance," *International Journal of Engine Research*, vol. 3, no. 3, pp. 127–138, 2002.

[208] A. Pesiridis and R. F. Martinez-Botas, "Experimental evaluation of active flow control mixed-flow turbine for automotive turbocharger application," *Journal of Turbomachinery*, vol. 129, no. 1, pp. 44–52, 2007.

[209] D. Palfreyman and R. F. Martinez-Botas, "The pulsating flow field in a mixed flow turbocharger turbine: an experimental and computational study," *Journal of turbomachinery*, vol. 127, no. 1, pp. 144–155, 2005.

[210] N. Karamanis, R. F. Martinez-Botas, and C. C. Su, "Mixed flow turbines: Inlet and exit flow under steady and pulsating conditions," *Journal of turbomachinery*, vol. 123, no. 2, pp. 359–371, 2001.

[211] B. Lüddecke, D. Filsinger, and J. Ehrhard, "On Mixed Flow Turbines for Automotive Turbocharger Applications," *International Journal of rotating machinery*, vol. 2012, 2012.

[212] H. Sun, "Advanced boost system development for diesel HCCI/LTC applications," presented at the 2011 Department of Energy Hydrogen Program and Vehicle Technologies Office Annual Merit Review and Peer Evaluation Meeting, Washington District of Columbia, United States, 2011.

[213] H. Sun, D. Hanna, L. Hu, J. Zhang, M.-C. Lai, E. Krivitzky, and C. Osborne, "Optimization of a turbocharger for high EGR applications," presented at the Directions in Engine Efficiency and Emissions Research Conference, Detroit, Michigan, 2011.

[214] W. J. Glewen, “Experimental Investigation of Transient Operation and Low Temperature Combustion in a Light Duty Diesel Engine,” THE UNIVERSITY OF WISCONSIN - MADISON, 2012.

[215] Y. Han, Z. Liu, J. Zhao, Y. Xu, J. Li, and K. Li, “EGR Response in a Turbo-charged and After-cooled DI Diesel Engine and Its Effects on Smoke Opacity,” SAE International, Warrendale, PA, SAE Technical Paper 2008-01–1677, Jun. 2008.

[216] G. Wright and CDX, *Fundamentals of Medium/Heavy Duty Diesel Engines*. Jones and Bartlett Publishers, 2015.

APPENDIX A: STOCK TURBOCHARGER TURBINE AND COMPRESSOR WHEEL MEASUREMENTS

This appendix details the steps taken to evaluate the turbine and compressor wheel diameters of the Honeywell Garrett M53 VGT. The turbine and compressor wheel each have an inducer and exducer as shown in Figure A1 below.

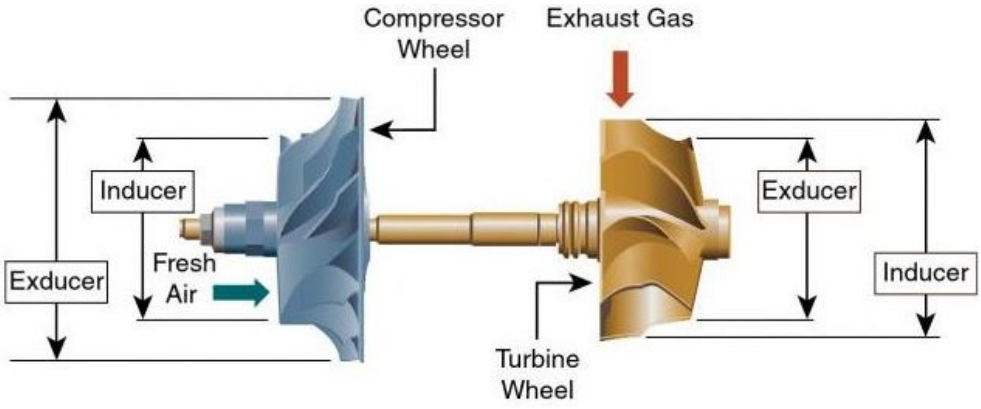

Figure A1: Turbocharger Wheel Schematic. (Source: [216])

Table A1: Turbine and Compressor Wheel Diameter Measurements

Turbine Wheel		**Compressor Wheel**	
Inducer Diameter/mm	**Exducer Diameter/mm**	**Inducer Diameter/mm**	**Exducer Diameter/mm**
42.26	37.7	34.99	48.88
42.18	37.58	35.2	48.26
42.21	37.64	35.39	48.01
41.84	37.33	35.74	48.73
42.24	37.74	35.38	48.59
Average Diameter/mm:			
42.15	37.60	35.34	48.49

The overall average wheel diameters were calculated by taking the average of the mean inducer diameter and the mean exducer diameter measurements. The average turbine wheel diameter was 39.87 mm while the average compressor wheel diameter was 41.92 mm.

APPENDIX B: EES CODES FOR ZERO-DIMENSIONAL ENGINE SIMULATION MODEL

In Appendix B, the EES codes (along with the appropriate comments) written to simulate the stock engine configuration and the Divided Exhaust Period will be included. Section B.1 will show the EES code for the stock engine configuration while Section B.2 will show the EES code for the DEP configuration.

B.1. EES Code for Stock Engine Configuration

```
"! CYLINDER EVACUATION GAS DYNAMICS - Version 16"
"! Written by: Anand Nageswaran Bharath"
"! September 18th 2015, University of Wisconsin Engine Research Center"
"! Program Description: This program models the entire engine cycle (720 Degree Crank Angle Duration) for a single cylinder version of the General Motors Z19 DTH 1.9 Liter Engine. The model is zero-dimensional, solving the equations of mass conservation and energy conservation for a control volume, for both the cylinder and the exhaust manifold."


"! Procedure for Exhaust Port Flow Computation: FLOW_EXHAUST"
procedure FLOW_EXHAUST(p_0, p_t_in, A_ex, T_0, gamma, R_Air, R_p_ex:dmdt_1)

    "Choked Flow in Exhaust Ports out of Cylinder (if p_0_exh/p_0 < 0.528)"
    if (R_p_ex < 0.528) then
     dmdt_1 := -p_0*A_ex/SQRT(T_0)*SQRT(gamma/R_Air*(2/(gamma+1))^((gamma+1)/(gamma-1)))
    endif

    "Non-critical Flow in Exhaust Ports out of Cylinder (if  0.528 < p_0_exh/p_0 < 1)"
    if (R_p_ex > 0.528) and (R_p_ex < 1) then
    dmdt_1 := -p_0*A_ex/SQRT(R_Air*T_0)*SQRT(2*gamma/(gamma-1)*(1-R_p_ex^((gamma-
1)/gamma)))*R_p_ex^(1/gamma)
    endif

    "Non-critical Flow in Exhaust Ports into Cylinder (if 1< p_0_exh/p_0 < 1.8939) - Flow Reversal"
    if (R_p_ex >= 1) and (R_p_ex < 1.8939) then
    dmdt_1 := p_t_in*A_ex/SQRT(R_Air*T_0)*SQRT(2*gamma/(gamma-1)*(1-(1/R_p_ex)^((gamma-
1)/gamma)))*(1/R_p_ex)^(1/gamma)
    endif

    "Choked Flow in Exhaust Ports into Cylinder (p_0_exh/p_0 > 1.8939) - Flow Reversal"
    if (R_p_ex >= 1.8939) then
    dmdt_1 := p_t_in*A_ex/SQRT(T_0)*SQRT(gamma/R_Air*(2/(gamma+1))^((gamma+1)/(gamma-1)))
    endif
end

"! Procedure for Intake Port Flow Computation: FLOW_INTAKE"
procedure FLOW_INTAKE(p_0, p_c_ex, A_in, T_0, T_in, gamma, gamma_rtp, R_Air, R_p_in:dmdt_2)

    "Choked Flow in Intake Ports into Cylinder (if p_c_ex/p_0 < 0.528)"
    if (R_p_in < 0.528) then
    dmdt_2 :=
p_c_ex*A_in/SQRT(T_in)*SQRT(gamma_rtp/R_Air*(2/(gamma_rtp+1))^((gamma_rtp+1)/(gamma_rtp-1)))
    endif
```

```
    "Non-critical Flow in Intake Ports into Cylinder (if  0.528 < p_c_ex/p_0 <
1)"
    if (R_p_in > 0.528) and (R_p_in < 1) then
    dmdt_2 := p_c_ex*A_in/SQRT(R_Air*T_in)*SQRT(2*gamma_rtp/(gamma_rtp-1)*(1-
R_p_in^((gamma_rtp-1)/gamma_rtp)))*R_p_in^(1/gamma_rtp)
    endif

    "Non-critical Flow in Intake Ports out of Cylinder (if 1< p_c_ex/p_0 < 1.8939) - Flow Reversal"
    if (R_p_in > 1) and (R_p_in < 1.8939) then
    dmdt_2 := -p_0*A_in/SQRT(R_Air*T_0)*SQRT(2*gamma/(gamma-1)*(1-(1/R_p_in)^((gamma-
1)/gamma)))*(1/R_p_in)^(1/gamma)
    endif

    "Choked Flow in Intake Ports out of Cylinder (if p_c_ex/p_0 > 1.8939) - Flow Reversal"
    if (R_p_in > 1.8939) then
    dmdt_2 := -p_0*A_in/SQRT(T_0)*SQRT(gamma/R_Air*(2/(gamma+1))^((gamma+1)/(gamma-1)))
    endif
end


"! Procedure for determining whether there is mass flow into or out of cylinder: MASSFLOW"
procedure MASSFLOW(m_dot_exh, m_dot_int, t, t_ivo, t_evc, t_fin, t_start, t_evo: dmdt_tot)

    "Flow during Valve Overlap Period; includes both intake and exhaust flow"
    if (t > t_ivo) and (t < t_evc) then
    dmdt_tot = m_dot_exh + m_dot_int
    endif

    "Flow between exhaust valve closure and intake valve closure - only intake flow"
    if (t >= t_evc) and (t < t_fin) then
    dmdt_tot = m_dot_int
    endif

    "Flow between exhaust valve opening and intake valve opening - only exhaust flow"
    if (t >= t_evo) and (t <= t_ivo) then
    dmdt_tot = m_dot_exh
    endif

    "Closed cycle - no flow into or out of cylinder"
    if (t >= t_start) and (t < t_evo) then
    dmdt_tot = 0
    endif
end

"! Procedure for determining Rate of Change of Internal Energy of Working Gas in Cylinder:
ENERGYFLOW"
procedure
ENERGYFLOW(t,t_start,t_soc,t_eoc,t_evo,t_ivo,t_evc,t_fin,dudV,V_dot,q_dot_loss_tot,q_dot_HR,h_cyl_
ex,h_cyl_in: dudt_tot)

    "Closed Cycle - Energy flow only involves boundary work and heat losses (before combustion)"
    if ((t >= t_start) and (t <= t_soc)) then
    dudt_tot = dudV*V_dot -  q_dot_loss_tot
    endif

    "Closed Cycle - Combustion process: Energy flow adds heat release from combustion"
```

```
    if ((t > t_soc) and (t <= t_eoc)) then
    dudt_tot = dudV*V_dot - q_dot_loss_tot + q_dot_HR
    endif

    "Closed Cycle - Expansion post-combustion: heat losses and boundary work only"
    if ((t > t_eoc) and (t <= t_evo)) then
    dudt_tot = dudV*V_dot - q_dot_loss_tot
    endif

    "Exhaust Valve Open Energy Flow"
    if (t > t_evo) and (t <= t_ivo) then
    dudt_tot = dudV*V_dot + h_cyl_ex - q_dot_loss_tot
    endif

    "Energy Flow due to Exhaust and Intake Flows - Valve Overlap Period"
    if (t > t_ivo) and (t < t_evc) then
    dudt_tot = dudV*V_dot + h_cyl_ex + h_cyl_in - q_dot_loss_tot
    endif

    "Intake Valve Open Energy Flow"
    if (t > t_evc) and (t < t_fin) then
    dudt_tot = dudV*V_dot + h_cyl_in - q_dot_loss_tot
    endif
end

"! Procedure for Determining Mach Number of Gas Flow through Exhaust Ports: MACH_EXHAUST"
procedure MACH_EXHAUST(R_p_ex, m_dot_exh_abs, gamma, t, t_evc, t_evo: M)

    "Mach Number = 1 (Sonic Flow at Throat)"
    if (R_p_ex < 0.528) and (m_dot_exh_abs > 0) then
    M = 1
    endif

    "Zero Flow, Mach Number = 0"
    if (m_dot_exh_abs = 0) then
    M = 0
    endif

    "Mach Number < 1 (Subsonic Flow)"
    if (R_p_ex > 0.528) and (R_p_ex < 1) then
    M = SQRT(2/(gamma-1)*((1/R_p_ex)^((gamma-1)/gamma)-1))
    endif

    "Mach Number < 1 (Subsonic Flow - Flow Reversal)"
    if (R_p_ex > 1) and (R_p_ex < 1.8939) then
    M = SQRT(2/(gamma-1)*((R_p_ex)^((gamma-1)/gamma)-1))
    endif

    "Valves closed; Mach Number = 0"
    if (t > t_evc) or (t < t_evo) then
    M = 0
    endif
end
```

```
"! Procedure for determining Exhaust Gas Static Properties at Exhaust Port"
procedure STATICEXHAUST (M, T_0, h_cyl_ex, gamma: T_e, h_e)

    "Mach Number = 0; Static Properties = Stagnation Properties"
    if (M = 0) then
    T_e = T_0
    h_e = ENTHALPY(Air,T = T_0)
    endif

    "Mach Number > 0"
    if (M > 0) then
    T_e = T_0/(1 + 0.5*(gamma -1)*M^2)
    h_e = ENTHALPY(Air,T = T_e)
    endif
end

"! Procedure for determining Mach Number of Gas Flow through Turbocharger Turbine:
MACH_TURBINE"
procedure MACH_TURBINE(R_p_turb, m_dot_turb, gamma: M_trb)
"NOTE: Turbine is modeled as a nozzle with work output."

    "Sonic Flow through Turbine (Mach Number = 1)"
    if (R_p_turb < 0.528) then
    M_trb = 1
    endif

    "Subsonic Flow through Turbine (Mach Number < 1)"
    if (R_p_turb >= 0.528) and (R_p_turb < 1) then
    M_trb = SQRT(2/(gamma-1)*((1/R_p_turb)^((gamma-1)/gamma)-1))
    endif

    "No Flow through Turbine (Mach Number = 0)"
    if (R_p_turb >= 1) or (m_dot_turb = 0) then
    M_trb = 0
    endif
end

"! Procedure for determining Exhaust Gas Static Density through Exhaust Ports: EXH_DENSITY"
procedure EXH_DENSITY(M, gamma, rho_0:rho_th)

    "Static Density at Sonic Condition"
    if (M = 1) then
    rho_th = rho_0/((gamma+1)*0.5)^(1/(gamma-1))
    endif

    "Static Density at Subsonic Condition"
    if (M < 1) then
    rho_th = rho_0/(1 + 0.5*(gamma-1)*M^2)^(1/(gamma-1))
    endif
end

"! Procedure for determining Exhaust Gas Static Density at Turbine Inlet: EXH_DENSITY_TURB"
procedure EXH_DENSITY_TURB(M_turb, gamma, rho_0_exh:rho_turb)

    "Static Density at Sonic Condition"
    if (M_turb = 1) then
```

```
    rho_turb = rho_0_exh/((gamma+1)*0.5)^(1/(gamma-1))
    endif

    "Static Density at Subsonic Condition"
    if (M_turb < 1) then
    rho_turb = rho_0_exh/(1 + 0.5*(gamma-1)*M_turb^2)^(1/(gamma-1))
    endif
end

"! Procedure for computing the Intake Valve Lift with respect to Crank Angle: VALVELIFTINTAKE. The polynomial equations for the lift profile and the discharge coefficients were obtained by curve fitting the valve lift profile and the discharge coefficient vs. L/D ratio values in MATLAB using the least squares method."
procedure VALVELIFTINTAKE(t, t_ivo, t_fin, D_in: C_D_in_1, C_D_in_2)
    if (t > t_ivo) and (t <= t_fin) then

    "Intake Valve Lift Profile:"
    tau_in = (t - 0.03322)/0.003937
    L_in = -0.025*tau_in^9 - 0.2506*tau_in^8 + 0.1468*tau_in^7 + 1.459*tau_in^6 - 0.2489*tau_in^5 -
1.365*tau_in^4 + 0.1024*tau_in^3 - 4.953*tau_in^2 - 0.01643*tau_in + 7.982

    "Lift-to-diameter L/D Ratio"
    epsilon_in = L_in/(D_in*1000)

    "Intake Valve Discharge Coefficients:"
    C_D_in_1 = -200.3*epsilon_in^5 + 260.8*epsilon_in^4 -114.4*epsilon_in^3 +14.54*epsilon_in^2 +
2.351*epsilon_in - 0.001114

    C_D_in_2 = -371.3*epsilon_in^5 + 449.6*epsilon_in^4 - 184.6*epsilon_in^3 +23.89*epsilon_in^2 +
1.998*epsilon_in - 0.0001521
    endif

    if (t =< t_ivo) or (t > t_fin) then
    C_D_in_1 = 0
    C_D_in_2 = 0
    endif
end

"! Procedure for computing the Exhaust Valve Lift with respect to Crank Angle: VALVELIFTEXHAUST. The polynomial equations for the lift profile and the discharge coefficients were obtained by curve fitting the valve lift profile and the discharge coefficient vs. L/D ratio values in MATLAB using the least squares method."
procedure VALVELIFTEXHAUST(t, t_evo, t_evc, D_ex: C_D_ex)
    if (t > t_evo) and (t < t_evc) then

    "Exhaust Valve Lift Profile:"
    tau_ex = (t-0.02089)/0.004258
    L_ex = -0.05157*tau_ex^9 - 0.1513*tau_ex^8 + 0.3153*tau_ex^7 + 0.9599*tau_ex^6 - 0.574*tau_ex^5
- 0.8069*tau_ex^4 + 0.2848*tau_ex^3 - 4.785*tau_ex^2 - 0.04103*tau_ex + 7.986

    "Lift-to-diameter L/D Ratio"
    epsilon_ex = L_ex/(D_ex*1000)

    "Exhaust Valve Discharge Coefficient"
    C_D_ex = 20.44*epsilon_ex^4 - 22.05*epsilon_ex^3 +3.791*epsilon_ex^2 + 2.641*epsilon_ex +
0.001286
```

```
    endif

    if (t =< t_evo) or (t >= t_evc) then
    C_D_ex = 0
    endif
end

"! Procedure for calculating the velocity of the exhaust gas at the exhaust port: EXHTHROATVELOCITY. Velocity w = (dm/dt)/[rho_th*A_ex]"
procedure EXHTHROATVELOCITY(A_ex, rho_th, m_dot_exh_abs, t, t_evo, t_evc: w)
    if (t > t_evo) and (t < t_evc) then
    w = m_dot_exh_abs/(A_ex*rho_th)
    endif

    if (t <= t_evo) or (t >= t_evc) then
    w = 0
    endif
end

"! Procedure for determining Mass Flow Rate of Exhaust Gas through Turbocharger Turbine: TURBINEFLOW"
procedure TURBINEFLOW (R_p_turb, p_0_exh, A_turb, T_0_exh, gamma, R_Air: m_dot_turb)

    "Subsonic Flow through Turbine (if Pressure Ratio 0.528 < p_atm/p_0_exh < 1)"
    if (R_p_turb > 0.528) and (R_p_turb < 1) then
    m_dot_turb = p_0_exh*A_turb/SQRT(R_Air*T_0_exh)*SQRT(2*gamma/(gamma-1)*(1-R_p_turb^((gamma-1)/gamma)))*R_p_turb^(1/gamma)
    endif

    "No flow through Turbine if Pressure Ratio >= 1 (We are assuming no flow reversal here.)"
    if (R_p_turb >= 1) then
    m_dot_turb = 0
    endif

    "Choked Flow through Turbine (if Pressure Ratio p_atm/p_0_exh < 0.528 - Sonic Condition)"
    if (R_p_turb < 0.528) then
    m_dot_turb = p_0_exh*A_turb/SQRT(T_0_exh)*SQRT(gamma/R_Air*(2/(gamma+1))^((gamma+1)/(gamma-1)))
    endif
end

"! Procedure for determining Exhaust Gas Velocity through Turbine: EXHTURBINEVELOCITY. Velocity w_turb_in = (dm/dt)/[rho_turb*A_turb]"
procedure EXHTURBINEVELOCITY(A_turb, rho_turb, m_dot_turb: w_turb_in)
    if (m_dot_turb > 0) then
    w_turb_in = m_dot_turb/(A_turb*rho_turb)
    endif

    if (m_dot_turb = 0) then
    w_turb_in = 0
    endif
end

"! Procedure for the Wiebe Function to model the Combustion Process: WIEBEMODEL"
procedure WIEBEMODEL (t, t_soc, t_eoc, q_in, a_w, m_w, N, theta_comb, k, theta_soc: q_dot_HR)
```

```
    "Wiebe Heat Release Rate between Start of Combustion (SOC) and End of Combustion (EOC)"
    if (t > t_soc) and (t <= t_eoc) then
    f = ABS(((PI*N*t)/30 - k - theta_soc)/theta_comb)

    q_dot_HR = q_in*(PI*a_w*m_w*N)/(30*theta_comb)*(((PI*N*t)/30 - k - theta_soc)/theta_comb)^(m_w-
1)*EXP(-a_w*f^m_w)
    endif

    if (t <= t_soc) or (t > t_eoc) then
    q_dot_HR = 0
    endif
end

"! Procedure for evaluating the In-cylinder Average Gas Velocity w_cyl for the Woschni Heat Transfer
Correlation: WOSCHNIGASVELOCITY"
procedure WOSCHNIGASVELOCITY (t, t_start, t_tdc, t_evo, t_fin, K_1_e, K_1_c, K_2, u_bar, V_d, T_r,
p_r, V_ivc, p_0, p_m: w_cyl)

    "Average Gas Velocity during the Compression Stroke"
    if (t >= t_start) and (t < t_tdc) then
    w_cyl = K_1_e*u_bar
    endif

    "Average Gas Velocity during the Expansion Stroke"
    if (t >= t_tdc) and (t < t_evo) then
    w_cyl = K_1_e*u_bar + K_2*(V_d*T_r)/(p_r*V_ivc)*(p_0 - p_m)
    endif

    "Average Gas Velocity during the Gas Exchange Process (between EVO and IVC)"
    if (t >= t_evo) and (t < t_fin) then
    w_cyl = K_1_c*u_bar
    endif
end

"! Geometry of the General Motors 1.9L Diesel Engine"
b = 0.082 [m]                                   "Bore"
s = 0.0904 [m]                                  "Stroke"
a = s/2                                         "Crank Radius"
L_crd = 0.14554 [m]                             "Connecting Rod Length"
R_c = 15.1                                      "Geometric Compression Ratio"
N = 3000                                        "Engine Speed (in RPM)"
V_d = (PI*b^2*s)/4                              "Displacement Volume of 1 cylinder"
V_c = V_d/(R_c-1)                               "Clearance Volume"

"Mean Piston Speed (for Heat Loss Calculations using Woschni Model)"
u_bar = 2*s*N/60

"! Fuel Properties, Fuel Mass, Trapped Air Mass, Load and Combustion Characteristics"
LHV_diesel = 4.4917e7 [J/kg]                    "Lower Heating Value of N-Heptane"
LHV_petrol = 4.4663e7 [J/kg]                    "Lower Heating Value of Iso-Octane"
eta_th = 0.45                                   "Thermal Efficiency"

m_fuel_cyc = 20.772 [mg]                        "Mass of fuel per cycle (in mg)"
lambda = 0.5                                    "Gasoline/Diesel Ratio"

m_dies_cyc=m_fuel_cyc*(1-lambda)*CONVERT(mg,kg) "Mass of N-Heptane"
```

```
m_gas_cyc = m_fuel_cyc*lambda*CONVERT(mg,kg)    "Mass of Iso-Octane"
eta_comb = 0.9624                               "Combustion Efficiency"

"Mass of Air needed for Stoichiometric mixture per cycle"
m_a_st_cyc = m_dies_cyc/0.0662 + m_gas_cyc/0.0664
phi = 0.4                                       "Equivalence Ratio"
m_a_cyc = m_a_st_cyc/phi                        "Actual Mass of Air per cycle"

"Mass Flow Rate of Air (kg/s) through Compressor"
m_a_tot = m_a_cyc*0.5*N/60*4

m_fuel_tot = m_fuel_cyc*CONVERT(mg,kg)*0.5*N/60*4 "Fuel Flow Rate for all Cylinders (kg/s)"
m_exh_tot = m_a_tot + m_fuel_tot                "Exhaust Mass Flow Rate through Turbine"

"! Air Properties"
"Specific Heat Ratio of Air at Room Temperature and Pressure (Used in the 1st iteration to create good
guess values for subsequent iterations)"
gamma_rtp = 1.4
{gamma = 1.4}
M_r_Air = MOLARMASS(Air)                        "Molecular Mass of Air"
R_bar = 8314 [J/kmol/K]                         "Universal Gas Constant"
R_Air = R_bar/M_r_Air                           "Specific Gas Constant of Air"
p_atm = 101325 [Pa]                             "Atmospheric Pressure"
T_atm = 298.15 [K]                              "Room Temperature"

"Specific Heat Capacity of Air at Room Temperature and Pressure"
c_p = CP(Air,T=T_atm)

"! Important Timepoints in each Engine Cycle"
theta_start_deg = -132          "Crank Angle (in Degrees) at start of cycle (Intake Valve Closure)"
theta_soc_deg = -10.48          "Crank Angle (in Degrees) at Start of Combustion (SOC)"
theta_eoc_deg = 24.23           "Crank Angle (in Degrees) at End of Combustion (EOC)"
theta_evo_deg = 112             "Crank Angle (in Degrees at Exhaust Valve Opening (EVO)"
theta_ivo_deg = 344             "Crank Angle (in Degrees) at Intake Valve Opening (IVO)"
theta_evc_deg = 376             "Crank Angle (in Degrees) at Exhaust Valve Closing (EVC)"
theta_fin_deg = 588             "Crank Angle (in Degrees) at end of cycle (Intake Valve Closure)"

theta_start = theta_start_deg*PI/180  "Crank angle (in Radians) at start of cycle (Intake Valve Closure)"
theta_soc = theta_soc_deg*PI/180      "Crank angle (in Radians) at Start of Combustion (SOC)"
theta_eoc = theta_eoc_deg*PI/180      "Crank angle (in Radians) at End of Combustion (EOC)"
theta_evo = theta_evo_deg*PI/180      "Crank angle at Exhaust Valve Opening (In Radians)"
theta_ivo = theta_ivo_deg*PI/180      "Crank angle at Intake Valve Opening (In Radians)"
theta_evc = theta_evc_deg*PI/180      "Crank angle at Exhaust Valve Closing (in Radians)"

"Crank angle (In Radians) at end of cycle (TDC - End of Compression)"
theta_fin = theta_fin_deg*PI/180

t_start = 0                                     "Time at Cycle Start (Intake Valve Closure)"

"Time at 1st Top Dead Center (at 0 Degrees Crank Angle)"
t_tdc = (0 - theta_start_deg)/360*(1/(N/60))
t_ivo = (theta_ivo_deg-theta_start_deg)/360*(1/(N/60))   "Intake Valve Opening (IVO) Time"
t_fin = (theta_fin_deg-theta_start_deg)/360*(1/(N/60))   "Time at Cycle End (Intake Valve Closure)"
t_evo = (theta_evo_deg-theta_start_deg)/360*(1/(N/60)) "Exhaust Valve Opening (EVO) Time"
t_evc = (theta_evc_deg-theta_start_deg)/360*(1/(N/60)) "Exhaust Valve Closing (EVC) Time"
t_soc = (theta_soc_deg-theta_start_deg)/360*(1/(N/60)) "Time at Start of Combustion (SOC)"
```

```
t_eoc = (theta_eoc_deg-theta_start_deg)/360*(1/(N/60)) "Time at End of Combustion (EOC)"

"! Engine Geometric Parameter Changes during Cycle"
"Piston Pin Position at Exhaust Valve Opening (EVO):"
x_evo = a*COS(theta_evo) + SQRT(L_crd^2 - (a*SIN(theta_evo))^2)

"Piston Pin Position at Cycle Start (Intake Valve Closure):"
x_start = a*COS(theta_start) + SQRT(L_crd^2 - (a*SIN(theta_start))^2)

V_ivc = V_c + 0.25*PI*b^2*(L_crd + a - x_start)          "Volume of cylinder at IVC"
V_evo = V_c + 0.25*PI*b^2*(L_crd + a - x_evo)            "Volume of cylinder at EVO"
V_start = V_c + 0.25*PI*b^2*(L_crd + a - x_start)        "Volume of cylinder at TDC (Cycle Start)"

"Piston Pin Position"
x = a*COS((PI*N)/30*t - (11*PI)/15) + SQRT(L_crd^2 - (a*SIN((PI*N)/30*t -
(11*PI)/15))^2)

"Rate of change of Piston Pin Position:"
x_dot = (-PI*a*N/30)*SIN((PI*N)/30*t - (11*PI)/15) - (PI*a^2*N/60)*SIN((PI*N)/15*t -
(22*PI)/15)/SQRT(L_crd^2-(a*SIN((PI*N)/30*t - (11*PI)/15))^2)

"Relationship between Crank Angle and Time"
theta = 6*N*t – 132

“Variation of cylinder volume with time (Slider-Crank Equation of Motion)"
V = V_c + 0.25*PI*b^2*(L_crd + a - x)

V_dot = -0.25*PI*b^2*x_dot                               "Rate of change of cylinder volume"

"! Intake Valve Operation"
"Call VALVELIFTINTAKE Procedure:"
call ValveLiftIntake(t, t_ivo, t_fin, D_in: C_D_in_1, C_D_in_2)
D_in = 24/1000                                           "Intake Valve Diameter"

A_in_1 = C_D_in_1*0.25*PI*D_in^2                         "Effective Intake Valve Area for Intake Valve 1"
A_in_2 = C_D_in_2*0.25*PI*D_in^2                         "Effective Intake Valve Area for Intake Valve 2"
A_in = A_in_1 + A_in_2                                   "Total Effective Intake Valve Area"

"Convert units of Effective Intake Valve Area to mm^2"
A_in_mm2 = A_in*1e6

"! Exhaust Valve Operation"
"Call VALVELIFTEXHAUST Procedure:"
call ValveLiftExhaust(t, t_evo, t_evc, D_ex: C_D_ex)
D_ex = 21.92/1000                                        "Exhaust Valve Diameter"
A_ex = C_D_ex*0.25*PI*D_ex^2*2                           "Effective Exhaust Valve Flow Area"

"Convert units of Effective Exhaust Valve Area to mm^2"
A_ex_mm2 = A_ex*1e6

"! Set up In-cylinder Initial Conditions"
{m_trap = m_a_cyc                                        "Mass trapped in cylinder (Initial Guess Value)"}
m_trap = 629.8e-6                                        "Initial Gas Mass trapped in cylinder"
T_1 = 354.6 [K]                                          "Temperature at Intake Valve Closure (IVC)"

T_init = T_1                                             "Initial Temperature - Temperature at IVC"
```

```
p_init*V_start = m_trap*R_Air*T_init                    "Initial Pressure - Pressure at IVC"

"Initial Motoring Pressure at IVC - Used for the computation of Average In-cylinder Gas Velocity for the
Woschni Heat Transfer Correlation"
p_m_init*V_start = m_trap*R_Air*T_init

m_init = m_trap                                         "Initial Gas Mass in cylinder at IVC"
u_init = INTENERGY(Air,T=T_init)*m_trap                 "Initial Internal Energy of Gas in cylinder at IVC"

"Initial Motoring Internal Energy of Gas in cylinder at IVC - Used for the computation of Average In-
cylinder Gas Velocity for the Woschni Heat Transfer Correlation"
u_m_init = INTENERGY(Air,T=T_init)*m_trap

"! Wiebe Combustion Model Parameters"
"Total Fuel Energy per cycle"
q_in = (LHV_diesel*m_dies_cyc + LHV_petrol*m_gas_cyc)

a_w = 3.281                                             "Wiebe Exponent a_w"
m_w = 2.269                                             "Wiebe Shape Parameter m_w"

theta_comb = 34.72/180*PI                               "Duration of Combustion"
k = 11*PI/15                                            "Phase Angle k (in Radians)"

"Call procedure WIEBEMODEL for simulating combustion using the Wiebe Model:"
call WiebeModel (t, t_soc, t_eoc, q_in, a_w, m_w, N, theta_comb, k, theta_soc: q_dot_HR)

"! Gas Exchange Process Calculations"
p_0*V = m_cyl*R_Air*T_0          "Ideal Gas Equation of State for gas remaining in cylinder"
p_0 = rho_0*R_Air*T_0            "Alternative form of Ideal Gas Equation to calculate Stagnation Density"
dudV = -p_0                      "dudV term for Gibbs' Equation (Energy Equation) for Control Volume"

"Call procedure FLOW_EXHAUST:"
call Flow_Exhaust(p_0, p_t_in, A_ex, T_0, gamma, R_Air, R_p_ex:m_dot_exh)

"Call procedure FLOW_INTAKE:"
call Flow_Intake(p_0, p_c_ex, A_in, T_0, T_in, gamma, gamma_rtp, R_Air, R_p_in:m_dot_int)

"Intake Temperature = Atmospheric Temperature (Assuming 100% Intercooler Effectiveness)"
T_in = T_atm

u_cyl = INTENERGY(Air,T=T_0)*m_cyl                      "Internal energy of gas remaining in cylinder"

"Stagnation Enthalpy of gas flowing out of cylinder"
h_cyl_ex = ENTHALPY(Air,T=T_0) * m_dot_exh

h_cyl_in = ENTHALPY(Air,T=T_in)*m_dot_int               "Stagnation Enthalpy of gas entering cylinder"

"Exhaust Manifold Properties and Geometric Information"
V_em = 1.20541e-3 [m^3]                                 "Volume of Exhaust Manifold"
p_exh_init = p_atm                                      "Initial Exhaust Pressure"

"Ideal Gas Equation of State for Exhaust Manifold - Initial Conditions"
p_exh_init*V_em = m_em_init*R_Air*T_in

"Initial Internal Energy of Gas in Exhaust Manifold at Cycle Start"
u_em_init = INTENERGY(Air,T=T_in)*m_em_init
```

```
"Internal Energy of Gas in Exhaust Manifold at time t > 0"
u_em = INTENERGY(Air,T=T_0_exh)*m_em

"Enthalpy of Exhaust Gas entering Exhaust Manifold"
h_in = -h_cyl_ex

"Enthalpy of Exhaust Gas leaving Exhaust Manifold"
h_out = m_dot_turb*ENTHALPY(Air,T=T_0_exh)

"Ideal Gas Equation of State for Gas in Exhaust Manifold"
p_0_exh*V_em = m_em*R_Air*T_0_exh

"Alternate Form of Ideal Gas Equation of State for Gas in Exhaust Manifold - To calculate Stagnation
Exhaust Density"
p_0_exh = rho_0_exh*R_Air*T_0_exh

"Turbine Inlet Pressure = Exhaust Manifold Stagnation Pressure"
p_t_in = p_0_exh

"Ratio of Exhaust Manifold Pressure to In-cylinder Pressure"
R_p_ex = p_0_exh/p_0

R_p_turb = p_atm/p_0_exh                    "Turbine to Atmosphere Pressure Ratio"
R_p_in = p_0/p_c_ex                         "Compressor to Cylinder Pressure Ratio"

"Call procedure MASSFLOW:"
call MassFlow(m_dot_exh, m_dot_int, t, t_ivo, t_evc, t_fin, t_start, t_evo: m_dot)

"Absolute value of Exhaust Mass Flow Rate out of Cylinder (Neglect Direction)"
m_dot_exh_ABS = ABS(m_dot_exh)

A_turb = 2.5e-4                             "Turbine Inlet Area (in m^2)"

"Call procedure TURBINEFLOW:"
call TurbineFlow (R_p_turb, p_0_exh, A_turb, T_0_exh, gamma_em, R_Air: m_dot_turb)

"Mass Conservation Equation for Gas in the Exhaust Manifold due to inflow from Cylinder and outflow to
Turbine"
m_dot_em = m_dot_exh_abs - m_dot_turb

"Energy Conservation Equation for Gas in Exhaust Manifold"
u_dot_em = h_in - h_out

"! Woschni Heat Transfer Model for In-cylinder Heat Loss"

"Energy Conservation Equation for the Motoring Pressure - Used for Computation of In-cylinder Average
Gas Velocity for Woschni Heat Transfer Correlation"
u_dot_m = -p_m*V_dot

"Integrate Motoring Energy Rate Change Equation above (with respect to time) to determine Motoring
Internal Energy at time t."
u_m = u_m_init + INTEGRAL(u_dot_m,t,t_start,t_fin)

"Motoring Internal Energy at Time t and Temperature T_m"
u_m = INTENERGY(Air,T=T_m)*m_cyl
```

```
p_m*V = m_cyl*R_Air*T_m                          "Ideal Gas Equation of State for Motoring"

"Woschni Model Constants"
K_1_e = 2.28
K_1_c = 6.18
K_2 = 3.24e-3

p_r = 141503                                     "Pressure at Intake Valve Closure (IVC)"
T_r = 354.6                                      "Temperature at Intake Valve Closure (IVC)"


"Call procedure WOSCHNIGASVELOCITY to evaluate the Average In-cylinder Gas Velocity:"
call WoschniGasVelocity (t, t_start, t_tdc, t_evo, t_fin, K_1_e, K_1_c, K_2, u_bar, V_d, T_r, p_r, V_ivc,
p_0, p_m: w_cyl)

"In-cylinder Spatially Averaged Heat Transfer Coefficient:"
h_bar_cyl = 3.26*(b^(-0.2))*((p_0/1000)^0.8)*(T_0^(-0.55))*w_cyl^0.8

A_PIst = (PI*b^2)/4                              "Area of Piston Surface"
A_head = (PI*b^2)/4                              "Area of Cylinder Head"
A_wall = PI*b*(L_crd + a - x)                    "Surface Area of Cylinder Wall at Time t"

T_pist = 465 [K]                                 "Piston Surface Temperature"
T_head = 465 [K]                                 "Cylinder Head Surface Temperature"
T_wall = 440 [K]                                 "Cylinder Wall Temperature"

q_dot_pist = h_bar_cyl*A_pist*(T_0 - T_pist)     "Heat Loss Rate to Piston Surface"
q_dot_head = h_bar_cyl*A_head*(T_0 - T_head)     "Heat Loss Rate to Cylinder Head"
q_dot_wall = h_bar_cyl*A_wall*(T_0 - T_wall)     "Heat Loss Rate to Cylinder Wall"
q_dot_loss_tot = q_dot_pist + q_dot_head + q_dot_wall  "Total Heat Loss Rate"

"Call procedure ENERGYFLOW:"
Call EnergyFlow(t,t_start,t_soc,t_eoc,t_evo,t_ivo,t_evc,t_fin,dudV,V_dot,q_dot_loss_tot,q_dot_HR,h_cyl_ex,h_cyl_in:
u_dot)

"Call procedure MACH_EXHAUST:"
call Mach_Exhaust(R_p_ex, m_dot_exh_abs, gamma, t, t_evc, t_evo: M)

"Call procedure EXH_DENSITY:"
call Exh_Density(M, gamma, rho_0:rho_th)

"Call procedure EXHTHROATVELOCITY:"
call ExhThroatVelocity(A_ex, rho_th, m_dot_exh_abs, t, t_evo, t_evc: w)

"Call procedure STATICEXHAUST:"
call StaticExhaust (M, T_0, h_cyl_ex, gamma: T_e, h_e)

"Call procedure MACH_TURBINE:"
call Mach_Turbine(R_p_turb, m_dot_turb, gamma_em: M_trb)

"Call procedure EXH_DENSITY_TURB:"
call Exh_Density_Turb(M_turb, gamma_em, rho_0_exh:rho_turb)

"Call procedure EXHTURBINEVELOCITY:"
call ExhTurbineVelocity(A_turb, rho_turb, m_dot_turb: w_turb_in)
```

```
"! Integration of Differential Equations with respect to Time"
$IntegralTable t:0.00002778 theta, p_0, T_0, V, m_cyl, u_cyl, c_p_cyl c_v_cyl gamma gamma_em M, w, R_p_ex, A_ex_mm2, A_in_mm2, m_dot_exh_abs, m_dot_int, R_p_turb, p_0_exh rho_0_exh T_0_exh m_dot_em m_em m_dot_turb W_dot_turb W_turb M_trb rho_turb w_turb_in T_e, h_e, m_exh m_air_cyl W_1 p_m w_cyl h_bar_cyl q_dot_loss_tot q_HR

$SaveTable 'IntegralTable' 'C:\Users\bharath\Box Sync\PhD Engine Research\Wisconsin RCCI Combustion Control\Simulation\Transients\EES_Results.csv'

q_HR_init = 0                                   "Initial Heat Release from Fuel"

"Heat Release over time as evaluated by Wiebe Combustion Model"
q_HR = INTEGRAL(q_dot_HR,t,t_start,t_evo)

"In-cylinder Gas Mass over time by integrating the Mass Conservation Equation for the Cylinder"
m_cyl = m_init + INTEGRAL(m_dot,t,t_start,t_fin)

"In-cylinder Internal Energy of Gas over time by integrating the Energy Conservation Equation for the Cylinder"
u_cyl = u_init + INTEGRAL(u_dot,t,t_start,t_fin)

"Exhaust Gas Mass in Exhaust Manifold over time by integrating the Mass Conservation Equation for the Exhaust Manifold"
m_em = m_em_init + INTEGRAL

"Exhaust Gas Internal Energy in Exhaust Manifold over time by integrating the Energy Conservation Equation for the Exhaust Manifold"
u_em = u_em_init + INTEGRAL(u_dot_em,t,t_evo,t_fin)

"! Turbocharger Operating Characteristics"
eta_mech = 1                                    "Mechanical Efficiency"
eta_t = 0.71                                    "Turbine Isentropic Efficiency"
eta_c = 0.71                                    "Compressor Isentropic Efficiency"
eta_otc = eta_mech*eta_t*eta_c                  "Overall Turbocharger Efficiency"

"Compressor Exit Pressure given by the Speed-Density Equation. Used in 1st iteration as a guess for Boost Pressure"
p_c_ex = 120*m_a_tot*0.25*R_Air*T_atm/(N*V_d)

{p_c_ex = 119400 [Pa]          "Compressor Exit Pressure (Actual Boost Pressure)"}


c_p_em = CP(Air,T=T_0_exh)     "Constant Pressure Specific Heat Capacity of Gas in Exhaust Manifold"
c_v_em = CV(Air,T=T_0_exh)     "Constant Volume Specific Heat Capacity of Gas in Exhaust Manifold"

"Constant Pressure Specific Heat Capacity of Air at Atmospheric Conditions:"
c_p_comp = CP(Air,T=T_atm)

"Specific Heat Ratio of Gas in Exhaust Manifold - Function of Temperature in Exhaust Manifold"
gamma_em = c_p_em/c_v_em

W_init = 0                                      "Initial Turbine Work Output"

"Instantaneous Turbine Power Output"
W_dot_turb =  m_dot_turb*c_p_em*T_0_exh*eta_t*(1-(p_atm/p_0_exh)^((gamma-1)/gamma))
```

```
W_turb = W_init + INTEGRAL(W_dot_turb,t,t_evo,t_fin)  "Evaluation of Turbine Work per Cycle"
m_turb = INTEGRAL(m_dot_turb,t,t_evo,t_fin)           "Total Mass Flow through Turbine"

"Energy Balance: Work extracted by Turbine = Work fed into Compressor"
 W_turb = W_comp

"Compressor Outlet Temperature:"
p_c_ex/p_atm = (T_0_comp/T_atm)^(gamma/(gamma-1))



"Constant Pressure Specific Heat Capacity of Gas in Cylinder"
c_p_cyl = CP(Air,T=T_0)

"Constant Volume Specific Heat Capacity of Gas in Cylinder"
c_v_cyl = CV(Air,T=T_0)

"Specific Heat Ratio of Gas in Cylinder - Function of In-cylinder Temperature"
gamma = c_p_cyl/c_v_cyl
```

B.2. EES Code for Divided Exhaust Period Concept

```
"! CYLINDER EVACUATION GAS DYNAMICS - Version 17"
"! By: Anand Nageswaran Bharath"
"! October 2015, University of Wisconsin Engine Research Center"
"! Program Description: This program models the gas exchange process for an engine cycle for a single cylinder version of the General Motors Z19 DTH 1.9 Liter Engine. The model is zero-dimensional, solving the equations of mass conservation and energy conservation for a control volume, for both the cylinder and the exhaust manifold."

"! Procedure for determining Mach Number of Gas Flow through Turbocharger Turbine: MACH_TURBINE"
procedure MACH_TURBINE(R_p_turb, m_dot_turb, gamma: M_turb)
"NOTE: Turbine is modeled as a nozzle with work output."

    "Sonic Flow through Turbine (Mach Number = 1)"
    if (R_p_turb < 0.528) then
    M_turb = 1
    endIF

    "Subsonic Flow through Turbine (Mach Number < 1)"
    if (R_p_turb >= 0.528) and (R_p_turb < 1) then
    M_turb = SQRT(2/(gamma-1)*((1/R_p_turb)^((gamma-1)/gamma)-1))
    endIF

    "No Flow through Turbine (Mach Number = 0)"
    if (R_p_turb >= 1) or (m_dot_turb = 0) then
    M_turb = 0
    ENDif
end

"! Procedure for determining Exhaust Gas Static Density through Blowdown Port: EXH_DENSITY_BLOWDOWN"
procedure EXH_DENSITY_BLOWDOWN(M_bd, gamma, rho_0:rho_bd)

    "Static Density at Sonic Condition"
    if (M_bd = 1) then
    rho_bd = rho_0/((gamma+1)*0.5)^(1/(gamma-1))
    endIF

    "Static Density at Subsonic Condition"
    if (M_bd < 1) then
    rho_bd = rho_0/(1 + 0.5*(gamma-1)*M_bd^2)^(1/(gamma-1))
    ENDif
end

"! Procedure for determining Exhaust Gas Static Density through Scavenging Port: EXH_DENSITY_SCAVENGE"
procedure EXH_DENSITY_SCAVENGE(M_sc, gamma, rho_0:rho_sc)

    "Static Density at Sonic Condition"
    if (M_sc >= 1) then
    rho_sc = rho_0/((gamma+1)*0.5)^(1/(gamma-1))
    endIF

    "Static Density at Subsonic Condition"
```

```
    if (M_sc < 1) then
    rho_sc = rho_0/(1 + 0.5*(gamma-1)*M_sc^2)^(1/(gamma-1))
    ENDif
end

"! Procedure for determining Exhaust Gas Static Density at Turbine Inlet: EXH_DENSITY_TURB"
procedure EXH_DENSITY_TURB(M_turb, gamma, rho_0_bd:rho_turb)

    "Static Density at Sonic Condition"
    if (M_turb = 1) then
    rho_turb = rho_0_bd/((gamma+1)*0.5)^(1/(gamma-1))
    endIF

    "Static Density at Subsonic Condition"
    if (M_turb < 1) then
    rho_turb = rho_0_bd/(1 + 0.5*(gamma-1)*M_turb^2)^(1/(gamma-1))
    ENDif
end

"! Procedure for Blowdown Port Flow Computation: FLOW_BLOWDOWN"
procedure FLOW_BLOWDOWN(p_0, p_t_in, A_bd, T_0, gamma, R_Air, R_p_bd:m_dot_bd)

    "Choked Flow in Blowdown Port out of Cylinder (if p_0_exh/p_0 <
0.528)"
    if (R_p_bd < 0.528) then
    m_dot_bd := -p_0*A_bd/SQRT(T_0)*SQRT(gamma/R_Air*(2/(gamma+1))^((gamma+1)/(gamma-1)))
    endif

    "Non-critical Flow in Blowdown Port out of Cylinder (if  0.528 < p_0_exh/p_0 < 1)"
    if (R_p_bd > 0.528) and (R_p_bd < 1) then
    m_dot_bd := -p_0*A_bd/SQRT(R_Air*T_0)*SQRT(2*gamma/(gamma-1)*(1-R_p_bd^((gamma-
1)/gamma)))*R_p_bd^(1/gamma)
    endif

    "Non-critical Flow in Blowdown Port into Cylinder (if 1< p_0_exh/p_0 < 1.8939) - Flow Reversal"
    if (R_p_bd > 1) and (R_p_bd < 1.8939) then
    m_dot_bd := p_t_in*A_bd/SQRT(R_Air*T_0)*SQRT(2*gamma/(gamma-1)*(1-(1/R_p_bd)^((gamma-
1)/gamma)))*(1/R_p_bd)^(1/gamma)
    endif

    "Choked Flow in Blowdown Port into Cylinder (p_0_exh/p_0 > 1.8939) - Flow Reversal"
    if (R_p_bd >= 1.8939) then
    m_dot_bd := p_t_in*A_bd/SQRT(T_0)*SQRT(gamma/R_Air*(2/(gamma+1))^((gamma+1)/(gamma-1)))
    endif

    "No Flow - Pressure Equilibrium"
    if (R_p_bd = 1) then
    m_dot_bd = 0
    endif
end

"! Procedure for Scavenging Port Flow Computation: FLOW_SCAVENGE"
procedure FLOW_SCAVENGE(p_0, p_0_sc, A_sc, T_0, gamma, R_Air, R_p_sc:m_dot_sc)
    if (R_p_sc < 0.528) then
    m_dot_sc := -p_0*A_sc/SQRT(T_0)*SQRT(gamma/R_Air*(2/(gamma+1))^((gamma+1)/(gamma-1)))
    endif
```

```
    if (R_p_sc > 0.528) and (R_p_sc < 1) then
    m_dot_sc := -p_0*A_sc/SQRT(R_Air*T_0)*SQRT(2*gamma/(gamma-1)*(1-R_p_sc^((gamma-
1)/gamma)))*R_p_sc^(1/gamma)
    endif
    if (R_p_sc > 1) and (R_p_sc < 1.8939) then
    m_dot_sc := p_0_sc*A_sc/SQRT(R_Air*T_0)*SQRT(2*gamma/(gamma-1)*(1-(1/R_p_sc)^((gamma-
1)/gamma)))*(1/R_p_sc)^(1/gamma)
    endif
    if (R_p_sc >= 1.8939) then
    m_dot_sc := p_0_sc*A_sc/SQRT(T_0)*SQRT(gamma/R_Air*(2/(gamma+1))^((gamma+1)/(gamma-
1)))
    endif
    if (R_p_sc = 1) then
    m_dot_sc = 0
    endif
end

"! Procedure for Intake Port Flow Computation: FLOW_INTAKE"
procedure FLOW_INTAKE(p_0, p_c_ex, A_in, T_0, T_in, gamma, gamma_rtp, R_Air, R_p_in:dmdt_2)

    "Choked Flow in Intake Ports into Cylinder (if p_c_ex/p_0 < 0.528)"
    if (R_p_in < 0.528) then
    dmdt_2 :=
p_c_ex*A_in/SQRT(T_in)*SQRT(gamma_rtp/R_Air*(2/(gamma_rtp+1))^((gamma_rtp+1)/(gamma_rtp-1)))
    endif

    "Non-critical Flow in Intake Ports into Cylinder (if  0.528 < p_c_ex/p_0 <
1)"
    if (R_p_in > 0.528) and (R_p_in < 1) then
    dmdt_2 := p_c_ex*A_in/SQRT(R_Air*T_in)*SQRT(2*gamma_rtp/(gamma_rtp-1)*(1-
R_p_in^((gamma_rtp-1)/gamma_rtp)))*R_p_in^(1/gamma_rtp)
    endif

    "Non-critical Flow in Intake Ports out of Cylinder (if 1< p_c_ex/p_0 < 1.8939) - Flow Reversal"
    if (R_p_in > 1) and (R_p_in < 1.8939) then
    dmdt_2 := -p_0*A_in/SQRT(R_Air*T_0)*SQRT(2*gamma/(gamma-1)*(1-(1/R_p_in)^((gamma-
1)/gamma)))*(1/R_p_in)^(1/gamma)
    endif

    "Choked Flow in Intake Ports out of Cylinder (if p_c_ex/p_0 > 1.8939) - Flow Reversal"
    if (R_p_in >= 1.8939) then
    dmdt_2 := -p_0*A_in/SQRT(T_0)*SQRT(gamma/R_Air*(2/(gamma+1))^((gamma+1)/(gamma-1)))
    endif

    if (R_p_in = 1) then
    dmdt_2 := 0
    endif
end

"! Procedure for determining whether there is mass flow into or out of cylinder: MASSFLOW_DEP"
procedure MASSFLOW_DEP(m_dot_bd, m_dot_sc, m_dot_int, t, t_evo_1, t_evo_2,
t_evc_1,t_ivo,t_evc_2, t_fin, t_start: dmdt_tot)

    "Exhaust Flow through Blowdown Valve, when only blowdown valve is open"
    if (t > t_evo_1) and (t < t_evo_2) then
    dmdt_tot = m_dot_bd
```

```
    endif

    "Exhaust Flow through both exhaust valves, when both blowdown and scavenging valves are
open"

    if (t >= t_evo_2) and (t < t_evc_1) then
    dmdt_tot = m_dot_bd + m_dot_sc
    endif

    "Exhaust Flow through Scavenging Valve, when only scavenging valve is open"
    if (t >= t_evc_1) and (t < t_ivo) then
    dmdt_tot = m_dot_sc
    endif

    "Flow through Intake and Exhaust Valves (Blowdown and/or Scavenging) depending on Valve Timings
- Valve Overlap Period"
    if (t >= t_ivo) and (t < t_evc_2) then
    dmdt_tot = m_dot_sc + m_dot_int
    endif

    "Flow through Intake Valves"
    if (t >= t_evc_2) and (t < t_fin) then
    dmdt_tot = m_dot_int
    endif

    "Closed cycle - no flow into or out of cylinder"
    if (t >= t_start) and (t <= t_evo_1) then
    dmdt_tot = 0
    endif
end

"! Procedure for determining whether there is energy flow into or out of cylinder: ENERGYFLOW_DEP"
procedure ENERGYFLOW_DEP(t, t_start, t_soc, t_eoc, t_evo_1, t_evo_2, t_evc_1, t_ivo, t_evc_2, t_fin,
dudV, V_dot, q_dot_loss_tot, q_dot_HR, h_cyl_bd, h_cyl_sc, h_cyl_in: dudt_tot)

    "Closed Cycle - Energy flow only involves boundary work and heat losses (before combustion)"
    if ((t >= t_start) and (t <= t_soc)) then
    dudt_tot = dudV*V_dot -  q_dot_loss_tot
    endif

    "Closed Cycle - Combustion process: Energy flow adds heat release from combustion"
    if ((t > t_soc) and (t <= t_eoc)) then
    dudt_tot = dudV*V_dot - q_dot_loss_tot + q_dot_HR
    endif

    "Closed Cycle - Expansion post-combustion: heat losses and boundary work only"
    if ((t > t_eoc) and (t <= t_evo_1)) then
    dudt_tot = dudV*V_dot - q_dot_loss_tot
    endif

    "Blowdown Valve Open Energy Flow"
    if (t > t_evo_1) and (t <= t_evo_2) then
    dudt_tot = dudV*V_dot + h_cyl_bd - q_dot_loss_tot
    endif

    "Exhaust Energy Flow thorugh both Blowdown and Scavenging Valves"
```

```
    if (t > t_evo_2) and (t <= t_evc_1) then
    dudt_tot = dudV*V_dot + h_cyl_bd + h_cyl_sc - q_dot_loss_tot
    endif

    "Scavenging Valve Open Energy Flow"
    if (t > t_evc_1) and (t <= t_ivo) then
    dudt_tot = dudV*V_dot + h_cyl_sc - q_dot_loss_tot
    endif

    "Energy Flow during Valve Overlap Period"
    if (t > t_ivo) and (t <= t_evc_2) then
    dudt_tot = dudV*V_dot + h_cyl_sc + h_cyl_in - q_dot_loss_tot
    endif

    "Intake Valve Open Energy Flow"
    if (t > t_evc_2) and (t < t_fin) then
    dudt_tot = dudV*V_dot + h_cyl_in - q_dot_loss_tot
    endif
end

"! Procedure for Determining Mach Number of Gas Flow through Blowdown Port: MACH_BLOWDOWN"
procedure MACH_BLOWDOWN(R_p_bd, m_dot_bd_abs, gamma, t, t_evc_1, t_evo_1: M_bd)

    "Mach Number = 1 (Sonic Flow at Throat)"
    if (R_p_bd < 0.528) and (m_dot_bd_abs > 0) then
    M_bd = 1
    endif

    "Zero Flow, Mach Number = 0"
    if (m_dot_bd_abs = 0) then
    M_bd = 0
    endif

    "Mach Number < 1 (Subsonic Flow)"
    if (R_p_bd > 0.528) and (R_p_bd < 1) then
    M_bd = SQRT(2/(gamma-1)*((1/R_p_bd)^((gamma-1)/gamma)-1))
    endif

    "Mach Number < 1 (Subsonic Flow - Flow Reversal)"
    if (R_p_bd > 1) and (R_p_bd < 1.8939) then
    M_bd = SQRT(2/(gamma-1)*((R_p_bd)^((gamma-1)/gamma)-1))
    endif

    "Valve closed; Mach Number = 0"
    if (t > t_evc_1) or (t < t_evo_1) then
    M_bd = 0
    endif
end

"! Procedure for Determining Mach Number of Gas Flow through Scavenging Port: MACH_SCAVENGE"
procedure MACH_SCAVENGE(R_p_sc, m_dot_sc_abs, gamma, t, t_evc_2, t_evo_2: M_sc)

    "Mach Number = 1 (Sonic Flow at Throat)"
    if (R_p_sc < 0.528) and (m_dot_sc_abs > 0) then
    M_sc = 1
    endif
```

```
    "Zero Flow, Mach Number = 0"
    if (m_dot_sc_abs = 0) then
    M_sc = 0
    endif

    "Mach Number < 1 (Subsonic Flow)"
    if (R_p_sc > 0.528) and (R_p_sc < 1) then
    M_sc = SQRT(2/(gamma-1)*((1/R_p_sc)^((gamma-1)/gamma)-1))
    endif

    "Mach Number < 1 (Subsonic Flow - Flow Reversal)"
    if (R_p_sc > 1) and (R_p_sc < 1.8939) then
    M_sc = SQRT(2/(gamma-1)*((R_p_sc)^((gamma-1)/gamma)-1))
    endif

    "Valve closed; Mach Number = 0"
    if (t > t_evc_2) or (t < t_evo_2) then
    M_sc = 0
    endif
end

"! Procedure for determining Exhaust Gas Static Properties at Blowdown Port: STATICBLOWDOWN"
procedure STATICBLOWDOWN (M_bd, T_0, gamma: T_e_bd, h_e_bd)

    "Mach Number = 0; Static Properties = Stagnation Properties"
    if (M_bd = 0) then
    T_e_bd = T_0
    h_e_bd = ENTHALPY(Air,T = T_0)
    endif

    "Mach Number > 0"
    if (M_bd > 0) then
    T_e_bd = T_0/(1 + 0.5*(gamma -1)*M_bd^2)
    h_e_bd = ENTHALPY(Air,T = T_e_bd)
    endif
end

"! Procedure for determining Exhaust Gas Static Properties at Scavenging Port: STATICSCAVENGE"
procedure STATICSCAVENGE (M_sc, T_0, gamma: T_e_sc, h_e_sc)

    "Mach Number = 0; Static Properties = Stagnation
Properties"
    if (M_sc = 0) then
    T_e_sc = T_0
    h_e_sc = ENTHALPY(Air,T = T_0)
    endif

    "Mach Number > 0"
    if (M_sc > 0) then
    T_e_sc = T_0/(1 + 0.5*(gamma -1)*M_sc^2)
    h_e_sc = ENTHALPY(Air,T = T_e_sc)
    endif
end
```

```
"! Procedure for computing the Intake Valve Lift with respect to Crank Angle: VALVELIFTINTAKE. The polynomial equations for the lift profile and the discharge coefficients were obtained by curve fitting the valve lift profile and the discharge coefficient vs. L/D ratio values in MATLAB using the least squares method."
procedure VALVELIFTINTAKE(t, t_ivo, t_fin, D_in: C_D_in_1, C_D_in_2)

    "Intake Valve Lift Profile:"
    if (t > t_ivo) and (t <= t_fin) then
    tau_in = (t - 0.03322)/0.003937
    L_in = -0.025*tau_in^9 - 0.2506*tau_in^8 + 0.1468*tau_in^7 + 1.459*tau_in^6 - 0.2489*tau_in^5 - 1.365*tau_in^4 + 0.1024*tau_in^3 - 4.953*tau_in^2 - 0.01643*tau_in + 7.982

    "Lift-to-diameter L/D Ratio"
    epsilon_in = L_in/(D_in*1000)

    "Intake Valve Discharge Coefficients"
    C_D_in_1 = -200.3*epsilon_in^5 + 260.8*epsilon_in^4 -114.4*epsilon_in^3 +14.54*epsilon_in^2 + 2.351*epsilon_in - 0.001114
    C_D_in_2 = -371.3*epsilon_in^5 + 449.6*epsilon_in^4 - 184.6*epsilon_in^3 +23.89*epsilon_in^2 + 1.998*epsilon_in - 0.0001521
    endif

    if (t =< t_ivo) or (t > t_fin) then
    C_D_in_1 = 0
    C_D_in_2 = 0
    endif
end

"! Procedure for computing the Blowdown Valve Lift with respect to Crank Angle: VALVELIFTBLOWDOWN. The polynomial equations for the lift profile and the discharge coefficients were obtained by curve fitting the valve lift profile and the discharge coefficient vs. L/D ratio values in MATLAB using the least squares method."
procedure VALVELIFTBLOWDOWN(t, t_evo_1, t_evc_1, D_bd: C_D_bd)
    if (t > t_evo_1) and (t < t_evc_1) then

    "Blowdown Valve Lift Profile"
    tau_bd = (t-0.02089)/0.004258
    L_bd = -0.05157*tau_bd^9 - 0.1513*tau_bd^8 + 0.3153*tau_bd^7 + 0.9599*tau_bd^6 - 0.574*tau_bd^5 - 0.8069*tau_bd^4 + 0.2848*tau_bd^3 - 4.785*tau_bd^2 - 0.04103*tau_bd + 7.986

    "Lift-over-Diameter (L/D) Ratio for Blowdown Valve"
    epsilon_bd = L_bd/(D_bd*1000)

    "Blowdown Valve Discharge Coefficient"
    C_D_bd = 20.44*epsilon_bd^4 - 22.05*epsilon_bd^3 +3.791*epsilon_bd^2 + 2.641*epsilon_bd + 0.001286
    endif

    if (t =< t_evo_1) or (t >= t_evc_1) then
    C_D_bd = 0
    endif
end

"! Procedure for computing the Scavenging Valve Lift with respect to Crank Angle: VALVELIFTSCAVENGE. The polynomial equations for the lift profile and the discharge coefficients were
```

```
obtained by curve fitting the valve lift profile and the discharge coefficient vs. L/D ratio values in MATLAB using the least squares method."
procedure VALVELIFTSCAVENGE(t, t_evo_2, t_evc_2, D_sc: C_D_sc)
    if (t > t_evo_2) and (t < t_evc_2) then

    "Scavenging Valve Lift Profile"
    tau_sc = (t-0.02572)/0.001452
    L_sc = -0.05157*tau_sc^9 - 0.1513*tau_sc^8 + 0.3153*tau_sc^7 + 0.9599*tau_sc^6 - 0.574*tau_sc^5
- 0.8069*tau_sc^4 + 0.2848*tau_sc^3 - 4.785*tau_sc^2 - 0.04103*tau_sc + 7.986

    "Lift-over-Diameter (L/D) Ratio for Scavenging Valve"
    epsilon_sc = L_sc/(D_sc*1000)

    "Scavenging Valve Discharge Coefficient"
    C_D_sc = 20.44*epsilon_sc^4 - 22.05*epsilon_sc^3 +3.791*epsilon_sc^2 + 2.641*epsilon_sc +
0.001286
    endif

    if (t =< t_evo_2) or (t >= t_evc_2) then
    C_D_sc = 0
    endif
end

"! Procedure for calculating the velocity of the exhaust gas at the blowdown port:
BLOWDOWN_THROATVELOCITY. Velocity w = (dm/dt)/[rho_th*A_ex]"
procedure BLOWDOWN_THROATVELOCITY(A_bd, rho_bd, m_dot_bd_abs, t, t_evo_1, t_evc_1: w_bd)
    if (t > t_evo_1) and (t < t_evc_1) then
    w_bd = m_dot_bd_abs/(A_bd*rho_bd)
    endif

    if (t <= t_evo_1) or (t >= t_evc_1) then
    w_bd = 0
    endif
end

"! Procedure for calculating the velocity of the exhaust gas at the scavenging port:
SCAVENGE_THROATVELOCITY. Velocity w = (dm/dt)/[rho_th*A_ex]"
procedure SCAVENGE_THROATVELOCITY(A_sc, rho_sc, m_dot_sc_abs, t, t_evo_2, t_evc_2: w_sc)
    if (t > t_evo_2) and (t < t_evc_2) then
    w_sc = m_dot_sc_abs/(A_sc*rho_sc)
    endif

    if (t <= t_evo_2) or (t >= t_evc_2) then
    w_sc = 0
    endif
end

"! Procedure for determining Mass Flow Rate of Exhaust Gas through Turbocharger Turbine:
TURBINEFLOW"
procedure TURBINEFLOW (R_p_turb, p_0_bd, A_turb, T_0_bd, gamma, R_Air: m_dot_turb)

    "Subsonic Flow through Turbine (if Pressure Ratio 0.528 < p_atm/p_0_bd < 1)"
    if (R_p_turb > 0.528) and (R_p_turb < 1) then
    m_dot_turb = p_0_bd*A_turb/SQRT(R_Air*T_0_bd)*SQRT(2*gamma/(gamma-1)*(1-
R_p_turb^((gamma-1)/gamma)))*R_p_turb^(1/gamma)
    endif
```

```
    "No flow through Turbine if Pressure Ratio >= 1 (We are assuming no flow reversal here.)"
    if (R_p_turb >= 1) then
    m_dot_turb = 0
    endif

    "Choked Flow through Turbine (if Pressure Ratio p_atm/p_0_bd < 0.528 - Sonic Condition)"
    if (R_p_turb < 0.528) then
    m_dot_turb =
p_0_bd*A_turb/SQRT(T_0_bd)*SQRT(gamma/R_Air*(2/(gamma+1))^((gamma+1)/(gamma-1)))
    endif
end

"! Procedure for determining Mass Flow Rate of Exhaust Gas out of Scavenging Manifold:
SCAVENGEFLOW. The exit of the scavenging manifold is modeled as a nozzle."
procedure SCAVENGEFLOW (R_p_surr, p_0_sc, A_surr, T_0_sc, gamma, R_Air: m_dot_surr)

    "Subsonic Flow out of Scavenging Manifold (if Pressure Ratio 0.528 < p_atm/p_0_sc < 1)"
    if (R_p_surr > 0.528) and (R_p_surr < 1) then
    m_dot_surr = p_0_sc*A_surr/SQRT(R_Air*T_0_sc)*SQRT(2*gamma/(gamma-1)*(1-
R_p_surr^((gamma-1)/gamma)))*R_p_surr^(1/gamma)
    endif

    "Now flow out of Scavenging Manifold if Pressure Ratio >= 1 (We are assuming no flow reversal
here.)"
    if (R_p_surr >= 1) then
    m_dot_surr = 0
    endif

    "Choked flow out of Scavenging Manifold (if Pressure Ratio p_atm/p_0_sc < 0.528 - Sonic Condition)"
    if (R_p_surr < 0.528) then
    m_dot_surr =
p_0_sc*A_surr/SQRT(T_0_sc)*SQRT(gamma/R_Air*(2/(gamma+1))^((gamma+1)/(gamma-1)))
    endif
end

"! Procedure for determining Exhaust Gas Velocity through Turbine: EXHTURBINEVELOCITY. Velocity
w_turb_in = (dm/dt)/[rho_turb*A_turb]"
procedure EXHTURBINEVELOCITY(A_turb, rho_turb, m_dot_turb: w_turb_in)
    if (m_dot_turb > 0) then
    w_turb_in = m_dot_turb/(A_turb*rho_turb)
    endif

    if (m_dot_turb = 0) then
    w_turb_in = 0
    endif
end

"! Procedure for the Wiebe Function to model the Combustion Process: WIEBEMODEL"
procedure WIEBEMODEL (t, t_soc, t_eoc, q_in, a_w, m_w, N, theta_comb, k, theta_soc: q_dot_HR)

    "Wiebe Heat Release Rate between Start of Combustion (SOC) and End of Combustion (EOC)"
    if (t > t_soc) and (t <= t_eoc) then
    f = ABS(((PI*N*t)/30 - k - theta_soc)/theta_comb)
    q_dot_HR = q_in*(PI*a_w*m_w*N)/(30*theta_comb)*(((PI*N*t)/30 - k - theta_soc)/theta_comb)^(m_w-
1)*EXP(-a_w*f^m_w)
```

```
    endif

    if (t <= t_soc) or (t > t_eoc) then
    q_dot_HR = 0
    endif
end

"! Procedure for evaluating the In-cylinder Average Gas Velocity w_cyl for the Woschni Heat Transfer
Correlation:
WOSCHNIGASVELOCITY"

procedure WOSCHNIGASVELOCITY (t, t_start, t_tdc, t_evo_1, t_fin, K_1_e, K_1_c, K_2, u_bar, V_d,
T_r, p_r, V_ivc, p_0, p_m: w_cyl)

    "Average Gas Velocity during the Compression Stroke"
    if (t >= t_start) and (t < t_tdc) then
    w_cyl = K_1_e*u_bar
    endif

    "Average Gas Velocity during the Expansion Stroke"
    if (t >= t_tdc) and (t < t_evo_1) then
    w_cyl = K_1_e*u_bar + K_2*(V_d*T_r)/(p_r*V_ivc)*(p_0 - p_m)
    endif

    "Average Gas Velocity during the Gas Exchange Process (between EVO and
IVC)"
    if (t >= t_evo_1) and (t < t_fin) then
    w_cyl = K_1_c*u_bar
    endif
end
"! Geometry of the General Motors 1.9L Diesel Engine"
b = 0.082 [m]                                          "Bore"
s = 0.0904 [m]                                         "Stroke"
a = s/2 [m]                                            "Crank Radius"
L_crd = 0.14554 [m]                                    "Connecting Rod Length"
R_c = 15.1                                             "Geometric Compression Ratio"
N = 3000                                               "Engine Speed (in RPM)"
V_d = (PI*b^2*s)/4                                     "Displacement Volume of 1 cylinder"
V_c = V_d/(R_c-1)                                      "Clearance Volume"
u_bar = 2*s*N/60 [m/s]                                 "Mean Piston Speed (for Heat Loss Calculations
using Woschni Model)"

"! Fuel Properties, Fuel Mass, Trapped Air Mass, Load and Combustion Characteristics"
LHV_diesel = 4.4917e7 [J/kg]                           "Lower Heating Value of N-Heptane"
LHV_petrol = 4.4663e7 [J/kg]                           "Lower Heating Value of Iso-Octane"
eta_th = 0.45                                          "Thermal Efficiency"

m_fuel_cyc = 20.772 [mg]                               "Mass of fuel per cycle (in mg)"
lambda = 0.5                                           "Gasoline/Diesel Ratio"

m_dies_cyc = m_fuel_cyc*(1-
lambda)*CONVERT(mg,kg)                                 "Mass of N-Heptane"
m_gas_cyc = m_fuel_cyc*lambda*CONVERT(mg,kg)           "Mass of Iso-Octane"
eta_comb = 0.9624                                      "Combustion Efficiency"

"Mass of Air needed for Stoichiometric mixture per cycle"
```

```
m_a_st_cyc = m_dies_cyc/0.0662 + m_gas_cyc/0.0664

phi = 0.4                                                    "Equivalence Ratio"
m_a_cyc = m_a_st_cyc/phi                                     "Actual Mass of Air per cycle"

"Mass Flow Rate of Air (kg/s) through Compressor"
m_a_tot = m_a_cyc*0.5*N/60*4

{p_c_ex = 120*m_a_tot*0.25*R_Air*T_atm/(N*V_d)}

m_fuel_tot = m_fuel_cyc*CONVERT(mg,kg)*0.5*N/60*4 "Fuel Flow Rate for all Cylinders (kg/s)"
m_exh_tot = m_a_tot + m_fuel_tot                             "Exhaust Mass Flow Rate through Turbine"

"! Air Properties"
gamma_rtp = 1.4                                              "Specific Heat Ratio of Air"
gamma = 1.4
M_r_Air = MOLARMASS(Air)                                     "Molecular Mass of Air"
R_bar = 8314 [J/kmol/K]                                      "Universal Gas Constant"
R_Air = R_bar/M_r_Air                                        "Specific Gas Constant of Air"
p_atm = 101325 [Pa]                                          "Atmospheric Pressure"
T_atm = 298.15 [K]                                           "Room Temperature"

"Specific Heat Capacity of Air at Room Temperature and Pressure"
c_p = CP(Air,T=T_atm)

"! Definition of Important Timepoints in each Engine Cycle"
theta_start_deg = -132          "Crank Angle at Start of Cycle: Intake Valve Closure (IVC) in Degrees"
theta_soc_deg = -10.48                  "Crank Angle at Start of Combustion (SOC) in Degrees"
theta_eoc_deg = 14.05                    "Crank Angle at End of Combustion (EOC) in Degrees"
theta_evo_1_deg = 112   "Crank Angle at Exhaust Valve Opening (EVO) in Degrees of Blowdown Valve"
theta_evo_2_deg = 286  "Crank Angle at Exhaust Valve Opening (EVO) in Degrees of Scavenging Valve"
theta_evc_1_deg = 376    "Crank Angle at Exhaust Valve Closing (EVC) in Degrees of Blowdown Valve"
theta_ivo_deg = 344                  "Crank Angle at Intake Valve Opening (IVO) in Degrees"
theta_evc_2_deg = 376  "Crank Angle at Exhaust Valve Closing (EVC) in Degrees of Scavenging Valve"
theta_fin_deg = 588          "Crank Angle at End of Cycle: Intake Valve Closure (IVC) in Degrees"

"Crank angle (in Radians) at Start of Cycle (IVC - Intake Valve Closure)"
theta_start = theta_start_deg*PI/180

theta_soc = theta_soc_deg*PI/180          "Crank angle (in Radians) at Start of Combustion (SOC)"
theta_eoc = theta_eoc_deg*PI/180           "Crank angle (in Radians) at End of Combustion (EOC)"

"Crank angle at Exhaust Valve Opening (In Radians) of Blowdown Valve"
theta_evo_1 = theta_evo_1_deg*PI/180

"Crank angle at Exhaust Valve Opening (In Radians) of Scavenging Valve"
theta_evo_2 = theta_evo_2_deg*PI/180

"Crank angle at Exhaust Valve Opening (In Radians) of Blowdown Valve"
theta_evc_1 = theta_evc_1_deg*PI/180

theta_ivo = theta_ivo_deg*PI/180                "Crank angle at Intake Valve Opening (In Radians)"

"Crank angle at Exhaust Valve Closing (in Radians) of Scavenging Valve"
theta_evc_2 = theta_evc_2_deg*PI/180
```

```
"Crank angle (In Radians) at End of Cycle (IVC - Intake Valve Closure)"
theta_fin = theta_fin_deg*PI/180
"Time at Cycle Start (IVC - Intake Valve Closure)"
t_start = 0

t_soc = (theta_soc_deg-theta_start_deg)/360*(1/(N/60)) "Time at Start of Combustion (SOC)"
t_eoc = (theta_eoc_deg-theta_start_deg)/360*(1/(N/60)) "Time at End of Combustion (EOC)"

"Time at 1st Top Dead Center (at 0 Degrees Crank Angle)"
t_tdc = (0 - theta_start_deg)/360*(1/(N/60))

"Time at Blowdown Valve Opening:"
t_evo_1 = (theta_evo_1_deg-theta_start_deg)/360*(1/(N/60))

"Time at Scavenging Valve Opening:"
t_evo_2 = (theta_evo_2_deg-theta_start_deg)/360*(1/(N/60))

"Time at Blowdown Valve Closing:"
t_evc_1 = (theta_evc_1_deg-theta_start_deg)/360*(1/(N/60))

t_ivo = (theta_ivo_deg-theta_start_deg)/360*(1/(N/60))   "Intake Valve Opening (IVO) Time"

"Time at Scavenging Valve Closing:"
t_evc_2 = (theta_evc_2_deg-theta_start_deg)/360*(1/(N/60))

"Time at Cycle End (IVC - Intake Valve Closure)"
t_fin = (theta_fin_deg-theta_start_deg)/360*(1/(N/60))

"! Engine Geometric Parameter Changes during Cycle"
"Piston Pin Position at Blowdown Valve Opening:"
x_evo_1 = a*COS(theta_evo_1) + SQRT(L_crd^2 - (a*SIN(theta_evo_1))^2)

"Piston Pin Position at Cycle Start (Intake Valve Closure):"
x_start = a*COS(theta_start) + SQRT(L_crd^2 - (a*SIN(theta_start))^2)

V_ivc = V_c + 0.25*PI*b^2*(L_crd + a - x_start)          "Volume in cylinder at IVC"
V_evo_1 = V_c + 0.25*PI*b^2*(L_crd + a - x_evo_1)        "Volume in cylinder at EVO"
V_start = V_c + 0.25*PI*b^2*(L_crd + a - x_start)        "Volume of cylinder at TDC (Cycle Start)"

"! Set up In-cylinder Initial Conditions"
m_trap = 870.8e-6                                        "Initial Gas Mass trapped in Cylinder"
T_1 = 348 [K]                                            "Temperature at Intake Valve Closure (IVC)"

T_init = T_1                                             "Initial Temperature - Temperature at IVC"
p_init*V_start = m_trap*R_Air*T_init                     "Initial Pressure - Pressure at IVC"

"Initial Motoring Pressure at IVC - Used for the computation of Average In-cylinder Gas Velocity for the
Woschni Heat Transfer Correlation"
p_m_init*V_start = m_trap*R_Air*T_init

m_init = m_trap                                          "Initial Gas Mass in cylinder at EVO"
u_init = INTENERGY(Air,T=T_init)*m_trap                  "Initial Internal Energy of Gas in cylinder at EVO"

"Initial Motoring Internal Energy of Gas in cylinder at IVC - Used for the computation of Average In-
cylinder Gas Velocity for the Woschni Heat Transfer Correlation"
u_m_init = INTENERGY(Air,T=T_init)*m_trap
```

```
"Piston Pin Position"
x = a*COS((PI*N)/30*t - (11*PI)/15) + SQRT(L_crd^2 - (a*SIN((PI*N)/30*t (11*PI)/15))^2)

“Conversion between Crank Angle and Time”
theta = 6*N*t - 132

"Variation of cylinder volume with time (Slider-Crank Equation of Motion)"
V = V_c + 0.25*PI*b^2*(L_crd + a - x)

V_dot = -0.25*PI*b^2*x_dot                    "Rate of change of cylinder volume"

"! Intake Valve Operation"
"Call VALVELIFTINTAKE Procedure:"
call ValveLiftIntake(t, t_ivo, t_fin, D_in: C_D_in_1, C_D_in_2)

D_in = 24/1000                                "Intake Valve Diameter"
A_in_1 = C_D_in_1*0.25*PI*D_in^2              "Effective Intake Valve Area for Intake Valve 1"
A_in_2 = C_D_in_2*0.25*PI*D_in^2              "Effective Intake Valve Area for Intake Valve 2"
A_in = A_in_1 + A_in_2                        "Total Effective Intake Valve Area"

"Convert units of Effective Intake Valve Area to mm^2"
A_in_mm2 = A_in*1e6


"! Exhaust Valve Operation"
"Call VALVELIFTBLOWDOWN Procedure:"
call VALVELIFTBLOWDOWN(t, t_evo_1, t_evc_1, D_bd: C_D_bd)

"Call VALVELIFTSCAVENGE Procedure:"
call VALVELIFTSCAVENGE(t, t_evo_2, t_evc_2, D_sc: C_D_sc)

D_bd = 21.92/1000                             "Blowdown Valve Diameter"
A_bd = C_D_bd*0.25*PI*D_bd^2                  "Effective Blowdown Valve Flow Area"

D_sc = 21.92/1000                             "Scavenging Valve Diameter"
A_sc = C_D_sc*0.25*PI*D_sc^2                  "Effective Scavenging Valve Flow Area"

"! Wiebe Combustion Model Parameters"
"Total Fuel Energy per cycle"
q_in = (LHV_diesel*m_dies_cyc + LHV_petrol*m_gas_cyc)

a_w = 3.281                                   "Wiebe Exponent a_w"
m_w = 2.269                                   "Wiebe Shape Parameter m_w"

theta_comb = 34.72/180*PI                     "Duration of Combustion"
k = 11*PI/15                                  "Phase Angle k (in Radians)"

"Call procedure WIEBEMODEL for simulating combustion using the Wiebe Model:"
call WiebeModel (t, t_soc, t_eoc, q_in, a_w, m_w, N, theta_comb, k, theta_soc: q_dot_HR)

"! Gas Exchange Process Calculations"
p_0*V = m_cyl*R_Air*T_0        "Ideal Gas Equation of State for gas remaining in cylinder"
p_0 = rho_0*R_Air*T_0          "Alternative form of Ideal Gas Equation to calculate Stagnation Density"
dudV = -p_0                    "dudV term for Gibbs' Equation (Energy Equation) for Control Volume"
```

```
“Call Procedure FLOW_BLOWDOWN:”
call Flow_Blowdown(p_0, p_t_in, A_bd, T_0, gamma, R_Air, R_p_bd:m_dot_bd)

“Call Procedure FLOW_SCAVENGE:”
call Flow_Scavenge(p_0, p_0_sc, A_sc, T_0, gamma, R_Air, R_p_sc:m_dot_sc)

“Call Procedure FLOW_INTAKE:”
call Flow_Intake(p_0, p_c_ex, A_in, T_0, T_in, gamma, gamma_rtp, R_Air, R_p_in:m_dot_int)

"Intake Temperature = Atmospheric Temperature (Assuming 100% Intercooler Effectiveness)"
T_in = T_atm

u_cyl = INTENERGY(Air,T=T_0)*m_cyl                    "Internal energy of gas remaining in cylinder"

"Stagnation Enthalpy of gas flowing out of cylinder into Blowdown Manifold"
h_cyl_bd = ENTHALPY(Air,T=T_0) * m_dot_bd

"Stagnation Enthalpy of gas flowing out of cylinder into Scavenging Manifold"
h_cyl_sc = ENTHALPY(Air,T=T_0) * m_dot_sc

"Stagnation Enthalpy of gas entering cylinder"
h_cyl_in = ENTHALPY(Air,T=T_in)*m_dot_int

"! Exhaust Manifold Properties and Geometric Information"
V_em = 3.0952e-4 [m^3]                                "Volume of Blowdown Manifold"
p_exh_init = 110000                                   "Initial Blowdown Pressure"
T_exh_init = 790                                      “Initial Blowdown Temperature”

"Ideal Gas Equation of State for Blowdown Manifold - Initial Conditions"
p_exh_init*V_em = m_em_init*R_Air*T_exh_init

"Initial Internal Energy of Gas in Blowdown Manifold at Cycle Start"
u_em_init = INTENERGY(Air,T=T_exh_init)*m_em_init

"Internal Energy of Gas in Blowdown Manifold at time t > 0"
u_em = INTENERGY(Air,T=T_0_bd)*m_em

"Enthalpy of Exhaust Gas entering Blowdown Manifold"
h_in = -h_cyl_bd

"Enthalpy of Exhaust Gas leaving Blowdown Manifold"
h_out = m_dot_turb*ENTHALPY(Air,T=T_0_bd)

"Ideal Gas Equation of State for Gas in Blowdown Manifold"
p_0_bd*V_em = m_em*R_Air*T_0_bd

"Alternate Form of Ideal Gas Equation of State for Gas in Blowdown Manifold - To calculate Stagnation
Blowdown Density"
p_0_bd = rho_0_bd*R_Air*T_0_bd

"Turbine Inlet Pressure = Blowdown Manifold Stagnation Pressure"
p_t_in = p_0_bd
p_backpres = 110000                                   “Turbine Outlet Pressure”

R_p_bd = p_0_bd/p_0                                   “Blowdown Manifold to Cylinder Pressure Ratio”
```

```
R_p_turb = p_backpres/p_0_bd                    "Turbine to Atmosphere Pressure Ratio"

R_p_in = p_0/p_c_ex                             "Compressor to Cylinder Pressure Ratio"

V_em_2 =3.0952e-4 [m^3]                         “Volume of Scavenging Manifold”
p_exh_2_init = 110000                           “Initial Scavenging Pressure”
T_exh_2_init = 756                              “Initial Scavenging Temperature”

"Ideal Gas Equation of State for Scavenging Manifold - Initial Conditions"
p_exh_2_init*V_em_2 = m_em_2_init*R_Air*T_exh_2_init

"Initial Internal Energy of Gas in Scavenging Manifold at Cycle Start"
u_em_2_init = INTENERGY(Air,T=T_exh_2_init)*m_em_2_init

"Internal Energy of Gas in Scavenging Manifold at time t > 0"
u_em_2 = INTENERGY(Air,T=T_0_sc)*m_em_2

"Enthalpy of Exhaust Gas entering Scavenging Manifold"
h_in_2 = -h_cyl_sc

"Enthalpy of Exhaust Gas leaving Scavenging Manifold"
h_out_2 = m_dot_surr*ENTHALPY(Air,T=T_0_sc)

"Ideal Gas Equation of State for Gas in Scavenging Manifold"
p_0_sc*V_em_2 = m_em_2*R_Air*T_0_sc

"Alternate Form of Ideal Gas Equation of State for Gas in Scavenging Manifold - To calculate Stagnation
Scavenging Density"
p_0_sc = rho_0_sc*R_Air*T_0_sc

“Scavenging Manifold to Cylinder Pressure Ratio”
R_p_sc = p_0_sc/p_0

“Scavenging Manifold to Atmosphere Pressure Ratio”
R_p_surr = p_backpres/p_0_sc

"Call procedure MASSFLOW_DEP:"
call MASSFLOW_DEP(m_dot_bd, m_dot_sc, m_dot_int, t, t_evo_1, t_evo_2, t_evc_1,t_ivo,t_evc_2, t_fin,
t_start: m_dot)

"Absolute value of Exhaust Mass Flow Rate out of Cylinder into Blowdown Manifold (Neglect Direction)"
m_dot_bd_abs = ABS(m_dot_bd)

"Absolute value of Exhaust Mass Flow Rate out of Cylinder into Scavenging Manifold (Neglect Direction)"
m_dot_sc_abs = ABS(m_dot_sc)

A_turb = 1.492e-4                               “Turbine Inlet Area (in m^2)”
A_surr = 1.408e-4                               “Scavenging Manifold Outlet Area (in m^2)”

“Call procedure TURBINEFLOW:”
call TURBINEFLOW (R_p_turb, p_0_bd, A_turb, T_0_bd, gamma, R_Air: m_dot_turb)

“Call procedure SCAVENGEFLOW:”
call SCAVENGEFLOW (R_p_surr, p_0_sc, A_surr, T_0_sc, gamma, R_Air: m_dot_surr)
```

"Mass Conservation Equation for Gas in the Blowdown Manifold due to inflow from Cylinder and outflow to Turbine"
m_dot_em = m_dot_bd_abs - m_dot_turb

"Energy Conservation Equation for Gas in Blowdown Manifold"
u_dot_em = h_in_1 - h_out

"Mass Conservation Equation for Gas in the Scavenging Manifold"
m_dot_em_2 = m_dot_sc_abs - m_dot_surr

"Energy Conservation Equation for Gas in Scavenging Manifold"
u_dot_em_2 = h_in_2 - h_out_2

"! Woschni Heat Transfer Model for In-cylinder Heat Loss"

"Energy Conservation Equation for the Motoring Pressure - Used for Computation of In-cylinder Average Gas Velocity for Woschni Heat Transfer Correlation"
u_dot_m = -p_m*V_dot

"Integrate Motoring Energy Rate Change Equation above (with respect to time) to determine Motoring Internal Energy at time t."
u_m = u_m_init + INTEGRAL(u_dot_m,t,t_start,t_fin)

"Motoring Internal Energy at Time t and Temperature T_m"
u_m = INTENERGY(Air,T=T_m)*m_cyl

p_m*V = m_cyl*R_Air*T_m "Ideal Gas Equation of State for Motoring"

“Woschni Model Constants”
K_1_e = 2.28
K_1_c = 6.18
K_2 = 3.24e-3

p_r = 228551 "Pressure at Intake Valve Closure (IVC)"
T_r = 381.5 "Temperature at Intake Valve Closure (IVC)"

"Call procedure WOSCHNIGASVELOCITY to evaluate the Average In-cylinder Gas Velocity:"
call WOSCHNIGASVELOCITY (t, t_start, t_tdc, t_evo_1, t_fin, K_1_e, K_1_c, K_2, u_bar, V_d, T_r, p_r, V_ivc, p_0, p_m: w_cyl)

"In-cylinder Spatially Averaged Heat Transfer Coefficient:"
h_bar_cyl = 3.26*(b^(-0.2))*((p_0/1000)^0.8)*(T_0^(-0.55))*w_cyl^0.8

A_Pist = (PI*b^2)/4 "Area of Piston Surface"
A_head = (PI*b^2)/4 "Area of Cylinder Head"
A_wall = PI*b*(L_crd + a - x) "Surface Area of Cylinder Wall at Time t"

T_pist = 450 [K] "Piston Surface Temperature"
T_head = 450 [K] "Cylinder Head Surface Temperature"
T_wall = 400 [K] "Cylinder Wall Temperature"

q_dot_pist = h_bar_cyl*A_pist*(T_0 - T_pist) "Heat Loss Rate to Piston Surface"
q_dot_head = h_bar_cyl*A_head*(T_0 - T_head) "Heat Loss Rate to Cylinder Head"
q_dot_wall = h_bar_cyl*A_wall*(T_0 - T_wall) "Heat Loss Rate to Cylinder Wall"
q_dot_loss_tot = q_dot_pist + q_dot_head + q_dot_wall "Total Heat Loss Rate"

"Call procedure ENERGYFLOW_DEP:"
call ENERGYFLOW_DEP(t, t_start, t_soc, t_eoc, t_evo_1, t_evo_2, t_evc_1, t_ivo, t_evc_2, t_fin, dudV, V_dot, q_dot_loss_tot, q_dot_HR, h_cyl_bd, h_cyl_sc, h_cyl_in: u_dot)

"Call procedure MACH_BLOWDOWN:"
call MACH_BLOWDOWN(R_p_bd, m_dot_bd_abs, gamma, t, t_evc_1, t_evo_1: M_bd)

"Call procedure MACH_SCAVENGE:"
call MACH_SCAVENGE(R_p_sc, m_dot_sc_abs, gamma, t, t_evc_2, t_evo_2: M_sc)

"Call procedure BLOWDOWN_THROATVELOCITY:"
call BLOWDOWN_THROATVELOCITY(A_bd, rho_bd, m_dot_bd_abs, t, t_evo_1, t_evc_1: w_bd)

"Call procedure SCAVENGE_THROATVELOCITY:"
call SCAVENGE_THROATVELOCITY(A_sc, rho_sc, m_dot_sc_abs, t, t_evo_2, t_evc_2: w_sc)

"Call procedure STATICBLOWDOWN:"
call STATICBLOWDOWN (M_bd, T_0, gamma: T_e_bd, h_e_bd)

"Call procedure STATICSCAVENGE:"
call STATICSCAVENGE (M_sc, T_0, gamma: T_e_sc, h_e_sc)

“Convert units of Blowdown Valve Area to mm^2”
A_bd_mm2 = A_bd*1e6

“Convert units of Scavenging Valve Area to mm^2”
A_sc_mm2 = A_sc*1e6

“Convert units of Intake Valve Area to mm^2”
A_in_mm2 = A_in*1e6

"Call procedure MACH_TURBINE:"
call MACH_TURBINE(R_p_turb, m_dot_turb, gamma: M_turb)

"Call procedure EXH_DENSITY_BLOWDOWN:"
call EXH_DENSITY_BLOWDOWN(M_bd, gamma, rho_0:rho_bd)

"Call procedure EXH_DENSITY_SCAVENGE:"
call EXH_DENSITY_SCAVENGE(M_sc, gamma, rho_0:rho_sc)

"Call procedure EXH_DENSITY_TURB:"
call EXH_DENSITY_TURB(M_turb, gamma, rho_0_bd:rho_turb)

"Call procedure EXHTURBINEVELOCITY:"
call ExhTurbineVelocity(A_turb, rho_turb, m_dot_turb: w_turb_in)

"! Integration of Differential Equations with respect to Time"
$IntegralTable t:0.00002778 theta, p_0, T_0, V, m_cyl, u_cyl, c_p_cyl c_v_cyl gamma gamma_em M_bd, M_sc, R_p_bd, R_p_sc, A_bd_mm2, A_sc_mm2, A_in_mm2, m_dot_bd_abs, m_dot_sc_abs, m_dot_int, R_p_turb, p_0_bd, p_0_sc, rho_0_bd, rho_0_sc, T_0_bd, T_0_sc, m_dot_em m_dot_em_2 m_dot_turb W_dot_turb W_turb M_turb rho_turb w_turb_in T_e, h_e, m_exh m_air_cyl W_1 p_m w_cyl h_bar_cyl q_dot_loss_tot q_HR h_cyl_bd h_cyl_sc h_cyl_in c_p_em c_v_em

$SaveTable 'IntegralTable' 'C:\Users\bharath\Box Sync\PhD Engine Research\Wisconsin RCCI Combustion Control\Simulation\Transients\18_BAR_DEP_VALVE_AREA+30_SVOD90.csv'

```
q_HR_init = 0                                   "Initial Heat Release from Fuel"

"Heat Release over time as evaluated by Wiebe Combustion Model"
q_HR = INTEGRAL(q_dot_HR,t,t_start,t_evo_1)

"In-cylinder Gas Mass over time by integrating the Mass Conservation Equation for the Cylinder"
m_cyl = m_init + INTEGRAL(m_dot,t,t_start,t_fin)

"In-cylinder Internal Energy of Gas over time by integrating the Energy Conservation Equation for the Cylinder"
u_cyl = u_init + INTEGRAL(u_dot,t,t_start,t_fin)

"Exhaust Gas Mass in Blowdown Manifold over time by integrating the Mass Conservation Equation for the Blowdown Manifold"
m_em = m_em_init + INTEGRAL(m_dot_em,t,t_start,t_fin)

"Exhaust Gas Internal Energy in Blowdown Manifold over time by integrating the Energy Conservation Equation for the Blowdown Manifold"
u_em = u_em_init + INTEGRAL(u_dot_em,t,t_start,t_fin)

"Exhaust Gas Mass in Scavenging Manifold over time by integrating the Mass Conservation Equation for the Scavenging Manifold"
m_em_2 = m_em_2_init + INTEGRAL(m_dot_em_2,t,t_start,t_fin)

"Exhaust Gas Internal Energy in Scavenging Manifold over time by integrating the Energy Conservation Equation for the Scavenging Manifold"
u_em_2 = u_em_2_init + INTEGRAL(u_dot_em_2,t,t_start,t_fin)

"! Turbocharger Operating Characteristics"
eta_mech = 1                                    "Mechanical Efficiency"
eta_t = 0.71                                    "Turbine Isentropic Efficiency"
eta_c = 0.71                                    "Compressor Isentropic Efficiency"
eta_otc = eta_mech*eta_t*eta_c                  "Overall Turbocharger Efficiency"

{p_c_ex = 120*m_a_tot*0.25*R_Air*T_atm/(N*V_d)      "Compressor Exit Pressure given by the Speed-Density Equation. Used in 1st iteration as a guess for Boost Pressure"}

p_c_ex = 195600 [Pa]    "Compressor Exit Pressure (Actual Boost Pressure)"

"Constant Pressure Specific Heat Capacity of Gas in Blowdown Manifold"
c_p_em = CP(Air,T=T_0_exh)

"Constant Volume Specific Heat Capacity of Gas in Exhaust Manifold"
c_v_em = CV(Air,T=T_0_exh)

"Constant Pressure Specific Heat Capacity of Air at Atmospheric Conditions"
c_p_comp = CP(Air,T=T_atm)

"Specific Heat Ratio of Gas in Exhaust Manifold - Function of Temperature in Exhaust Manifold"
gamma_em = c_p_em/c_v_em

W_init = 0                                      "Initial Turbine Work Output"

"Instantaneous Turbine Power Output"
W_dot_turb =  m_dot_turb*c_p_em*T_0_exh*eta_t*(1-(p_atm/p_0_exh)^((gamma_em-1)/gamma_em))
```

```
W_turb = W_init + INTEGRAL(W_dot_turb,t,t_evo,t_fin)  "Evaluation of Turbine Work per Cycle"
m_turb = INTEGRAL(m_dot_turb,t,t_evo,t_fin)           "Total Mass Flow through Turbine"

"Energy Balance: Work extracted by Turbine = Work fed into Compressor"
 W_turb = W_comp

"Compressor Outlet Temperature:"
p_c_ex/p_atm = (T_0_comp/T_atm)^(gamma/(gamma-1))

"Constant Pressure Specific Heat Capacity of Gas in Cylinder"
c_p_cyl = CP(Air,T=T_0)

"Constant Volume Specific Heat Capacity of Gas in Cylinder"
c_v_cyl = CV(Air,T=T_0)

"Specific Heat Ratio of Gas in Cylinder - Function of In-cylinder Temperature"
gamma = c_p_cyl/c_v_cyl
```

B.3 Polynomial Curve Fits used in Stock Engine Configuration Code

This section gives the coefficients of the polynomial curve fits of the valve lift profiles and the valve discharge coefficient used in the EES code. The MATLAB curve fitting tool was used to perform the curve fits using the least squares method.

The polynomial fitted equation for the exhaust valve discharge coefficient is of the form:

$$C_{D,ex} = A_1 \cdot \epsilon^4 + A_2 \cdot \epsilon^3 + A_3 \cdot \epsilon^2 + A_4 \cdot \epsilon + A_5 \quad \text{(B-1)}$$

Where ϵ is the lift-to-diameter (L/D) ratio. The L/D ratio is in turn a function of the valve lift profile, which itself can be represented by a curve fit equation as follows:

$$L(\tau) = B_1 \cdot \tau^9 + B_2 \cdot \tau^8 + B_3 \cdot \tau^7 + B_4 \cdot \tau^6 + B_5 \cdot \tau^5 + B_6 \cdot \tau^4 + B_7 \cdot \tau^3 + B_8 \cdot \tau^2 + B_9 \cdot \tau + B_{10} \quad \text{(B-2)}$$

In Equation B-2, the variable τ is given as follows:

$$\tau(t) = \frac{t - k_1}{k_2} \quad \text{(B-3)}$$

Where t is the time in seconds, and k_1 and k_2 are curve-fit constants which will vary depending on the valve opening and closing times as well as engine speed.

Table B.3-1 gives the polynomial coefficients for the exhaust valve discharge coefficient expression. As the table shows, the polynomial coefficients vary with valve diameter, as the discharge coefficients have to be re-scaled when the exhaust valve area is changed:

Table B.3-1: Discharge Coefficient Polynomial Curve Fit Coefficient Values for Exhaust Valves

Exhaust Area Increase (%)	Valve Diameter/mm	C_D Polynomial Curve Fit Coefficients				
		A_1	A_2	A_3	A_4	A_5
0	21.92	20.44	-22.05	3.791	2.641	0.001286
5	22.46	22.54	-23.73	3.98	2.706	0.001286
10	22.99	24.74	-25.44	4.17	2.77	0.001286
15	23.51	27.04	-27.19	4.359	2.832	0.001286
20	24.01	29.44	-28.99	4.549	2.893	0.001286
25	24.51	31.94	-30.82	4.738	2.953	0.001286
30	24.99	34.55	-32.68	4.928	3.011	0.001286

Table B.3-2 gives the polynomial coefficients for the intake and exhaust valve lift profile curve fit equation B-2.

Table B.3-2: Polynomial Curve Fit Coefficient Values for Valve Lift Profiles

Coefficients B_n	Exhaust Valves	Intake Valves
B_1	-0.05157	-0.025
B_2	-0.1513	-0.2506
B_3	0.3153	0.1468
B_4	0.9599	1.459
B_5	-0.574	-0.2489
B_6	-0.8069	-1.365
B_7	0.2848	0.1024
B_8	-4.785	-4.953
B_9	-0.04103	-0.01643
B_{10}	7.986	7.982

For the intake valves, the polynomial curve fit is given as a quintic equation of the form:

$$C_{D,in} = k_1 \cdot \epsilon^5 + k_2 \cdot \epsilon^4 + k_3 \cdot \epsilon^3 + k_4 \cdot \epsilon^2 + k_5 \cdot \epsilon + k_6 \quad \text{(B-4)}$$

The polynomial coefficients for Equation B-4 are given in Table B.3-3:

Table B.3-3: Intake Valve Discharge Coefficient Polynomial Curve Fit Coefficients

Intake Valve Number	C_D Polynomial Curve Fit Coefficients for Intake Valves					
	k_1	k_2	k_3	k_4	k_5	k_6
1	-200.3	-260.8	114.4	14.54	2.351	0.001114
2	-371.3	449.6	-184.6	23.89	1.998	-0.0001521

APPENDIX C: STOCK AND NON-DIMENSIONAL TURBINE MAPS FOR THE HONEYWELL GARRETT M53 VARIABLE GEOMETRY TURBOCHARGER

In this appendix, the stock and non-dimensional turbine maps for each rack position of the stock Honeywell Garrett M53 Variable Geometry Turbocharger (VGT) are shown. The raw maps for each rack position were first preprocessed in GT-Power, following which they were non-dimensionalized using the methods described in the turbocharger scaling paper by Bell et al. [177].

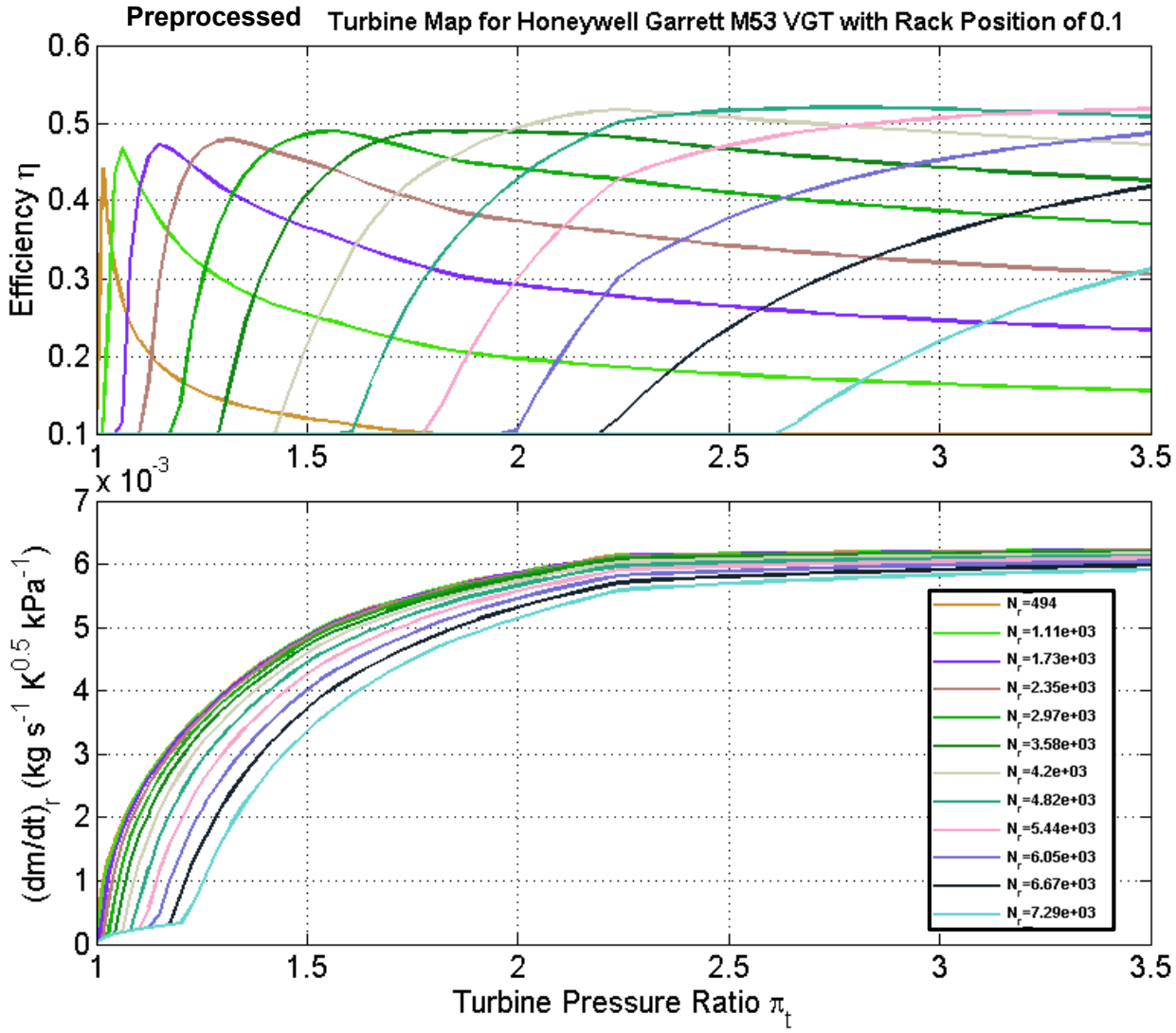

Figure C1: Preprocessed and Fitted Turbine Map from GT-Power for the Honeywell Garrett M53 Stock VGT at a Rack Position of 0.1 (T10 Family of Speed Lines).

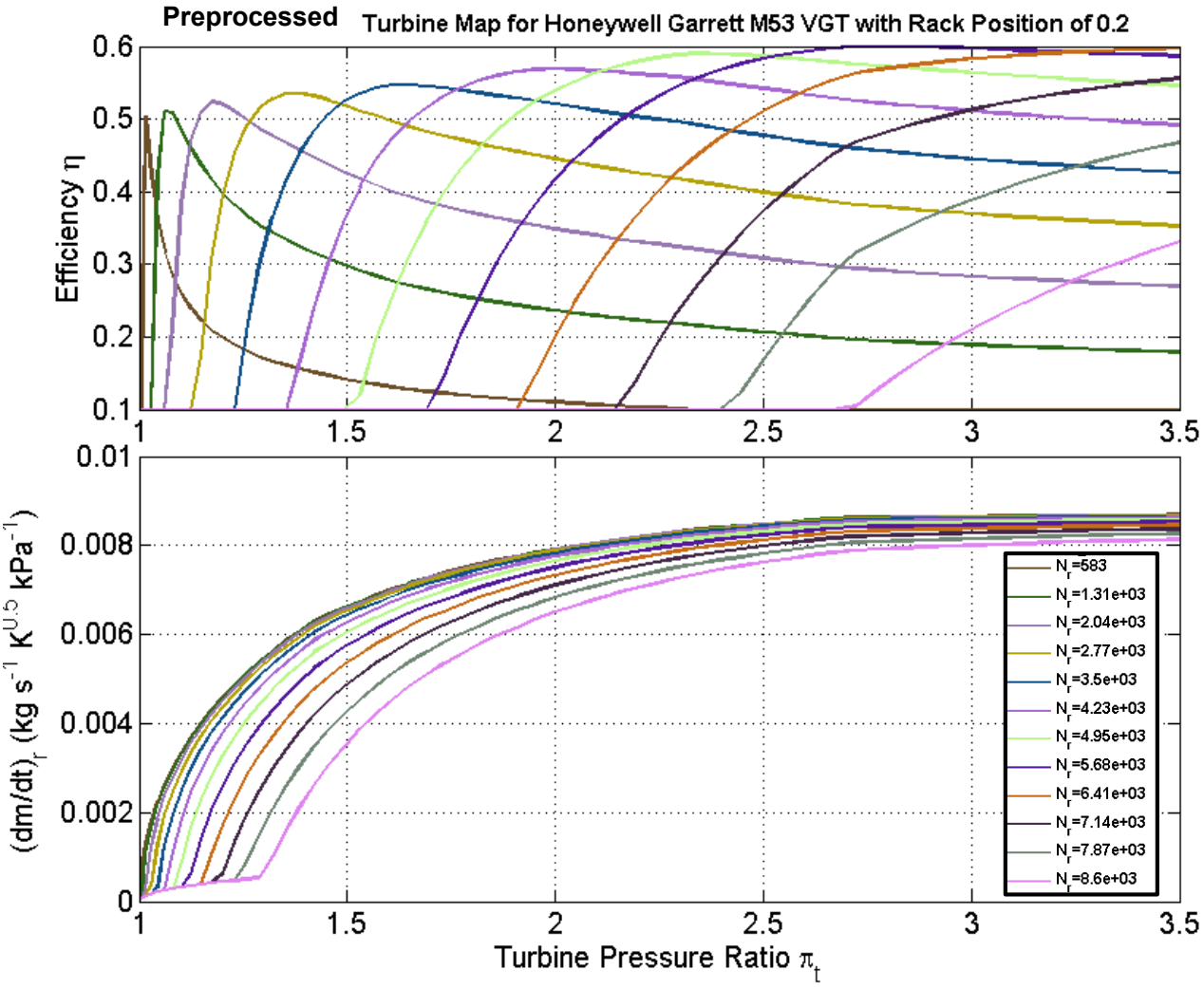

Figure C2: Preprocessed and Fitted Turbine Map from GT-Power for the Honeywell Garrett M53 Stock VGT at a Rack Position of 0.2 (T20 Family of Speed Lines).

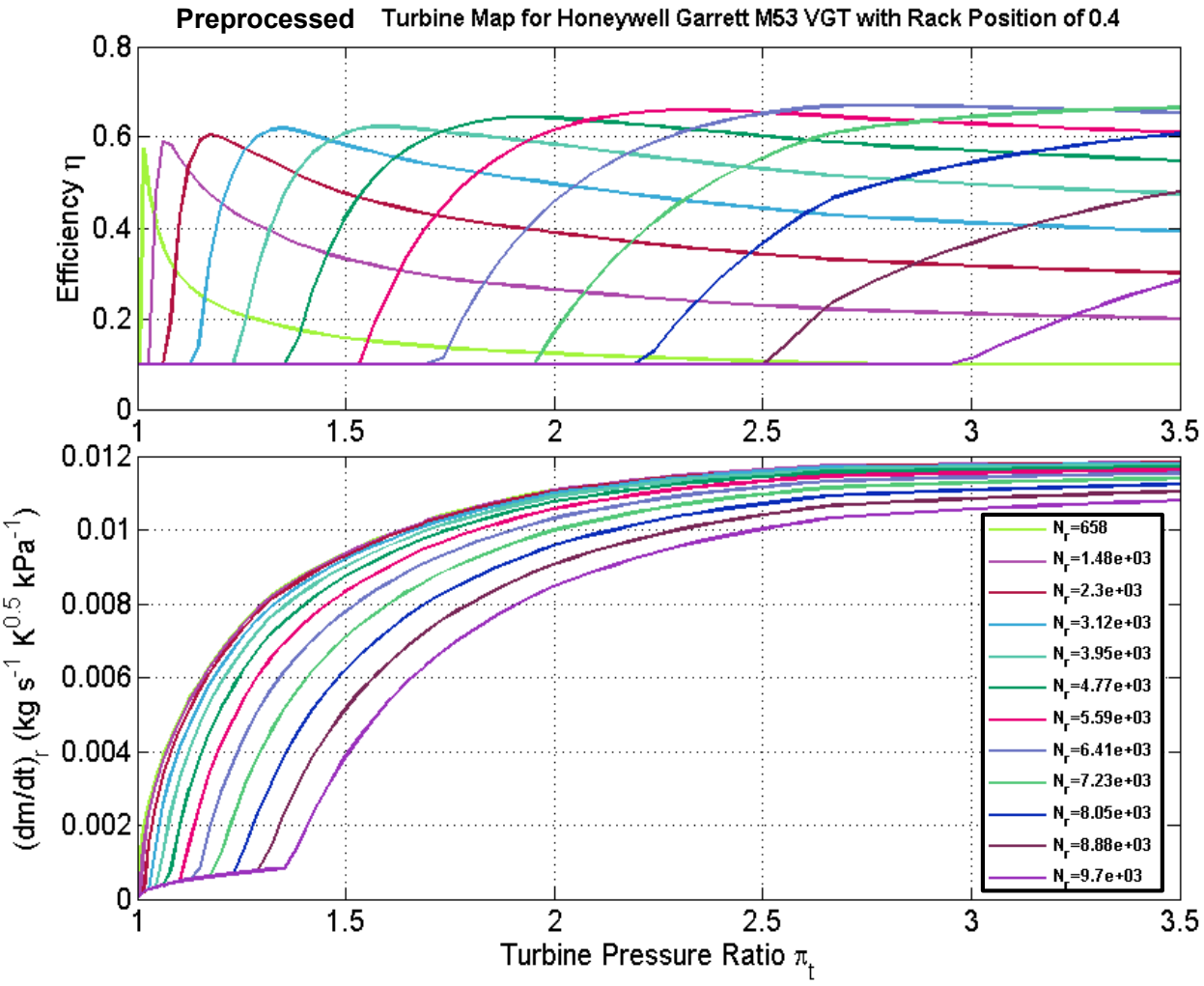

Figure C3: Preprocessed and Fitted Turbine Map from GT-Power for the Honeywell Garrett M53 Stock VGT at a Rack Position of 0.4 (T40 Family of Speed Lines).

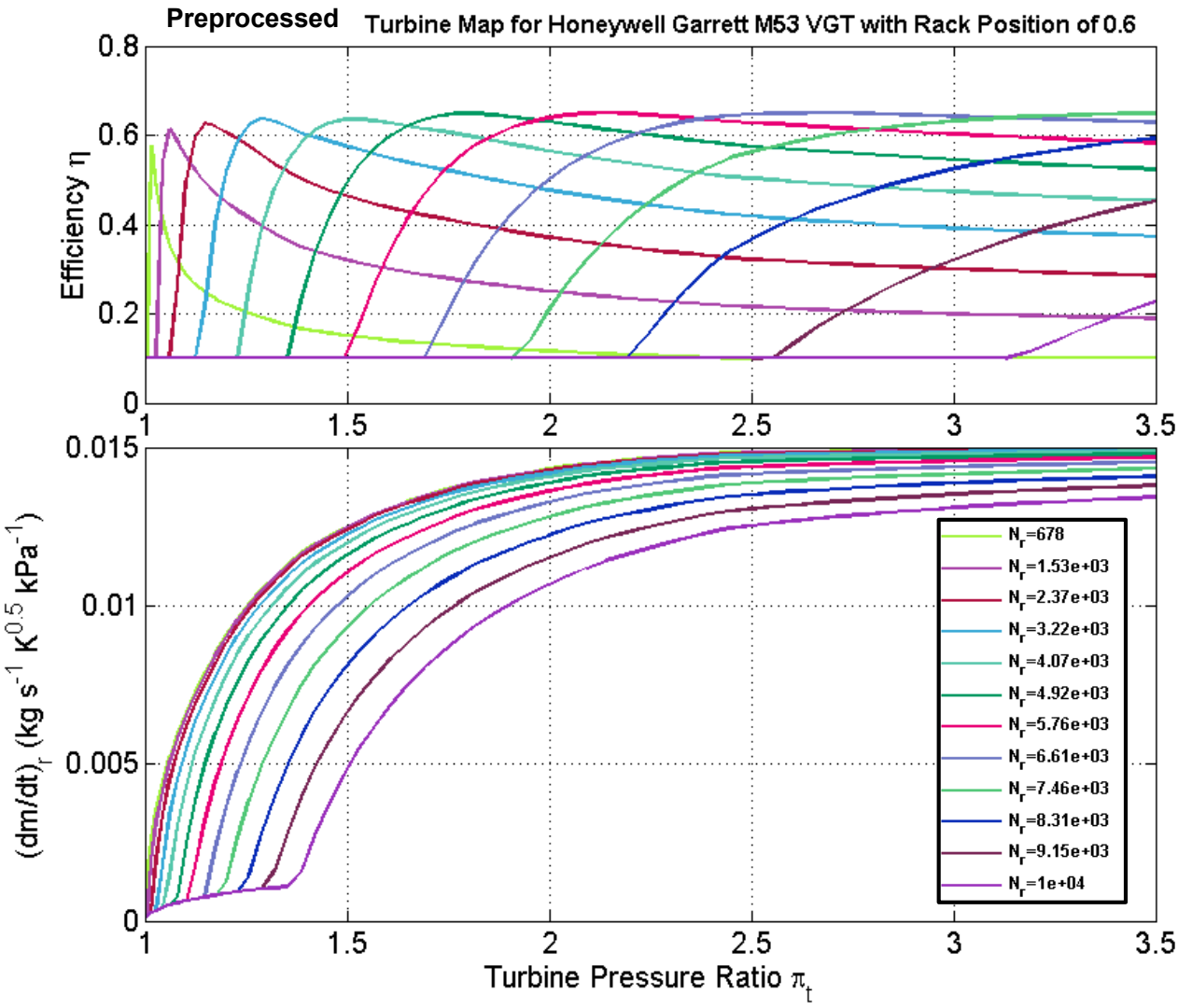

Figure C4: Preprocessed and Fitted Turbine Map from GT-Power for the Honeywell Garrett M53 Stock VGT at a Rack Position of 0.6 (T60 Family of Speed Lines).

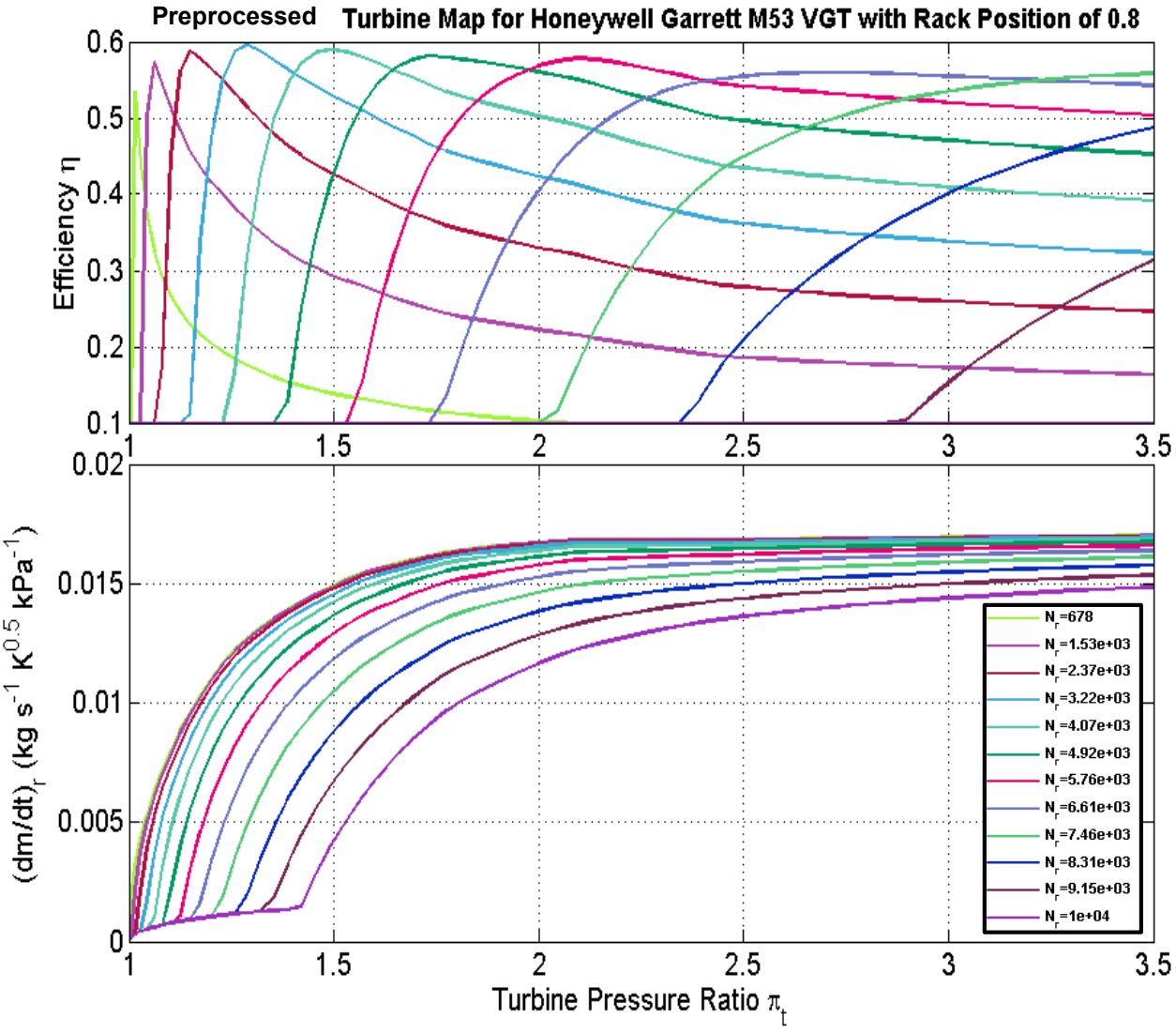

Figure C5: Preprocessed and Fitted Turbine Map from GT-Power for the Honeywell Garrett M53 Stock VGT at a Rack Position of 0.8 (T80 Family of Speed Lines).

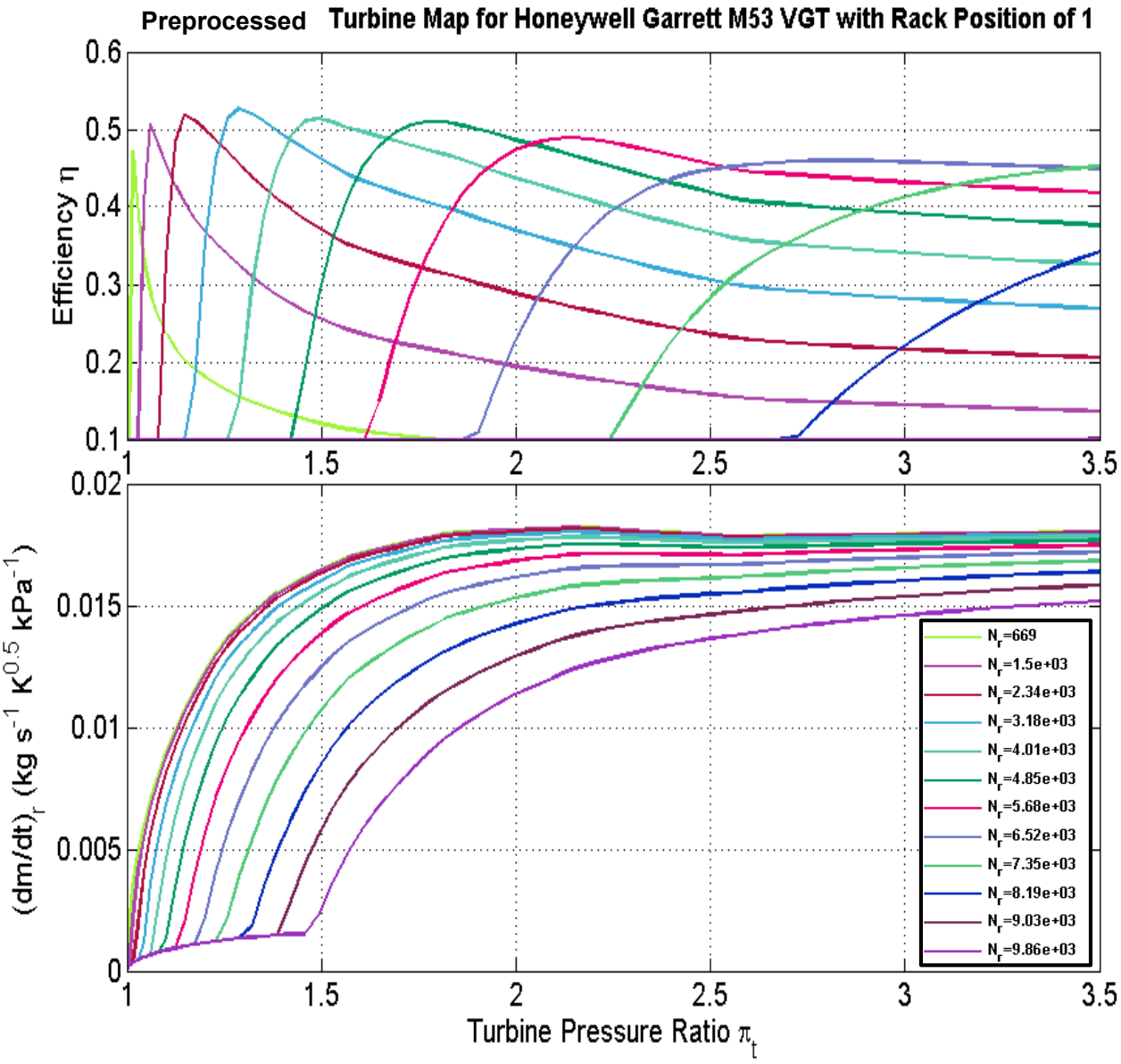

Figure C6: Preprocessed and Fitted Turbine Map from GT-Power for the Honeywell Garrett M53 Stock VGT at a Rack Position of 1 (T100 Family of Speed Lines).

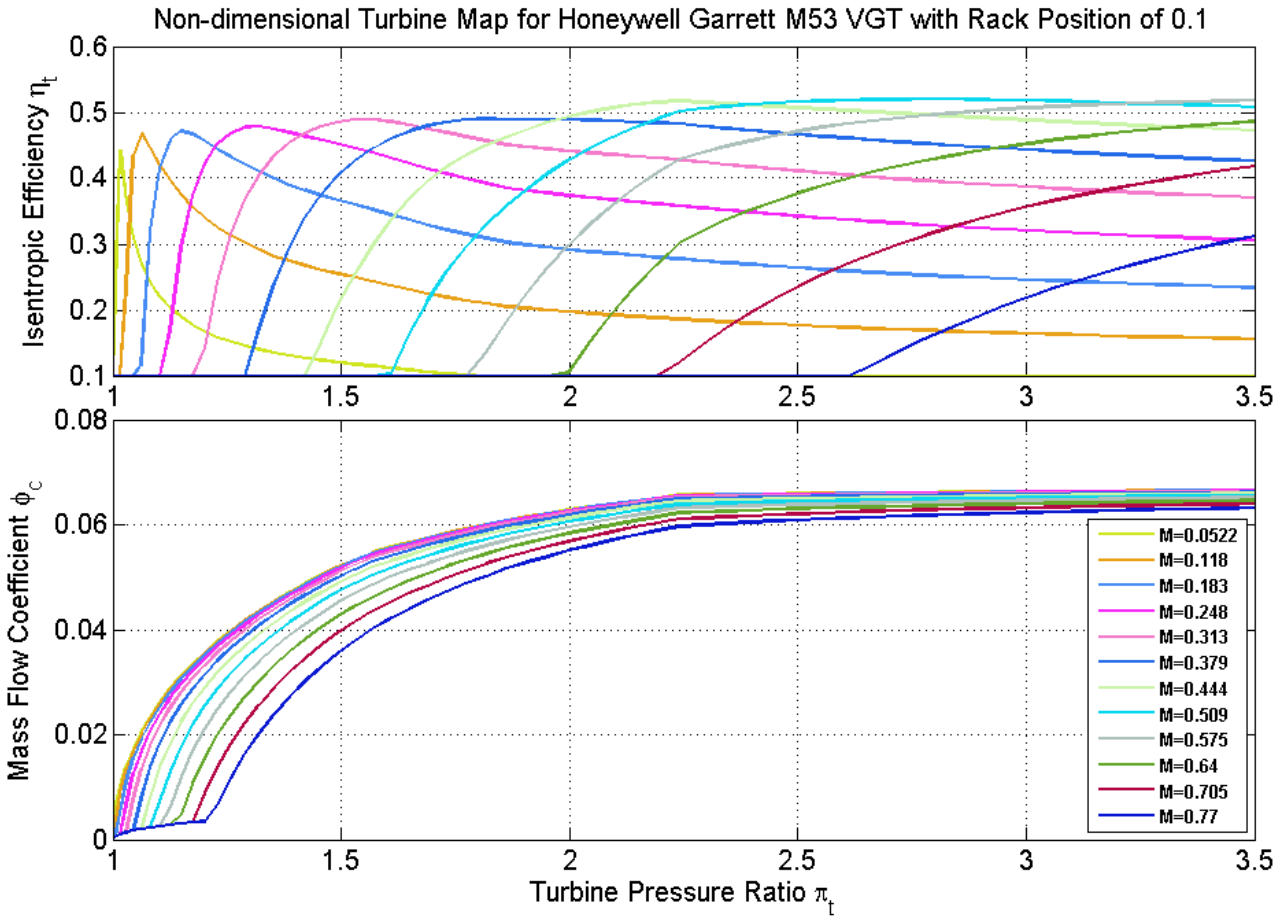

Figure C7: Non-dimensional Turbine Map from GT-Power for the Honeywell Garrett M53 Stock VGT at a Rack Position of 0.1 (T10 Family of Speed Lines).

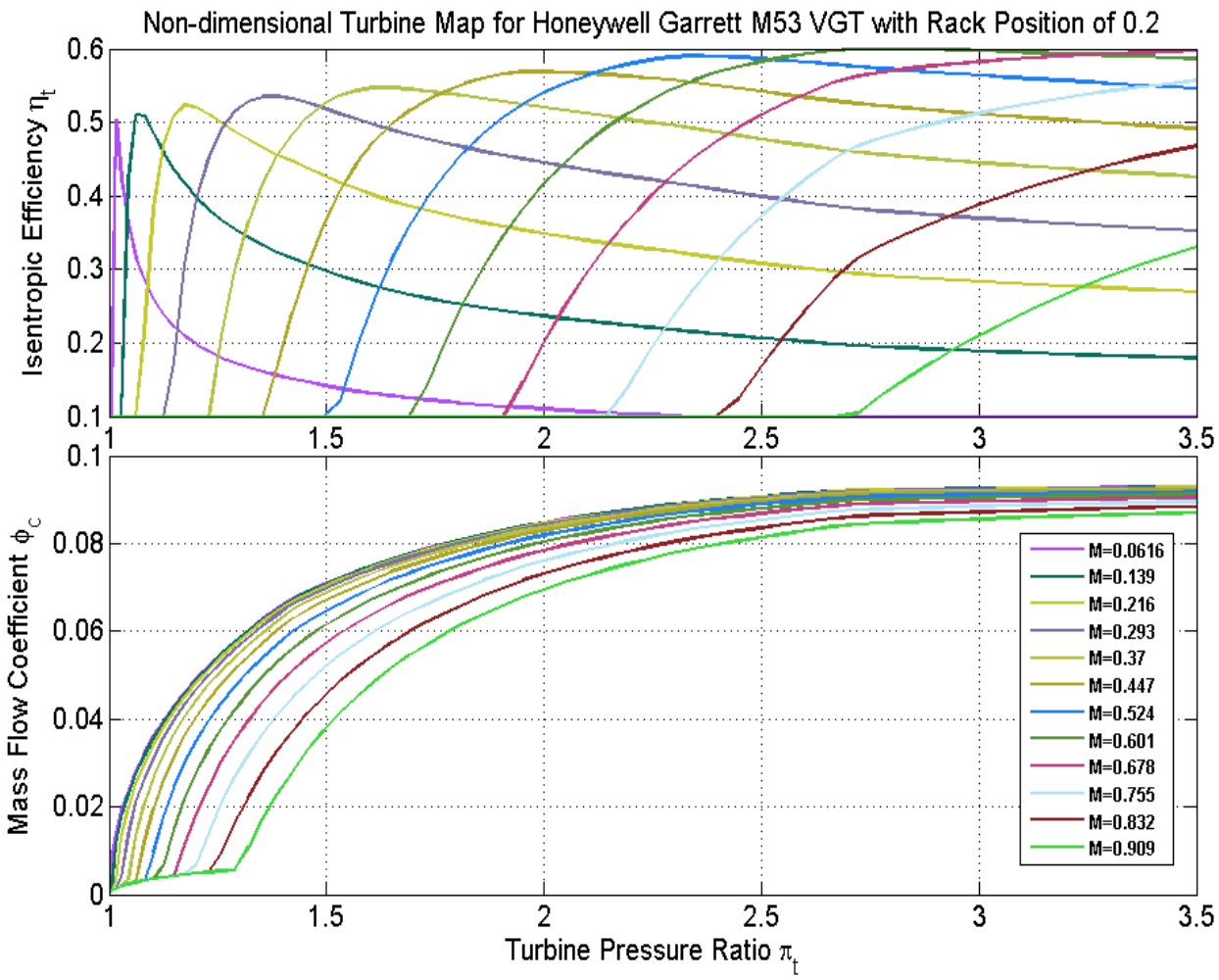

Figure C8: Non-dimensional Turbine Map from GT-Power for the Honeywell Garrett M53 Stock VGT at a Rack Position of 0.2 (T20 Family of Speed Lines).

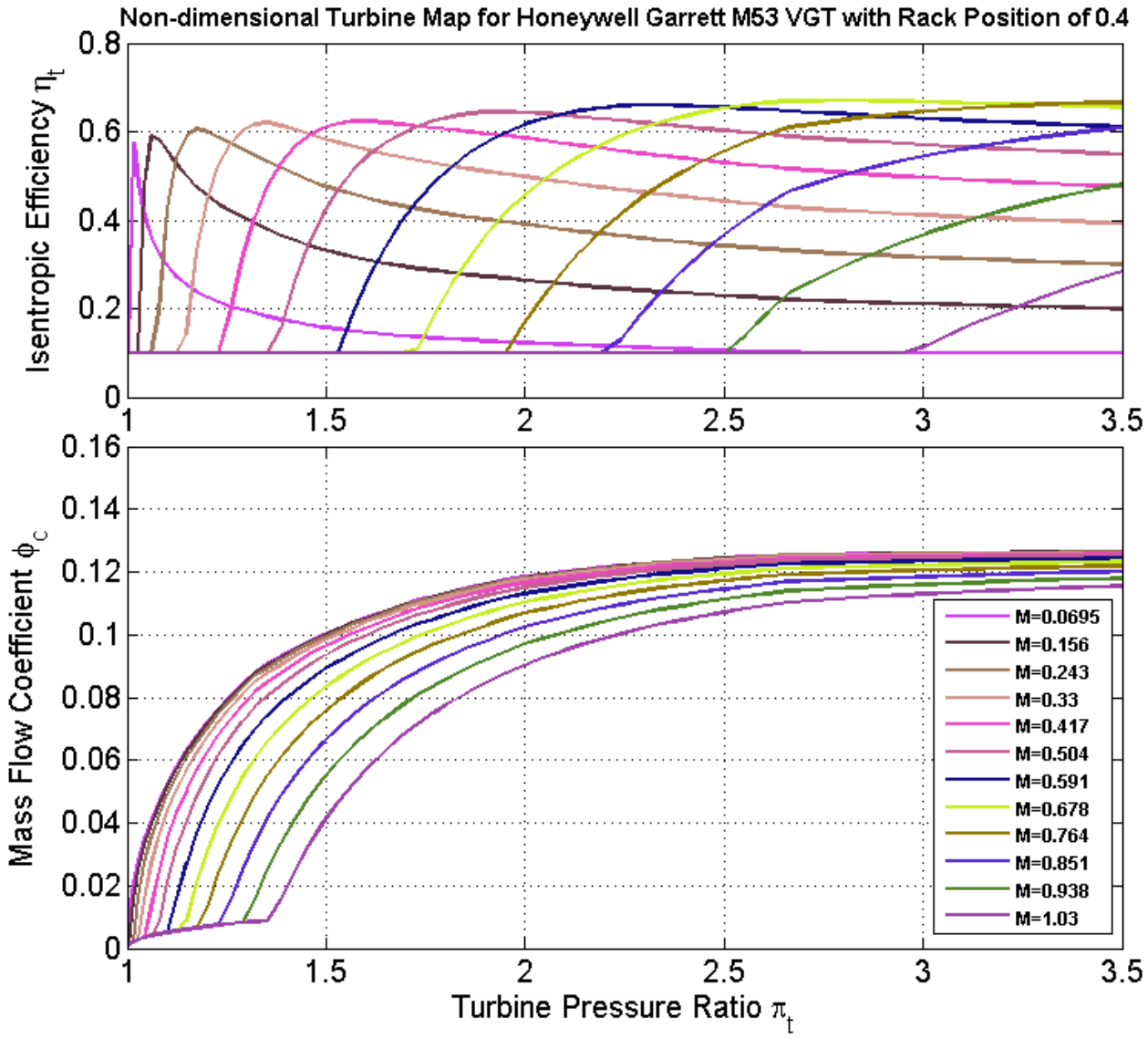

Figure C9: Non-dimensional Turbine Map from GT-Power for the Honeywell Garrett M53 Stock VGT at a Rack Position of 0.4 (T40 Family of Speed Lines).

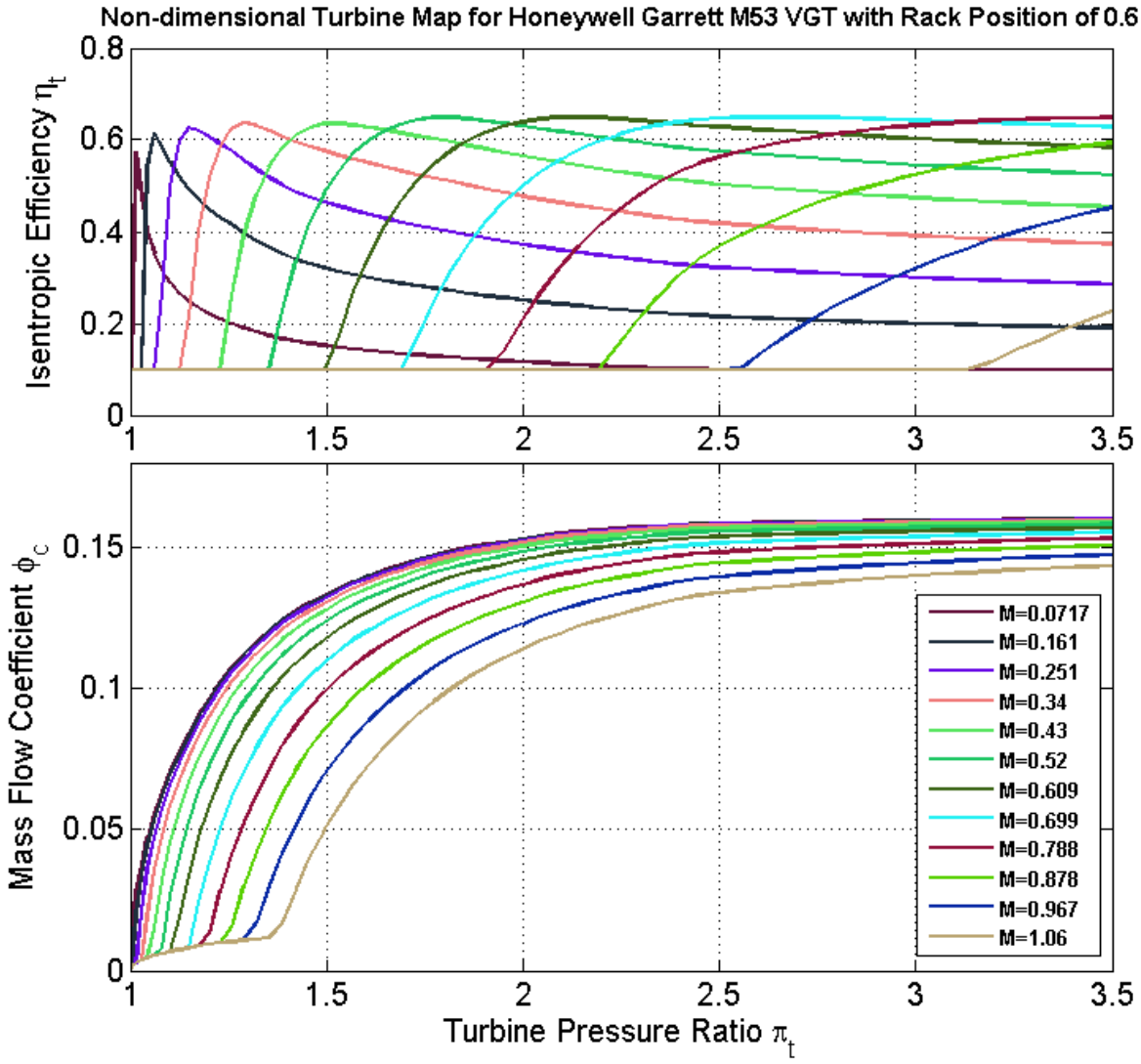

Figure C10: Non-dimensional Turbine Map from GT-Power for the Honeywell Garrett M53 Stock VGT at a Rack Position of 0.6 (T60 Family of Speed Lines).

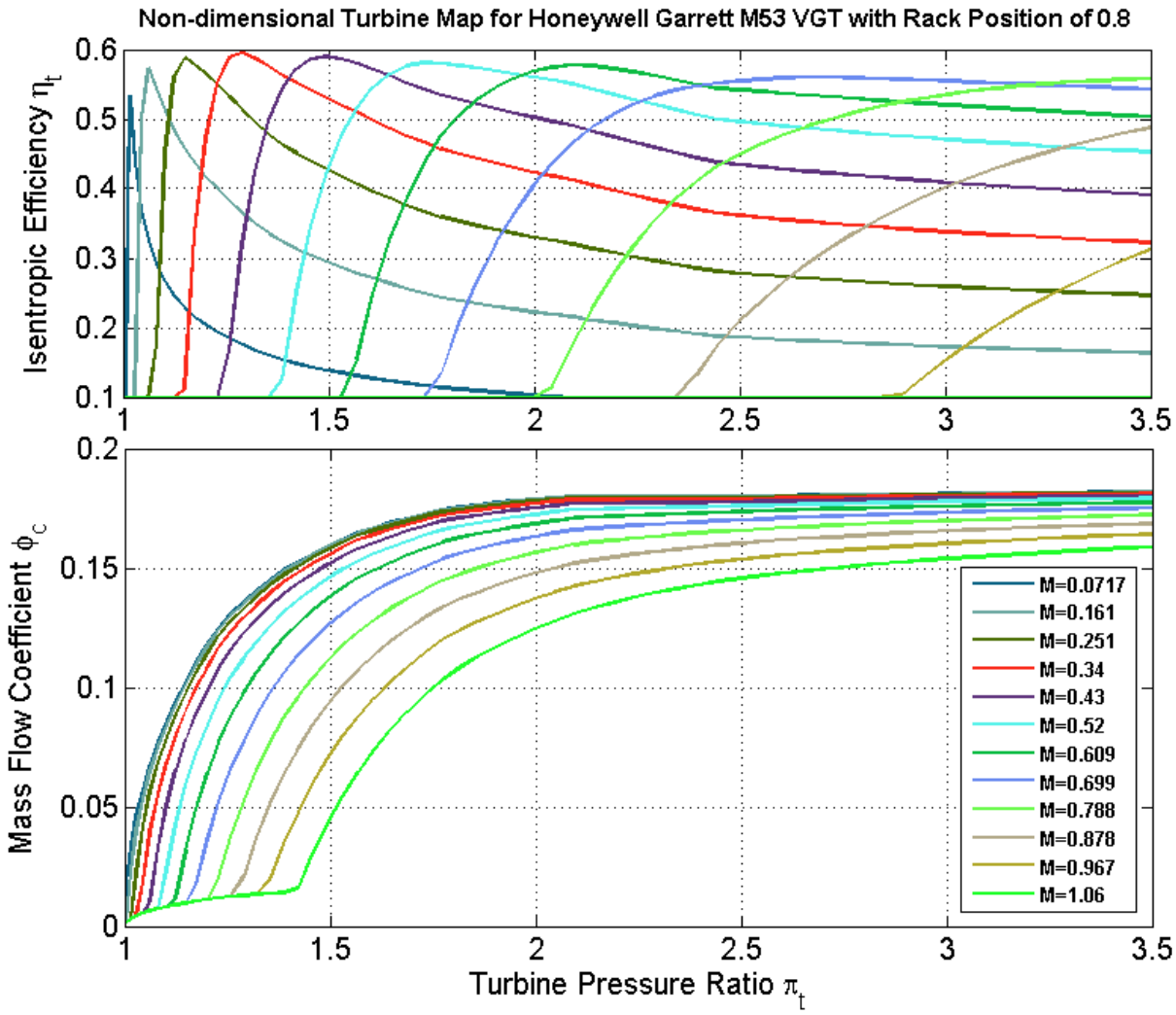

Figure C11: Non-dimensional Turbine Map from GT-Power for the Honeywell Garrett M53 Stock VGT at a Rack Position of 0.8 (T80 Family of Speed Lines).

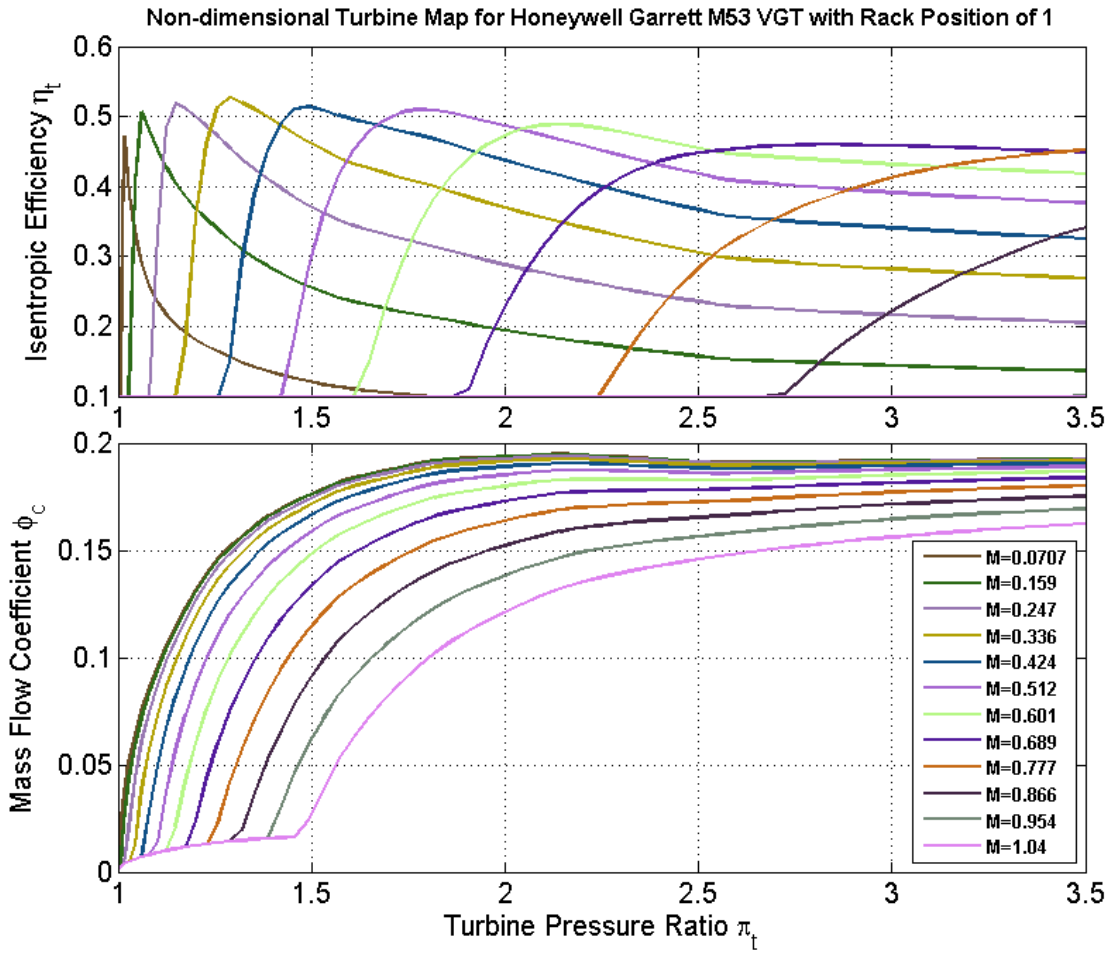

Figure C12: Non-dimensional Turbine Map from GT-Power for the Honeywell Garrett M53 Stock VGT at a Rack Position of 1 (T100 Family of Speed Lines).

APPENDIX D: CHEMICAL KINETIC MECHANISM FOR KIVA-3V

This Appendix gives the Reduced Primary Reference Fuel (PRF) Mechanism developed by Wang et. al [167] that was used in the KIVA-3V multi-dimensional simulations. The mechanism consists of 48 species and 142 reactions. Iso-octane is used as the surrogate fuel to model the chemical and physical properties of gasoline, while n-heptane is used as the surrogate to model diesel chemistry.

Table D1: Elements Considered in Mechanism

ELEMENTS CONSIDERED	ATOMIC WEIGHT
1. h	1.00797
2. c	12.0112
3. o	15.9994
4. n	14.0067

Table D2: Species Considered in Mechanism

SPECIES CONSIDERED	PHASE	CHARGE	MOLECULAR WEIGHT	TEMPERATURE LOW	TEMPERATURE HIGH	ELEMENT COUNT h	c	o	n
1. nc7h16	G	0	100.20557	300.0	5000.0	16	7	0	0
2. o2	G	0	31.99880	300.0	5000.0	0	0	2	0
3. n2	G	0	28.01340	300.0	5000.0	0	0	0	2
4. co2	G	0	44.00995	300.0	5000.0	0	1	2	0
5. h2o	G	0	18.01534	300.0	5000.0	2	0	1	0
6. co	G	0	28.01055	300.0	5000.0	0	1	1	0
7. h2	G	0	2.01594	300.0	5000.0	2	0	0	0
8. oh	G	0	17.00737	300.0	5000.0	1	0	1	0
9. h2o2	G	0	34.01474	300.0	5000.0	2	0	2	0
10. ho2	G	0	33.00677	300.0	5000.0	1	0	2	0
11. h	G	0	1.00797	300.0	5000.0	1	0	0	0
12. o	G	0	15.99940	300.0	5000.0	0	0	1	0
13. ch3o	G	0	31.03446	300.0	3000.0	3	1	1	0
14. ch2o	G	0	30.02649	300.0	5000.0	2	1	1	0
15. hco	G	0	29.01852	300.0	5000.0	1	1	1	0
16. ch2	G	0	14.02709	250.0	4000.0	2	1	0	0
17. ch3	G	0	15.03506	300.0	5000.0	3	1	0	0
18. ch4	G	0	16.04303	300.0	5000.0	4	1	0	0
19. c2h2	G	0	26.03824	300.0	5000.0	2	2	0	0
20. c2h3	G	0	27.04621	300.0	5000.0	3	2	0	0
21. c2h4	G	0	28.05418	300.0	5000.0	4	2	0	0
22. c2h5	G	0	29.06215	300.0	5000.0	5	2	0	0
23. c3h4	G	0	40.06533	200.0	6000.0	4	3	0	0

24.	c3h5	G	0	41.07330	300.0	5000.0	5	3	0	0
25.	c3h6	G	0	42.08127	300.0	5000.0	6	3	0	0
26.	c3h7	G	0	43.08924	300.0	5000.0	7	3	0	0
27.	c7h15-2	G	0	99.19760	300.0	5000.0	15	7	0	0
28.	c7h15o2	G	0	131.19640	300.0	5000.0	15	7	2	0
29.	c7ket12	G	0	146.18783	300.0	5000.0	14	7	3	0
30.	c5h11co	G	0	99.15397	300.0	5000.0	11	6	1	0
31.	n	G	0	14.00670	300.0	5000.0	0	0	0	1
32.	n2o	G	0	44.01280	300.0	5000.0	0	0	1	2
33.	no	G	0	30.00610	300.0	5000.0	0	0	1	1
34.	no2	G	0	46.00550	300.0	5000.0	0	0	2	1
35.	ic8h18	G	0	114.23266	300.0	5000.0	18	8	0	0
36.	c8h17	G	0	113.22469	300.0	5000.0	17	8	0	0
37.	c8h17oo	G	0	145.22349	300.0	5000.0	17	8	2	0
38.	ic8ket21	G	0	160.21492	300.0	5000.0	16	8	3	0
39.	c6h13co	G	0	113.18106	300.0	5000.0	13	7	1	0
40.	c4h9	G	0	57.11633	300.0	5000.0	9	4	0	0
41.	c2h6	G	0	30.07012	300.0	4000.0	6	2	0	0
42.	ch2cho	G	0	43.04561	300.0	5000.0	3	2	1	0
43.	ch2co	G	0	42.03764	300.0	5000.0	2	2	1	0
44.	ch3o2	G	0	47.03386	300.0	5000.0	3	1	2	0
45.	ch3o2h	G	0	48.04183	300.0	5000.0	4	1	2	0
46.	soot	G	0	960.89203	200.0	5000.0	0	80	0	0
47.	nox	G	0	30.00610	300.0	5000.0	0	0	1	1
48.	c14h30	G	0	198.39520	300.0	5000.0	30	14	0	0

Table D3: Reactions Considered in Mechanism

	REACTIONS CONSIDERED	(k = A T**b exp(-E/RT)) A	b	E
1.	ic8h18+h=c8h17+h2	4.38E+07	2.0	7760.0
2.	ic8h18+oh=c8h17+h2o	3.47E+07	1.8	278.2
3.	ic8h18+ho2=c8h17+h2o2	2.23E+14	0.0	18950.0
4.	ic8h18+o2=c8h17+ho2	2.22E+15	0.0	42904.0
5.	c8h17+o2=c8h17oo	1.05E+11	0.0	0.0
6.	c8h17oo+o2=ic8ket21+oh	1.74E+16	0.0	21233.0
7.	ic8ket21=ch2o+c6h13co+oh	1.78E+14	0.0	39100.0
8.	c6h13co=c4h9+c2h4+co	4.92E+16	0.0	40200.0
9.	c4h9=c3h6+ch3	4.56E+13	0.0	36900.0
10.	c8h17=c3h7+c2h4+c3h6	2.16E+16	0.0	36600.0
11.	ic8h18+c7h15-2<=>nc7h16+c8h17	5.01E+10	0.0	0.0
12.	nc7h16+h=c7h15-2+h2	4.38E+07	2.0	4760.0
13.	nc7h16+oh=c7h15-2+h2o	1.36E+10	1.3	690.0
14.	nc7h16+ho2=c7h15-2+h2o2	3.30E+14	0.0	16950.0
15.	nc7h16+o2=c7h15-2+ho2	1.25E+14	0.0	37904.0
16.	c7h15-2+o2=c7h15o2	2.34E+12	0.0	0.0
17.	c7h15o2+o2=c7ket12+oh	3.29E+14	0.0	18232.7
18.	c7ket12=c5h11co+ch2o+oh	6.00E+14	0.0	41100.0
19.	c5h11co=c2h4+c3h7+co	9.84E+15	0.0	40200.0
20.	c7h15-2=c2h5+c2h4+c3h6	4.04E+15	0.0	34600.0
21.	c3h7=c2h4+ch3	9.60E+13	0.0	30950.0
22.	c3h7=c3h6+h	1.25E+14	0.0	36900.0
23.	c3h6+ch3=c3h5+ch4	9.00E+12	0.0	8480.0
24.	c3h5+o2=c3h4+ho2	6.00E+11	0.0	10000.0
25.	c3h4+oh=c2h3+ch2o	1.00E+12	0.0	0.0
26.	c3h4+oh=c2h4+hco	1.00E+12	0.0	0.0
27.	ch3+ho2=ch3o+oh	5.00E+13	0.0	0.0
28.	ch3+oh=ch2+h2o	7.50E+06	2.0	5000.0

```
29. ch2+oh=ch2o+h                                   2.50E+13    0.0        0.0
30. ch2+o2=hco+oh                                   4.30E+10    0.0     -500.0
31. ch2+o2=co2+h2                                   6.90E+11    0.0      500.0
32. ch2+o2=co+h2o                                   2.00E+10    0.0    -1000.0
33. ch2+o2=ch2o+o                                   5.00E+13    0.0     9000.0
34. ch2+o2=co2+h+h                                  1.60E+12    0.0     1000.0
35. ch2+o2=co+oh+h                                  8.60E+10    0.0     -500.0
36. ch3o+co=ch3+co2                                 3.92E+13    0.0    11800.0
37. co+oh=co2+h                                     1.26E+07    1.3     -758.0
38. o+co(+m)<=>co2(+m)                              1.80E+10    0.0     2385.0
    Low pressure limit:  0.60200E+15  0.00000E+00  0.30000E+04
       h2               Enhanced by    2.000E+00
       o2               Enhanced by    6.000E+00
       h2o              Enhanced by    6.000E+00
       co               Enhanced by    1.500E+00
       co2              Enhanced by    3.500E+00
39. o2+co<=>o+co2                                   2.50E+12    0.0    47800.0
40. ho2+co<=>oh+co2                                 4.76E+13    0.0    23600.0
41. o+oh=o2+h                                       4.00E+14   -0.5        0.0
42. h+ho2=oh+oh                                     1.70E+14    0.0      875.0
43. oh+oh=o+h2o                                     6.00E+08    1.3        0.0
44. h+o2(+m)=ho2(+m)                                1.48E+12    0.6        0.0
    Low pressure limit:  0.35000E+17 -0.41000E+00 -0.11160E+04
    TROE centering:      0.50000E+00  0.10000E-29  0.10000E+31
       h2               Enhanced by    2.000E+00
       h2o              Enhanced by    1.200E+01
       co               Enhanced by    1.900E+00
       co2              Enhanced by    3.800E+00
45. oh+oh(+m)=h2o2(+m)                              1.24E+14   -0.4        0.0
    Low pressure limit:  0.30410E+31 -0.46300E+01  0.20490E+04
    TROE centering:      0.47000E+00  0.10000E+03  0.20000E+04  0.10000E+16
       h2               Enhanced by    2.000E+00
       h2o              Enhanced by    1.200E+01
       co               Enhanced by    1.900E+00
       co2              Enhanced by    3.800E+00
46. h2o2+h=ho2+h2                                   1.98E+06    2.0     2435.0
47. h2o2+h=oh+h2o                                   3.07E+13    0.0     4217.0
48. h2o2+o=oh+ho2                                   9.55E+06    2.0     3970.0
49. h2o2+oh=h2o+ho2                                 2.40E+00    4.0    -2162.0
50. h2+oh=h2o+h                                     1.17E+09    1.3     3626.0
51. ho2+ho2=h2o2+o2                                 3.00E+12    0.0        0.0
52. ch2o+oh=hco+h2o                                 5.56E+10    1.1      -76.5
53. ch2o+ho2=hco+h2o2                               3.00E+12    0.0     8000.0
54. hco+o2=ho2+co                                   3.30E+13   -0.4        0.0
55. hco+m=h+co+m                                    1.59E+18    0.9    56712.3
56. ch3+ch3o=ch4+ch2o                               4.30E+13    0.0        0.0
57. c2h4+oh=ch2o+ch3                                1.20E+14    0.0      960.0
58. c2h4+oh=c2h3+h2o                                8.02E+13    0.0     5955.0
59. c2h3+o2=ch2o+hco                                4.00E+12    0.0     -250.0
60. c2h3+hco=c2h4+co                                6.03E+13    0.0        0.0
61. c2h5+o2=c2h4+ho2                                2.00E+10    0.0    -2200.0
62. ch4+o2=ch3+ho2                                  7.90E+13    0.0    56000.0
63. oh+ho2=h2o+o2                                   7.50E+12    0.0        0.0
64. ch3+o2=ch2o+oh                                  3.80E+11    0.0     9000.0
65. ch4+h=ch3+h2                                    6.60E+08    1.6    10840.0
66. ch4+oh=ch3+h2o                                  1.60E+06    2.1     2460.0
67. ch4+o=ch3+oh                                    1.02E+09    1.5     8604.0
68. ch4+ho2=ch3+h2o2                                9.00E+11    0.0    18700.0
69. ch4+ch2=ch3+ch3                                 4.00E+12    0.0     -570.0
70. c3h6=c2h3+ch3                                   3.15E+15    0.0    85500.0
71. ch2+ch2=c2h2+h2                                 1.20E+13    0.0      800.0
72. ch2+ch2=c2h2+h+h                                1.20E+14    0.0      800.0
73. c2h4+m=c2h2+h2+m                                1.50E+15    0.0    55800.0
```

```
 74. c2h2+o2=hco+hco                                   4.00E+12    0.0    28000.0
 75. c2h2+o=ch2+co                                     1.02E+07    2.0     1900.0
 76. c2h2+h+m=c2h3+m                                   5.54E+12    0.0     2410.0
 77. c2h3+h=c2h2+h2                                    4.00E+13    0.0        0.0
 78. c2h3+oh=c2h2+h2o                                  3.00E+13    0.0        0.0
 79. c2h3+ch2=c2h2+ch3                                 3.00E+13    0.0        0.0
 80. c2h3+c2h3=c2h2+c2h4                               1.45E+13    0.0        0.0
 81. c2h3+o=c2h2+oh                                    1.00E+13    0.0        0.0
 82. c2h2+oh=ch3+co                                    4.83E-04    4.0    -2000.0
 83. c2h3=c2h2+h                                       4.60E+40   -8.8    46200.0
 84. n+no<=>n2+o                                       3.50E+13    0.0      330.0
 85. n+o2<=>no+o                                       2.65E+12    0.0     6400.0
 86. n+oh<=>no+h                                       7.33E+13    0.0     1120.0
 87. n2o+o<=>n2+o2                                     1.40E+12    0.0    10810.0
 88. n2o+o<=>2no                                       2.90E+13    0.0    23150.0
 89. n2o+h<=>n2+oh                                     4.40E+14    0.0    18880.0
 90. n2o+oh<=>n2+ho2                                   2.00E+12    0.0    21060.0
 91. n2o(+m)<=>n2+o(+m)                                1.30E+11    0.0    59620.0
     Low pressure limit:  0.62000E+15  0.00000E+00  0.56100E+05
        h2               Enhanced by    2.000E+00
        h2o              Enhanced by    6.000E+00
        ch4              Enhanced by    2.000E+00
        co               Enhanced by    1.500E+00
        co2              Enhanced by    2.000E+00
 92. ho2+no<=>no2+oh                                   2.11E+12    0.0     -480.0
 93. no+o+m<=>no2+m                                    1.06E+20   -1.4        0.0
        h2               Enhanced by    2.000E+00
        h2o              Enhanced by    6.000E+00
        ch4              Enhanced by    2.000E+00
        co               Enhanced by    1.500E+00
        co2              Enhanced by    2.000E+00
 94. no2+o<=>no+o2                                     3.90E+12    0.0     -240.0
 95. no2+h<=>no+oh                                     1.32E+14    0.0      360.0
 96. c3h6+h=c3h5+h2                                    5.00E+12    0.0     1500.0
 97. c3h6+o2=c3h5+ho2                                  4.00E+12    0.0    39900.0
 98. ch2cho+h=ch3+hco                                  2.20E+13    0.0        0.0
 99. ch2o+o2=hco+ho2                                   6.20E+13    0.0    39000.0
100. ch2o+o=hco+oh                                     4.10E+11    0.6     2760.0
101. ch2o+h=hco+h2                                     2.19E+08    1.8     3000.0
102. ch2o+m=co+h2+m                                    6.25E+15    0.0    69540.0
103. ch2o+m=hco+h+m                                    3.30E+16    0.0    81000.0
104. hco+oh=h2o+co                                     1.00E+14    0.0        0.0
105. hco+o=oh+co                                       3.00E+13    0.0        0.0
106. hco+o=h+co2                                       3.00E+13    0.0        0.0
107. hco+ho2=co2+oh+h                                  3.00E+13    0.0        0.0
108. c2h6+ch3=c2h5+ch4                                 1.51E-07    6.0     6047.0
        Reverse Arrhenius coefficients:                9.65E-10    6.6    10220.0
109. c2h6+h=c2h5+h2                                    5.37E+02    3.5     5200.0
        Reverse Arrhenius coefficients:                9.72E+02    3.5    27320.0
110. c2h6+oh=c2h5+h2o                                  5.12E+06    2.1      855.0
        Reverse Arrhenius coefficients:                1.01E+07    2.1    22980.0
111. c2h6+o=c2h5+oh                                    1.13E+14    0.0     7850.0
        Reverse Arrhenius coefficients:                2.08E+13    0.0    12720.0
112. ch3+ch3(+m)=c2h6(+m)                              7.37E+16   -1.2      635.8
     Low pressure limit:  0.90880E+36 -0.52460E+01  0.17050E+04
     TROE centering:      0.40500E+00  0.11200E+04  0.69600E+02  0.10000E+16
113. c2h6+o2=c2h5+ho2                                  4.00E+13    0.0    50900.0
        Reverse Arrhenius coefficients:                3.00E+11    0.0        0.0
114. c2h6+ho2=c2h5+h2o2                                1.70E+13    0.0    20460.0
        Reverse Arrhenius coefficients:                1.07E+11    0.2     7842.0
115. c2h6+c2h4=c2h5+c2h5                               5.00E+11    0.0    60000.0
        Reverse Arrhenius coefficients:                5.00E+11    0.0        0.0
116. c2h6+m=c2h5+h+m                                   8.85E+20   -1.2   102200.0
```

```
       Reverse Arrhenius coefficients:            1.15E+13    0.3    -1550.0
117. c2h6+ch2=c2h5+ch3                            2.20E+13    0.0     8670.0
       Reverse Arrhenius coefficients:            2.66E+10    0.6    17060.0
118. c2h6+ch3o2=c2h5+ch3o2h                       1.70E+13    0.0    20460.0
       Reverse Arrhenius coefficients:            7.50E+11    0.0     1280.0
119. c3h6+c2h5=c3h5+c2h6                          1.00E+11    0.0     9800.0
       Reverse Arrhenius coefficients:            5.37E+05    1.3    16440.0
120. c3h5+c2h5=c2h6+c3h4                          4.00E+11    0.0        0.0
       Reverse Arrhenius coefficients:            1.80E+12    0.1    40330.0
121. c2h4+o=ch2cho+h                              3.39E+06    1.9      179.0
122. c2h3+o2=ch2cho+o                             3.50E+14   -0.6     5260.0
123. ch2cho+o2=ch2o+co+oh                         2.00E+13    0.0    42000.0
124. c2h2+oh=ch2co+h                              2.19E-04    4.5    -1000.0
125. ch2co+h=ch3+co                               1.10E+13    0.0     3400.0
126. ch2co+o=ch2+co2                              1.75E+12    0.0     1350.0
127. ch2co(+m)=ch2+co(+m)                         3.00E+14    0.0    70980.0
     Low pressure limit:  0.36000E+16  0.00000E+00  0.59270E+05
128. c3h6+o=ch2co+ch3+h                           2.50E+07    1.8       76.0
129. ch2cho=ch2co+h                               3.09E+15   -0.3    50820.0
130. ch3+o2+m=ch3o2+m                             5.44E+25   -3.3        0.0
131. ch3o2+ch3=ch3o+ch3o                          2.41E+12    0.0        0.0
132. ch3o2+o=ch3o+o2                              3.61E+13    0.0        0.0
133. ch3o2+h=ch3o+oh                              9.64E+13    0.0        0.0
134. ch3o+h=ch3+oh                                1.00E+14    0.0        0.0
135. ch3+o=ch2o+h                                 8.00E+13    0.0        0.0
136. ch3+o2=ch3o+o                                2.00E+18   -1.6    29210.0
       Reverse Arrhenius coefficients:            3.58E+18   -1.6    -1631.0
137. ch3+h(+m)=ch4(+m)                            2.14E+15   -0.4        0.0
     Low pressure limit:  0.33100E+31 -0.40000E+01  0.21080E+04
     TROE centering:      0.00000E+00  0.10000E-14  0.10000E-14  0.40000E+02
        h2               Enhanced by    2.000E+00
        h2o              Enhanced by    5.000E+00
        co               Enhanced by    2.000E+00
        co2              Enhanced by    3.000E+00
138. ch3o2h=ch3o+oh                               6.31E+14    0.0    42300.0
139. ch3o2+ch2o=ch3o2h+hco                        1.99E+12    0.0    11670.0
140. c2h4+ch3o2=c2h3+ch3o2h                       1.13E+13    0.0    30430.0
141. ch4+ch3o2=ch3+ch3o2h                         1.81E+11    0.0    18480.0
142. ch3o2+ho2=ch3o2h+o2                          1.75E+10    0.0    -3275.0

 NOTE:  A units mole-cm-sec-K, E units cal/mole
```